1-1-1980

Hydraulics of floating boundaries.

Mohamed Reda Ibrahim Haggag
University of Windsor

HYDRAULICS OF FLOATING BOUNDARIES

A Dissertation
Submitted to the Faculty of Graduate Studies through the
Department of Civil Engineering in Partial Fulfilment
of the Requirements for the Degree of
Doctor of Philosophy at the
University of Windsor

by

Mohamed Reda Ibrahim Haggag

B.Sc. (Honour), M.A.Sc, P. Eng.

Windsor, Ontario, Canada
1980

ABSTRACT

The problems associated with the hydraulics of floating boundaries as well as the flow in covered channels were investigated theoretically and experimentaly.

A mathematical model was developed to predict the velocity and shear profiles in two and three dimensional channels. An empirical friction factor for the cover underside that accounts for both the skin and form resistances was introduced. To aid in solving these models, a method for estimating the composite roughness was also presented.

A generalized non-uniform flow equation was developed to predict the sedimentary pattern in channels with loose floating covers. A study of the behavior of an arrested block at the leading edge of the cover was also presented. The different forces and the stability conditions were investigated for a general block stability case.

A comprehensive experimental program was carried out to verify the developed mathematical models and to aid in obtaining the necessary empirical coefficients. Based on these experiments, an empirical relation for the block stability problem, was also obtained. Good agreement was found between the theory and the experimental data within the tested limits.

To my wife,

with all my love, THANK YOU

ACKNOWLEDGEMENTS

I wish to express my appreciation and gratitude to my advisor Dr. S. P. Chee for his continuous and patient guidance throughout the course of my study. My admiration and thanks to him go far beyond words.

The encouragement and support of Dr. C. MacInnis, Dean of Engineering, and Dr. J. McCorquodale are sincerely appreciated.

I also wish to thank the Civil Engineering Department technicians Mr. G. Michalczuk and Mr. P. Feimer for their help during the experimental investigation.

The financial support of the National Research Council and the Civil Engineering Department of the University of Windsor is appreciated.

The encouragement of my parents and my mother-in-law is greatly appreciated.

Finally, I am deeply grateful to my wife for her assistance, patience and understanding. I am very thankful for her effort in typing this thesis, and I truly appreciate her constant support.

TABLE OF CONTENTS

Table of Contents Continued: PAGE

Table of Contents Continued: PAGE

Table of Contents Continued:

Table of Contents Continued:

LIST OF FIGURES

Figure (Continued) PAGE

Figure (Continued) PAGE

Figures (Continued) PAGE

LIST OF TABLES

CHAPTER I

INTRODUCTION

INTRODUCTION

Much of the earth's surface experiences annually recurring periods of low temperatures which result in partial or total freezing of a great number of natural bodies of water, and in the formation of a floating boundary on its surface called ice cover.

Ice covers are not the only known types of floating boundaries. Floating plants such as the Nile Rose or tree logs transported by rivers are other types of floating covers. This work is an investigation of the problems of floating boundaries with direct application to ice covers.

1.1 Definition of the Problem

In an open channel, Figure 1.1, when the temperature drops to or below a certain point water starts to freeze, forming ice. The ice accumulates, forming ice floes which travel downstream until they strike an obstacle that stops them and the formation of an ice cover begins.

The formation of ice covers is always associated with many hydraulic problems. One of the key problems is the flow pattern; that is, the velocity and shear profiles. These profiles, in turn, depend on the sedimentary pattern in the channel as well as the friction factors of the different boundaries.

On the other hand, when an ice block reaches an existing cover, it either remains stable and extends the cover or rides above or turns under the cover to thicken it. This depends on its properties and the flow conditions.

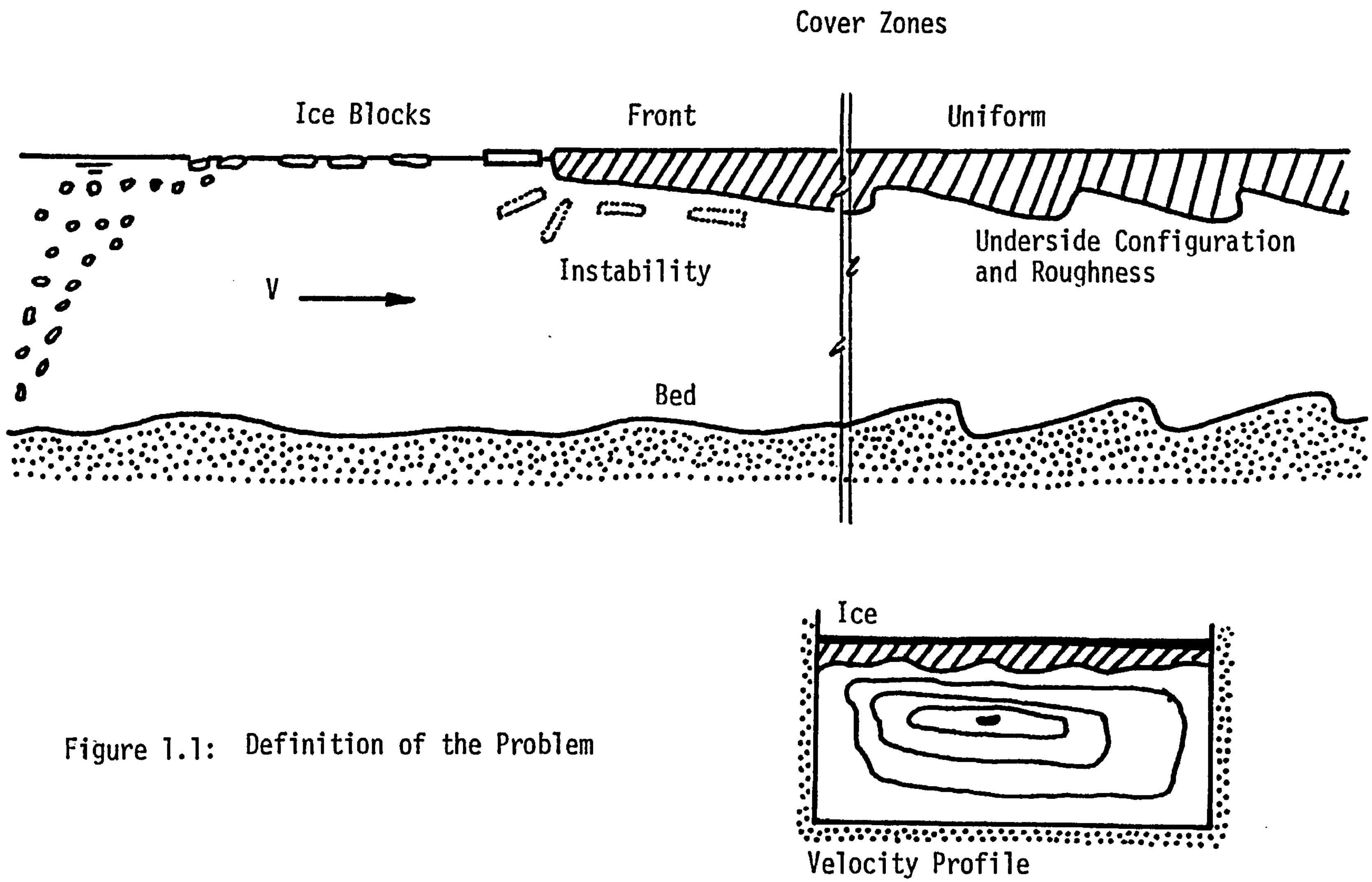

Figure 1.1: Definition of the Problem

Although the ice cover problem has many other aspects, these problems are among the more basic ones that warrant further investigation. This thesis deals only with these aspects of the problem.

The thesis will proceed with the development of the theoretical model, which is presented in Chapter III, after reviewing the literature in Chapter II. Then the experimental investigation will be described in Chapter IV, followed by the analysis of the model and its results in Chapter V. An empirical relation to predict the leading edge stability condition is presented separately in Chapter VI.

The necessary mathematical details and computer program listings along with the analysis of the significant error limits of the experimental results are presented in separate appendices in order not to disturb the fluency of the subject presentation.

CHAPTER II

LITERATURE SURVEY

II LITERATURE SURVEY

This chapter reviews some of the literature that deals with those ice cover problems mentioned in Chapter I. For the sake of simplicity the notations used in the different literature reports were modified to agree with those adopted in this thesis.

2.1 Definitions and Basic Assumptions

In all the literature surveyed certain basic assumptions with regard to ice-covered channel flow were generally agreed upon. These assumptions can be summarized as follows:

1. The flow in an ice-covered channel is gravity open channel flow with a floating boundary. Only gravity forces can exist and no pressure gradient will be found.
2. The channel cross-section can be divided into two subsections, Figure 2.1. Subsection (1) flows under the effect of the bottom and sides, while subsection (2) is dominated by the cover.
3. The separation surface between the two subsections is the locus of no shear. With reference to a vertical line it is also the locus of the points of maximum velocity.
4. The equations of continuity, momentum and energy can be applied to the channel cross-section in total and to each subsection on its own.

In addition some common assumptions are applied to each specific problem associated with the cover. These specific assumptions will be

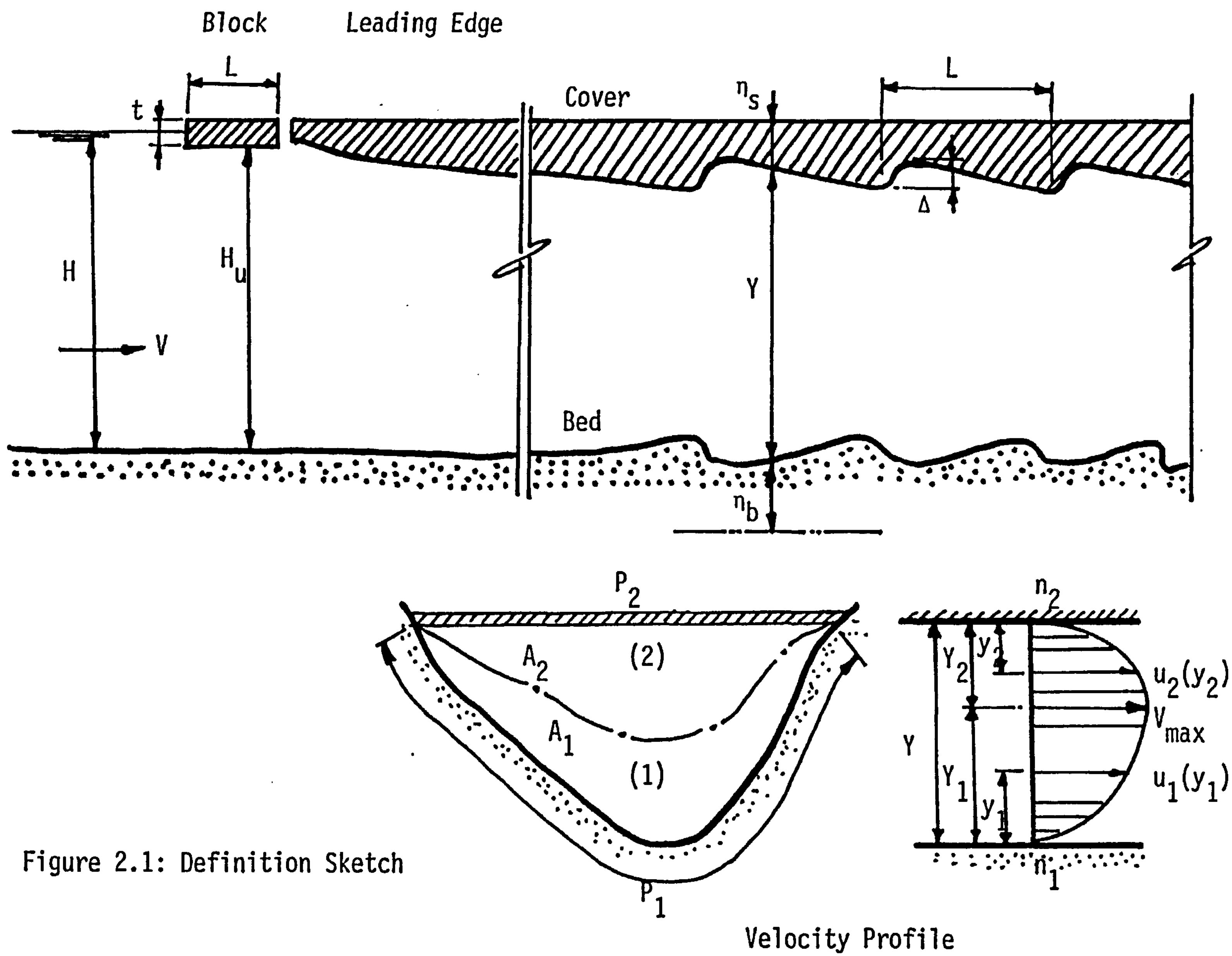

Figure 2.1: Definition Sketch

presented at the appropriate point.

The different variables used in this work and the notations given to them are shown in Figure 2.1 and listed in Appendix F. In addition an explanation of each notation will be presented when it first appears.

2.2 Velocity Profiles in Covered Channels

As early as 1938, Belokon(after(39)) adopted a power-law velocity distribution with an exponent of 1.5 for each subsection. He also suggested that the mean velocities of each subsection are equal and also equal to that of the total channel, i.e. $V_1 = V_2 = V$, an assumption which became very popular later in spite of its inaccuracy.

In 1948, Levi (after(39)), considering the case of a wide channel, applied a logarithmic velocity profile in the form

$$u_i(y_i) = (V_{*i}/\sqrt{2}\,\kappa) \text{ Ln } y_i/k_i \qquad , i = 1,2 \qquad 2.1$$

where, κ = Von Karman's constant,

k_i = roughness height,

V_{*i} = shear velocity,

u_i = velocity at point y_i away from the boundary,

and i = 1 or 2, and refers to the bed and cover subsections respectively.

This equation was used to predict the mean velocity and hence to develop an expression for the composite roughness.

In 1959, Barrows et al(after(2))presented some field measurements of the velocity profiles at Chemung River, N.Y., during different stages of ice formation. They gave only descriptive analyses of their data and suggested the use of a parabolic velocity profile. Also in 1964, Devik (2) reported field measurmenets of velocity profiles in rivers.

Synotin (32) in 1965 suggested that the velocity structure of the flow under the ice cover can be described by the relation

$$V_i/V_{*i} = 6.45 \text{ Log } Y_i/k_i + 5.6 + 2.8\ (1 - k_i/Y_i) \quad , i = 1,2 \qquad 2.2$$

which was developed using Russian data obtained by Nikitin.

In 1966, Carey (4) affirmed once more the suggestion that the mean velocities of each subsection are equal and equal to that of the total channel. He also suggested the use of the Karaman-Prandtl lograithmic velocity profile and resistance equation.

Hancu (after (39)) in 1937, suggested the application of the velocity defect law to each subsection as follows

$$V_{max} - u_i(y_i) = (\ V_{*i}/\kappa\ ) \text{ Ln } y_i/Y_i \quad , i = 1,2 \qquad 2.3$$

He also presented some graphs which can be used to estimate V_1, V_2, V, Y_1 and Y_2 and to establish the velocity profile.

In 1968, Yu, Graf and Levine (45) suggested the use of a modified Manning relation to determine the mean velocity for each subsection in the form

$$V_i = \frac{1.49}{n_i}\ S^{\frac{1}{2}}\ (\ A_i/\ P_i^{\ Z}\ )^{r+\frac{1}{2}} \quad , i = 1,2 \qquad 2.4$$

where Z equals $(n_2/n_1)^{1/6}$ and r = 1/6 on the average but should be determined experimentally.

In 1969, Larsen (18) suggested the use of the logarithmic velocity profile for each subsection in the form

$$u_i(y_i) = 2.5\, V_{*i} \,\mathrm{Ln}\, 30\, Y_i/k_i \qquad , i = 1,2 \qquad 2.5$$

which he used to determine Y_1, Y_2 and the composite roughness.

Ohashi et al(after(25))in 1970, gave the measurements of the velocity profiles both under irregular ice covers and in the open sections for the Hokaido River. In the same year Tsang (38) showed that the presence of frazil ice under the cover alters the vertical velocity profile to a great extent. Also he reported increases in the head loss and the velocity between the frazil layer and the bed.

In 1970, Tesaker (37) suggested the use of the Prandtl type logarithmic velocity profile to predict the average subsection velocity. while the measurements of the slope can be used to estimate the channel average velocity.

Zhidkikh, Sinotin and Guenkin (46) in 1974 pointed out the importance of the absolute values of the boundary roughness in determining the position of the maximum velocity rather than their relative magnitude.

In 1975, Kanavin (14) presented some empirical relations for the velocities in ice-covered as well as open channels. He also presented some field data for ice formation in River Daugava at Koknese, Norway.

Drage and Carlson (11) suggested in 1977, the application of the regime theory to ice-covered rivers. They proposed a flow equation in the form

$$V = K\, Q^m \qquad 2.6$$

where K and m are constants that should be determined experimentally.

Ismail, Abd EL-Hadi and Davar (13) in the same year adopted a logarithmic velocity profile in the form

$$u_i / V_{*i} = \phi + \psi \ \mathrm{Ln}\ y_i/Y_i \qquad , i = 1,2 \qquad 2.7$$

where ϕ and ψ were given graphically as a function of the spacing and height of the roughness elements and were determined experimentally in a wind tunnel simulating the ice cover by steel angles fixed to its top surface.

In 1978, Burgi (3) presented a descriptive analysis of the flow in Gunnison River while Hirayama (25) reported some velocity measurements and a method for computing the flow-rate in ice-covered channels.

2.3 Underside Configuration and Friction Factor

The importance of the determination of the underside configuration of an ice cover lies in its effect on the sedimentary pattern and its control of the flow carrying capacity of the channel. The prediction of the underside configuration of the cover requires the study of the behavior of the cover as a loose boundary similar to that of sediment transport in open channels.

On the other hand, the friction factor plays a significant role in the establishment of the velocity profile, the determination of the energy losses and their mutual dependence on the underside configuration.

The total carrying capacity of an ice-covered channel is usually obtained using the flow equation. This requires the determination of a total friction factor, usually referred to as the composite roughness, that represents the different effects of each boundary involved. Reviews of the different methods of the composite roughness estimation were given by Haggag (12) and Uzuner (39).

In 1759 Brahms (9) suggested the application of the momentum equation to uniform flow in open channels. He then applied the equation to the prism shown in Figure 2.2 and it resulted in

$$\text{Total Shear} = \gamma . A.L.S \qquad 2.8$$

Chezy (9) in 1769 proceeded with Brahms' assumption and suggested the use of an average shear (τ) for the channel boundary related to the mean velocity of the flow in the form

$$\tau = K.\ V^2 \qquad 2.9$$

which Chezy combined with Equation 2.8 to obtain

$$V = C\sqrt{RS} \qquad 2.10$$

where R is the hydraulic radius and equals A/P, and C is a factor that latter became known as Chezy's coefficient. This equation is widely referred to as Chezy's equation.

Since Chezy introduced his equation some 200 years ago many investigators introduced different relations to evaluate Chezy's C. These relations are readily available in the literature and will not be repeated here (9), (33), (44).

The investigation of the cover underside configuration started

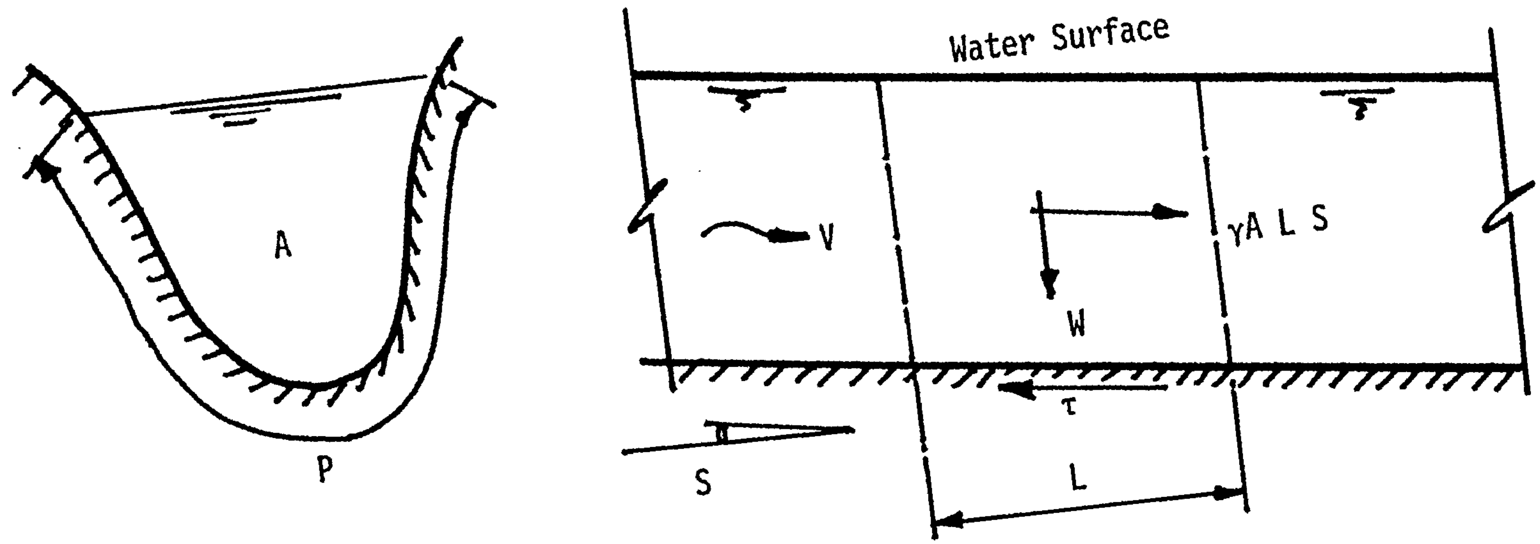

Figure 2.2: Uniform Flow in Channels

in 1963, when Williams(after(2)) presented some probability charts for the prediction of the average ice thickness. In his analysis he assumed a constant thickness jam profile with no underside configuration.

In 1966, Carey (4,5,6), presented some field measurements of the St. Croix River, Wis, U.S.A., taken during the two succeeding winters of 1965 and 1966 as the first attempt to study the underside configuration of an ice cover. His observations can be summarized as follows:

1. A non-similar sharp-crested dune formation was observed accompanied with some ripples oriented transverse to the flow direction.
2. The dunes had no standard profile. Their wave lengths ranged from 0.5 to 1.0 ft with heights ranging from 0.03 to 0.14 ft. The greatest amplitudes did not necessarily occur with the greatest wave lengths. Also, the upstream face slopes were steeper than the downstream ones.

As a result Carey introduced the hypothesis that the variation in the intensity of turbulence from point to point within the flow results in a differential temperature gradient. This causes intermittent freezing or melting of the ice thereby determining its underside configuration.

In 1966, Larsen (17), presented some field measurements for the cover underside. His experiments involved successive measurements of underside configuration of real ice after exposure to actual flow conditions.

Ohashi et al(after(25)),in 1970, proposed an estimation technique for n_2 by using the actual measurements of velocity profiles and the position of the maximum velocity in the form

$$n_2 = n_1 \left(\frac{Y}{Y_2} - 1\right)^{3/4} \qquad 2.11$$

which is in fact Pavlovskiy's relation for composite roughness determination.

In the same year Tesaker (37) reported his observations of three Norwegian rivers. He measured the head losses and velocity profiles and suggested the use of the Nikuradse equation to express the friction coefficient as

$$1/\sqrt{f_i} = 2 \text{ Log } (14.8 R_i/k_i) \qquad , i = 1,2 \qquad 2.12$$

Ashton and Kennedy (1) introduced a mathematical model in 1972, based on Carey's hypothesis, to relate the local heat flux to the normal component of the turbulent velocity near the boundary. They also presented experimental results for a study of a bed formed of ice in addition to some field data.

In 1973, Larsen (18), obtained field data from both the Kilforsen and Gailjaur channels in Sweden. He introduced the bed effect as a factor in the heat transfer process and showed that the cover is thicker near the banks than at the mid-channel with a gradual variation in between. He observed wave steepnesses of not more than 0.1 with wave lengths of up to 1.2 ft and heights of up to .12 ft for flow depths and velocities ranging from 3.0 -34.0 ft. and 1.6-4.0 fps respectively. He noticed a proportional relation between the wave steepness and the friction factor for which he reported an n value of up to 0.03.

Cowley and Hyden ,(after (25)), in 1977, described a model study of St. Mary's River ice in which they studied the navigational feasibilities and jam formation. In their experiments, specially treated plastic blocks were used to simulate the cover as well as its sticking and crushing properties.

In 1977, Tatinclaux (35) reported an experimental investigation of the jam profile using 3" x 2.5" blocks made of both real ice and plastic. The jam produced in this manner was short in length which made it difficult to judge its profile. He reported some wavy formation, but his main aim was to determine an average equilibrium thickness.

Ismail, Abd EL-Hadi and Davar (13), in 1977, suggested the use of Darcy's equation and presented experimental results for the underside of the simulated cover graphically, while Mercer and Cooper (21) presented an analysis of a major ice jam. Petryk (29), in 1978, suggested a method to estimate jam profiles based on a modified backwater curve analysis along with the criteria for the stability of floating floes.

In the same year Osterkamp (26) presented some concepts limited to frazil ice formation. He did not relate any of his analysis to the jam profiles or friction factors, while Zsilak (47) presented some analyses of the configuration of jams in which he utilized the continuity relation as well as the force-balance concept.

The National Research Council Working Group on Hydraulics of Ice-Covered Rivers (25), in 1979, presented a summary of the work on the resistance to the flow in ice-covered rivers. In this study Pratte stated that a variation in the n value coincided with the variation of the cover thickness in the cross-sectional direction as well as the longitudinal one. He reported that the cover is always thicker near the banks and suggested a value of n_1/n_2 that equals Y_1/Y_2.

2.4 Instability of Cover Blocks

The first report about ice floe stability was made by Mclachlan in 1926 (after(40)) based on his observations of the St. Lawrence River ice. He concluded that a very regular ice cover is formed in rivers at water velocities not exceeding 1.25 fps. He also noted that ice-covers may thicken and progress at velocities up to 2.25 fps without floes passing underneath.

Estiveef in 1958(after(2)) gave the critical velocity value as 2.3 to 2.6 fps after his observations in Russian rivers. While Kivisild (16), in 1959, pointed out that the Froude number of the flow in front of the cover should be the criterion for the floe stability and suggested that its limiting value should be F_{nc} = .08.

Pariset and Hausser's work in the same year (27) showed that the cover will not progress at velocities greater than $0.109\sqrt{2gH}$. This result was verified in Cartier's Flume but failed to hold in the St. Lawrence River; so they proposed another critical velocity in the form

$$(V_c/C)^2 = 0.00375\, d + 0.005\, q_i^{2/3} \qquad 2.13$$

where V_c = critical velocity for stability conditions

C = Chezy's coefficient

d = mean equivalent diameter of ice blocks

q_i = ice discharge

They also reported some variation in V_c, due to the existence of adjacent blocks to the floes.

Cartier in 1956 (after(2)) reported velocities of 2.0-1.2 fps to limit the cover advancing and 1.6-3.2 fps for overturning of the blocks; the variation depends upon the block shape and dimensions. He also found experimentally that it was impossible to obtain upstream progression of an ice cover fed with big ice floes at velocities higher than 2.3 fps.

In the same year Michel (23) introduced an analytical solution to the problem. His analysis was based on the moment equilibrium of a single block arrested in front of an obstruction. He also introduced a form coeffecient to describe the block geometry and determined its value experimentally using right paralleleppiped blocks.

Pariset and Hausser (28), in 1961, based their analysis on the continuity principle and the conservation of energy between the sections with and without a cover. They introduced the no-spill condition, when the upper leading edge of the block is at the same elevation as the water surface, as the stability criterion. They suggested the use of Equation 5 Table 2.1 to estimate the critical Froude number.

Devik (10), in 1964, reported a limiting velocity for diving blocks of 2.0 fps for Norwegian rivers. In the same year Cousineau (after(40)) confirmed Mclachlan's V_c = 2.25 fps observation adding that in fact this velocity was an upper limit which can be reached only under ideal conditions.

Michel (22), in 1966, presented a more elaborate analysis based on the same assumptions of Parisset et al . In addition he introduced the effect of the porosity into the problem and suggested the value of the critical Froude number as given by Equation 6 Table 2.1.

In 1967, Mathieu (20), reported that the critical Froude number should be 0.11, while Oudshoorn (40), in 1970, reported after his observations of the Rhine River that F_{nc} should be in the range of 0.06 to 0.09. Also in 1970, Synotin et al (after(40)), obtained an empirical expression for the critical velocity V_c, using paraffin blocks, as

$$V_c = (0.035\, g\, L)^{\frac{1}{2}} \qquad 2.14$$

where L is the block length.

Uzuner and Kennedy (41), in 1972, analyzed the equilibrium of the forces and moments acting on the block. They used the no-spill condition as the stability criterion and ended with Eqution 7 of Table 2.1.Their analysis was extended by Ashton (1) , in 1974, where he introduced Equation 8 of Table 2.1 to predict the critical stability condition.

In 1974, Uzuner and Kennedy (42), suggested the adoption of a jam collapse mechanism rather than a transport one in investigating the stability problem. In the same year, Osterkamp (25) reported, after his observation of the Tanana River, that at a velocity and a water depth of 4.5 fps and 18 ft respectively the floes were observed to ride on the upstream edge of the jam.

Michel and Abdelnour (24), in 1974, reported an experimental investigation using wax blocks to simulate real ice floes. They expressed their findings as

$$\sqrt{\rho/\sigma}\quad (V - \sqrt{2g\, S_{g1}\, H}\,) = 0.055\ (Y/B)^{3.816} \qquad 2.15$$

where σ and ρ are the modulus of flexural strength and the unit mass respectively. This equation can be solved to obtain the critical velocity.

In 1977, Mercer and Cooper (21), based on Shield's relation, gave the value of the critical velocity as

$$V_c = 0.46\ \sqrt{g}\ H^{1/6}\ L^{1/3} \qquad 2.16$$

while Petryk (29) in the following year suggested another relation to express V_c as

$$V_c = 2.27\ \sqrt{d}\ (1 - d/H) \qquad 2.17$$

where d is the cover size in ft. He also reported that while thermal cover stability is maximum during the central period of winter, it is minimum during the cover formation or break-up.

Tatinclaux and Chung(36), in 1978, presented the following relation to estimate the critical velocity of instability

$$V_* / V_c = 5.48\ t/L + 1.53 \qquad 2.18$$

which is limited to their experimental data. In the same year Tatinclaux and Lee (35), based on an earlier investigation by Tatinclaux (34) suggested the use of Equation 11 of Table 2.1 to evaluate the stability conditions of ice floes.

2.4.1 Generalized Formula

The literature equations reported in the previous article can be expressed in the general form

$$F_m = F_{nc} / \sqrt{2\, S_{g1}\, t/H} = A + B\,(1 - t/H) \qquad 2.19$$

where F_m = a modified Froude number

S_{g1} = the specific gravity difference = $1 - S_g$

and F_{nc} = the critical Froude number = $V_c / \sqrt{g\,H}$.

The different literature equations, modified to the general form, are given in Table 2.1. The behavior of the coeffecients A and B, as given by these equations, is shown in Figures 2.3 and 2.4 respectively. From these figures it can be seen that the literature equations are divided into two groups, one that considered F_m as constant (B=0) and the second relates it to t/H variation (A=0). Further discussions of the literature equations are given in Chapter VI.

Investigator	A	B	Remarks
1 Mclachlan (1926)	$2.25/\sqrt{2g\, S_{g1}\, t}$	0	
2 Michel (1957)	K_o	0	K_o is the shape factor
3 Sinotin (1970)	$\left[\dfrac{.035\, L/H}{2\, S_{g1}\, \frac{t}{H}}\right]^{½}$	0	L is the block length.
4 Kivisild (1959)	$\dfrac{0.08}{\sqrt{2\, S_{g1}\, t/H}}$	0	
5 Pariset & Hausser (1961)	0	1	Analysis of sinking blocks.
6 Michel (1966)	0	(1 - P)	P is the porosity of the cover

Table 2.1 Generalized Stability Equations

Investigator	A	B	Remarks
7 Uzuner and Kennedy (1972)	0	$[1 + (C_s - \beta - 1)(1 - t/H)^2]^{-\frac{1}{2}}$	C_s, β are surface velocity and moment coefficients respectively.
8 Ashton (1974)	0 0	$[2.5 - 1.5(1 - t/H)^2]^{\frac{1}{2}}$ Static $[1.5 - (1 - t/H)^2]^{\frac{1}{2}}$ Dynamic	Static and dynamic stability of the blocks
9 Tetanclaux (1977)	0	$(S_g t_c/t - 1)^{\frac{1}{2}} (1 - t/H) \ (\beta)^{-\frac{1}{2}}$ $\times (1 + a S_g c(t/H)/(1-P))^{-1}$ $\times ((V/V_c)^2 (1 - S_g t_c/H)^2 - 1)$	t_c = the cover thickness $c = q_i / V t$ V_c = critical velocity a and β = experimental coef.
10 Patryk (1978)	$\dfrac{2.27 (\frac{d}{H})^{\frac{1}{2}} (1 - \frac{d}{H})}{\sqrt{2g S_{g1} t/H}}$	0	Used in his computer program. d is an indicative size.
11 Tetanclaux and Lee (1978)	0	$[2.5 - 1.5(1 - \frac{t}{H})^2]^{\frac{1}{2}} \left[\dfrac{1 - S_g + \quad /t}{2 S_{g1}}\right]^{\frac{1}{2}}$	Δ= the block displacement

Table 2.1 continued

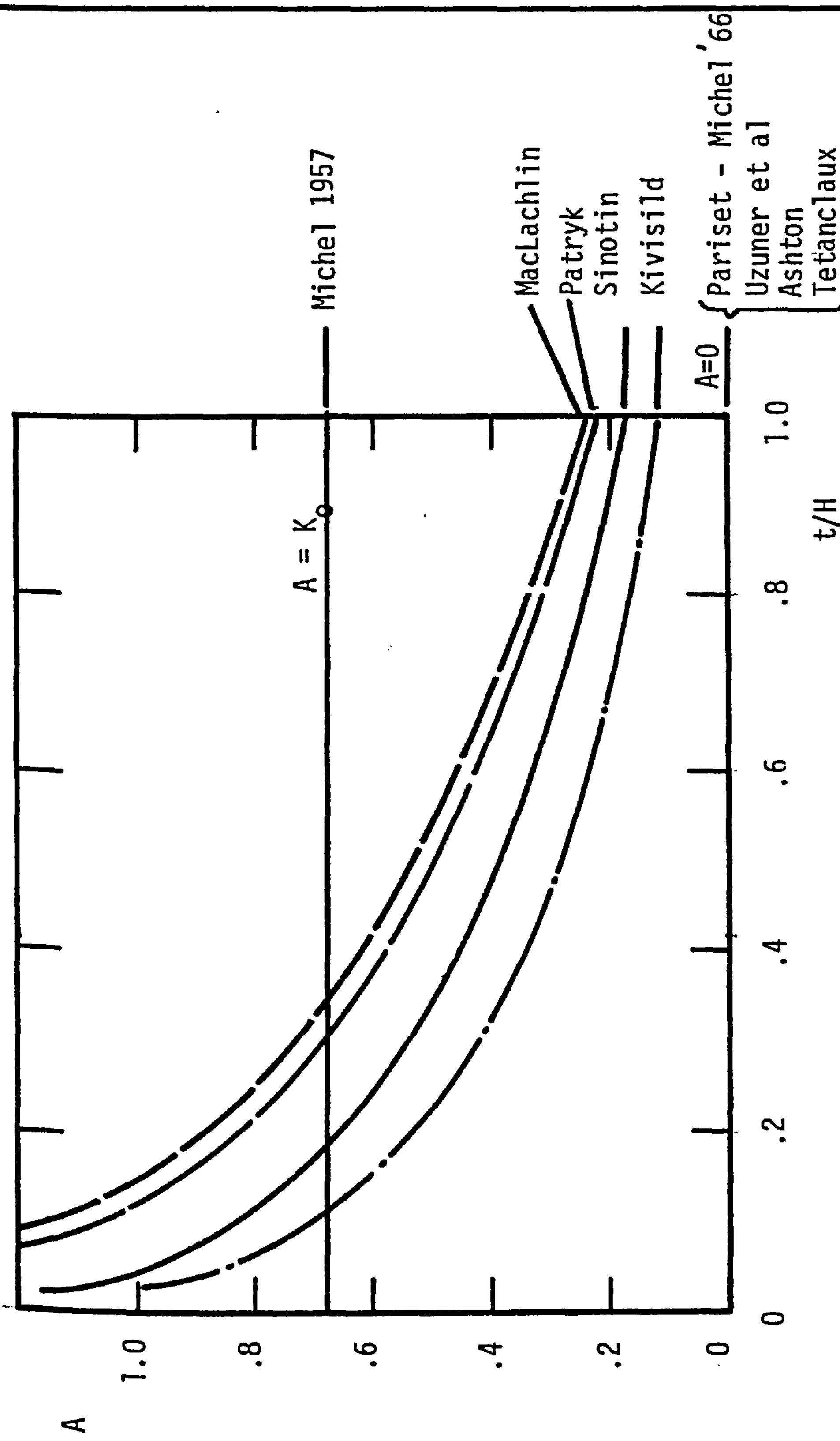

Figure 2.3: Behavior of Generalized Function A

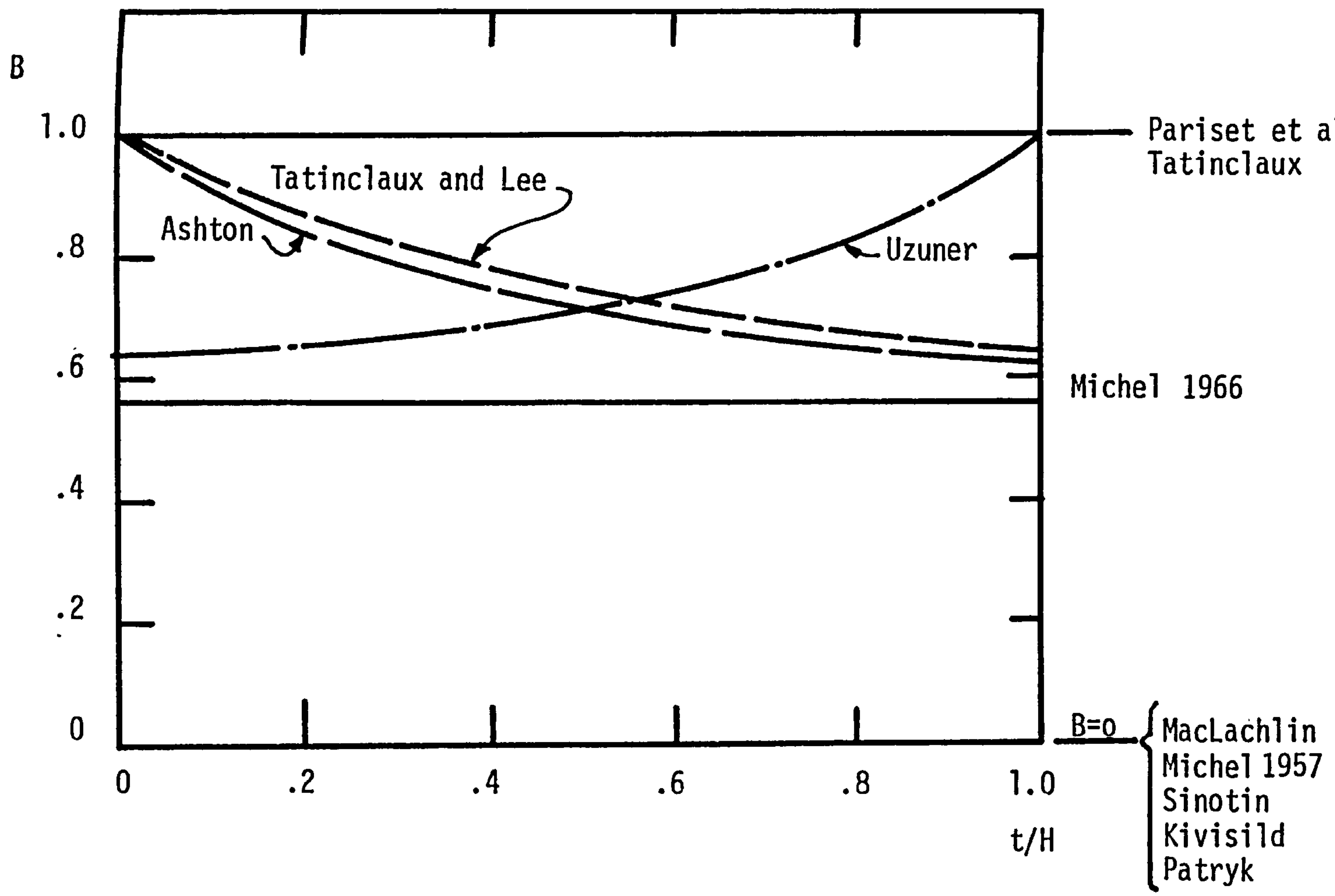

Figure 2.4: Behavior of Generalized Function B

CHAPTER III

THEORETICAL INVESTIGATION

III. THEORETICAL INVESTIGATION

In this chapter the theoretical models for the problems mentioned in Chaper I are developed. The analysis proceeds by first developing the equations that describe the velocity distribution in a covered channel. Then the relation between the cover underside configuration and the bed-form is presented following an empirical expression for the cover underside friction factor. Finally, the block stability at the cover leading edge is investigated.

3.1 Basic Assumptions

The following assumptions were made throughout the course of the theoretical analysis:

1. The flow is quasi-steady.
2. The channel cross-section is divided into two distinct subsections, Figure 3.1; subsection (1) is governed by the bottom and sides while subsection (2) is controlled by the cover.
3. The separation line between the two subsections is the locus of the points of maximum velocity which in turn are the points of no shear.
4. The wetted perimeters ratio, α, and the hydraulic radii ratio, λ, are defined as

$$\alpha = P_1/P,$$

$$\lambda = R_2/R_1 \tag{3.1}$$

and $R_i = A_i / P_i$, $i = 1, 2$

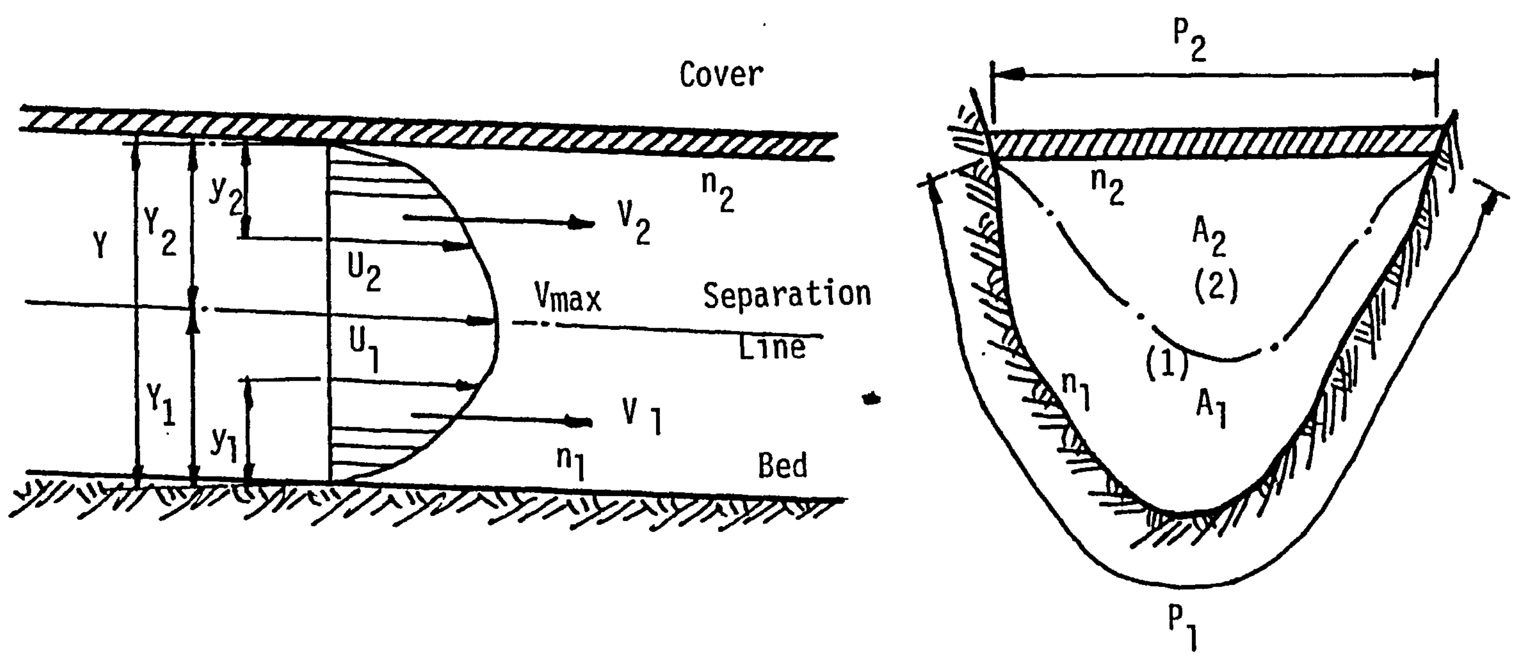

$$\alpha = P_1/P$$

$$\lambda = R_2/R_1 = \frac{A_2/P_2}{A_1/P_1}$$

Figure 3.1: Definition Sketch

where P_1, P_2 and P are the wetted perimeters of the bed and cover subsections and the total channel respectively, and A_1, A_2 and A are the corresponding flow areas.

3.2 Flow Pattern

The problem under investigation can be phrased in the following manner: for a covered channel of a known cross-section and boundary roughnesses, what is the flow pattern at a given flow-rate or energy slope? The reason for using the term "given flow-rate or energy slope" arises from the fact that they are related by the flow equation.

3.2.1 General approach

The difficulty of solving the general equation of motion, Reynolds' equation, arises from the existence of a differential shear on the opposite faces of any flow element parallel to the direction along which the equation is integrated.

If this differential shear vanishes, the equation can be integrated; this is the case of two dimensional flow. This concept will be used to develop the velocity profile in a prismatic channel in the absence of any cross-currents.

In the channel shown in Figure 3.2, vertical and horizontal strips of a unit width are drawn around an arbitrary point P. A two-dimensional solution will be carried out for the vertical strip, as if it is a portion of a wide channel, neglecting the horizontal differential shear and utilizing the local depth Y_p and local roughnesses n_1 and n_2 to yield the vertical shape function of the local relative velocity

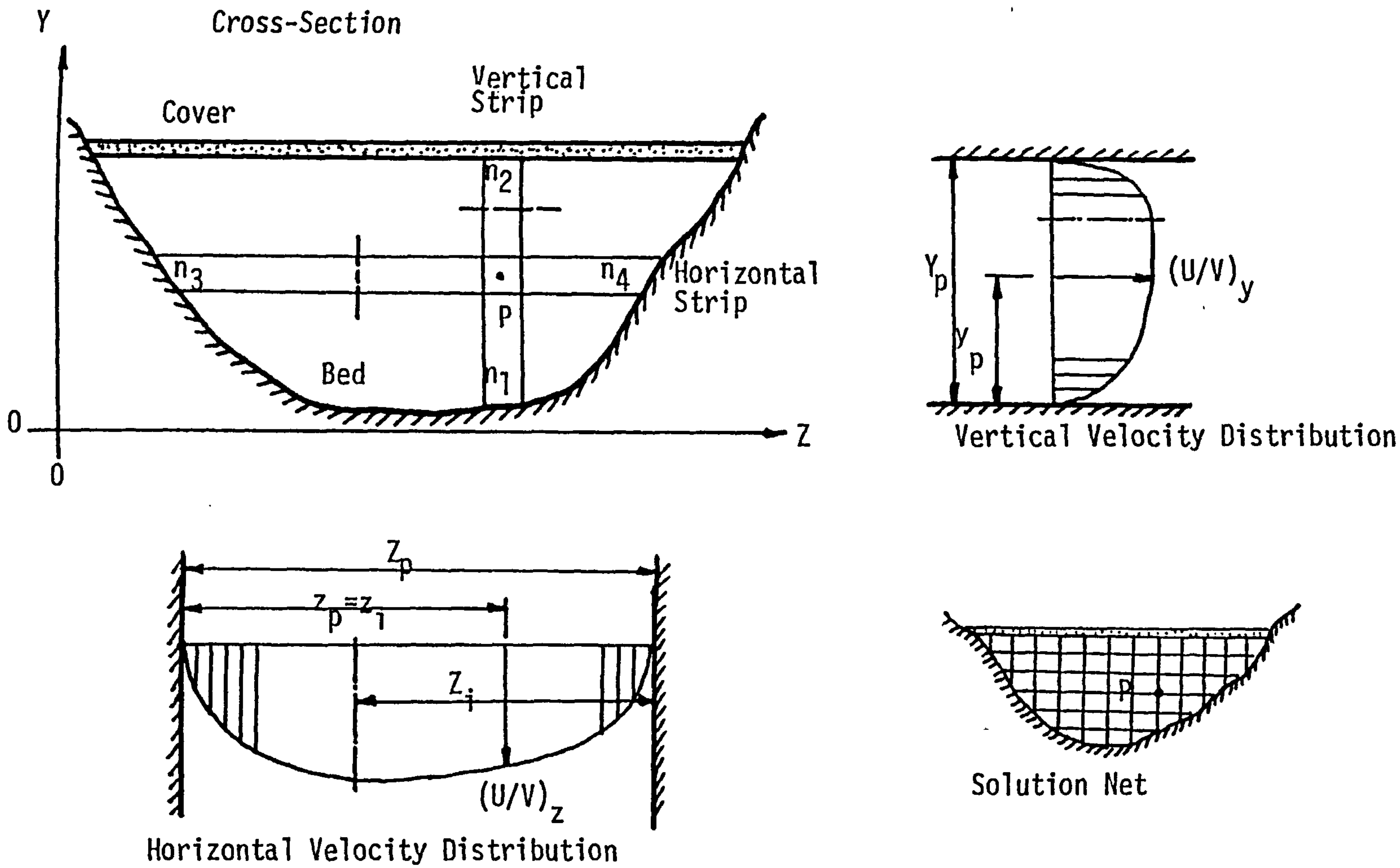

Figure 3.2: General Technique for Velocity Profile Determination

$(U/V)_y$. A similar solution will be carried out for the horizontal strip using its local width Z_p and roughnesses n_3 and n_4 to yield the transverse shape function of the local relative velocity $(U/V)_z$, where (U/V) is the ratio between the velocity at point P and the mean velocity of each strip.

If these two solutions are used as coefficients of each other, through a coefficient equation, the relative velocity at the point P can be estimated. The successive application of the equation at every point within the cross-section will result in the complete determination of the velocity profile and boundary shear distribution in the channel.

The following form of the coefficient equation was adopted in this research

$$U/V = E \left((U/V)_y \cdot (U/V)_z \right)^{EE} / (V_{max}/V) \qquad 3.2$$

where, V_{max} is the maximum velocity in the channel cross-section, E is the velocity coefficent, and EE is the velocity exponent. This form satisfies the necessary conditions dictated by the observed velocity profiles. The (V_{max}/V) is the ratio of the maximum to the mean velocity of the channel. This ratio is constant for a given flow condition and it depends on the developed velocity profile. The velocity exponent, EE, relates to and affects the velocity gradient steepness while the coeffecient, E relates to and affects the total flow in the section.

The solution of Equation 3.2 necessitates the evaluation of (V_{max}/V), E and EE. This can be achieved by satisfying the following conditions:

1. The flow-rate should equal the integration of the velocity profile with respect to the cross-sectional area, i.e.

$$Q = \int_A U \, dA \tag{3.3}$$

2. The total driving force, the gravity force here, should equal the total boundary shear, i.e.

$$\int_P \tau \, dP = \gamma . A . S \tag{3.4}$$

where τ is the local boundary shear and P is the wetted perimeter.

3. The flow equation should be satisfied.

The satisfying of these conditions will result in the necessary parameters needed to define the velocity pattern in the channel.

3.2.2 Two Dimensional Determination of Velocity Profile

The general Reynolds' form of the Navier-Stokes equation in two dimensional flow can be written for the vertical strip as

$$\overline{U}(\partial\overline{U}/\partial x) + \overline{V}(\partial\overline{U}/\partial y) + \partial\overline{U'U'}/\partial x + \partial\overline{V'U'}/\partial y =$$

$$- \frac{\partial}{\partial x} (\overline{P}/\rho + gh) + \frac{\mu}{\rho} \left(\frac{\partial^2\overline{U}}{\partial x^2} + \frac{\partial^2\overline{U}}{\partial y^2}\right) \tag{3.5}$$

in which $\overline{U}$, $\overline{V}$, are the average velocities in the x and y directions, U', V' are the variations in the $\overline{U}$ and $\overline{V}$ values, ρ and μ are the fluid density and viscosity, and $\overline{P}$ = average pressure. For gravity, as well as a steady and uniform flow with no cross-currents, Equation 3.5, following Chang et al (8), reduces to

$$\frac{\partial}{\partial y} \left(\mu \frac{\partial \overline{U}}{\partial y} - \rho \overline{U'V'} \right) = -\rho\ g\ S \qquad 3.6$$

where S is the bed slope and g is the acceleration due to gravity. The laminar shear is denoted by the first term in Equation 3.6 while the second quantity represents the turbulent shear.

The integration of Equation 3.6 for each subsection on its own, noting that the shear vanishes at the separation line, yields the shear distribution, Figure 3.3, as

$$\tau_{ti} + \tau_{Li} = \rho\ g\ S\ (\ Y_i - y_i) \qquad ,i = 1,2 \qquad 3.7$$

in which the turbulent shear is denoted by τ_{ti}, the laminar shear is τ_{Li}, Y_i = distance from the bed or ice cover to the division line, y_i is the distance measured from the bed or the cover; and the subscript i = 1,2, refers to the bed and cover subsections respectively.

The laminar shear is very small outside the laminar sublayer, hence, only the turbulent shear is retained. Within the turbulent core, the shear distribution can be represnted by the equation,

$$\tau_{ti} = \rho\ g\ S\ (\ Y_i - y_i\ ) \qquad ,i = 1,2 \qquad 3.8$$

Using the Prandtl-Karman mixing length theory, the turbulent shear can be expressed as

$$\tau_{ti} = \rho\ y_i^2\ \kappa^2\ (\ dU_i/dy_i)\ |(dU_i/dy_i)| \qquad ,i = 1,2 \qquad 3.9$$

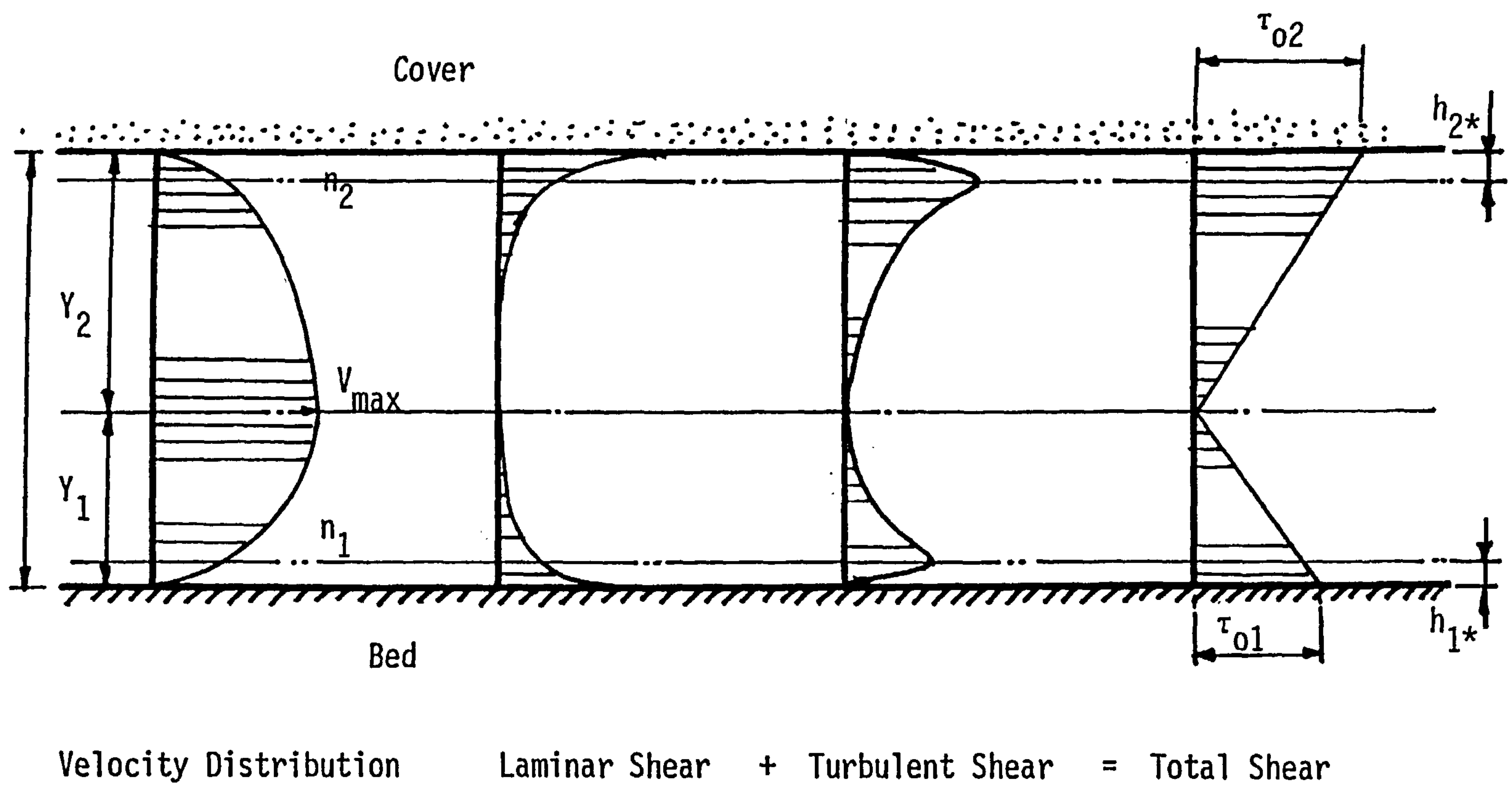

Figure 3.3: Two-Dimensional Shear Distribution

where κ is Von Karman's constant. Combining the previous equations, noting that $\varepsilon_i = y_i/Y_i$ = the relative depth, results in

$$dU_i/d\varepsilon_i = (V_{*i}/\kappa) \sqrt{1 - \varepsilon_i} / \varepsilon_i \qquad ,i = 1,2 \qquad 3.10$$

where V_{*i} = shear velocity = $\sqrt{g\ Y_i\ S_o}$.

The integration of this equation yields

$$U_i(\varepsilon_i) = (V_{*i}/\kappa)\ F'(\varepsilon_i) + C_i \qquad ,i = 1,2 \qquad 3.11$$

where $F'(\varepsilon_i)$ is given as

$$F'(\varepsilon_i) = 2\sqrt{1 - \varepsilon_i} - \mathrm{Ln}\,\frac{1 + \sqrt{1 - \varepsilon_i}}{1 - \sqrt{1 - \varepsilon_i}} \qquad ,i = 1,2 \qquad 3.12$$

The velocity profile should satisfy two boundary conditions:

1. The computed mean velocities should equal the existing one, i.e.

$$(1/A) \int U_i(y_i)\ dy_i = V_i \qquad ,i = 1,2 \qquad 3.13$$

hence, the integration constant C_i is

$$C_i = V_i + 2\ V_{*i}/\ 3\kappa \qquad ,i = 1,2 \qquad 3.14$$

2. At the point of separation, $\varepsilon = 1$, the velocity is maximum, and C_i should be

$$C_i = V_{max} \qquad ,i = 1,2 \qquad 3.15$$

The velocity profile can then be defined by the following two equations:

$$V_i - U_i(\varepsilon_i) = V_{*i}\ F_1(\varepsilon_i) \qquad ,i = 1,2 \qquad 3.16$$

and

$$V_{max} - U_i(\varepsilon_i) = V_{*i}\ F_2(\varepsilon_i) \qquad ,i = 1,2 \qquad 3.17$$

where $F_1\ (\varepsilon_i)$ and $F_2\ (\varepsilon_i)$ are given graphically in Figure 3.4 and their values are respectively

$$F_1(\varepsilon_i) = \frac{2}{\kappa}\left(Ln(\sqrt{\varepsilon_i}/(1 - \sqrt{1-\varepsilon_i})) - \sqrt{1-\varepsilon_i} - 1/3\right) \qquad 3.18a$$

and $\qquad ,i = 1,2$

$$F_2(\varepsilon_i) = \frac{1}{\kappa}\left(Ln\ \frac{1 + \sqrt{1-\varepsilon_i}}{1 - \sqrt{1-\varepsilon_i}} - 2\sqrt{1-\varepsilon_i}\ \right) \qquad 3.18b$$

and the maximum velocity is related to the mean velocities in the form

$$V_i = V_{max} - 2\ V_{*i}/\ 3\ \kappa \qquad ,i = 1,2 \qquad 3.19$$

To use the developed velocity profile, the position of the maximum velocity, i.e. Y_1 and Y_2, should be estimated. These values depend upon the roughness of each boundary and the depth, and can be obtained using the equations developed in Appendix A.

Similar relations can be developed for the horizontal strip with the substitution of

$$\varepsilon_i = z_i\ /\ Z_i \qquad ,i = 1,2 \qquad 3.20$$

where z_i and Z_i are defined in Figure 3.2.

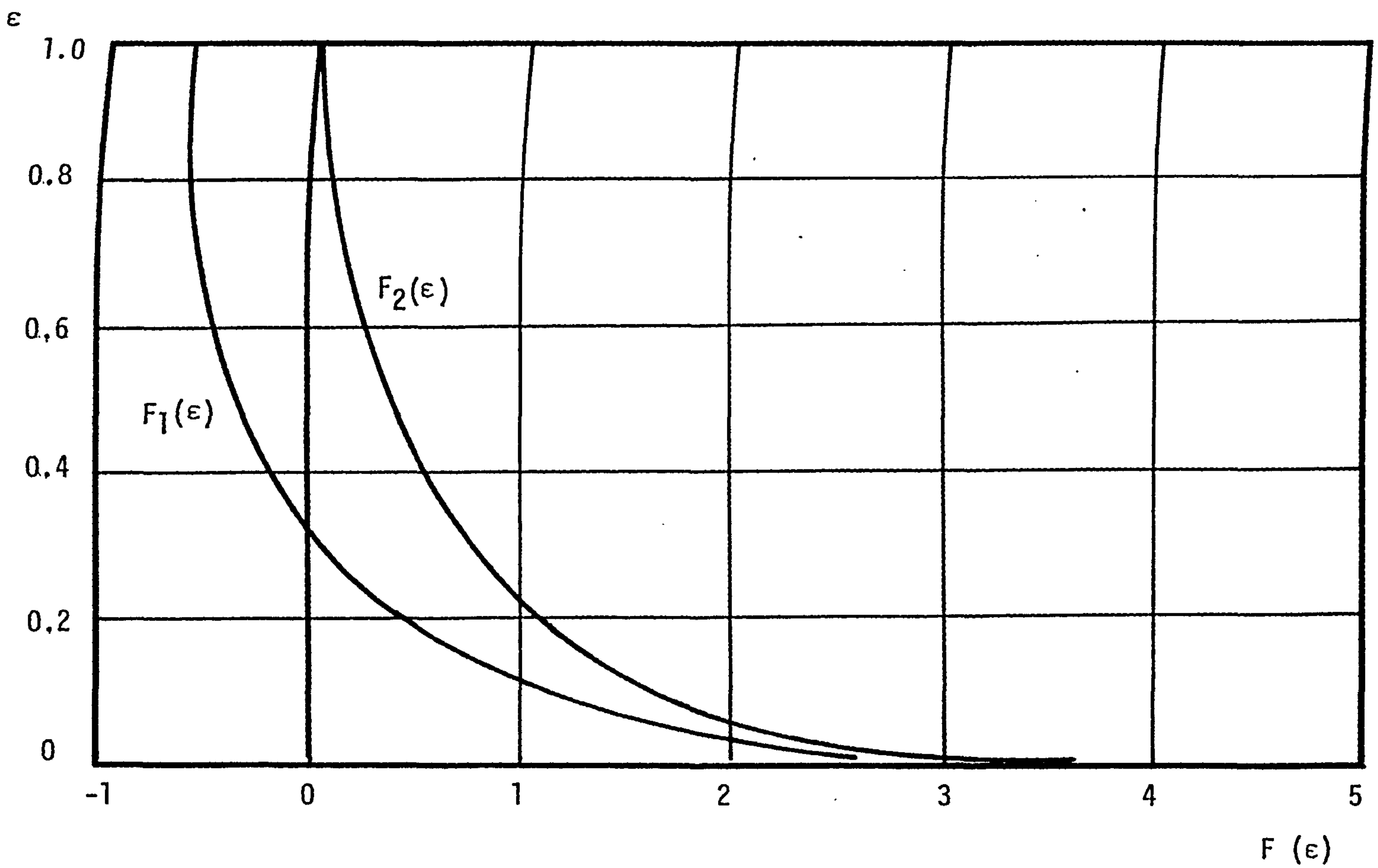

Figure 3.4: Velocity Profile Functions

3.2.3 General Solution

The velocity profile can be obtained by combining all the previously derived equations with the coefficient equation. The solution can only be performed numerically.

The suggested numerical solution is explained in the flow-chart, Figure 3.5. The program proceeds by creating and assigning dimensions to a traverse, Figure 3.2, inside the channel. The points of the traverse were not taken at constant intervals along the horizontal lines to eliminate the difficulty of integrating the shear profile. The number of points along each horizontal line was assumed to be constant to allow for the introduction of the zero boundary velocity to the solution.

The roughnesses at the four sides were determined by extending horizontal and vertical lines through each node to the surrounding boundaries. The method introduced in Appendix A along with the two-dimensional velocity profiles developed were then used to estimate the (U/V) values for both the horizontal and vertical strips at each node.

The unknown value of either S or Q was estimated through the flow equation utilizing a weighted average composite roughness. This assumed value was corrected as the solution progresses. The velocity profile was developed and hence the shear distribution was determined. The slope was estimated using Equation 3.4.

An iteration process, controlled by the comparison between the computed and assumed slopes, continued until the final solution was reached. The program listing as well as its typical results are

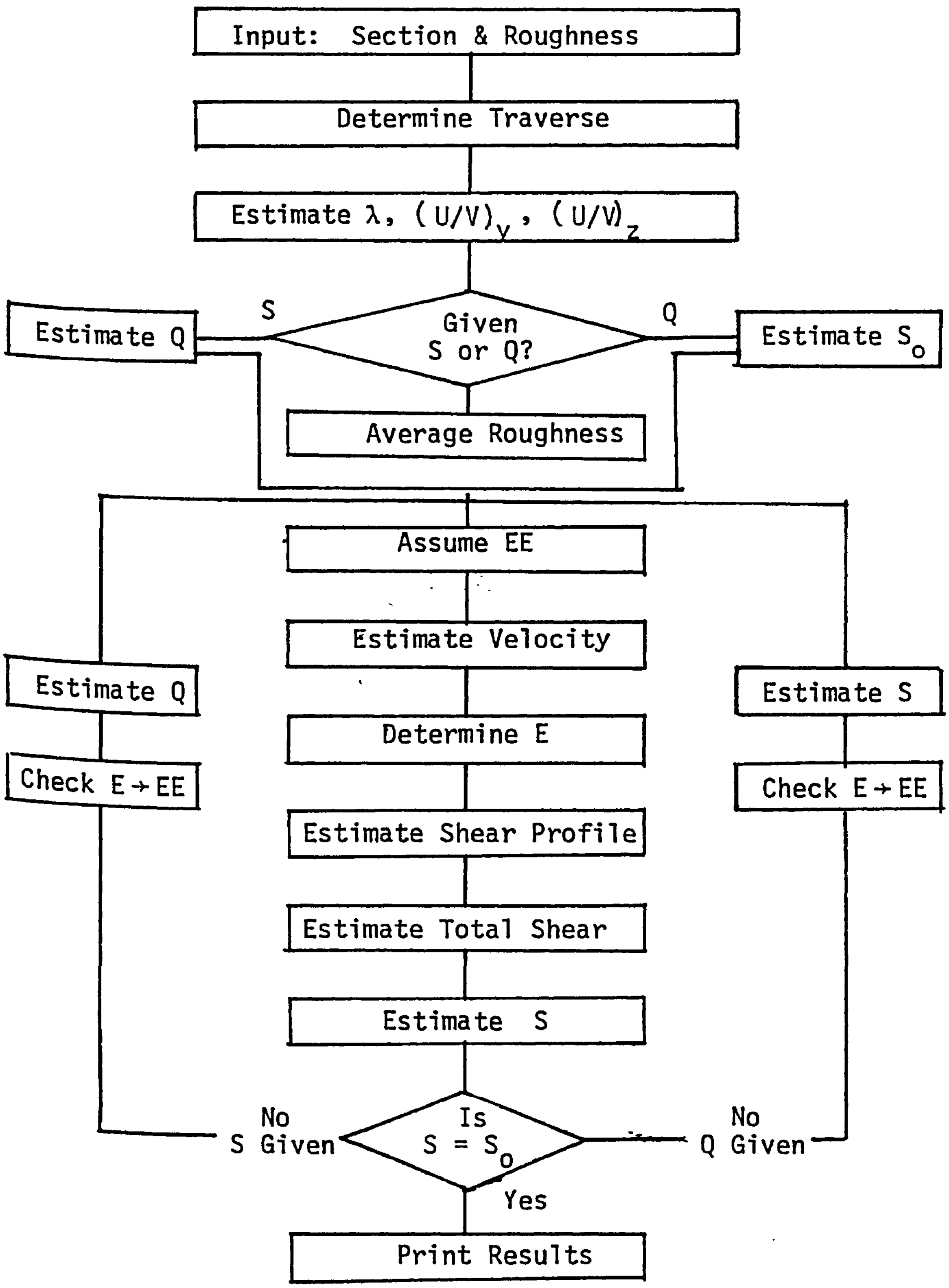

Figure 3.5 : Flow Chart for Flow Patterns

reproduced in Appendix C. A general cross-section to describe polygonal channels, Figure 3.6, was used to feed the data to the developed computer program. This section covers the rectangular, trapezoidal, triangular and compound channels.

To avoid the singularity of using B = 0 in the triangular and compound triangular cases, the program modifies B to a value equals to 0.05 of the top width BT. This modification is not expected to affect the solution by more than 5% which is well within the practical limits.

The presented solution is valid for both open and covered channels. For the open channel case the roughness of the cover underside should be considered as zero and the wetted perimeter, hydraulic radius, and separation line should be modified accordingly.

Chapter V presents a detailed study of the behavior of the model, its practical applications and typical results. Also a comparison of the theory with both the literature and the experimental results is presented.

3.3 Cover Underside Friction Factor

In this article an expression for the cover underside friction factor with no suspended material in the flow is developed. The flow equation used in this analysis is in the form

$$V = C_m \sqrt{g R S} \qquad 3.21$$

where C_m is a dimensionless Chezy's type friction factor.

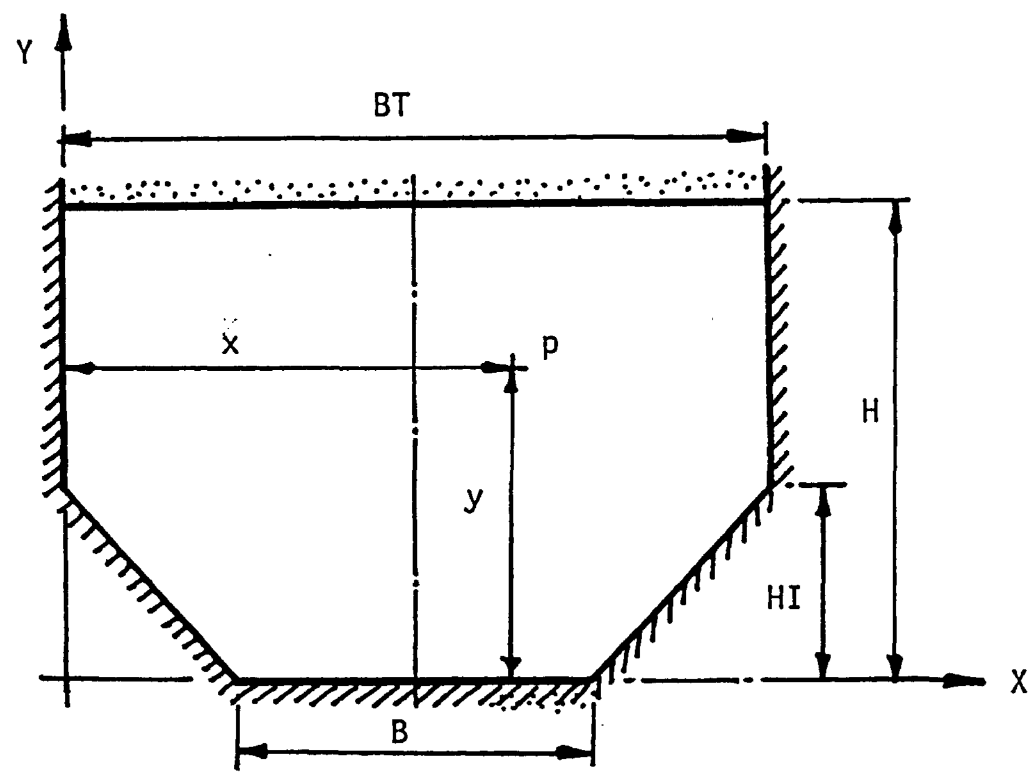

General Cross-section

For Rectangular Sections: BT = B , HI = 0

For Trapezoidal Sections: H = HI

For Triangular Sections : B = 0 , HI = H

For Compound Sections : Triangular B = 0
Trapezoidal as given

Figure 3.6: General Cross-section

3.3.1 The Friction Factor Expression

The resistance caused by the cover is attributed to its skin friction and the form resistance caused by its underside configuration. Hence, the total energy loss for the cover subsection, E_{2L}, can be expressed as the sum of two energy losses E'_{2L} and E''_{2L} caused by the skin and form resistances respectively, i.e.

$$E_{2L} = E'_{2L} + E''_{2L} \qquad 3.22$$

Differentiating this expression with respect to the channel longitudinal axis, the friction slope for the cover subsection S_{2f} can be written as

$$S_{2f} = S'_{2f} + S''_{2f} \qquad 3.23$$

where S'_{2f} and S''_{2f} are the energy slopes due to skin and form resistances respectively. This relation can be combined with the flow equation for the cover subsection, same R and V, to yield

$$(1/ C_{2m})^2 = (1/ C'_{2m})^2 + (1/ C''_{2m})^2 \qquad 3.24$$

where C_{2m}, C'_{2m} and C''_{2m} are the friction factors for the cover underside, the skin friction and configuration respectively. Rearranging the different terms in this relation yields

$$C'_{2m} = C_{2m} \left(1 - \left(C_{2m}/C''_{2m} \right)^2 \right)^{-\frac{1}{2}} \qquad 3.25$$

which can be expanded to

$$C_{2m}^{'} = C_{2m} \left(1 + \tfrac{1}{2}(C_{2m}/C_{2m}^{''})^2 + \ldots\ldots\ldots\ldots \right)$$

or in short

$$C_{2m} = C_{2m}^{'} - \delta C_{2m} \qquad 3.26$$

where δC_{2m} is a correction function that describes the contribution of the form resistance to the total cover friction factor.

The skin friction term is readily available in the literature (8), (9), (31). In this research it will be adopted in the form given by Senturek (31) as

$$C_{2m}^{'} = 6.25 + 5.75 \text{ Log } R/k \qquad 3.27$$

where R is the hydraulic radius and k is the roughness height of the cover underside surface.

On the other hand, the form resistance function was shown,(44), to depend on the underside configuration wave height Δ and length L as well as the flow depth Y. These variables are illustrated in Fig 3.7 for both actual and simulated cover undersides. By dimensional analysis this function can be expressed as

$$\delta C_{2m} = a \left(\frac{\Delta}{L} \; \frac{\Delta}{Y} \right)^b \qquad 3.28$$

where a and b are constants to be determined experimentally.

The general expression for the cover underside friction factor can then be written as

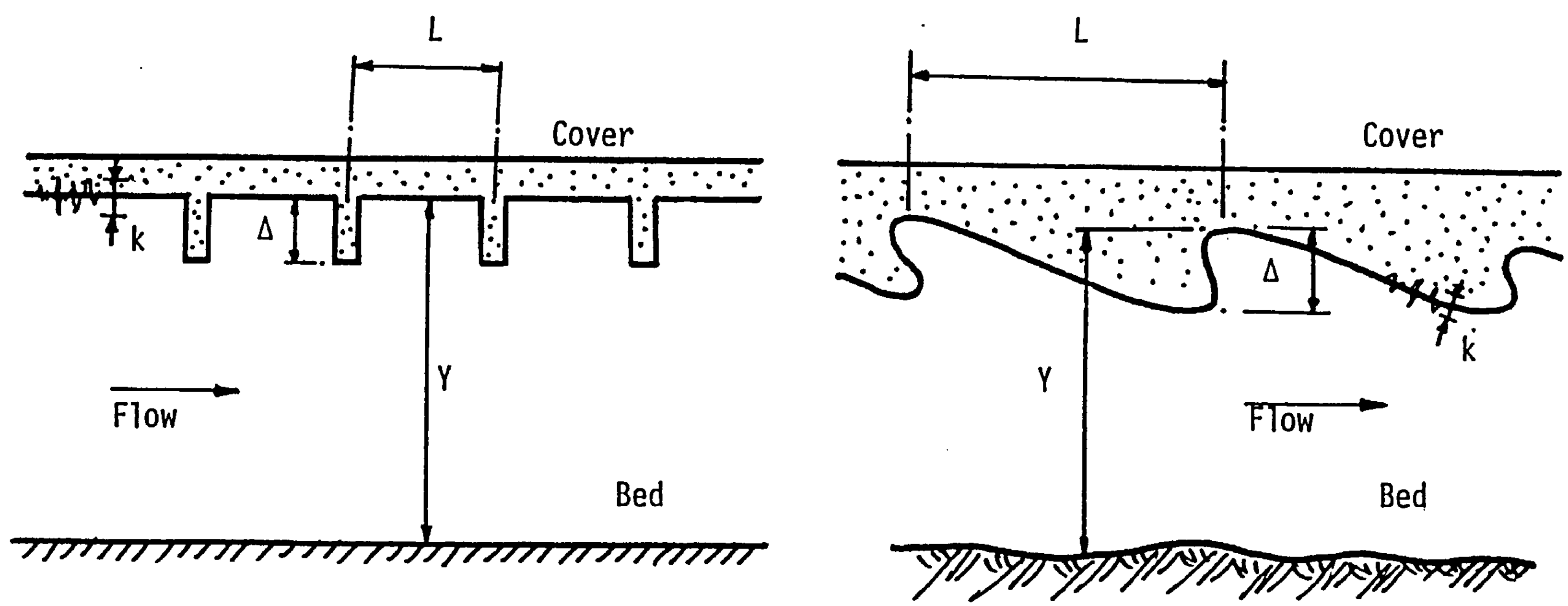

Fixed Bed and Cover,

Mobile Bed and Cover

Experimental Arrangement

Figure 3.7: Cover Underside Friction Factor

$$C_{2m} = 6.25 + 5.75 \text{ Log } R/k - a \left(\frac{\Delta}{L} \frac{\Delta}{Y} \right)^b \qquad 3.29$$

The details of the experimental procedure used to obtain the a and b values and to verify the adopted skin friction expression are given in Chapter V.

3.4 Underside Configuration of Loose Cover

This problem can be phrased as follows: in a certain covered channel of known bed material and flow conditions, what is the relation between the bed-form and the configuration of a loose cover underside?

A general solution for a steady two dimensional flow will be presented for the case of no phase change between the cover and the flow or seepage through the cover or the bed. The different variables involved in the problem are defined in Figure 3.8.

3.4.1 Derivation of General Equations

At any general section along the channel the rate of flow, q, is defined by the continuity equation as

$$q = V\ Y$$

where V and Y are the flow velocity and depth respectively. Differentiating with respect to x yields

$$dq/dx = V\ dY/dx + Y\ dV/dx \qquad 3.30$$

The conservation of energy principle can also be written for

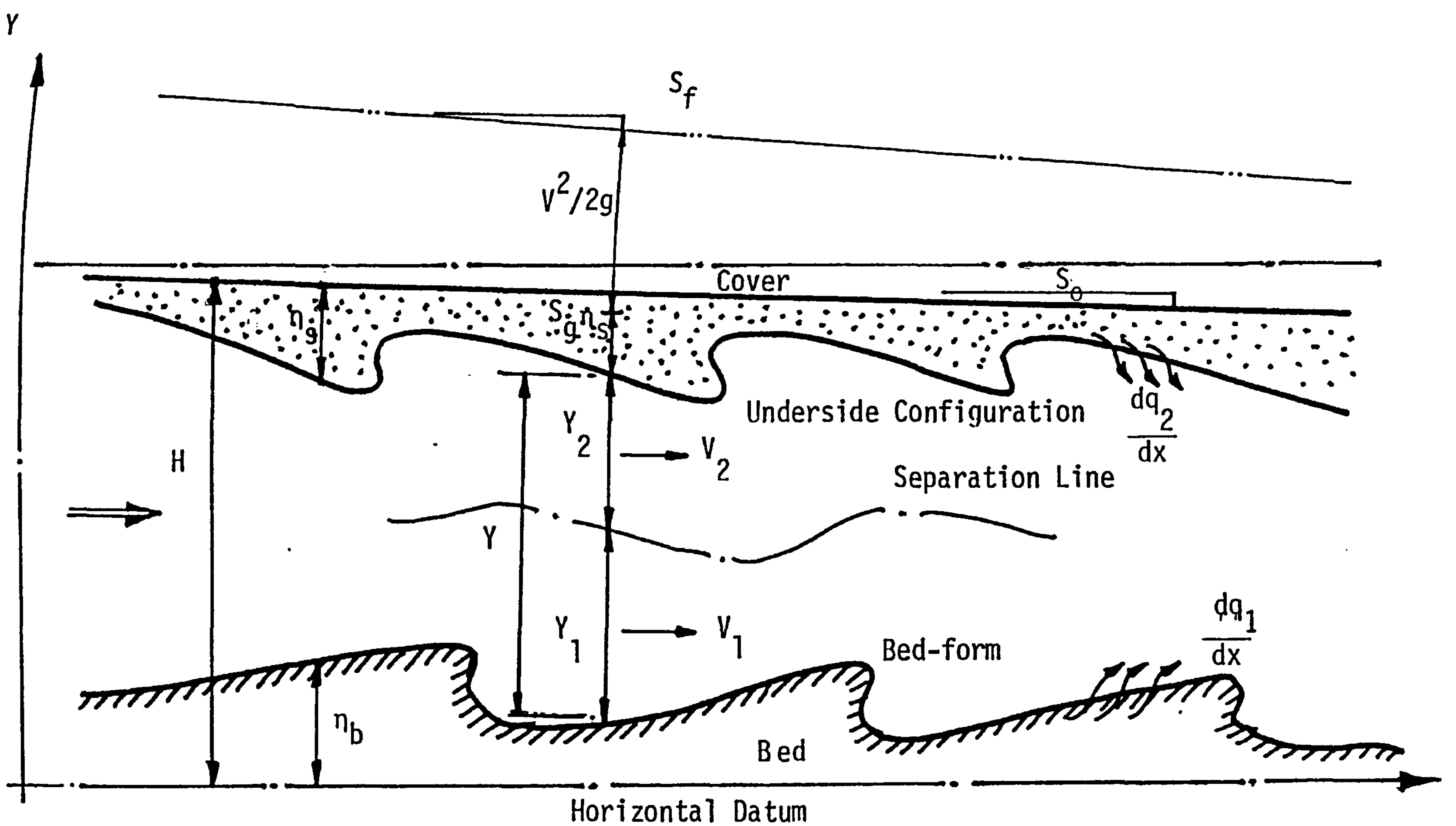

Figure 3.8: Cover Underside Configuration

the same section, as

$$E = \eta_b + V^2/2g + Y + S_g\ \eta_s \tag{3.31}$$

where E is the total energy at this section, η_b is the height of the bottom surface from a lower horizontal datum, η_s is the cover thickness and V is the average velocity in the cross-section, Figure 3.8. Differentiating with respect to x the slope of the total energy line S_f can be expressed as

$$S_f = -\frac{dE}{dx} = -\left(\frac{d\eta_b}{dx} + \frac{d}{dx}\frac{V^2}{2g} + \frac{dY}{dx} + S_g \frac{d\eta_s}{dx} \right) \tag{3.32}$$

in which the rate of change of the velocity head equals

$$\frac{d}{dx}\frac{V^2}{2g} = \frac{V}{gY}\frac{dq}{dx} - F_n^{\,2}\frac{dY}{dx} \tag{3.33}$$

and $F_n = V/\sqrt{gY}$ is the local Froude number.

Both field and experimental observations suggested the equality of the cover top surface slope and the general average slope of the channel bed. The height of the cover top surface above the datum, H, can be written as

$$H = \eta_b + Y + \eta_s \tag{3.34}$$

Differentiating with respect to x the slope of the cover top surface S_o will be

$$S_o = -\frac{dH}{dx} = -\left(\frac{d\eta_b}{dx} + \frac{dY}{dx} + \frac{d\eta_s}{dx} \right) \tag{3.35}$$

Equations 3.30 through 3.35 can be combined to yield the general underside configuration relation in the form

$$\frac{d\eta_s}{dx} = \left(-S_f + (1-F_n^2)S_o - \frac{V}{gY}\frac{dq}{dx} - F_n^2 \frac{d\eta_b}{dx} \right) / \left(F_n^2 - S_{g1} \right) \quad 3.36$$

where F_n = local Froude number = $V/\sqrt{gY}$

and $S_{g1} = 1 - S_g$

where S_g is the specific gravity of the cover material. The flow depth can also be expressed in the form

$$\frac{dY}{dx} = \left(-S_f + S_g S_o - S_{g1}\frac{d\eta_b}{dx} - \frac{V}{gY}\frac{dq}{dx} \right) / \left(S_{g1} - F_n^2 \right) \quad 3.37$$

Equations 3.36 and 3.37 are the general equations that relate the underside configuration to the bed-form and the different flow conditions. The solution of these equations requires the determination of the local friction slope S_f; this will be done next.

3.4.2 The Energy Slope

The energy slope is the rate of variation of the total energy with respect to the channel longitudinal axis. If the channel boundaries are uniform over its length, the energy slope will be constant. This is generally the case of a uniform flow with a solid boundary.

However, the existence of the bed-forms and the cover underside configuration cause a redistribution of the energy losses resulting in local variations of the energy slope around its average value as shown in Figure 3.9.

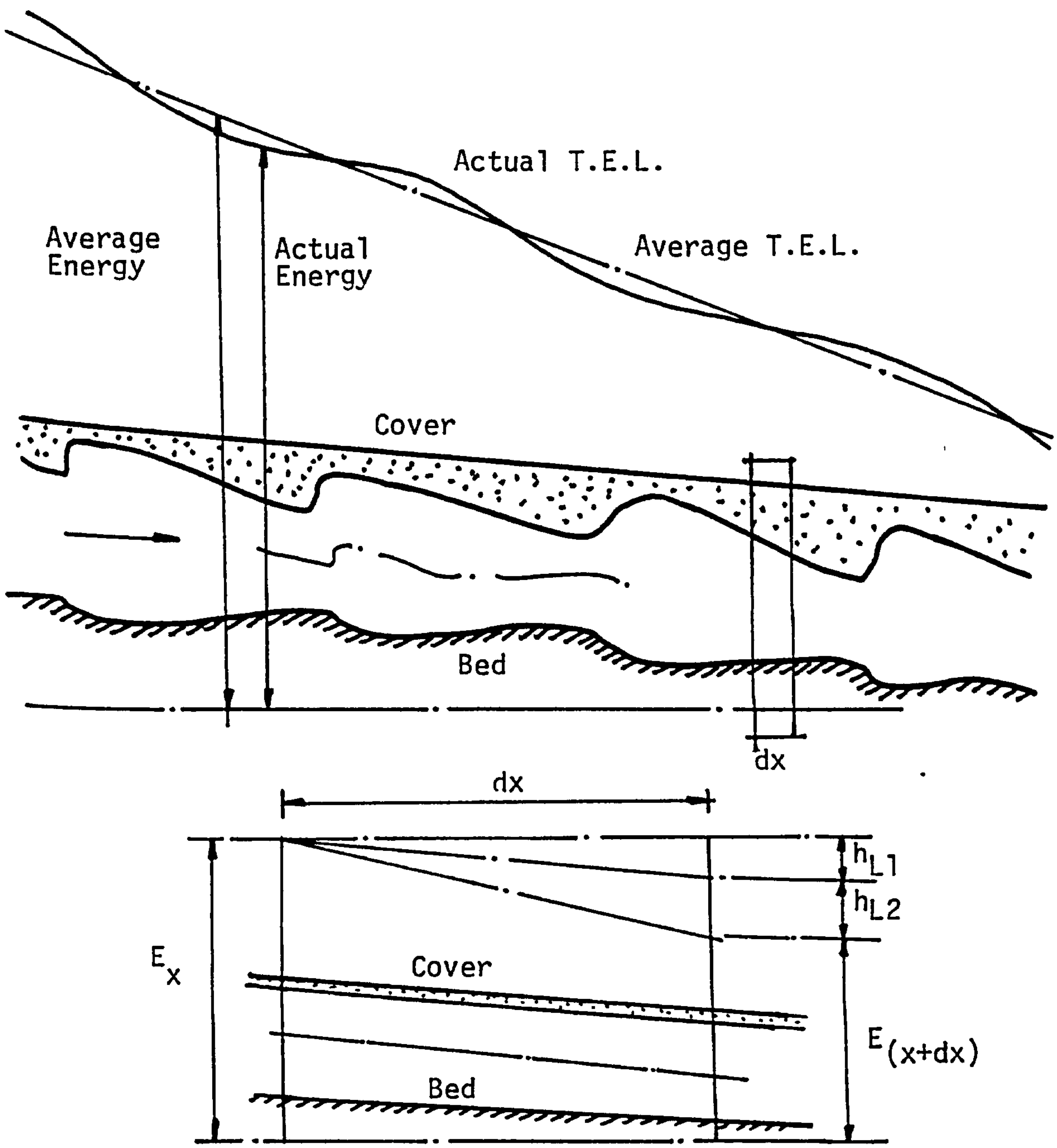

Figure 3. 9 : Average and Actual Energy Lines

The total energy loss is the sum of the losses of each subsection; hence the friction slope at a certain section of the channel will be the sum of the two subsection's friction slopes, i.e.

$$S_f = S_{f1} + S_{f2} \qquad 3.38$$

The friction slope is also related to the boundary shear through the known relation (9)

$$S_{fi} = \tau_i \,/\, \gamma Y_i \qquad ,i = 1,2 \qquad 3.39$$

At this point estimation of the boundary shear becomes necessary to evaluate the friction slope.

3.4.3 Determination of the Boundary Friction

This boundary friction will be estimated using the momentum principle in each subsection.

3.4.3.1 The Cover Subsection

Figure 3.10 shows the different forces acting on an element of the cover subsection. The application of the momentum principle in the horizontal direction to this element will result in

$$P_{2x} - P_{2(x+dx)} - \tau_{2x} dx = \rho q_2 \,(V_{2(x+dx)} - V_{2x}) \qquad 3.40$$

The total pressure is assumed to be proportional to the static pressure. This total pressure per unit width will be

$$P_{2x} = C_p \,\gamma\, Y_2 \,(\, S_g \, n_s + \tfrac{1}{2} Y_2 \,)$$

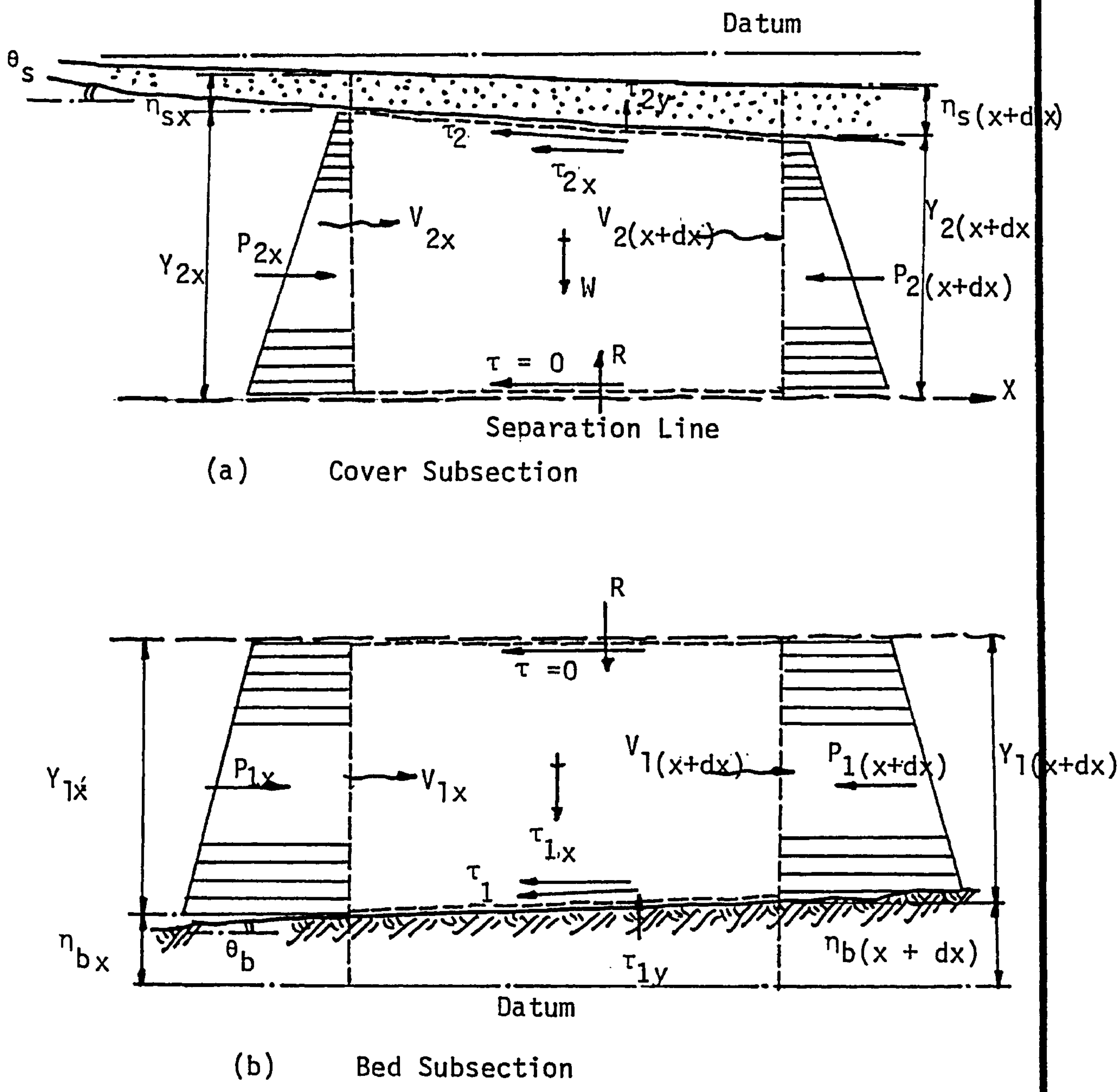

Figure 3.10: Forces on Each Subsection

The continuity relation is

$$q_2 = Y_2 V_2$$

Therefore, the horizontal force applying on the cover can be estimated as

$$\tau_{2x} = - (\gamma C_p S_g Y_2 \frac{d\eta_s}{dx} + \frac{\gamma}{g} V_2 \frac{dq_2}{dx} + \gamma \frac{dY_2}{dx}$$

$$(C_p S_g \eta_s + C_p Y_2 - V_2^2/g)) \qquad 3.41$$

Similarly the application of the momentum equation in the vertical direction will result in

$$\tau_{2y} = \gamma S_g \eta_s \qquad 3.42$$

where τ_{2y} is the vertical component of the cover force. From the force diagram, Figure 3.10, the total cover shear can be expressed as

$$\tau_2 = \tau_{2x} \text{ Cos } \theta_s - \tau_{2y} \text{ Sin } \theta_s \qquad 3.43$$

where θ_s is the slope of the cover underside. For practical purposes the following assumptions can be made

$$\text{Cos } \theta_s = 1 \qquad \text{and} \qquad \text{Sin } \theta_s = d\eta_s / dx$$

which can be combined with Equation 3.39, noting that from the discussion in Appendix A,

$$Y_2 = Y \lambda / (1 + \lambda)$$

to yield the following expression for the cover subsection friction slope:

$$- S_{f2} = S_g \left(C_p + \frac{n_s}{Y} \frac{1+\lambda}{\lambda} \right) \frac{dn_s}{dx} + \frac{V_2}{gY} \frac{1+\lambda}{\lambda} \frac{dq_2}{dx}$$

$$+ \frac{dY}{dx} \left(C_p S_g n_s/Y + C_p\lambda/(1+\lambda) - V_2^2/gY \right) \qquad 3.44$$

3.4.3.2 The Bed Subsection

Figure 3.10 shows the different forces acting on a bed subsection element. Applying the momentum equation in the vertical direction gives

$$\tau_{1y} = \gamma \left(S_g n_s + Y \right) \qquad 3.45$$

where τ_{1y} is the vertical component of the bed reaction, while its application in the horizontal direction yields

$$\tau_{1x} = - dP_1/dx - \rho q_1 dV_1/dx \qquad 3.46$$

where the pressure can be expressed in the form

$$P_{1x} = C_p \gamma Y_1 \left(S_g n_s + Y_2 + \tfrac{1}{2} Y_1 \right)$$

and the continuity equation as

$$q_1 = V_1 Y_1$$

The balance of the forces on the bed surface gives the friction shear value as

$$\tau_1 = \tau_{1x} \operatorname{Cos} \theta_b - \tau_{1y} \operatorname{Sin} \theta_b \qquad 3.47$$

Combined with the previous relations, and noting that for practical purposes

$$\cos\theta_b = 1 \qquad \text{and} \qquad \sin\theta_b = d\eta_b/\,dx$$

and from Appendix A

$$Y_1 = Y\,/\,(1+\lambda)$$

this equation gives the friction slope for the bed subsection S_{f1} as

$$- S_{f1} = C_p\, S_g\, d\eta_s/dx + (1+\lambda)\,(1 + S_g\, \eta_s/Y)\, d\eta_b/dx$$
$$+(1+\lambda)\,\frac{V_1}{gY}\,\frac{dq_1}{dx} + \frac{dY}{dx}\,\left(C_p S_g\,\frac{\eta_s}{Y} + C_p + \frac{\lambda}{1+\lambda}\,C_p - \frac{V_1^{\,2}}{gY}\right) \qquad 3.48$$

The total friction slope, S_f, can be written from the previous equations as

$$- S_f = (\,d\eta_s/dx\,)\,\left(2\,C_p\,S_g + S_g\,\frac{1+\lambda}{\lambda}\,\frac{\eta_s}{Y}\right)$$
$$+ (\,d\eta_b/dx\,)\,(1+\lambda)\,(1 + S_g\,\eta_s\,/\,Y\,)$$
$$+ (\,dY\,/dx\,)\,\left(2C_pS_g\eta_s/Y + C_p - \frac{V^2}{gY}\left(\frac{V_1^{\,2}}{V^2} + \frac{V_2^{\,2}}{V^2}\right) +\right.$$
$$\left. C_p\,\frac{2\,\lambda}{1+\lambda}\right) + (1+\lambda)\,\frac{V}{g\,Y}\,\left(\frac{V_1}{V}\,\frac{dq_1}{dx} + \frac{V_2}{\lambda V}\,\frac{dq_2}{dx}\right) \qquad 3.49$$

The determination of the friction slope requires the estimation of the values of λ as well as V_1 and V_2. These values can be obtained using the equations developed in Appendix A.

3.4.4 The General Solution

The general equation 3.36 can be solved at each section using Equation 3.49 to predict the underside configuration of the cover for a given bed configuration.

The exact solution of these equations is mathematically difficult due to the implicity of the factors involved in them, and a numerical solution becomes necessary. Details of the proposed techniques for solving the equations as well as a comparison between the theory and the experimental results are presented in Chapter V.

3.5 The Growth of the Cover and its Mechanism

In this section the stability of a block arrested at the leading edge of the cover is presented.

The behavior of the loose cover as well as observations of actual ice covers suggested the use of blocks with different shaped edges other than the popular rectangular shape. This change proves to be a very important factor in the stability process.

Throughout the instability process only the block was assumed to move while the cover was considered stationary. The problem was solved only in two-dimensions. The reference axes X and Y were taken as the static water surface and the contact face (Figure 3.11), with the positive X and Y axes pointing upstream and downward respectively.

The different variables used in this analysis were defined, as shown in Figure 3.11, as

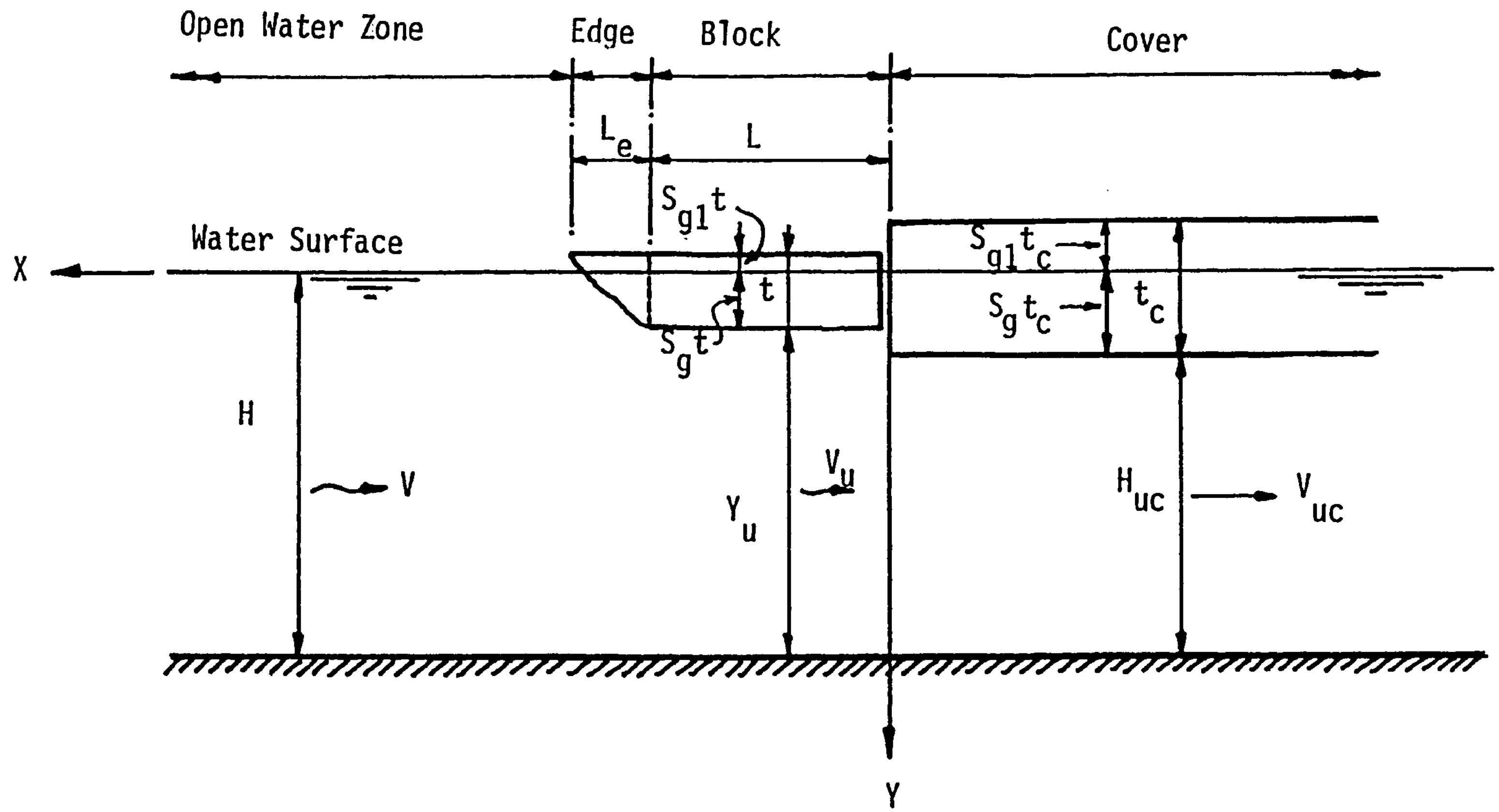

Figure 3.11: Definitions and Original Position

L = block core length

L_e = edge length

t = block thickness

t_c = cover thickness

S_g = specific gravity of cover and block

H, V = depth and velocity upstream of blocks

H_{uc}, V_{uc} = depth and velocity underneath the cover

H_u, V_u = depth and velocity under the block

In the following analysis the modes of instability are discussed first; then the different forces acting on the block are defined. Finally the equilibrium criteria and the numerical solution are presented.

3.5.1 Modes of Instability

The block is free to pursue any of three types of motion, namely horizontal, vertical or rotational. Figure 3.12 illustrates graphically these possible motions and explains the sign convention adopted to describe them.

A horizontal motion downstream of the cover will be prevented by the cover while an upstream one will move the block away from the cover resulting in a no-contact situation. Hence no horizontal motion was tolerated in this mathematical model.

A vertical motion will either sink the block or lift it. This vertical displacement is tolerated as long as it keeps the block in contact with the cover.

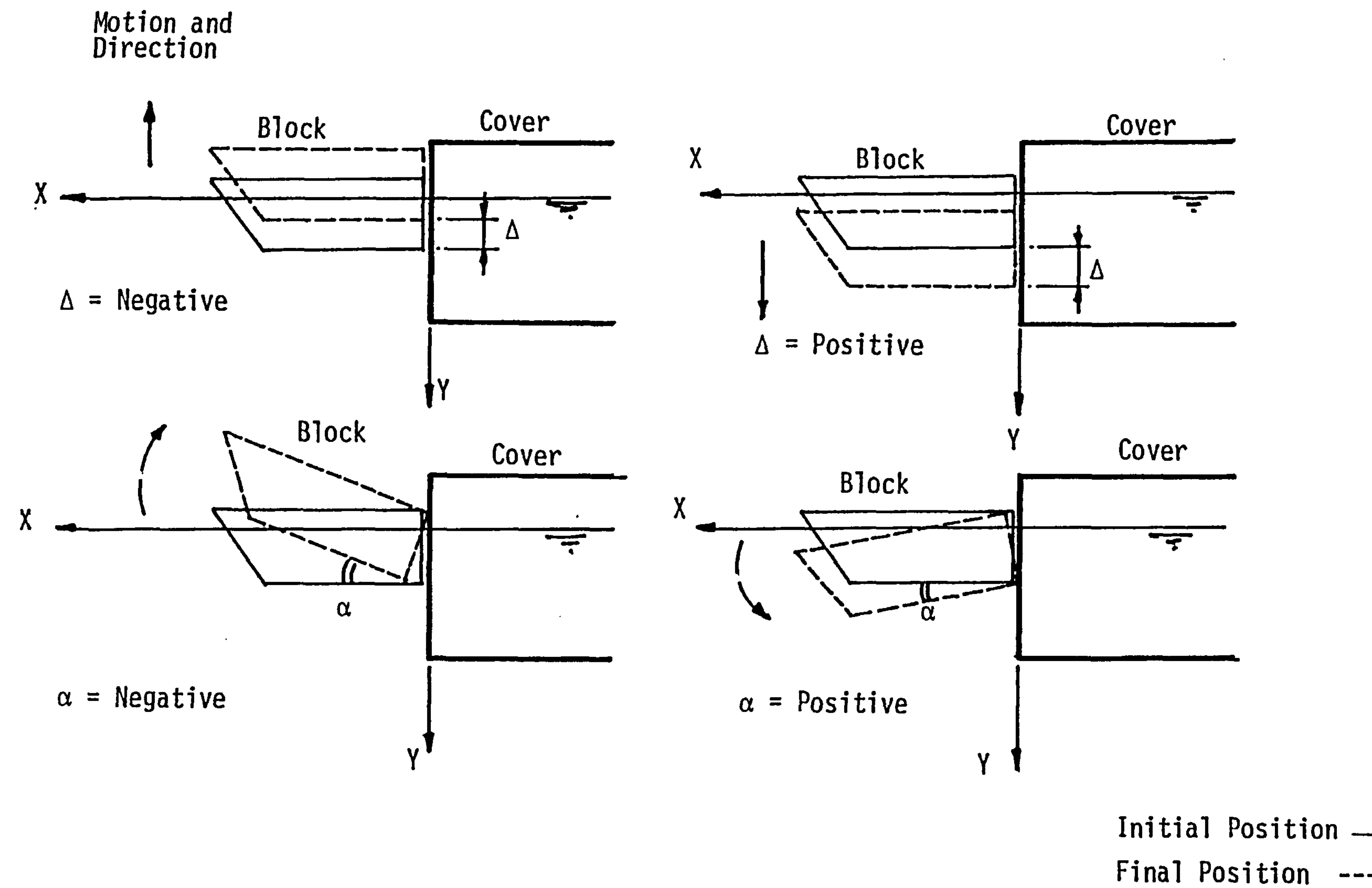

Figure 3.12: Basic Step Displacements of Block

The rotational movement is a rotation about the point of contact of the block and the cover. A positive rotation will drive the block underneath the cover while a negative rotation will force it to override the cover as shown in Figure 3.12.

The actual block movement was considered to be a combination of The vertical displacement Δ , and the rotation α . Depending upon these values, different modes of instability can exist. The term "mode of instability refers to the path followed by the block from its original position until it attains its instability.

The different possible modes of instability are shown in Figure 3.13. A brief description of these modes follows.

1. Absolute Stability: this is the original stable position when $\Delta = 0$ and $\alpha = 0$.
2. Pure Sinking Mode: if no rotation is encountered and only positive displacement exists the block will sink parallel to the cover face, and then it will be pushed underneath the cover.
3. Pure Lifting Mode: similar to pure sinking mode but with negative displacement. This mode can be interrupted by the shear failure of the cover edge in the way shown in Figure 3.14.
4. Pure Underturning: in this mode only rotation can occur with no displacement and the block will rotate about its lower corner.
5. Pure Upturn Rotation Mode: similar to pure underturning mode

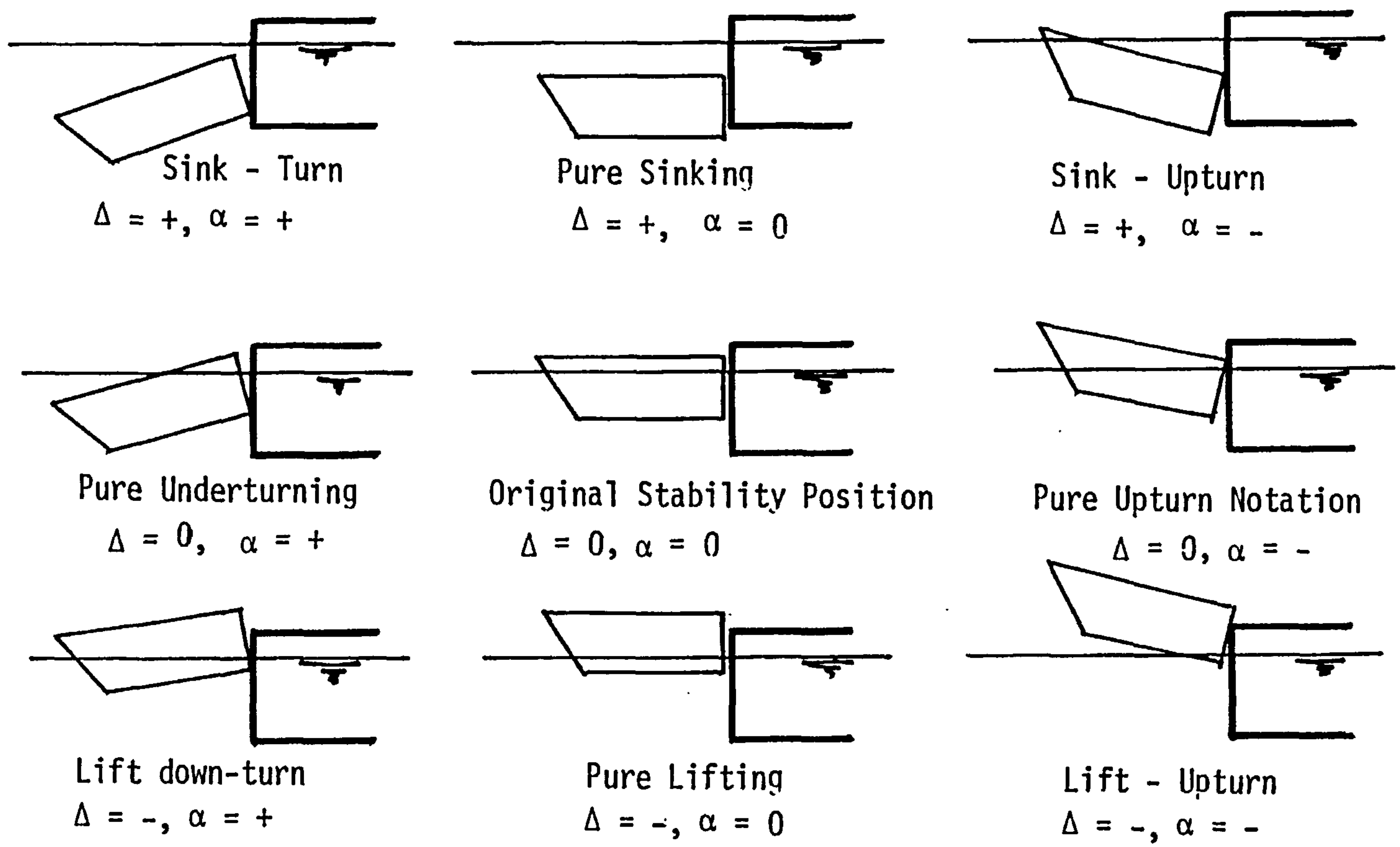

Figure 3.13: Modes of Instability

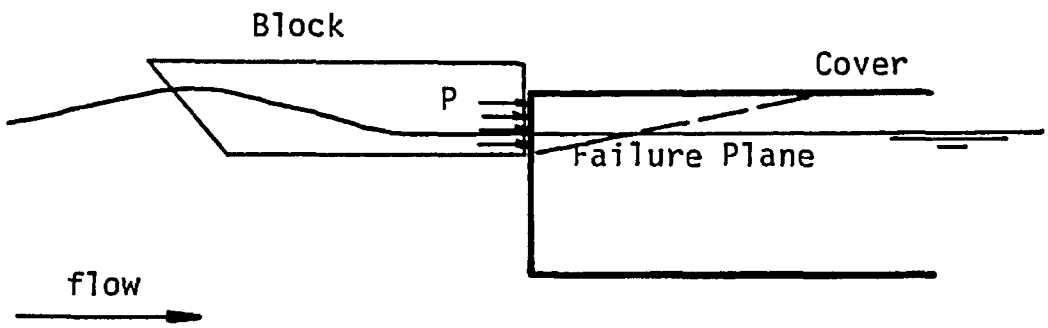

Figure 3.14: Edge Breaking

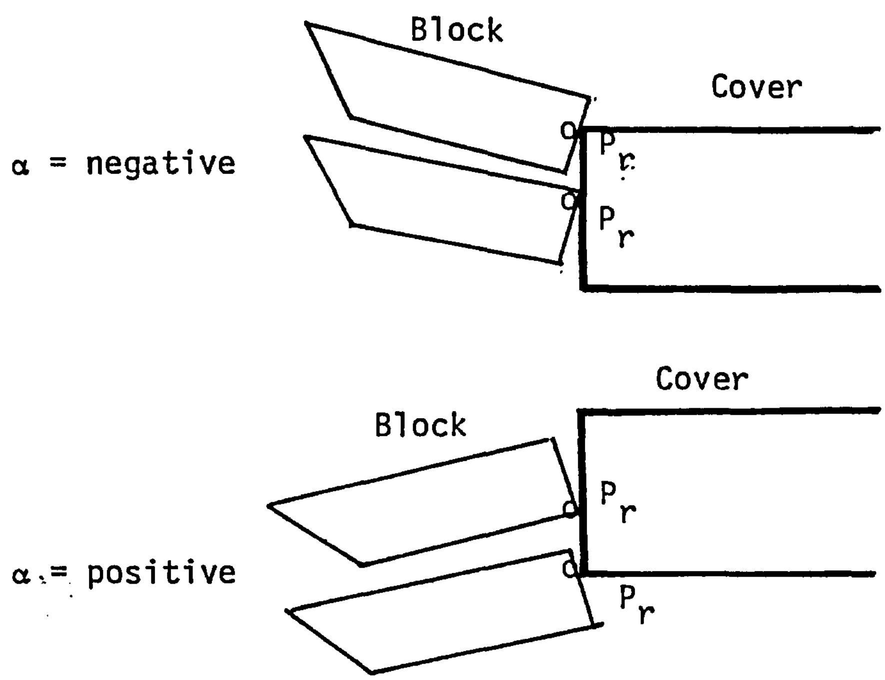

Figure 3.15: Point of Rotation

but with rotation about the upper corner.

6. Sink Turn Mode: this is the most frequently encountered mode. In this mode a positive displacement is acompanied by an underturning rotation.

7. Sink Upturn Mode: similar to the previous one but with negative rotation.

8. Lift Downturn Mode: the block will be turning down but with some lift. This usually occurs at the beginning of the instability process.

9. Lift Upturn Mode: in this mode the block will be lifted with upturning; hence it will be thrown over the cover. The cover edge might experience a crushing failure in the middle of this mode and a pushing mode might develop.

3.5.2 General Position of the Block

As the block points experience the displacement Δ and rotation α, a point originally at a position X_0 and Y_0 will move to a new position X and Y. This new position depends on the Δ and α values as well as the position of the center of rotation.

The position of the center of rotation depends on the mode of instability. The possible locations of this centre are shown in Figure 3.15. Once the position of the point of rotation is known, the ordinates of any point on the block can be estimated in the rotated position (Figure 3.16) using the following equations:

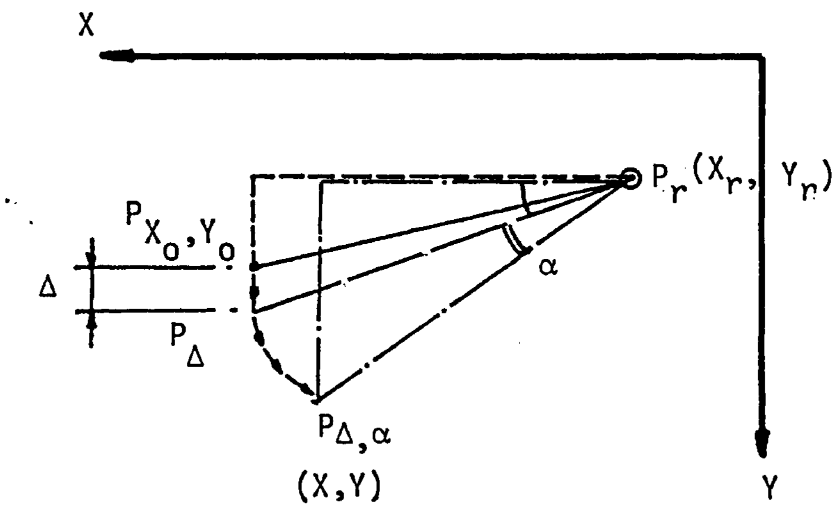

General Coordinates

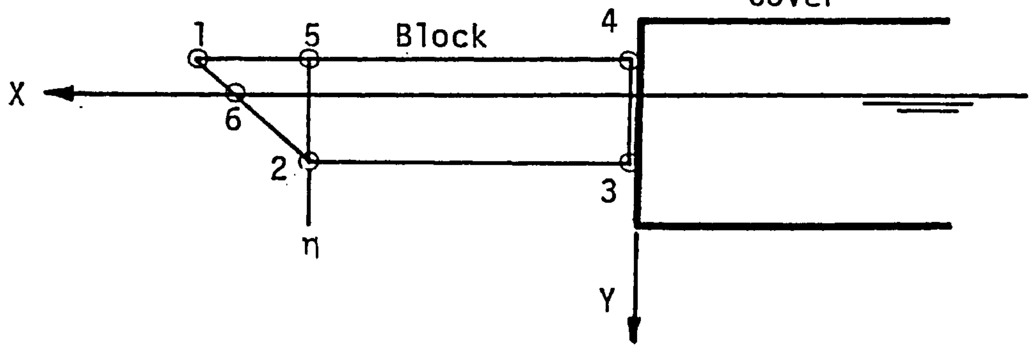

Main Points on Block

Figure 3.16: General Position of a Point

$$X = X_o \text{ Cos } \alpha - Y_o \text{ Sin}\alpha + (\Delta - Y_r) \text{ Sin } \alpha$$

and 3.50

$$Y = X_o \text{ Sin } \alpha + Y_o \text{ Cos}\alpha + Y_r (1 - \text{Cos}\alpha) + \Delta \text{ Cos } \alpha$$

3.5.3 Forces Acting on the Block

The different forces acting on the block are shown in Figure 3.17. These forces are:

1. The block core weight, W. acting vertically.
2. The block edge weight, W_e.
3. The additional weight due to submergence W_a which only appears if the block sinks under the static water surface while being stable.
4. The surface tension force due to the fluid between the contact faces of the block and the cover.
5. The edge force F_e which is the force acting on the leading edge due to the flow. Its two components are horizontally F_{xe} and vertically F_{ye}.
6. The force on the block underside, F_u. Its two components are horizontally F_{xu} and vertically F_{yu}.
7. The reaction force at the contact point R_x and R_y.

The details of the mathematical determination of these different forces are given in Appendix B.

3.5.4 Stability Criteria

The free block will be stable if the resultant of all the forces and moments acting on it vanishes. The resultant of all the applied

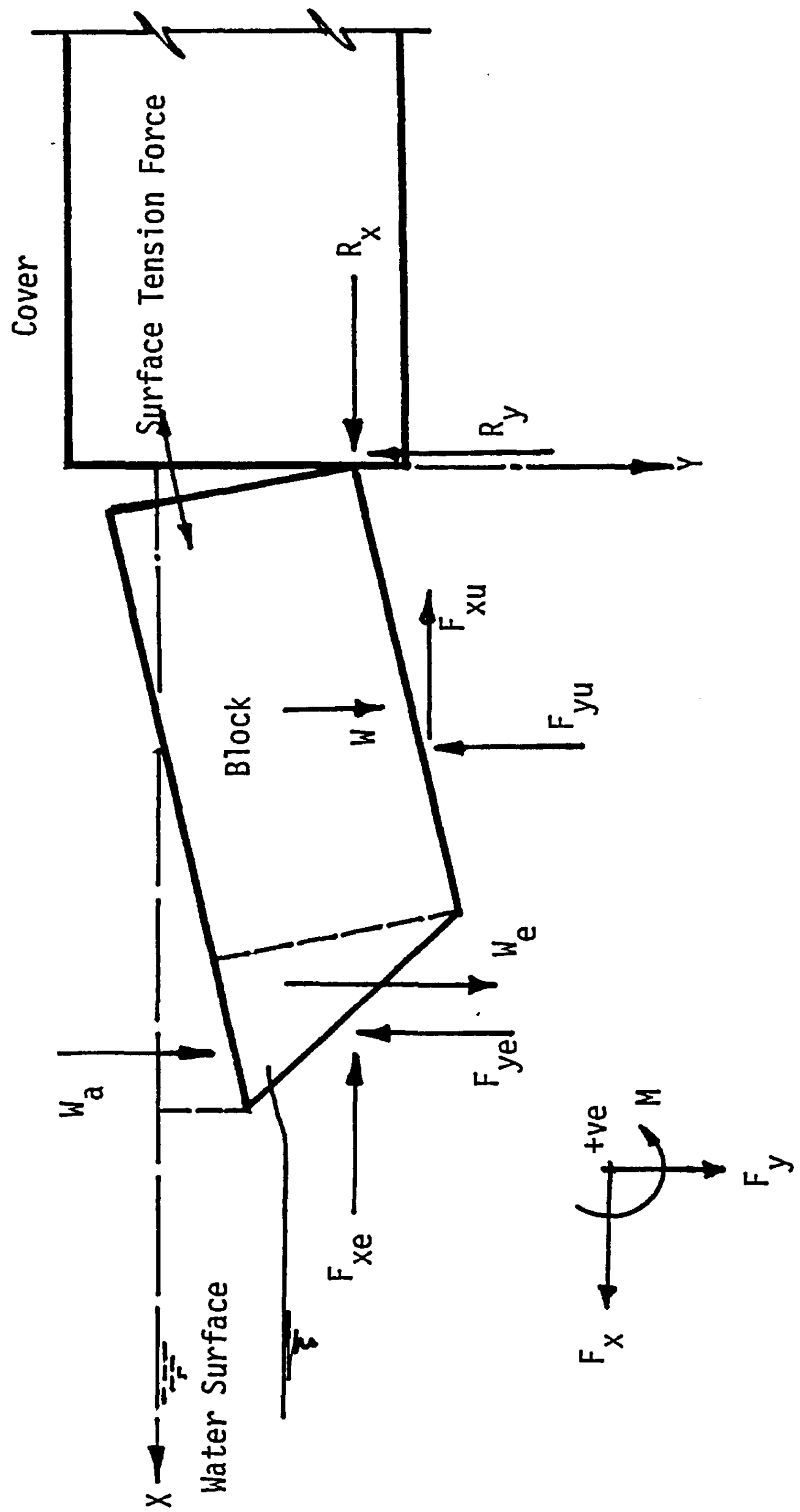

Figure 3.17: Forces on Block

forces on the block has to be counteracted by the cover reactions. If the direction of this resultant is such that the cover can offer no resistance, the block will be free to move in that direction indefinitely, and it becomes unstable.

For the block to be stable, the horizontal component of the reaction R_x has to be positive, because the cover can not pull the block. The contact surface between the block and the cover was assumed to offer a very small frictional resistance to any relative motion; hence, no tangential reaction is assumed to exist on a stable block, Figure 3.18.

The forementioned conditions of stability can be expressed mathematically as

The sum of moments @ point of rotation $= 0$

The reaction $R_y = 0$ if $Y_r < S_g t_c$

and $Y_r > S_{g1} t_c$

Otherwise The Reaction $R_t = 0$ 3.51

where $R_t = R_x \text{ Cos } \alpha - R_y \text{ Sin } \alpha$

and

R_t is the tangential reaction, Figure 3.18.

These equations can be solved for the unknowns Δ and α to yield the exact position of the stable block and the different forces acting on it.

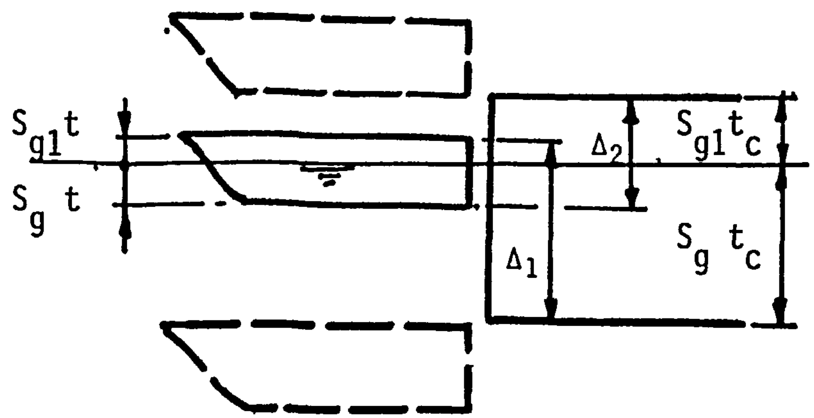

$-\Delta < \Delta_2 \quad , \Delta_2 = S_g\ t + S_{g1}t_c$

$\Delta < \Delta_1 \quad , \Delta_1 = S_{g1}t + S_g\ t_c$

Stability Range

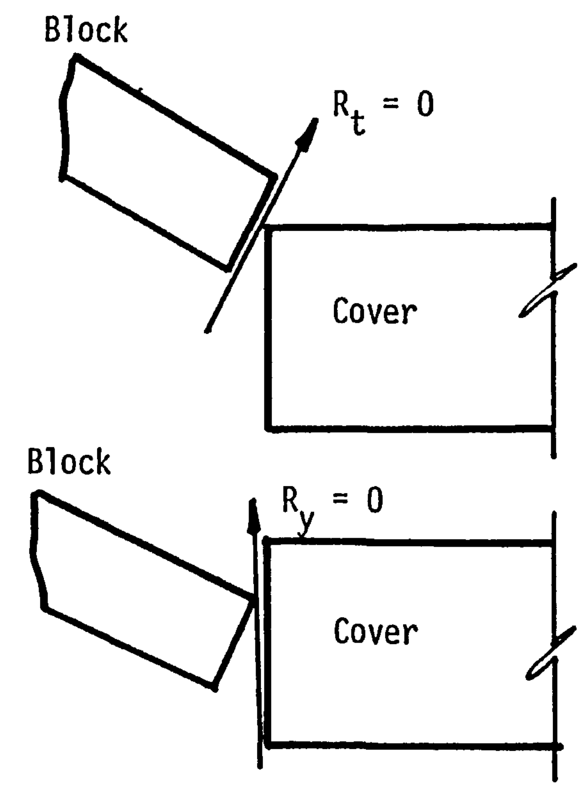

Stability Criteria

Figure 3.18: Stability Criteria and Range

3.5.5 Numerical Solution

The purpose of the mathematical model is to test the stability of the block under given flow conditions and / or to determine the critical stability conditions for this block. The model also can be used to determine the mode of stability, the final stable position of the block and the different forces acting on both the block and the cover at this position of stability.

The direct solution of the stability criteria equations will yield the corresponding Δ and α for a given block and cover under the defined flow conditions. There are three possibilities for the solution of the Δ and α values:

1. No solution is found, hence no force balance can exist in the tested position. In this case the block will be unstable.
2. Both Δ and α have definite values that satisfy the stability criteria requirements but are outside the stability range. In this case also the block will be considered unstable.
3. The values of Δ and α are definite and within the stability range. Hence the block is stable and the cover will extend.

The stable range is the range at which the Δ and α are physically possible. This range, Figure 3.18, can be expressed mathematically as:

1. The vertical displacement, Δ, is limited to

$$\Delta < S_g t_c + S_{g1} t \qquad ,\Delta \text{ is positive}$$

$$-\Delta > S_g t + S_{g1} t_c \qquad ,\Delta \text{ is negative}$$

otherwise the whole block will have no point of contact and the cover can not prevent it from moving.

2. For the rotation:

α corresponding to submerged upper edge if α is positive.

α corresponding to exposed lower edge if α is negative.

In the solution either the flow rate or the flow depth was kept constant while the other increased steadily until the point of instability was reached. The empirical method presented in Chapter VI can be used as an estimate of the critical condition.

The solution of the problem is generally numerical due to the complexity of the expressions for different forces and the nonlinearity of the equations in both Δ and α . The necessary program for the suggested numerical solution is presented in Appendix C while the behavior of the model and its typical results are discussed in Chapter V.

CHAPTER IV

EXPERIMENTAL INVESTIGATION

IV EXPERIMENTAL INVESTIGATION

4.1 Introduction

In this chapter the following subjects will be described:

1. The test equipment and the laboratory facilities,
2. The measurement equipment including point gauges, Pitot-tubes, miniature current meter, and the shear apparatus,
3. The experimental program and procedure including spatial. arrangements for each experiment,
4. The experimental results, and
5. The experimental errors.

4.2 The Test Equipment

4.2.1 Laboratory Facilities

Three different flumes were used, an 18" wide flume in which most of the experimental work was carried out, and a 6" wide and a 56" wide flumes in which the loose cover experiments were carried out.

4.2.1.1 The 18 Inch Flume

As shown in Figure 4.1, the test flume is 24' (7.315 m) long with a rectangular cross-section of 1.5' (.457 m) width and 2'(.61 m) depth. The bottom and right side of the flume were made of plywood while the left side was made of clear plexiglass.

A gauze screen was provided at the upstream end to ensure suitable flow inlet conditions from the head tank. The head tank was 4.25' (1.419 m) by 3.66' (1.18 m) in cross-section and 4' (1.219 m) in

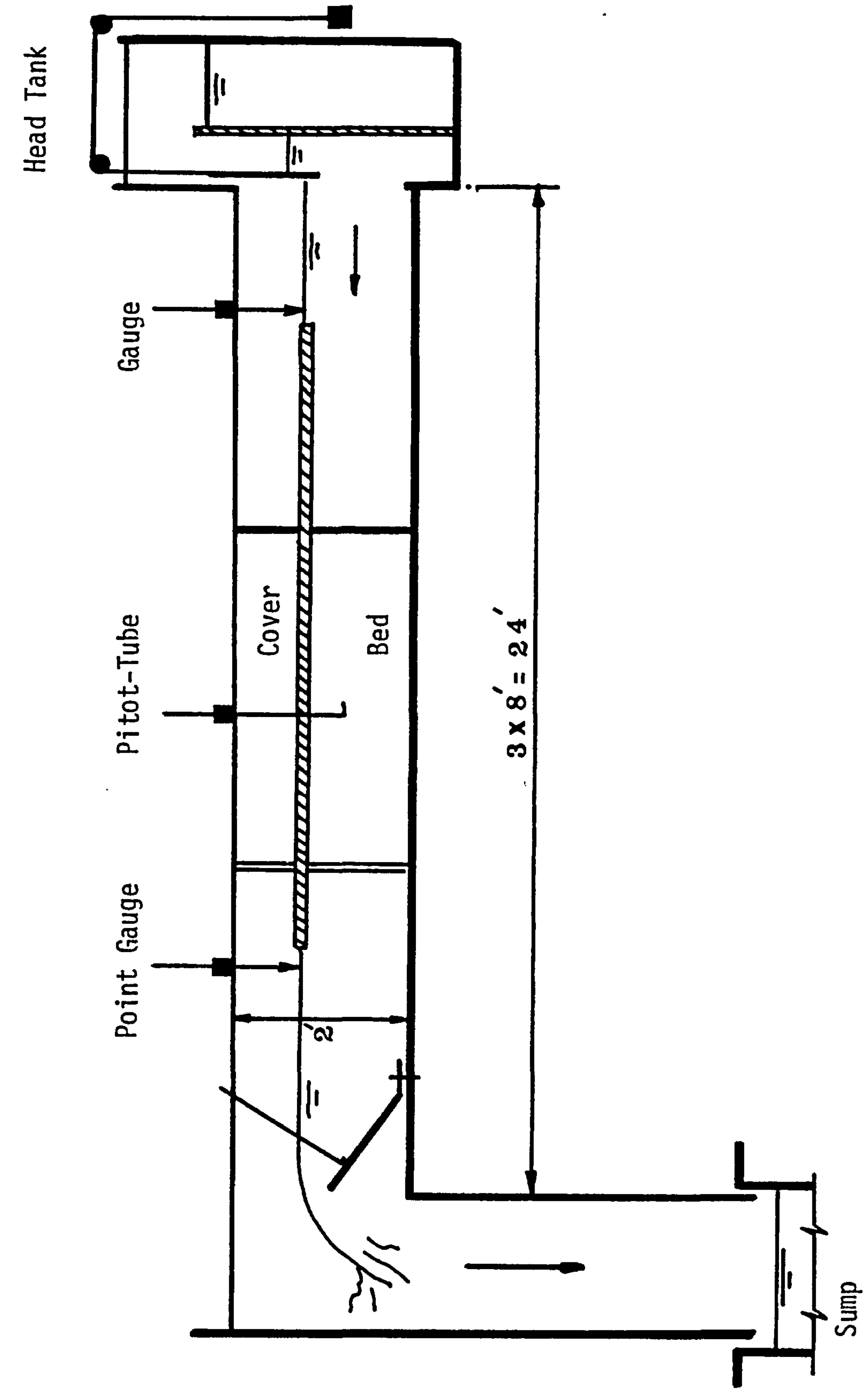

Figure 4.1: Layout of 18" Wide Test Flume

height. An adjustable gate to control the depth was fixed at the downstream end. The flume was served by a centrifugal pump capable of delivering up to 3500 USGPM (.2267 m^3/sec) in discharge with a 22.0'(6.71 m) head. A magnetic flow meter calibrated to 10 USGPM (6.5×10^{-5} m^3/sec) was used for discharge measurements.

4.2.1.2 The 6 Inch Flume

As shown in Figure 4.2 the portable self-circulating test flume is 10'(3.05 m) long with a 6"x 12"(15 x 30 cm) rectangular cross section and was made of plexiglass. The flow was supplied to the head tank through a centrifugal pump of 500 USGPM capacity and pump heads of up to 15'(4.5 m). A movable downstream vertical gate was used to control the flow depth, while a calibrated lever was used to change the bed slope by rotating the flume around its central hinge. A Venturimeter, installed on the delivery pipe of the pump was used to measure the flow discharge.

4.2.1.3 The 56 Inch Flume

A 56"(1.42 m) wide by 15'(4.6 m) long and 3'(.91 m) deep flume was used to study the loose cover behavior in wide channels. The flume, as shown in Figure 4.3 has a 1200 USGPM capacity pump that supplies up to 25'(7.6 m) head of water to the head tank and flows through a distributor to the main flume, which in turn recirculates it. An orifice meter on the delivery pipe was installed to measure the discharge using a calibrated manometer. Various kinds of end wiers were used to control the flow depth. The sides of the flume were made of plexiglass while its floor was made of aluminum.

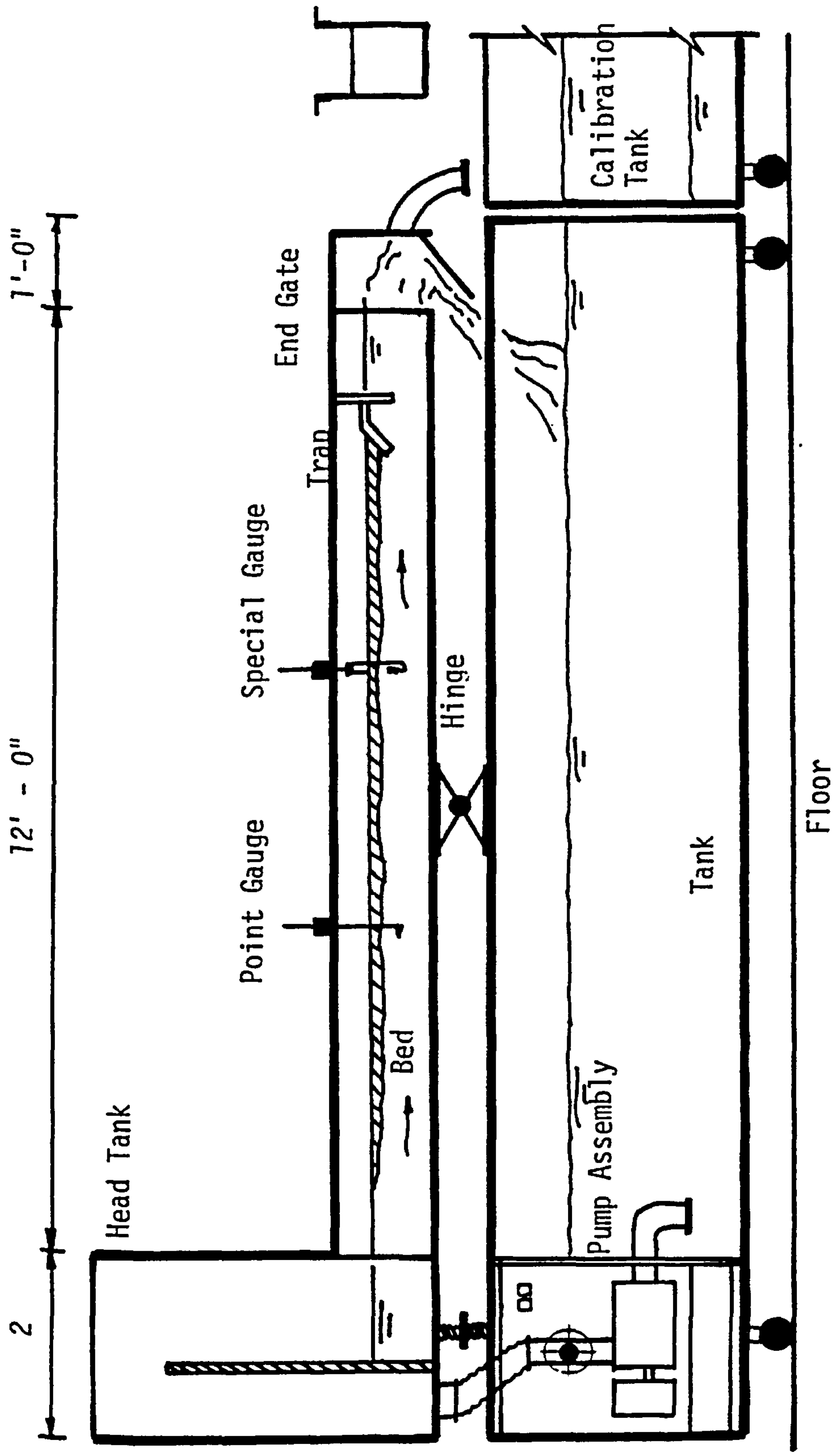

Figure 4.2: Layout of 6" Wide Test Flume

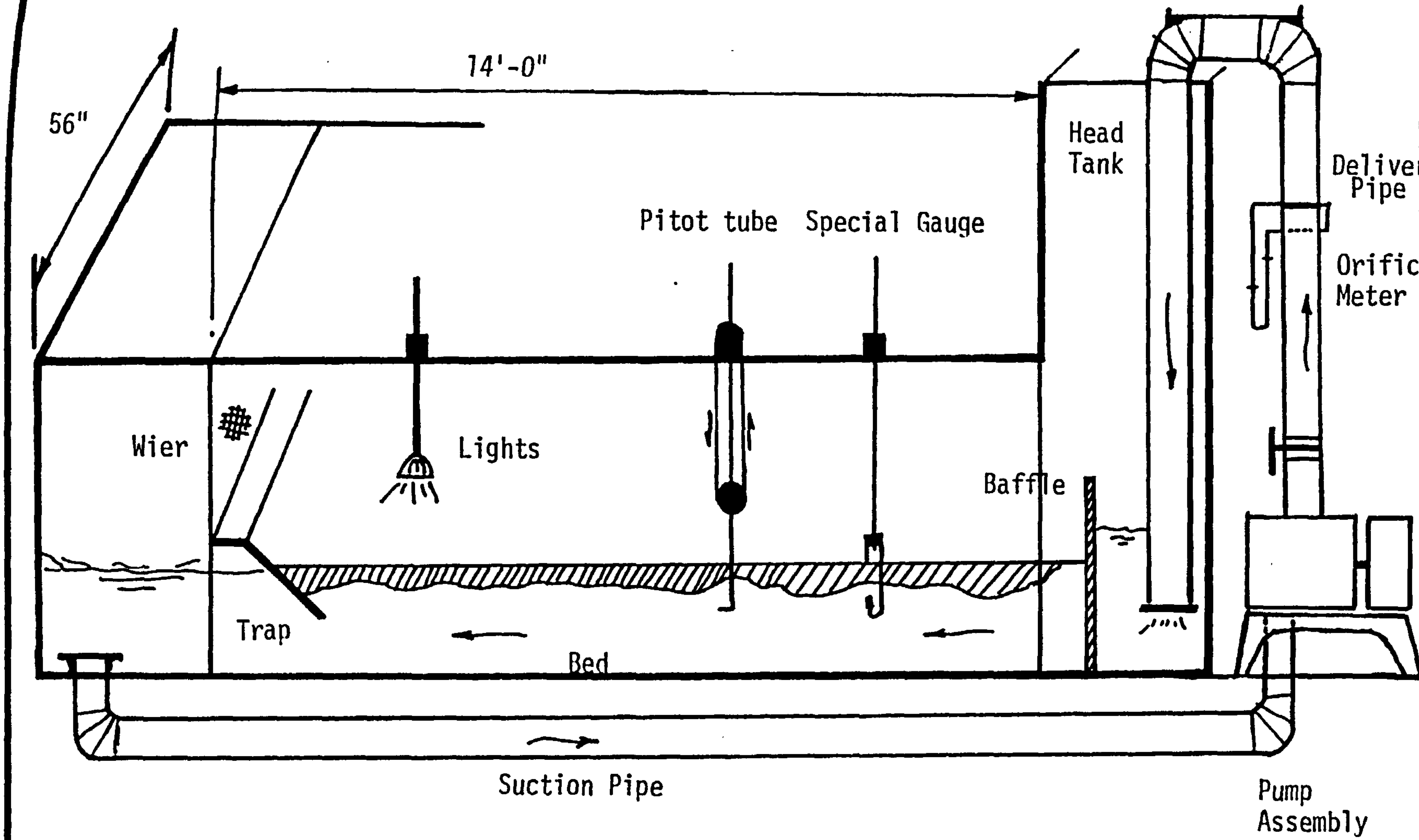

Figure 4.3: Layout of 56" Wide Test Flume

4.3 The Measuring Equipment

4.3.1 Point Gauges

Point gauges with electric bulb indicators were used to measure the water depths. The gauges were calibrated to read directly to 0.01" (0.025 cm).

4.3.2 Pitot-Tube

A Pitot-Tube was used for the velocity measurements with a vertical manometer reading directly to 0.01"(0.025 cm).

4.3.3 Miniature Current Meter

A miniature current meter was used for the velocity measurements as shown in Figure 4.4

4.3.4 Loose Cover Underside Configuration

The loose cover underside configuration was measured using the special hook gauge shown in Figure 4.5.

4.3.5 The Shear Apparatus

A simple pendulum apparatus Figure 4.6 was designed to measure the horizontal force acting on the block. The pendulum consisted of a 1.7 Ib (.75 kg) bar hinged to a bridge by means of two strings which acted as an indicator to the attached balance scale. The block end was provided with two vertical nails to transmit the shear acting on the block underside to the pendulum and hence the total horizontal force can be read on the scale.

4.4 Experimental Program

The experimental program was carried out with the objective of

Figure 4.4: Miniature Current Meter

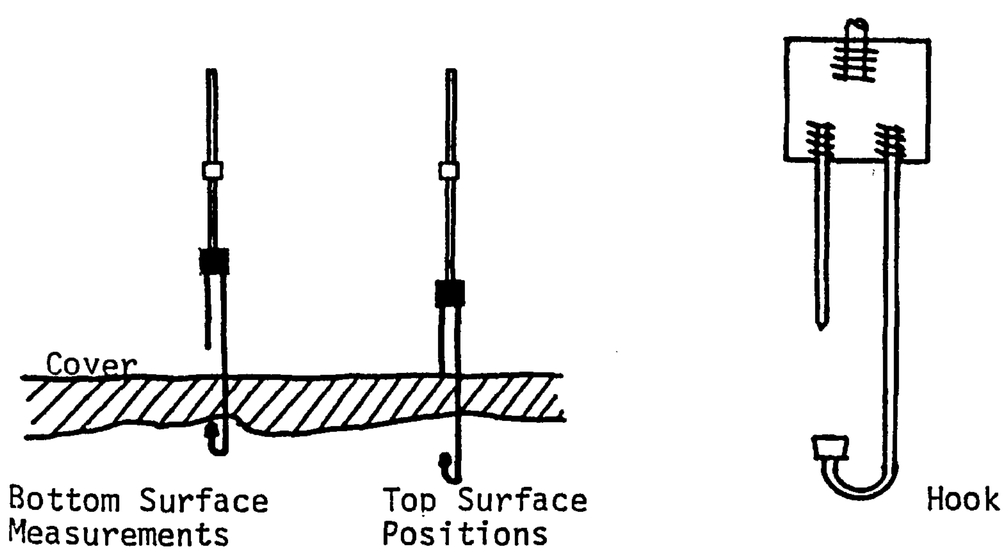

Figure 4.5: Special Hook Gauge

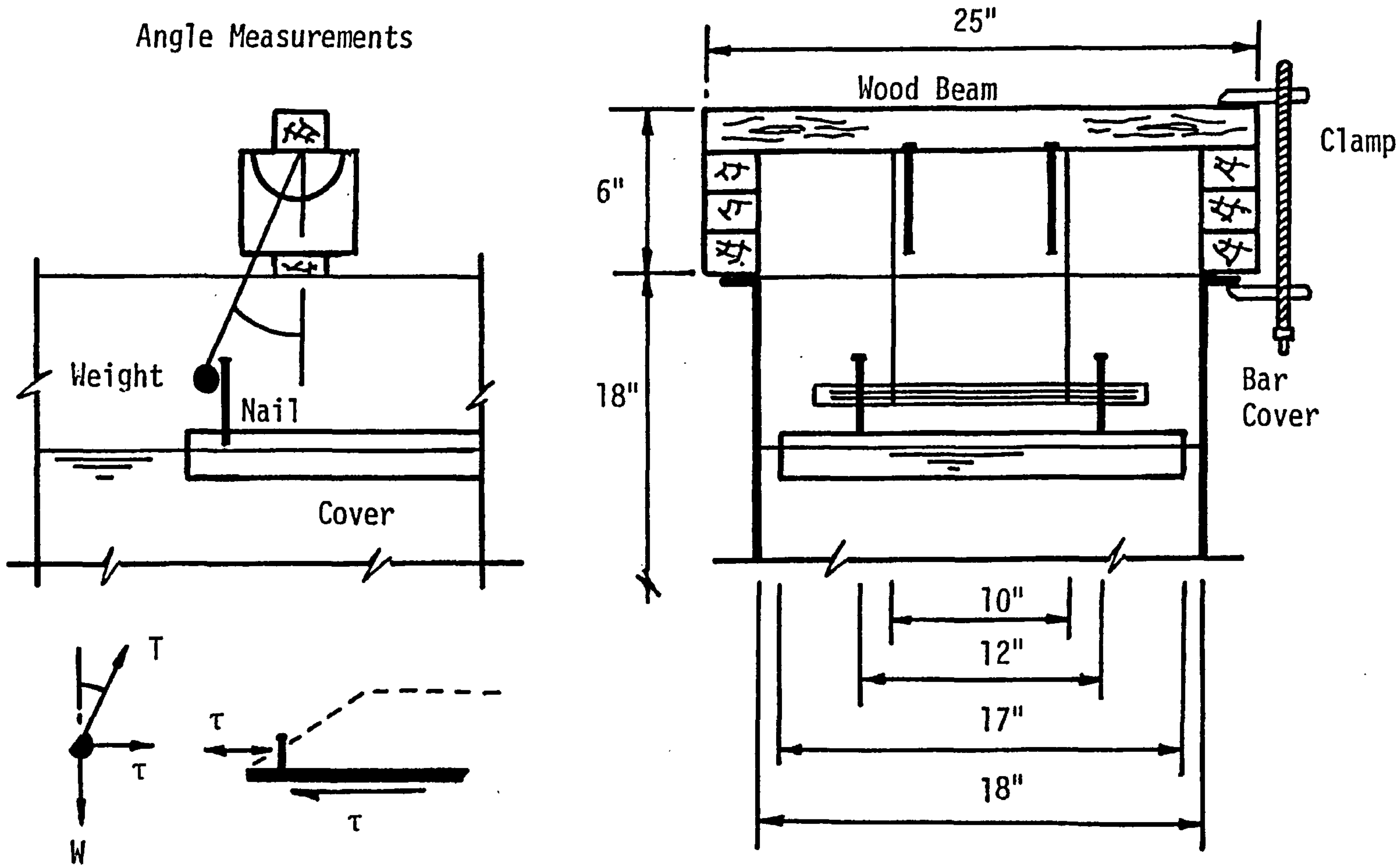

Figure 4.6: Shear Apparatus

investigating those problems defined in Chapter I and to verify the mathematical models developed in Chapter III. In the following sections a brief summary is made of the arrangements and procedures used in each group of experiments.

4.4.1 Study of the Velocity Profile

In this part of the investigation the velocity profiles were measured through the covered cross-section in the 18"wide flume. These measurements were taken beyond an initial length of 40 times the cover thickness to ensure the establishment of uniform flow away from the leading edge effect.

Two types of covers were used to study the effct of the boundary roughness on the velocity. First a flat wooden cover was used. Then the same cover was roughened by nailing a metal screen to its underside. This increased the Manning's roughness n_2 from 0.011 to 0.032. The underside roughness of each cover was determined by lining the channel bottom and sides with the cover material in the way shown in Figure 4.7. The n_2 value was then determined as if for an open channel.

4.4.2 Study of the Cover Underside Roughness

The cover underside roughness was studied, in the 18" wide flume, using roughness elements to simulate its configuration. These elements, Figure 4.4, have a rectangular section of 1"width (2.54 cm) and different heights of 0.0, 0.75", 1.5"and 2.25"respectively and were spaced at 6", 12"and 18". Both the cover and the roughness elements were made of neatly finished wood.

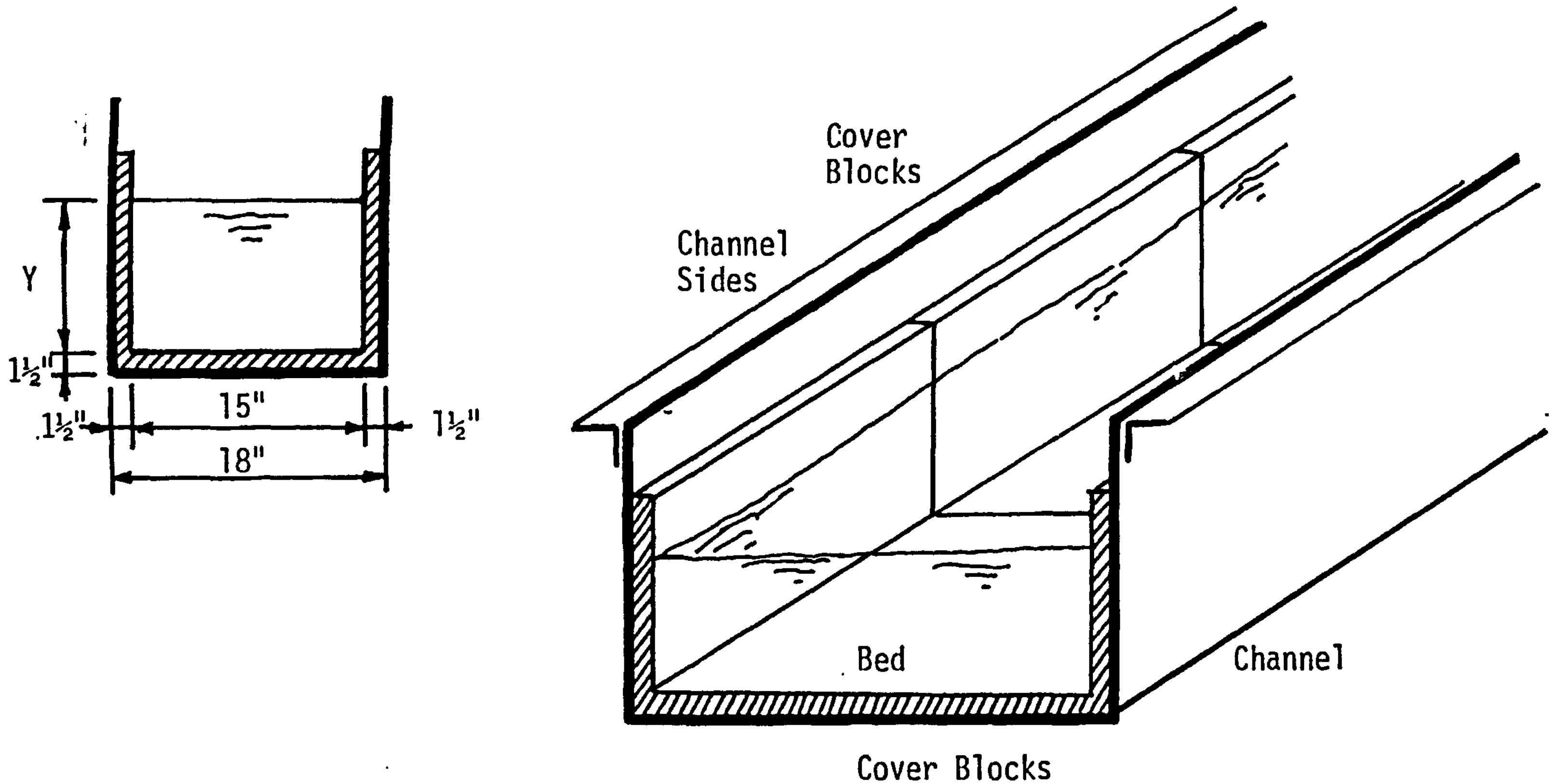

Lining of Channel Bottom and Sides to Determine the n_2 values

Figure 4.7: Determintation of n_2

All the possible combinations of the roughness elements heights and spacings were tested under different flow conditions. In each run the velocity distribution and the friction slope were measured. The underside roughness coefficient was then estimated as explained in Chapter V.

4.4.3 Study of the Cover Underside Configuration

In these experiments the cover was simulated by means of white polyethelene pellets with a specific gravity of 0.92. They have a disc-like shape 4mm in diameter, 2mm in core height, and 1mm in side height as shown in Figure 4.8. These particles were then placed on the flow surface and allowed to take any shape dictated by the flow. The underside configuration was measured by means of the hook gauge described earlier.

Three different types of bed-forms were used to study the effect of the bottom configuration on the underside shape.

1. A flat bed, formed of the natural flume bottom, was tested in all three flumes.
2. Dune bed-form, consisting of ten adjacent identical concrete blocks, was tested in the 18"flume. A typical block is shown in Figure 4.9.
3. Triangular bed-form, made of thin smooth sheet metal on a wooden frame, was tested in the 6"wide flume only. Typical dimensions of these forms are given in Figure 5.23.

Two traps were used to avoid losing the pellets into the pumping system. The two types of traps used were:

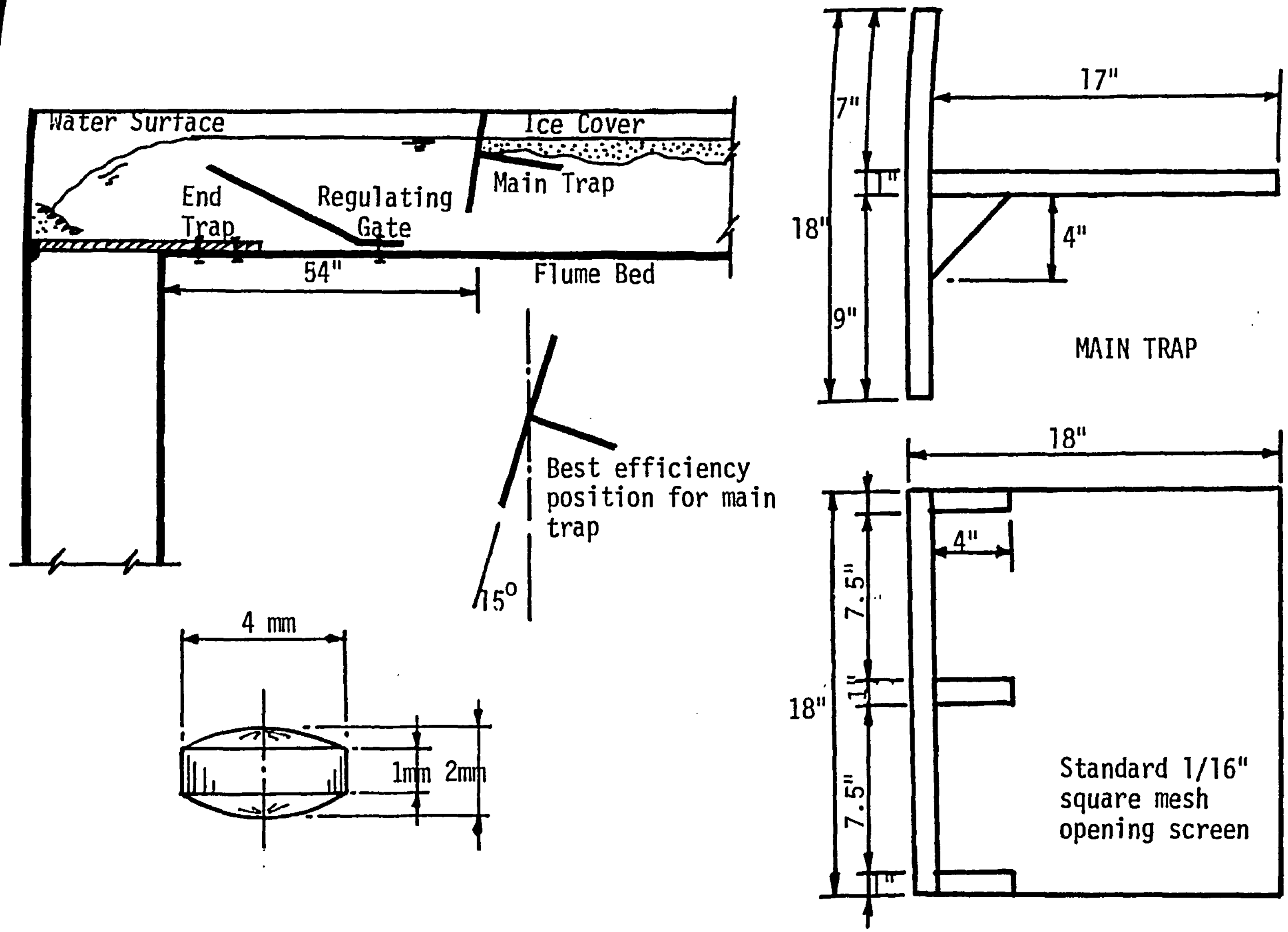

Figure 4.8 : Loose Cover Traps

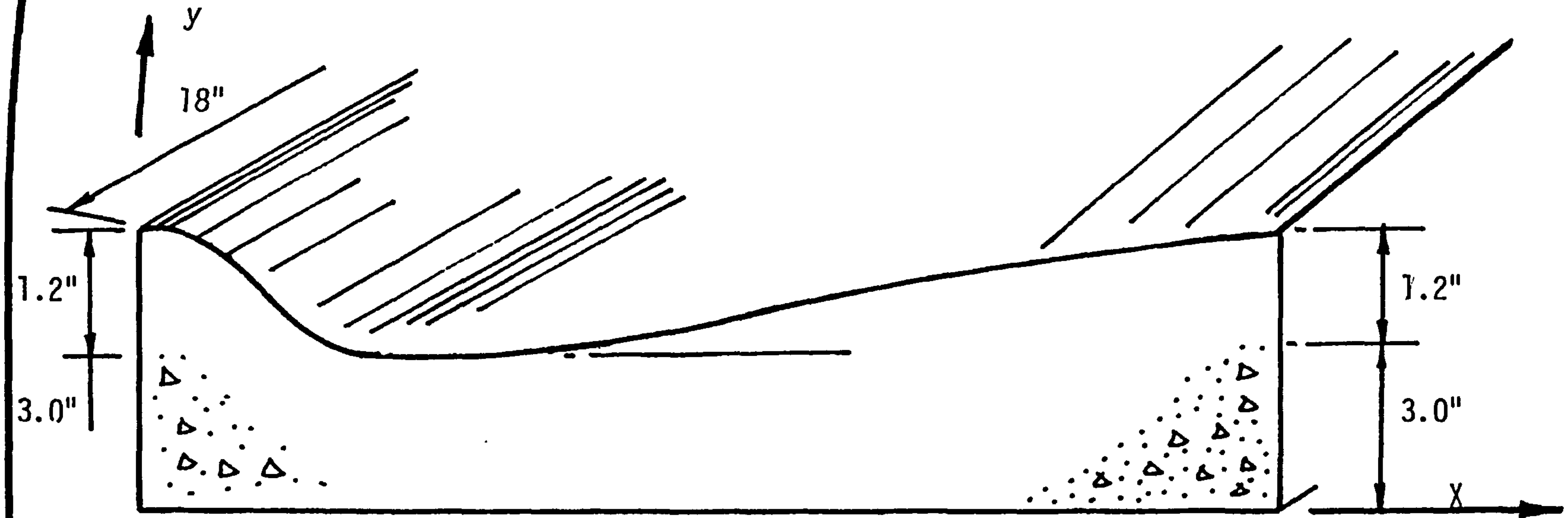

Station	0.0	1.0	2.0	2.5	3.0	4.0	5.0	6.0	7.0	8.0	9.0	10.0	11.0	12.0
X Inch	0.0	1.0	2.0	2.5	3.0	4.0	5.0	6.0	7.0	8.0	9.0	10.0	11.0	12.0
Y Inch	1.2	0.825	0.09	0.00	0.03	0.09	0.10	0.30	0.465	0.63	0.825	0.975	1.128	1.200

Figure 4.9 : Typical Dimensions of Dune Bed-form

1. A downstream horizontal end trap with a wooden frame covered with an 0.08"(2mm) opening square mesh.
2. A main control trap consisted of a vertical square frame of side dimenions equal to the width of the flume, and attached to another frame of the same size slightly inclined to the horizontal.. Figure 4.8 shows the details of the traps used in the 18" flume.

4.4.4 Study of Block Instability

In these experiments the instability criteria of the block and the forces acting on it were studied. Wooden blocks of 17" (0.43 m) width and lengths of 1.5", 2.0", 6.0", 15.0" and 17.0" were tested. Four wooden interchangeable edges (see Figure 4.10) 1:1 and 2:1 sloped as well as circular and rectangular, were used.

In each run the flow was increased slowly and the horizontal forces acting on the block were recorded at each step. The block was watched until the instability condition was reached, i.e, the point after which the block moves without any possibility of being stable again. The critical discharge and flow depth corresponding to this point were then recorded.

To ensure measurable pressures a larger block measuring 17" wide, 36" long, and 2.25" thick was tested, using similar types of edges. Twenty holes were drilled along the block's centerline, at 2" intervals, and the water level inside each hole was measured to obtain a representative pressure distribution.

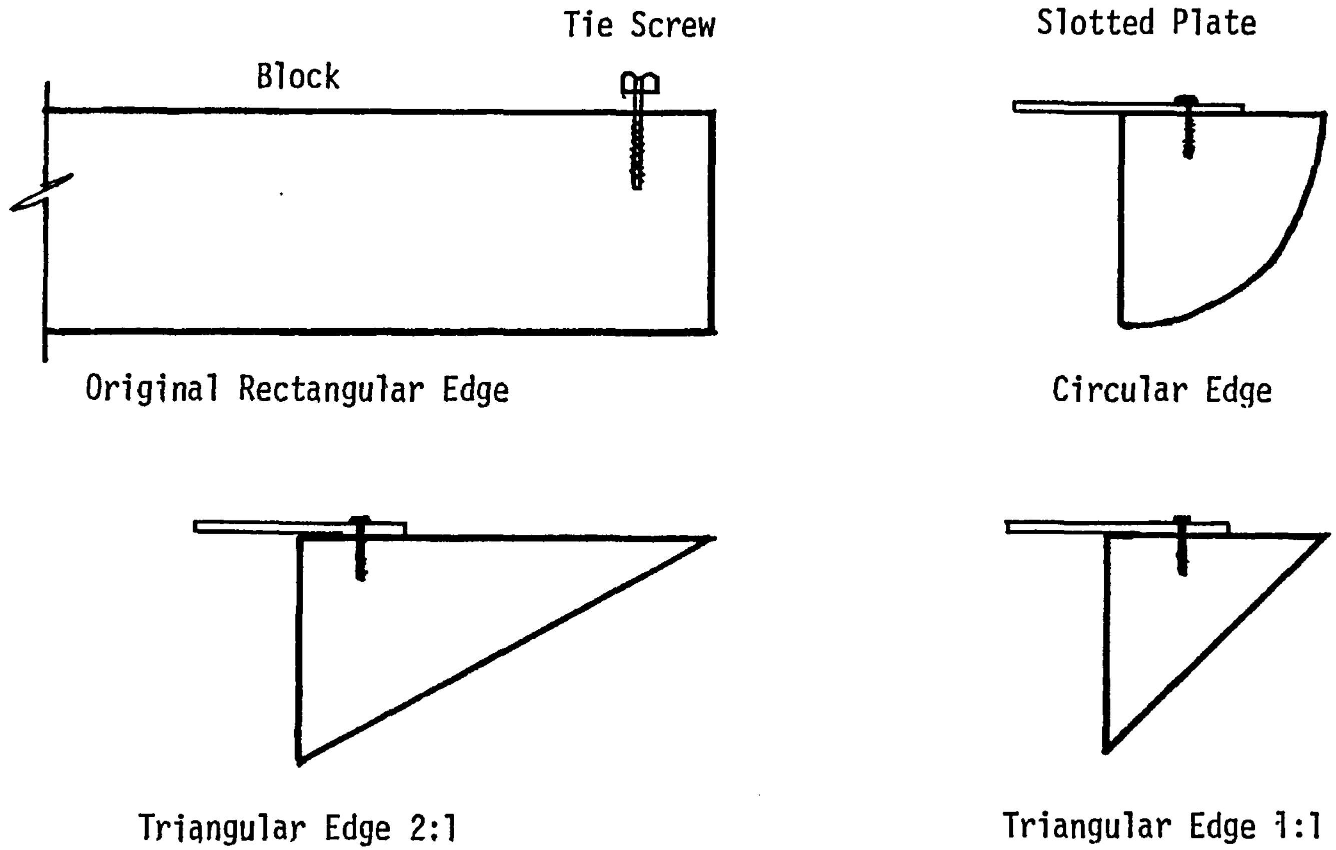

Figure 4.10: Different Edges Used in Instability Study

4.5 Experimental Results

A summary of the results obtained in the experimental investigation is given in Appendix E.

4.6 Experimental Errors

The sources of the experimental errors along with their expected values are summarized in Appendix D.

CHAPTER V

DISCUSSION OF THEORETICAL AND EXPERIMENTAL RESULTS

V. DISCUSSION OF THEORETICAL AND EXPERIMENTAL RESULTS

In this chapter the utilization of the mathematical model developed in Chapter III is discussed. First the behavior of the model under different conditions is analyzed, then the applicability and limitations of its different aspects are investigated. Finally a comparison between the results obtained through the application of the theory and those obtained experimentally is presented.

5.1 Flow Patterns

In this article the velocity profile solution will be discussed for the two -dimensional case followed by the three-dimensional sections.

5.1.1 Two-Dimensional Solutions

As was mentioned in Chaper III, a wide covered channel can be divided into two subsections to which the velocity profile relations, Equations 3.16 and 3.17, are applicable. It was further shown that the maximum velocity occurs at the separation line, and its position can be found using the relations developed in Appendix A.

The difference between the two subsection mean velocities was given as

$$V_1 - V_2 = \frac{-2}{3\kappa} (V_{*1} - V_{*2}) \qquad 5.1$$

and hence the rougher the boundary the smaller its subsection velocity. In fact the same applies to the mean and maximum velocities of the whole section. The ratio of these two velocities can be evaluated as

$$\frac{V_{max}}{V} = 1 + \frac{2}{3\kappa} \left(\frac{V_{*1}}{V} \frac{A_2}{A} + \frac{V_{*2}}{V} \frac{A_1}{A} \right). \qquad 5.2$$

and the rougher the boundaries, the higher this ratio will be. The numerical examples presented in Figures 5.1 and 5.2 further clarify these facts.

To test the applicability of the developed velocity profile, the velocities were measured at the center of the wide flume described in Chapter IV. The bottom Manning's roughness n_1 was .011 while the cover underside roughness n_2 was measured on a lined channel at .032. The measured flow rates were used to develop the theoretical velocity profiles and the results were compared to the measured velocities as shown in figure 5.3.

Good agreement between the theoretical and measured velocity profiles was obtained. The measured velocities were slightly greater than the predicted ones near the cover boundary, but this can be attributed to the release of the cover resistance due to the gap through which the Pitot-tube was introduced.

A comparison between the theoretically predicted velocity profile and those of Larsen, Krishnamurthy and Shen is presented in Figure 5.4. Since none of these velocity profiles suggested a method of defining the position of the maximum velocity, Equation A.12 was used to find this position.

Most of the velocity profiles in the literature do not agree on the value of the computed velocity at and near the point of separation, where they have a discontinuous profile. To have a continuous profile, a

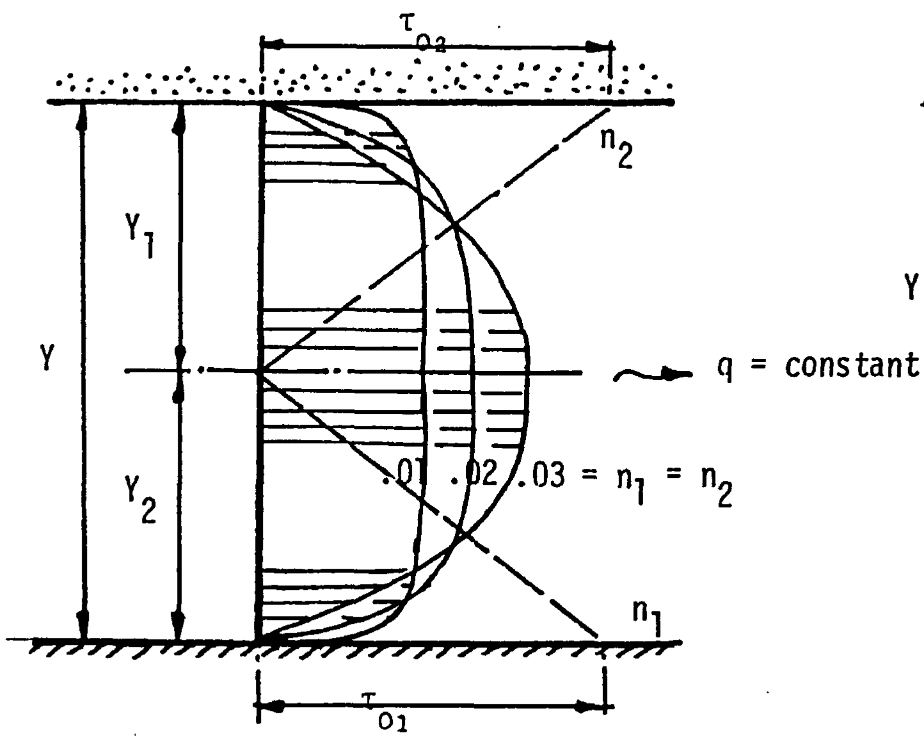

Figure 5.1: Effect of Boundary Roughness

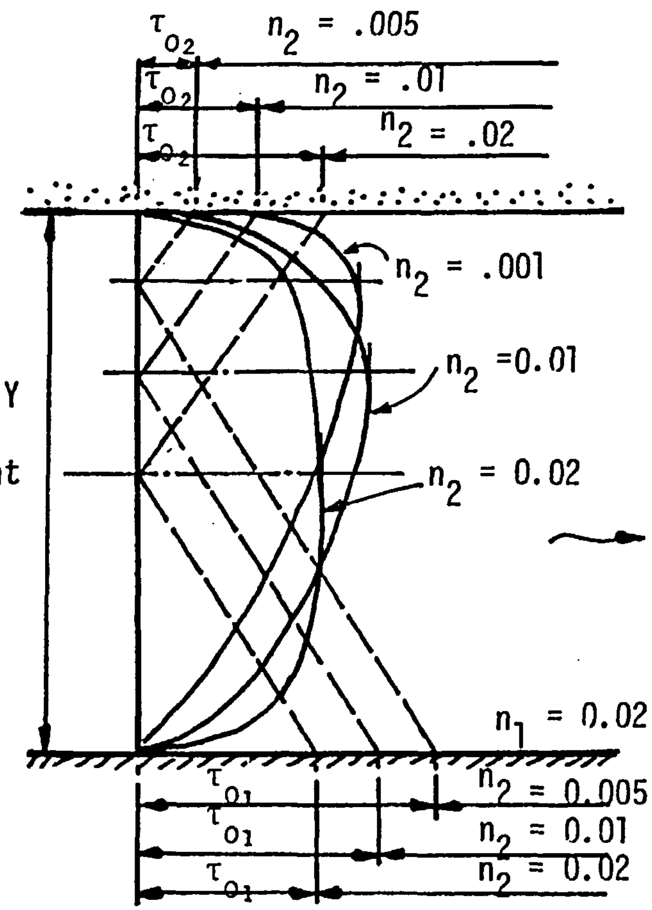

Figure 5.2: Effect of Relative Roughness

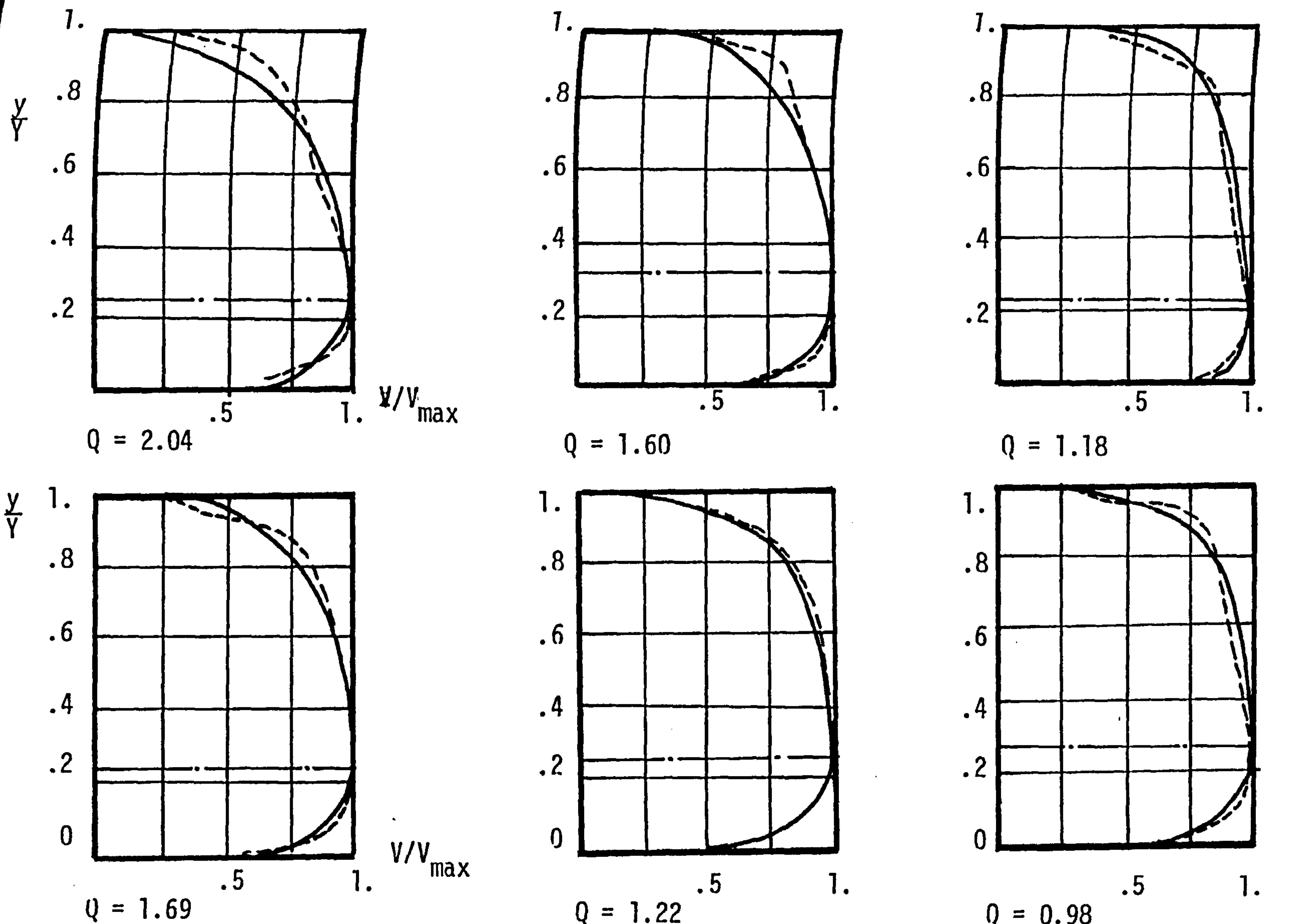

Figure 5.3: Velocity Comparison with Experimental Data

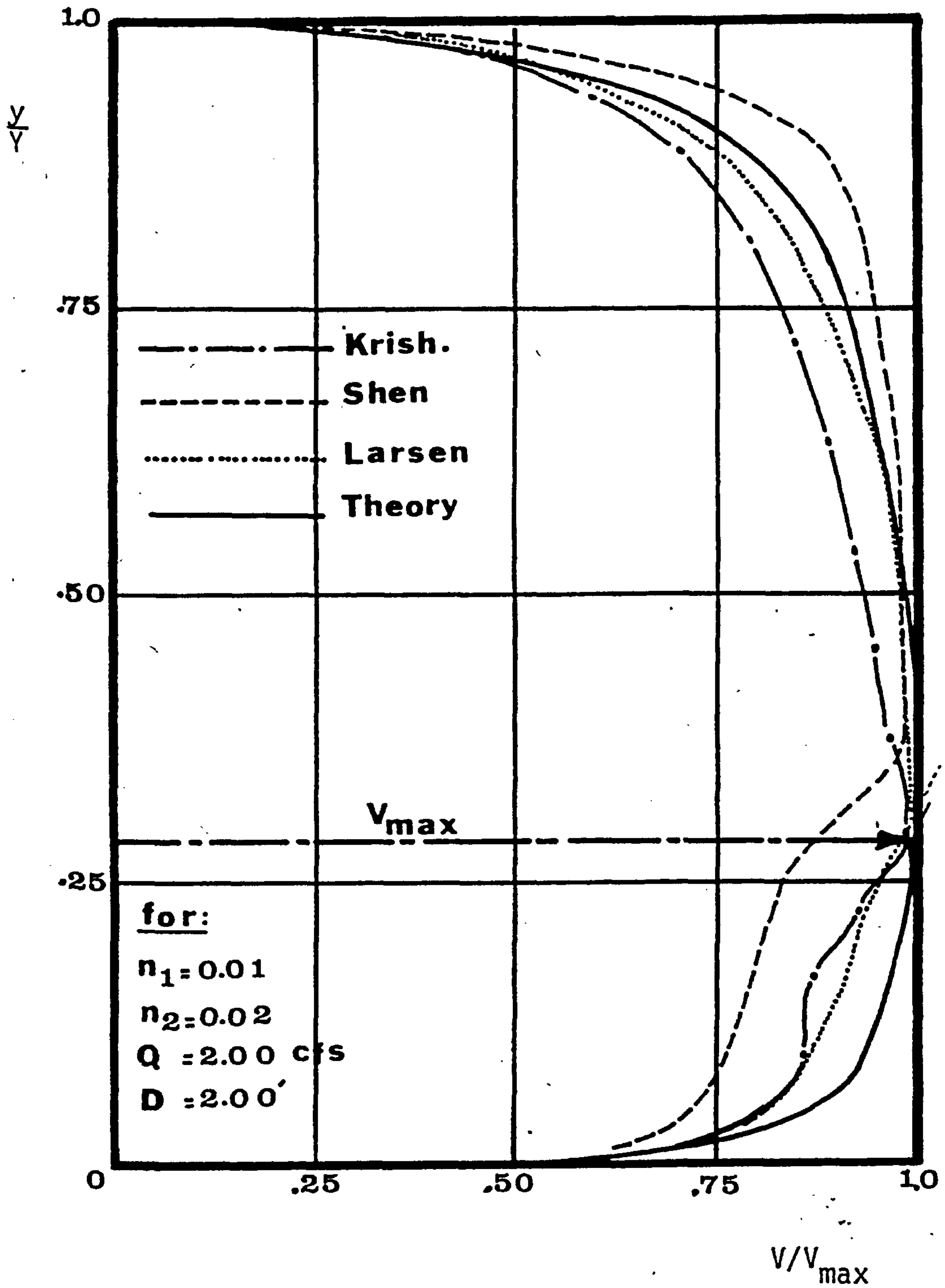

Figure 5.4: Velocity Comparison with Literature

maximum velocity has to occur at the separation point when computed from both sides. This does not appear to be the case when applying the direct logarithmic velocity profiles commonly used in the literature.

5.1.2 General Flow Patterns

In Chapter III, the velocity profile for narrow channels was developed. The suggested method applies to free as well as covered channels of different boundary roughnesses.

The behavior of the mathematical model can best be illustrated through numerical examples. In the following articles different channels of polygonal type cross-section were tested. The numerical technique developed in Chapter III was utilized to obtain the results of these models.

In all examples, the channel dimensions, the roughnesses of different boundaries, and the flow rate were assumed to be known. Using the computer program listed in Appendix C, the velocities were determined at the nodal points of the traverse, then, the isovels, lines of constant velocity, were plotted. The maximum velocity points, along a series of vertical strips taken across the channel section, were connected by a smooth curve to obtain the separation line.

The extrapolation of the shear at the internal points was used to determine the shear at the boundaries. This shear was then used to estimate the friction slope in the manner given in Chaper III. The composite roughness was calculated using the flow equation and the computed friction slope.

5.1.2.1 Effect of Channel Roughness

Figures 5.5 to 5.7 represent the flow and shear distributions in a 1' x 1' square covered channel with equal boundary roughnesses of 0.01, 0.02 and 0.03 respectively. The flow rate was maintained at 1.0 cfs.

It can be noticed that the smoother the boundary, the flatter the velocity profile and the smaller the (V_{max}/V) ratio become. Also the rougher the boundary, the steeper the energy slope required to pass the same amount of flow. The separation line was difficult to distinguish for smoother boundaries while it becomes more visible as the boundary gets rougher. The estimated energy slope and composite roughness agrees with their expected values.

In the example of Figure 5.8 the velocity and shear profiles were computed for the same channel using the same bottom and side roughnesses while the cover roughness was increased to $n_2 = .03$. The position of the maximum velocity was noticed to shift from the center of the channel Figure 5.7, to the lower portion, that is, away from the rougher boundary. But because of the equal side roughnesses, the maximum velocity stayed at the centerline of the section.

The shear was noticed to be greater at the rougher boundary which makes the rougher boundary responsible for larger share of energy dissipation. The side shear was also found to be greater at the lower part of the channel. The separation line in this case is distinct and assumes a trapezoidal shape in general.

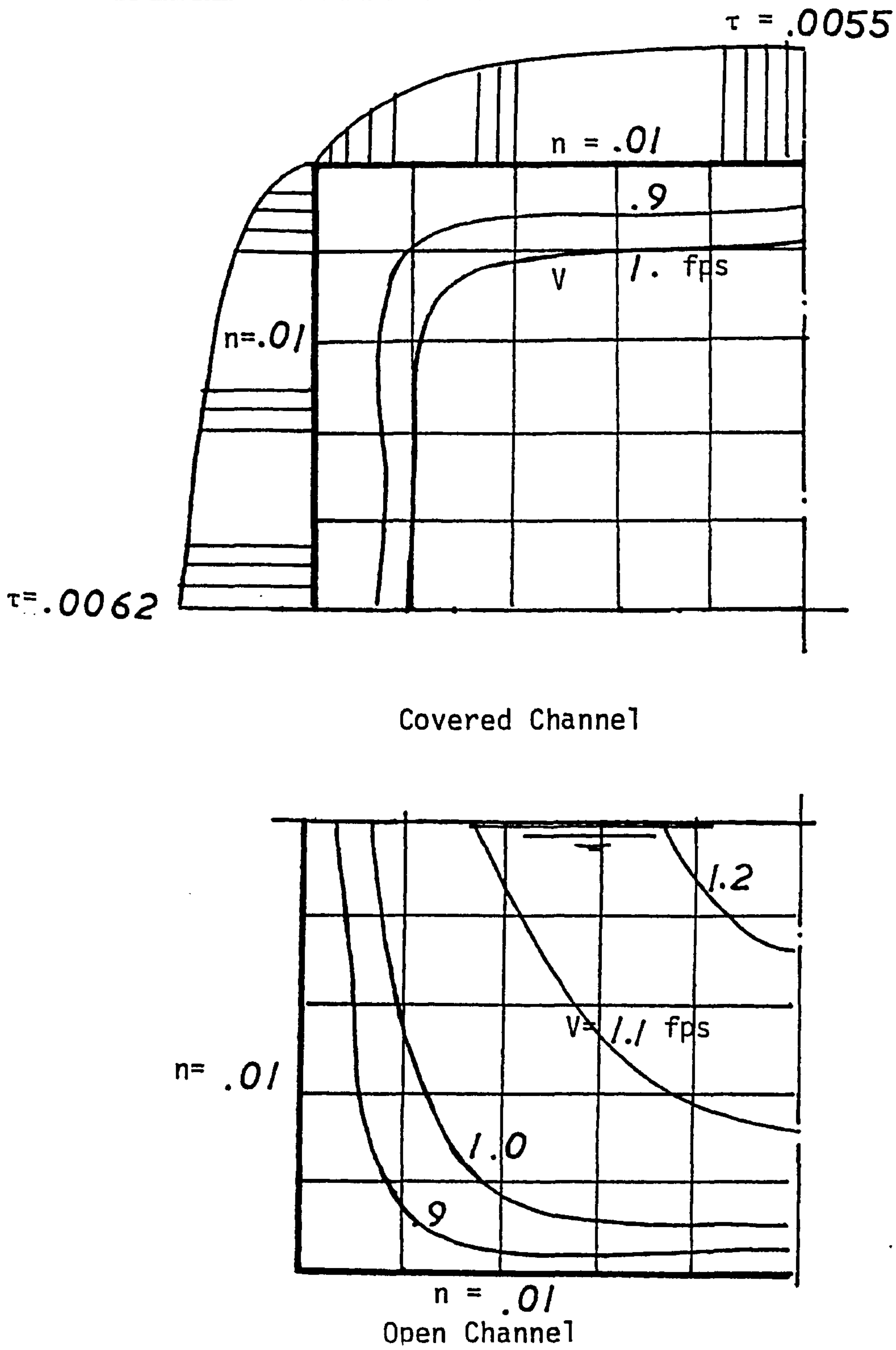

Figure 5.5: Velocity Profile in Channel

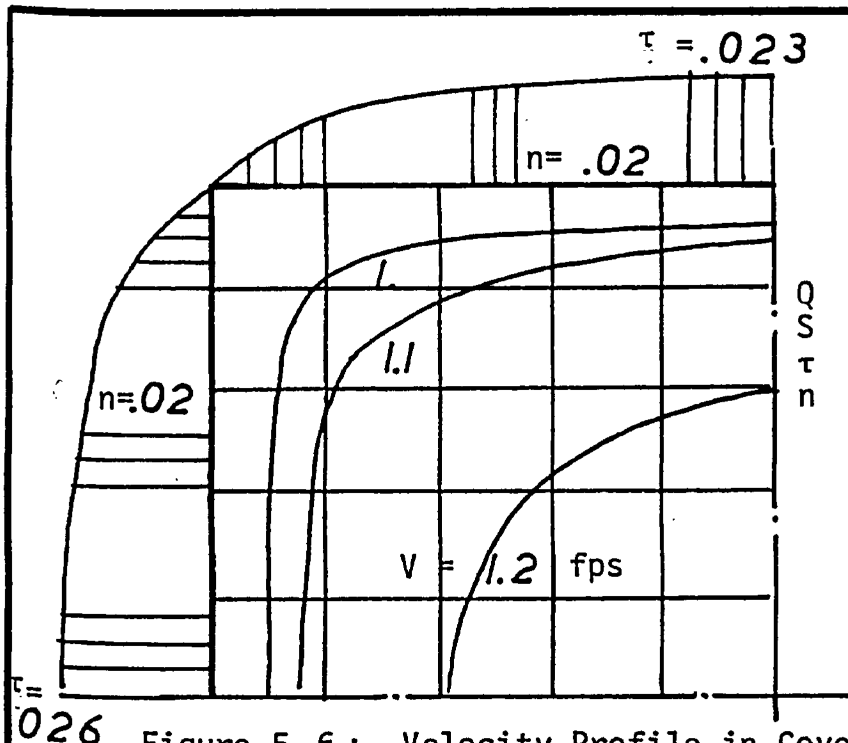

	Theory	Expected
Q	1.0	1.0
S	0.00114	0.0013
τ	0.071	0.0809
n	0.02	0.0213

Figure 5.6 : Velocity Profile in Covered Channel

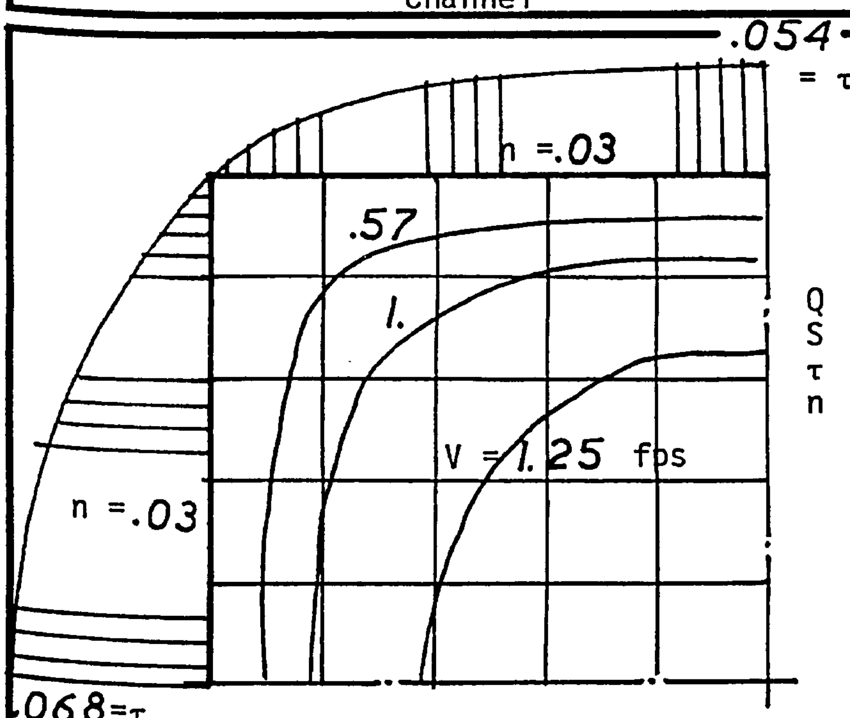

	Theory	Expected
Q	1.0	1.0
S	0.0025	0.00282
τ	0.161	0.176
n	0.03	0.031

Figure 5.7 : Rectangular Covered Channel Velocity Profile

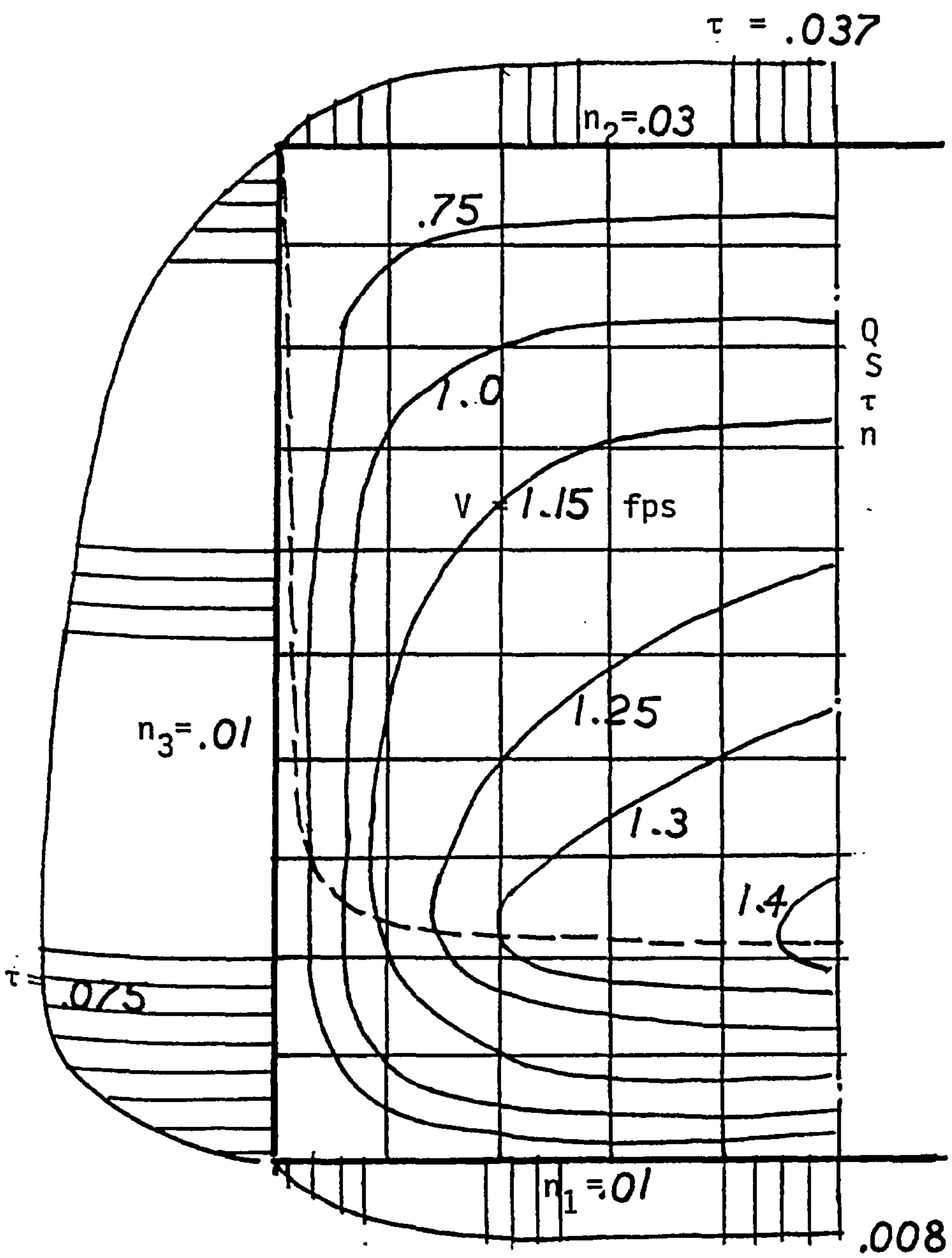

	Theory	Expected
Q	1.0	1.0
S	0.00076	0.0008
τ	0.047	0.050
n	0.016	0.0157

Figure 5.8 : Effect of Cover Roughness on Velocity Profile

The numerical examples presented in Figures 5.8 to 5.10 show the effect of the side roughness. It was again noticed that the rougher side will carry a larger amount of shear. The maximum velocity was found to move away from the rougher side, Figure 5.10.

5.1.2.2 Effect of Channel Size

To study the effect of the channel size on the flow pattern, three models of aspect ratios of 1,2 and 10 were tested. Different roughnesses were assigned to each boundary as shown in Figures 5.10 to 5.12. The aspect ratio is defined as the channel width to depth ratio.

It can be seen that as the aspect ratio increases, the zone, in which the channel acts as if it is wide, increases. This increase agrees with the previous literature reports. The maximum velocity moves towards the smoother side resulting in lower shear. Both the maximum velocity and the average shear decrease at higher aspect ratio. The effect of the variation in the side roughness decreases with the increase in the aspect ratio. This widens the separation line shape as shown in Figures 5.12.

5.1.2.3 Effect of Channel Geometry

To illustrate the effect of the channel cross-section shape on the velocity and shear distributions, different models including triangular, trapezoidal and compound channels, Figures 5.13 to 5.16, were tested.

It is clear that the closer the channel section is to that of a gently rounded shape, the more uniform the velocity and shear distributions are. This is especially apparent when comparing the combined triangular

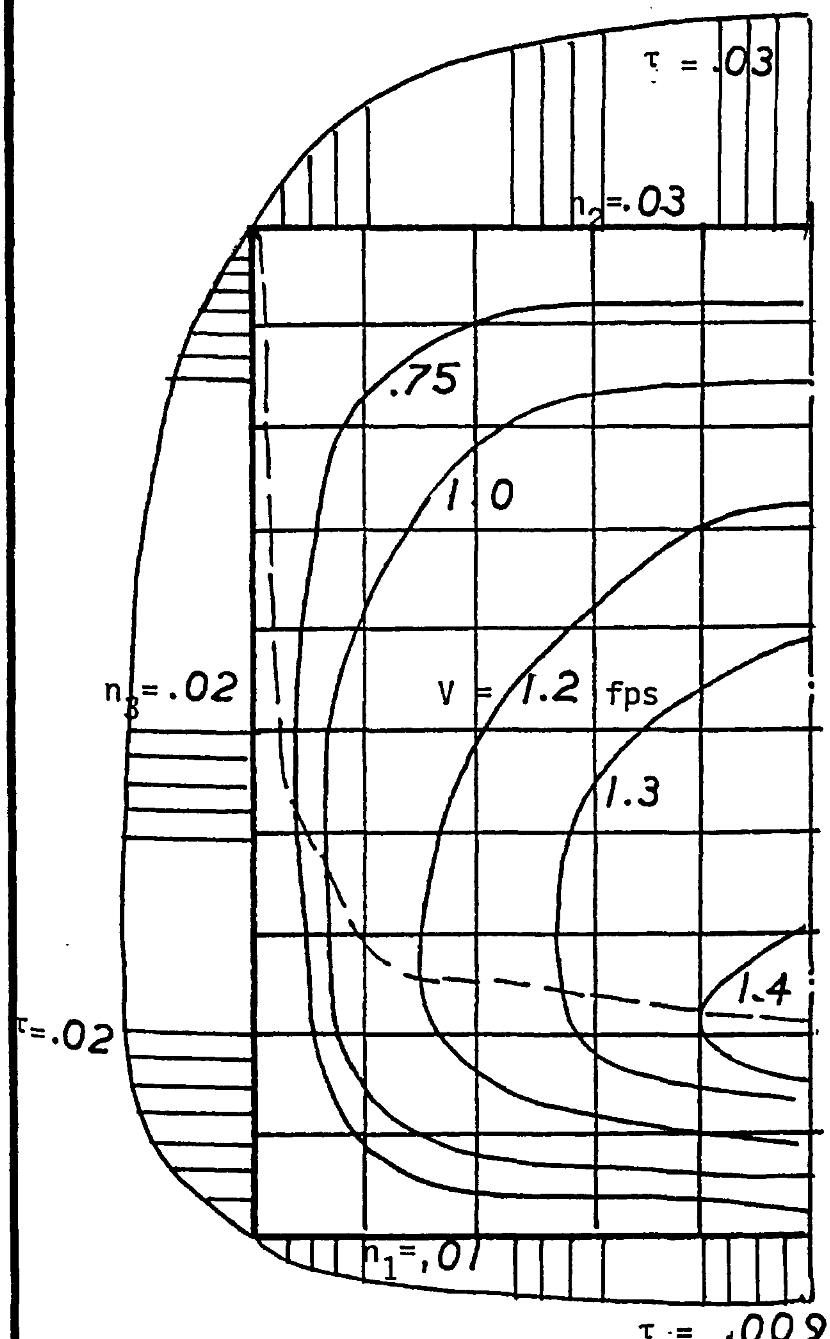

	Theory	Expected
Q	1.0	1.0
S	0.0012	0.0013
τ	0.08	0.079
n	0.02	0.021

Figure 5.9 : Effect of Side Roughness on Velocity Profile

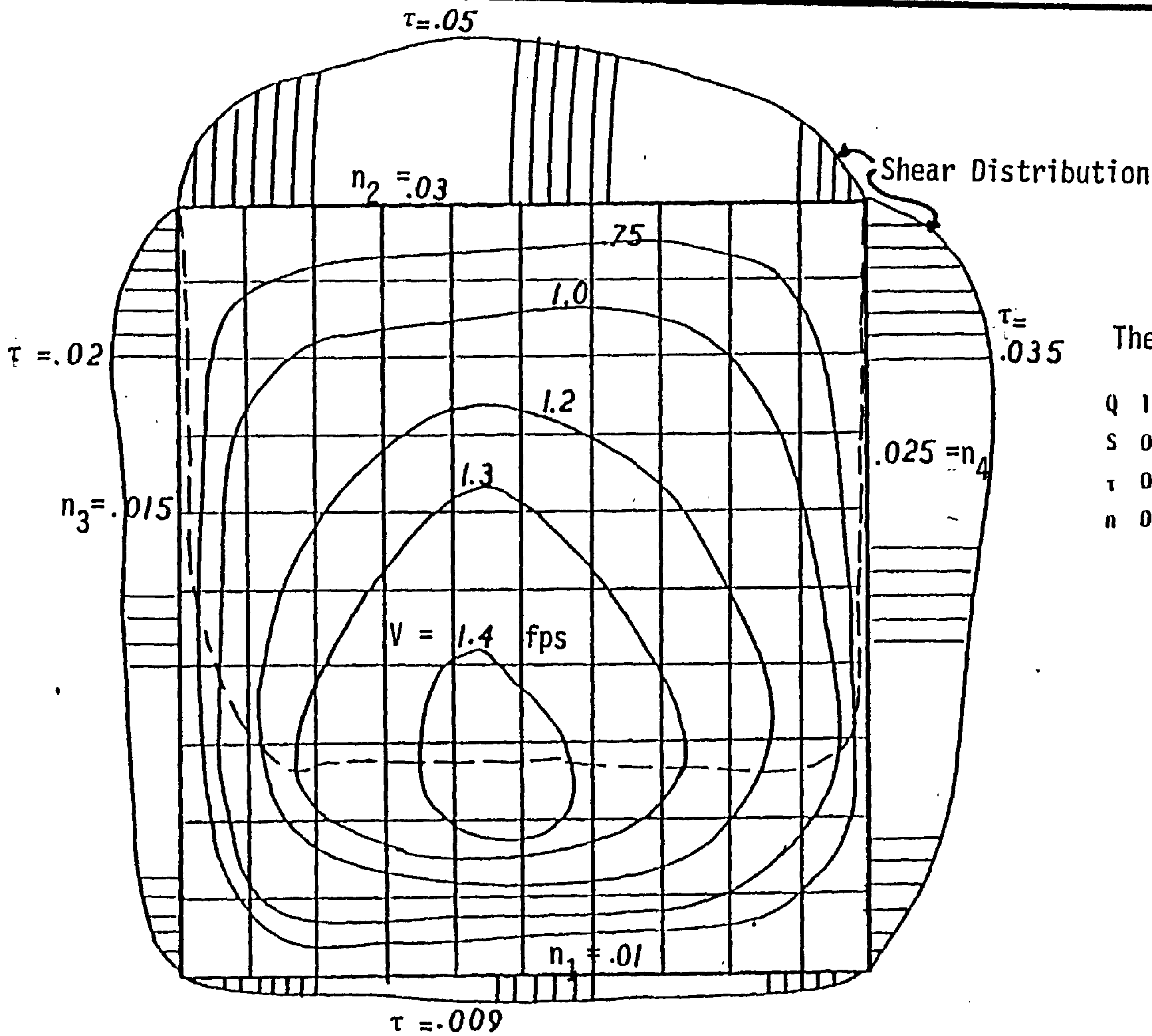

	Theory	Expected
Q	1.00	1.00
S	0.0013	0.00129
τ	0.079	0.08
n	0.02	0.021

Figure 5.10: Effect of Channel Size and Roughness on Velocity Profile

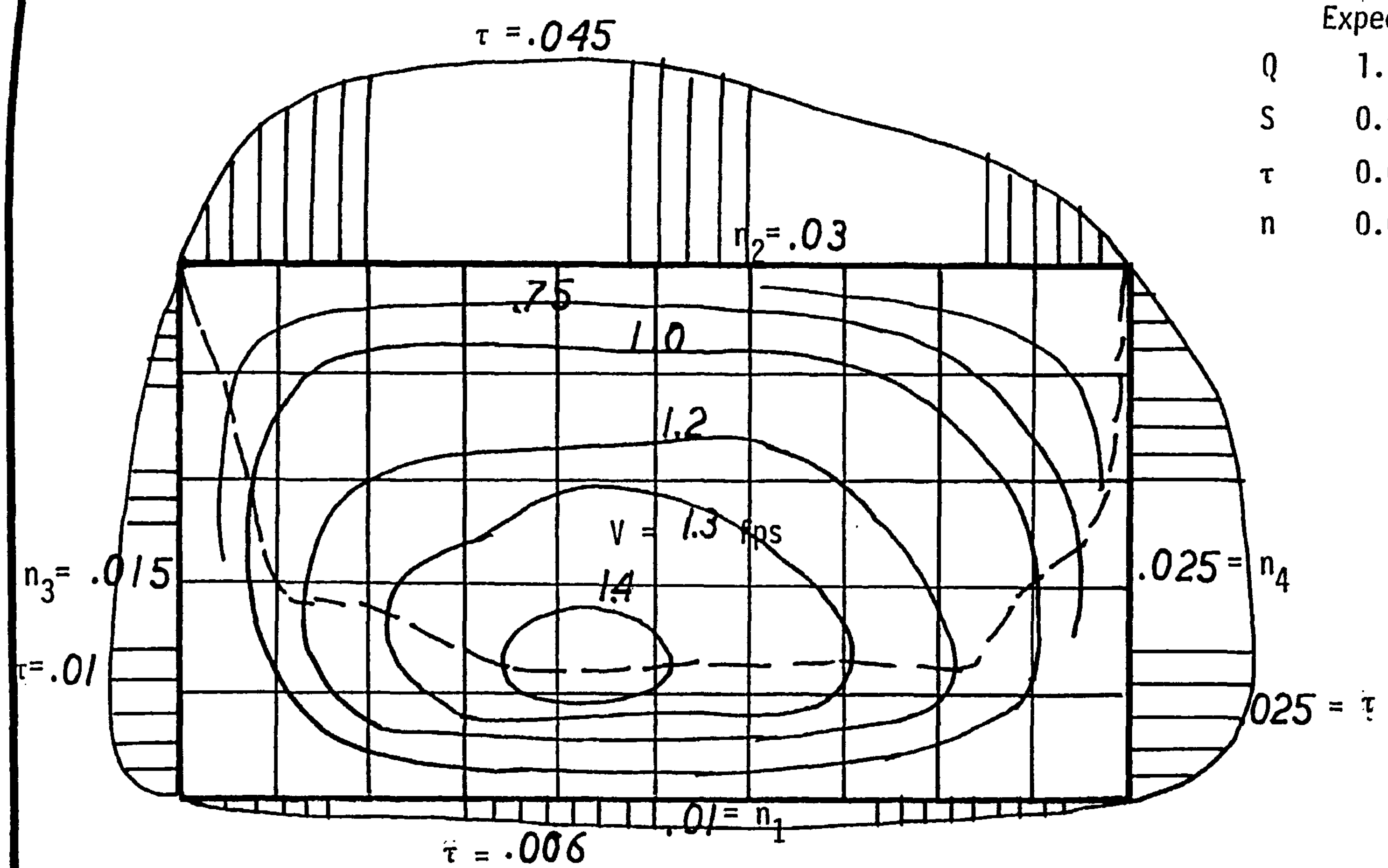

	Expected	Theory
Q	1.0	1.0
S	0.009	0.001
τ	0.011	0.01
n	0.0214	0.023

Figure 5.11: Effect of Size and Roughness on Velocity Profile

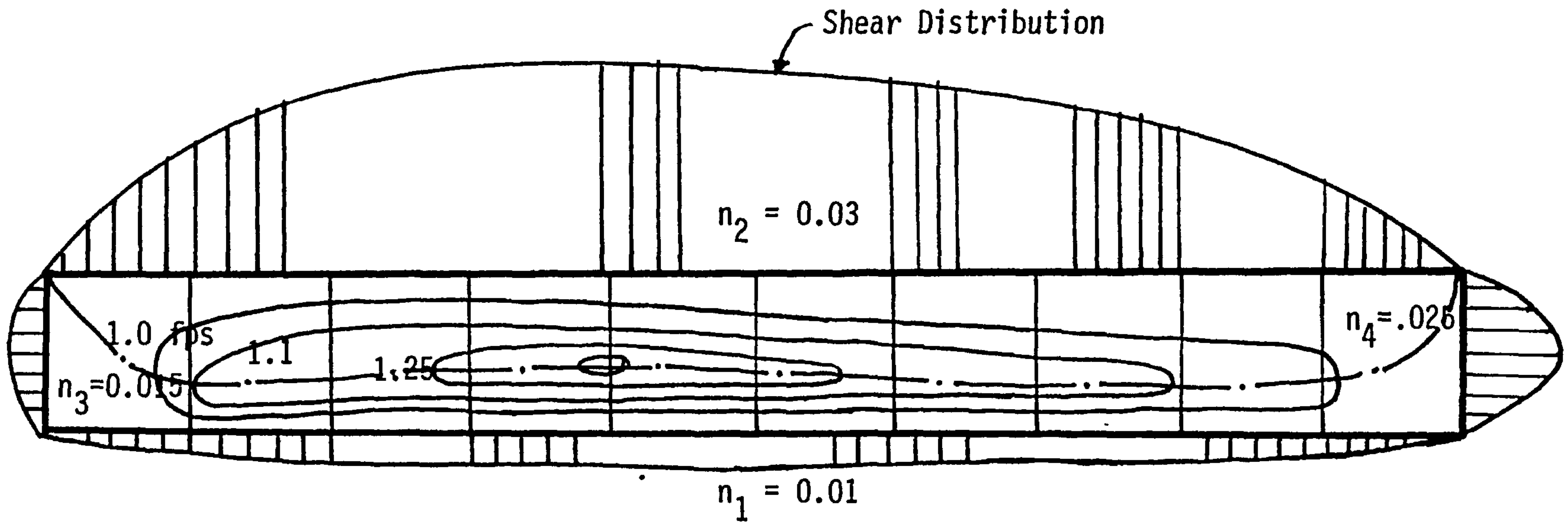

Figure 5.12: Effect of Channel Size on Velocity Profile

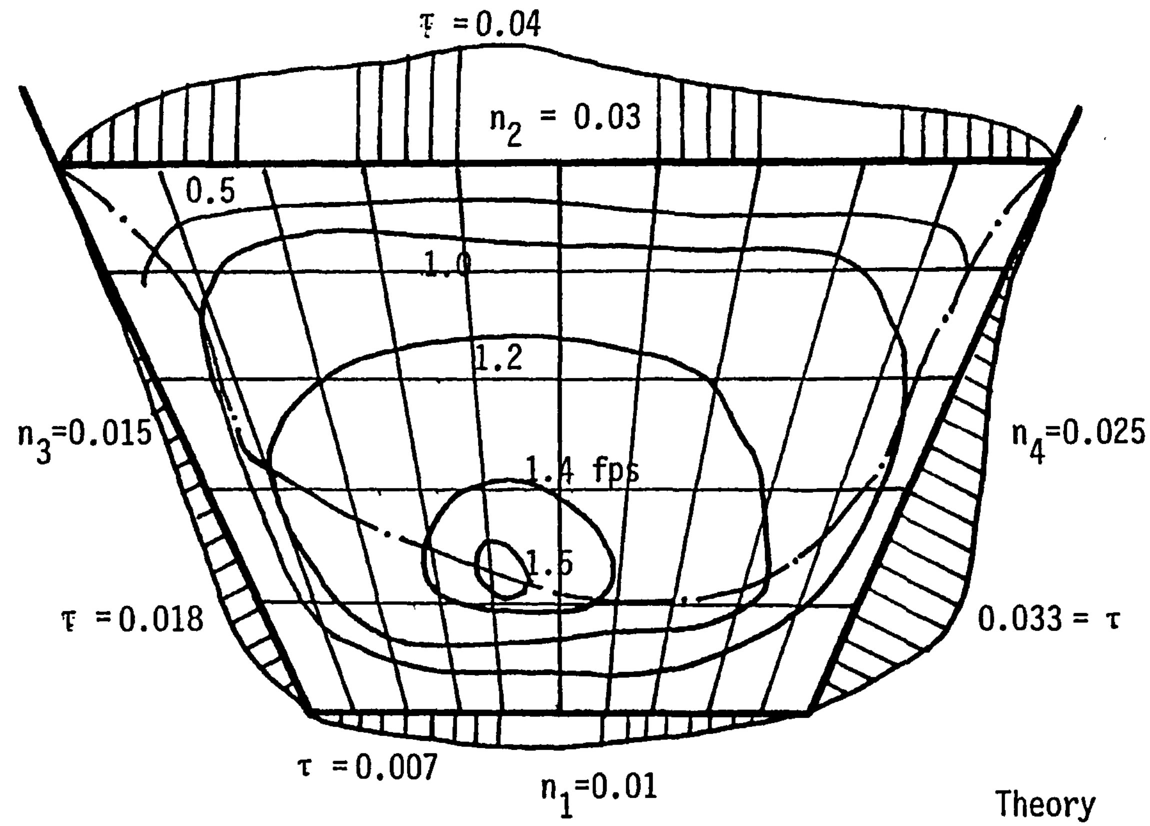

	Theory	Expected	
Q	1.50	1.50	cfs
S	0.001	0.0011	
n	0.021	0.023	

Figure 5.13: Trapezoidal Channel Velocity Profile

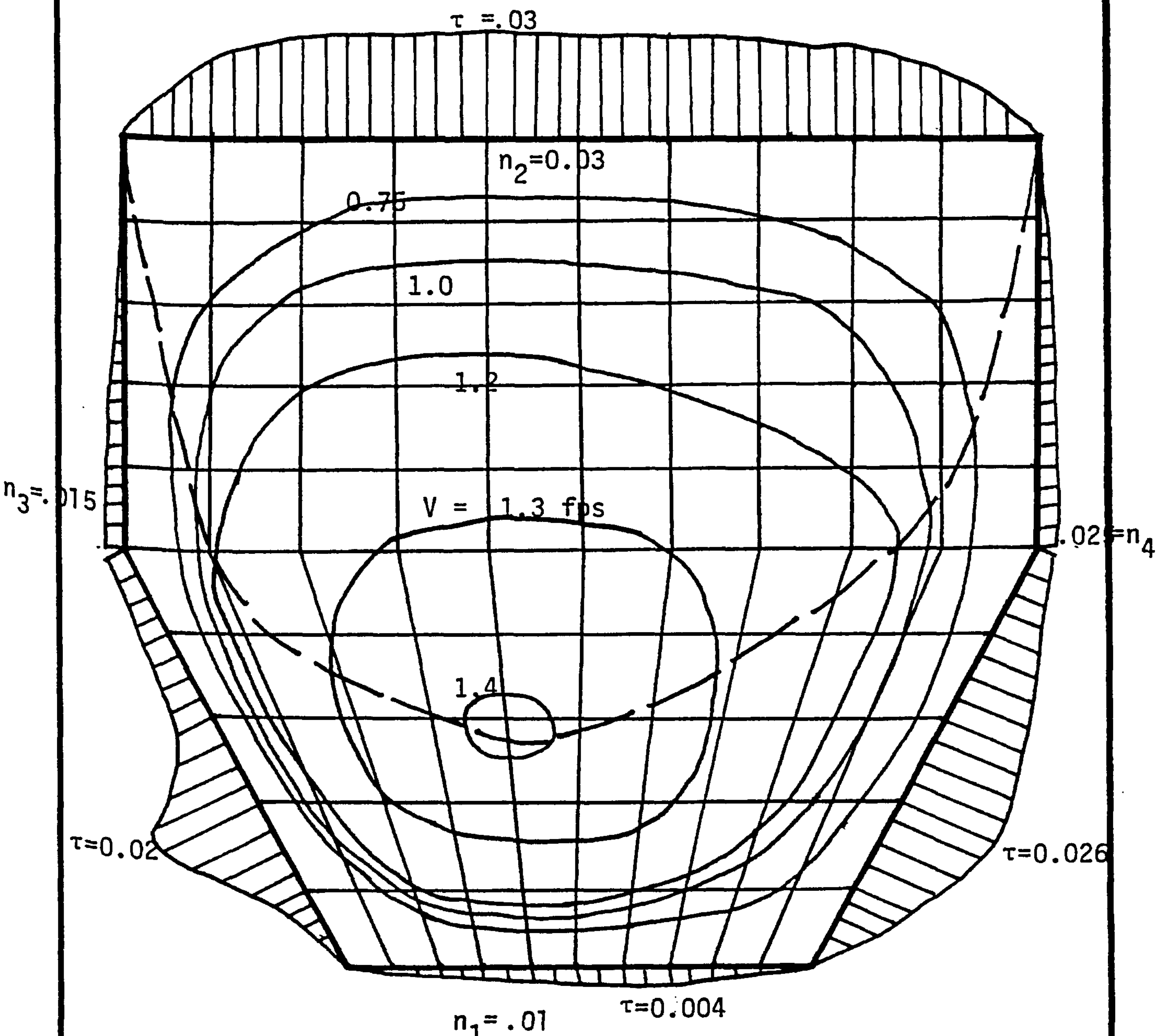

Q 3.0
S 0.0037

Figure 5.14: Compound Trapezoidal Channel Velocity Profile

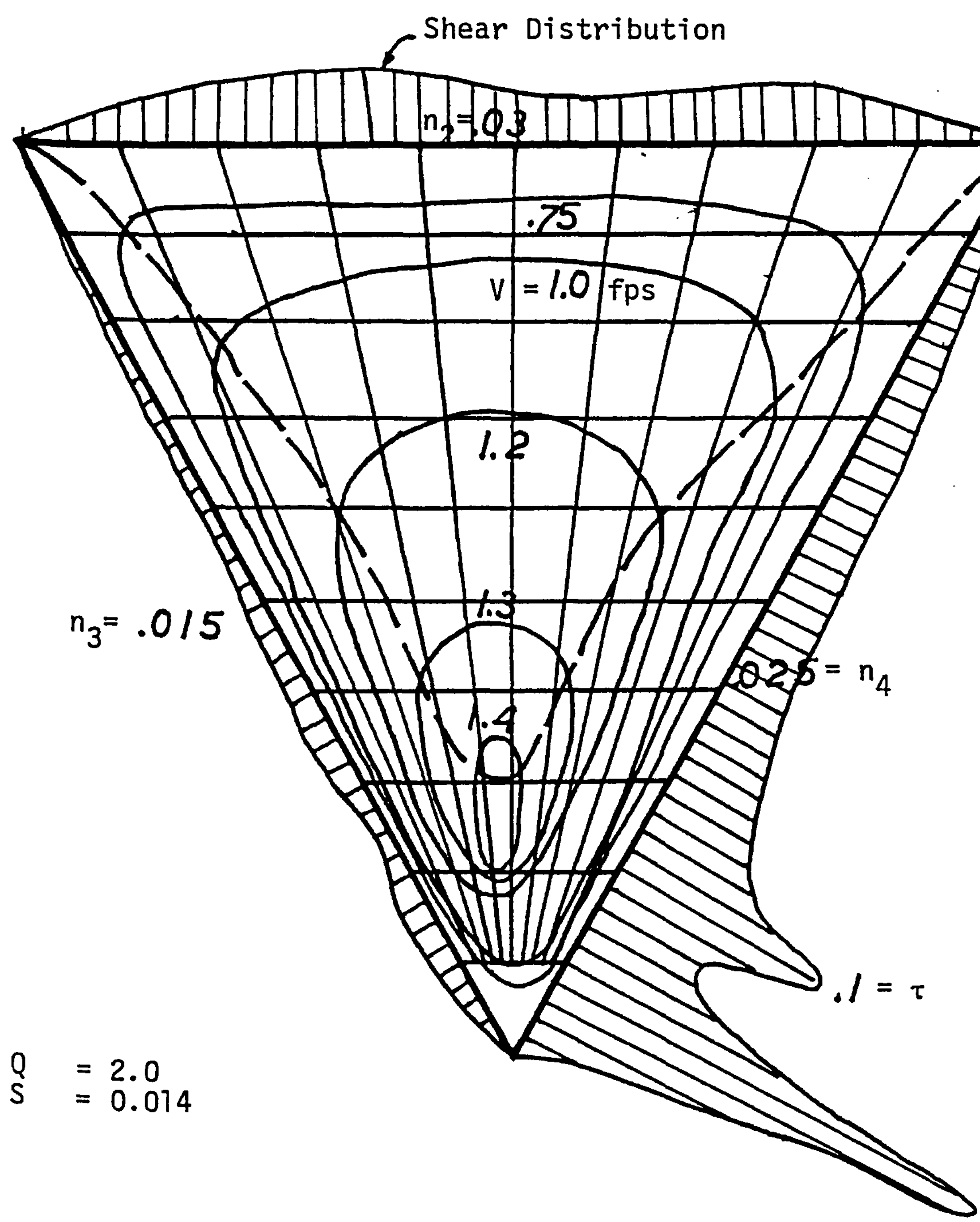

Figure 5.15 : Triangular Channel Velocity Profile

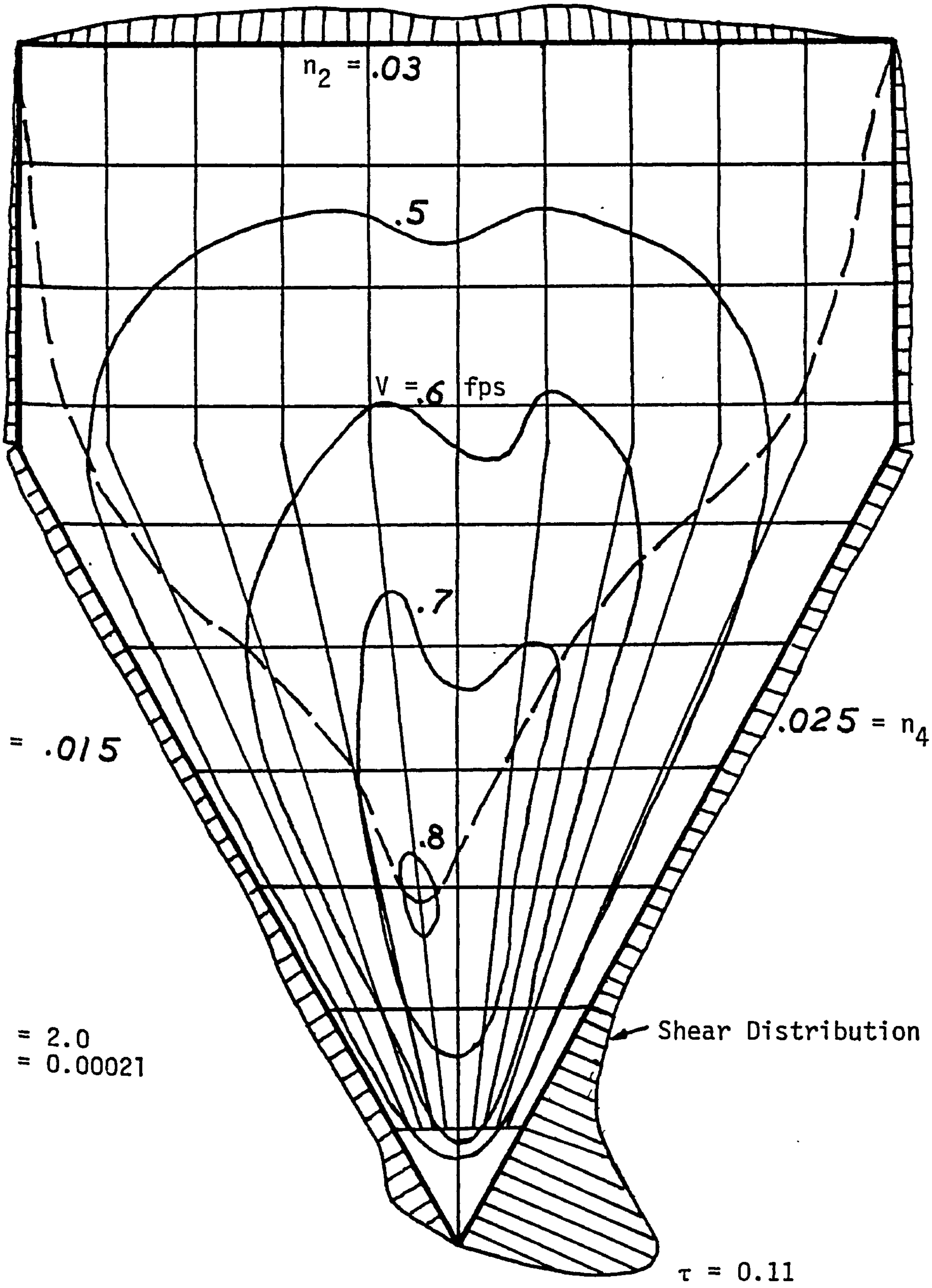

Figure 5.16: Compound Triangular Channel Velocity Profile

and the trapezoidal shapes.

The shear on the vertical sides of the compound cross-sections was very small and the major portion of the shear was taken by the sloping sides in these cases. The drop in the middle part of the velocity and shear distributions at the cover underside for triangular and compound triangular sections was due to the shape effect. The sudden sharp increase in the shear near the bottom in these two cross-sections was most likely due to the very high velocity gradient encountered at the bottom, since theoretically the bottom width diminishes at these locations.

The separation line was generally found to follow the channel cross-section except for the compound trapezoidal section where it was more parabolic in shape.

5.1.3 Comparison with Measured Results

The velocity profiles and composite roughnesses for different cross-sections were tested against those reported by Wong (43), Figures 5.17 to 5.20. No shear distributions were reported in his study; hence, they will not be discussed here.

It can be seen, from these comparisons, that the prediction is in good agreement with the measurements. The agreement also was good for the computed and measured composite roughnesses as well as the friction slopes.

5.2 Friction Factor For The Cover Underside

5.2.1 Determination of Constants:

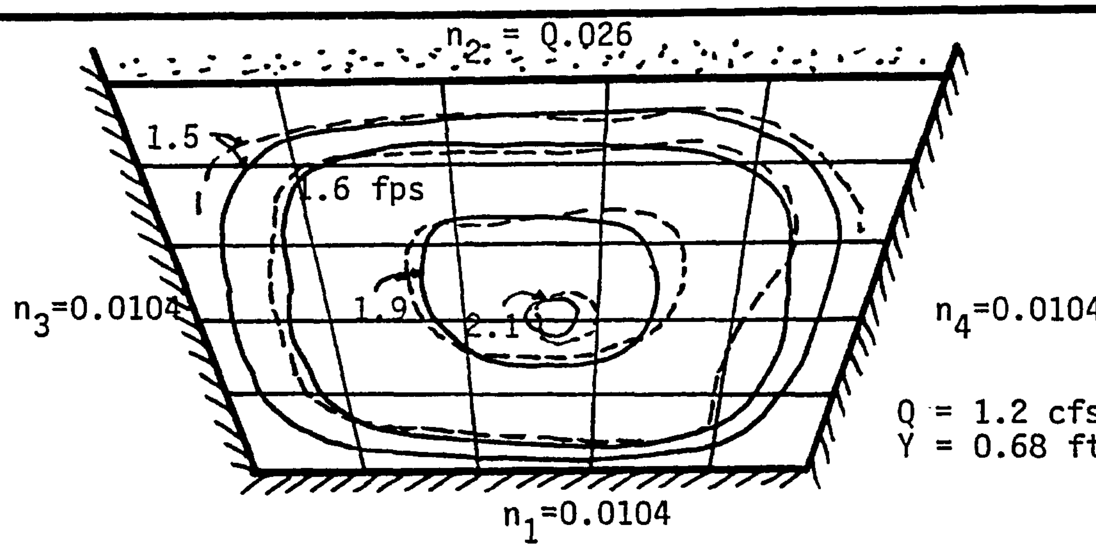

Figure 5.17: Velocity Comparison for Trapezoidal Channel

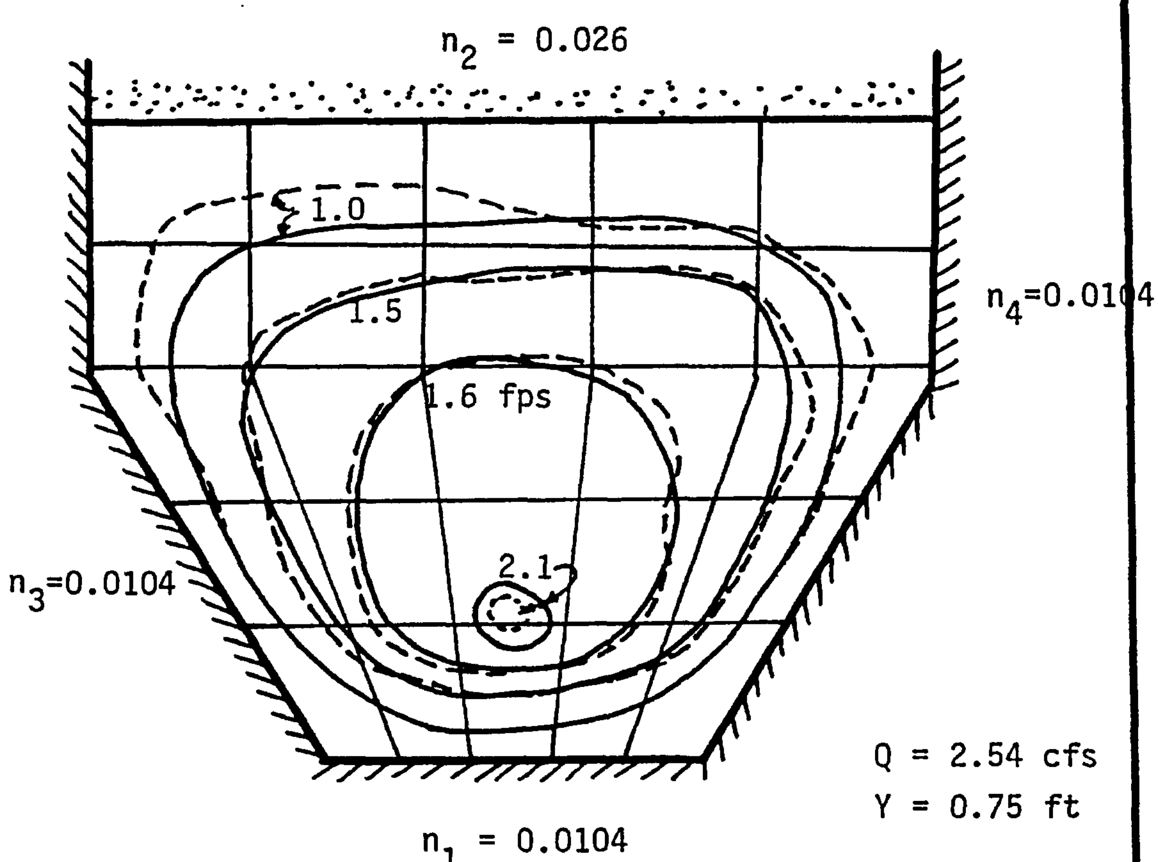

Figure 5.18: Velocity Comparison for Compound Trapezoidal Channel

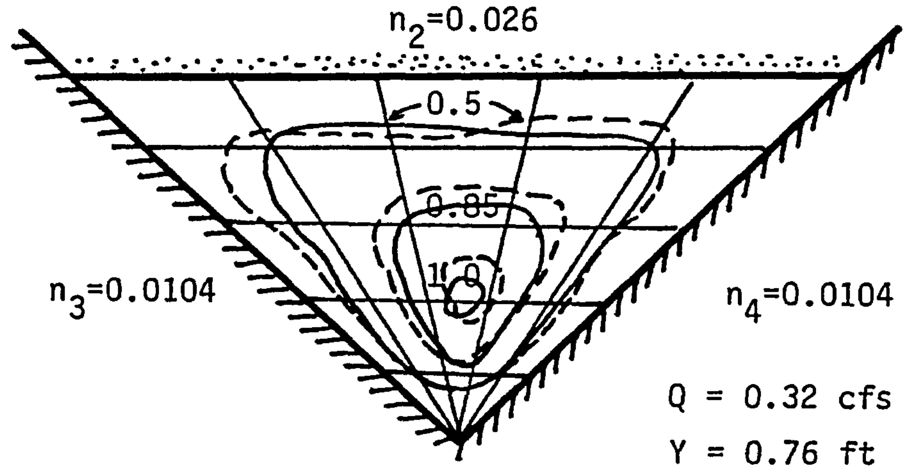

Figure 5.19: Velocity Comparison for Triangular Channel

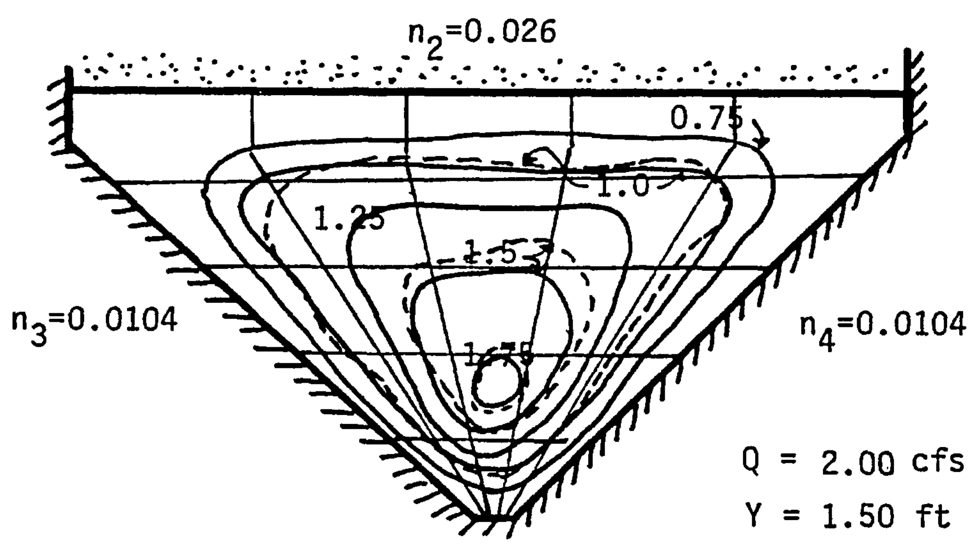

Figure 5.20: Velocity Comparison for Compound Triangular Channel

In Chapter III the general expression for the cover underside roughness was written as

$$C_{2m} = 6.25 + 5.75 \text{ Log } \frac{R}{K} - a \left(\frac{\Delta}{L} \cdot \frac{\Delta}{Y} \right)^{b} \qquad 3.29$$

The experimental investigation of the flat cover underside was used to verify the adopted skin friction expression. In these experiments the friction factor for the channel without cover was measured first; then, the cover was introduced and the channel composite roughness was measured. The equations developed in Appendix A were used to determine the cover underside Chezy's factor C_2 and hence the modified factor C_{2m} was obtained using the relation

$$C_{2m} = C_2 / \sqrt{g} \qquad 3.21$$

The underside configuration, in the form of rectangular roughness elements with height Δ and spacing L, was attached to the cover underside as explained in Chapter IV. The forementioned procedure was repeated to determine the cover underside friction factor C_{2m}, and the form resistance function δC_{2m} was found from the relation

$$\delta C_{2m} = 6.25 + 5.75 \text{ Log } \frac{R}{K} - C_{2m} \qquad 5.3$$

where the value of k for well finished wood was adopted as .001', following that reported by Chow (9). A summary of the experimental results is presented in Table E-1 in Appendix E.

The experimental data were plotted and a curve was obtained as shown in Figure 5.21. The least square method was used to develop an

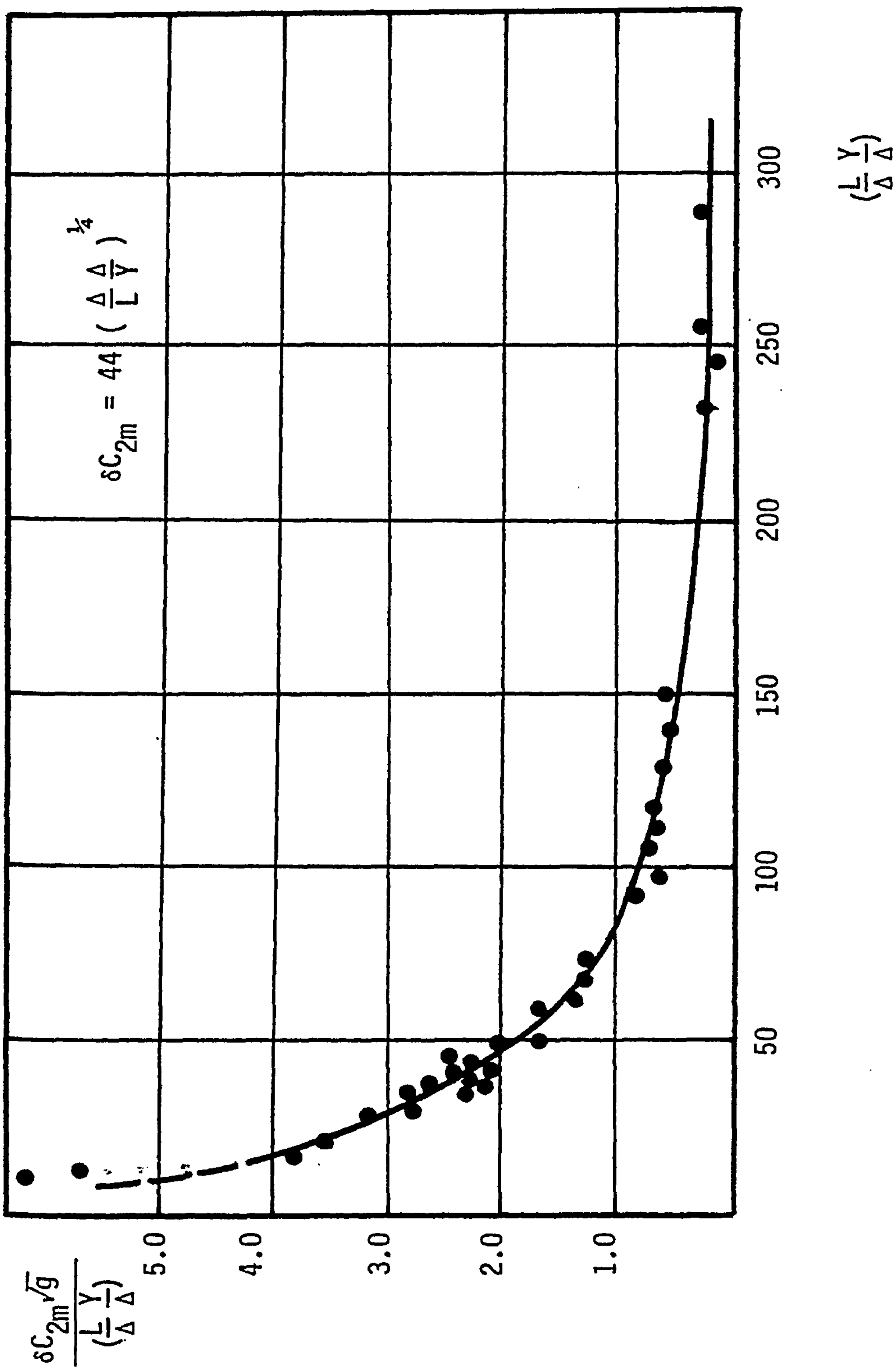

Figure 5.21: Form Resistance Function

expression for the form resistance function as

$$\delta C_{2m} = 44 \left(\frac{\Delta}{L} \cdot \frac{\Delta}{Y} \right)^{1/4} \tag{5.4}$$

with a correlation coefficient of 0.95.

The general expression for the cover underside friction factor can then be written in the form

$$C_{2m} = 6.25 + 5.75 \text{ Log } \frac{R}{k} - 44 \left(\frac{\Delta}{L} \cdot \frac{\Delta}{Y} \right)^{1/4} \tag{5.5}$$

which was found to describe well the experimental data for the range $(.29 < R < .34)$ and $(.0025 < \frac{\Delta}{L} \cdot \frac{\Delta}{Y} < .05)$. Further experimental and field data are needed to test the equation's applicability beyond the laboratory limits.

5.2.2 Behavior of the Friction Factor Equation

The first two terms in Equation 5.5 express the skin friction contribution to the total cover underside resistance. This expression was adopted from the literature (8), (9), (31) where its behavior is well documented and it will be not discussed further here.

The last term in Equation 5.5 represents the change in the total cover underside friction factor due to the existence of the underside configuration. The general tendency of this term is to decrease the C_{2m} value by retarding the flow and can be explained by the added resistance of such a configuration. In the absence of such forms this term will vanish and the skin friction will be the only source of resistance.

It can be seen from the form resistance expression that a cover with steeper underside waves will cause more resistance than a cover with a flatter bottom. On the other hand, the projected depth ratio Δ/Y reflects the degree by which the flow is affected by the disturbance caused by the forms. As the channel depth increases the disturbance zone relatively decreases and less resistance should be expected.

The added form resistance increases with ($\frac{\Delta}{L} \cdot \frac{\Delta}{Y}$) value as shown in Figure 5.21. Since the added resistance cannot increase indefinitely, it is expected that the δC_{2m} value will increase to a certain limit at which a type of a skimming flow (9) will appear, and the resistance will be limited to the quasi-smooth one. This phenomenon was not investigated in this research.

5.3 Underside Configuration

In Chapter III the general equation for the underside configuration, Equation 3.31, was developed along with the necessary expression for the local friction slope S_f.

A frictionless model and an average friction slope model were tested and the results were found to be physically impossible (e.g. negative flow depth). This confirmed the necessity of using the local friction slope to obtain realistic results.

Different methods can be used to integrate the general equation. In the following articles the direct integration is presented for the case of a flat-bed. A modified step-by-step method, similar to the one used with the general dynamic equation, was adopted in solving the triangular and dune bed-form cases. A comparison between the predicted and the experimental data will be presented for each case.

5.3.1 Direct Integration Method

This is the case of a channel with flat-bed sloping at a constant value. The general differential equation in this case, after the proper simplifications, is written as

$$\frac{dY}{dx}\left(\frac{\lambda-1}{\lambda}\ \frac{H-\eta_b}{Y} - B / Y^3 + C \right) = S_o \left((1+\lambda)(H-\eta_b)/ Y - 1 - \lambda + \lambda / S_g \right) \qquad 5.6$$

which can be directly integrated to yield

$$\frac{EA - E^3B - CD^3}{E^2D^2}\ \mathrm{Ln}(D + EY) + \frac{BE + CD\ Y^2}{DE\ Y} + \frac{EB}{D^2}\ \mathrm{Ln}\ Y = X + \mathrm{Constant} \qquad 5.7$$

where $A = (H - \eta_b)\ (\lambda - 1) / \lambda$

$$B = (q^2 / (g\ S_g))\ (V_1^{\,2}/V^2 + V_2^{\,2}/V^2 - 1)$$

$$C = 1/\lambda + 2\lambda/(S_g\ (1+\lambda)) - 2 \qquad 5.8$$

$$D = S_o\ (H - \eta_b)\ (1+\lambda)$$

$$E = S_o\ (\lambda/S_g - 1 - \lambda)$$

and the integration constant can be estimated for any known boundary condition. Substituting the local values at certain distance X, and solving, the flow depth Y can be obtained. The cover thickness η_s can then be estimated from the relation

$$\eta_s = H - Y - \eta_b \qquad 3.34$$

The successive application of the equation at different intervals will result in the longitudinal profile of the underside configuration.

In Figure 5.22 experimental and theoretical results of the underside configuration corresponding to a flat bed of 0.005 slope were drawn. A good agreement was obtained for the tested case.

5.3.2 Direct Step Method

The integration of the general differential equation, Equation 3.36, is sometimes difficult because of the shape of the bed-forms. In this case a numerical integration becomes necessary. The direct step method was adoped here because of its simplicity.

Table 5.1 illustrates the procedure followed in the application of the method. The values of $d\eta_b/dx$ are assumed to be known along the channel. If at any point (X_o) the flow depth (Y_o) is known, the value of $(dY/dx)_o$ can be calculated and the expected Y at (X_o + dx) can be determined as

$$Y_{(X_o + dx)} = Y_o + (dY/dx)_o \, (dx) \qquad 5.9$$

Then Equation 3.34 can be used to predict the cover thickness.

The solution is then progressed along the channel to obtain the underside configuration. If an initial solution cannot be found, the point at the leading edge of the cover, $\eta_s = 0$, can be used if its location is known. If this point was far upstream from the reach of

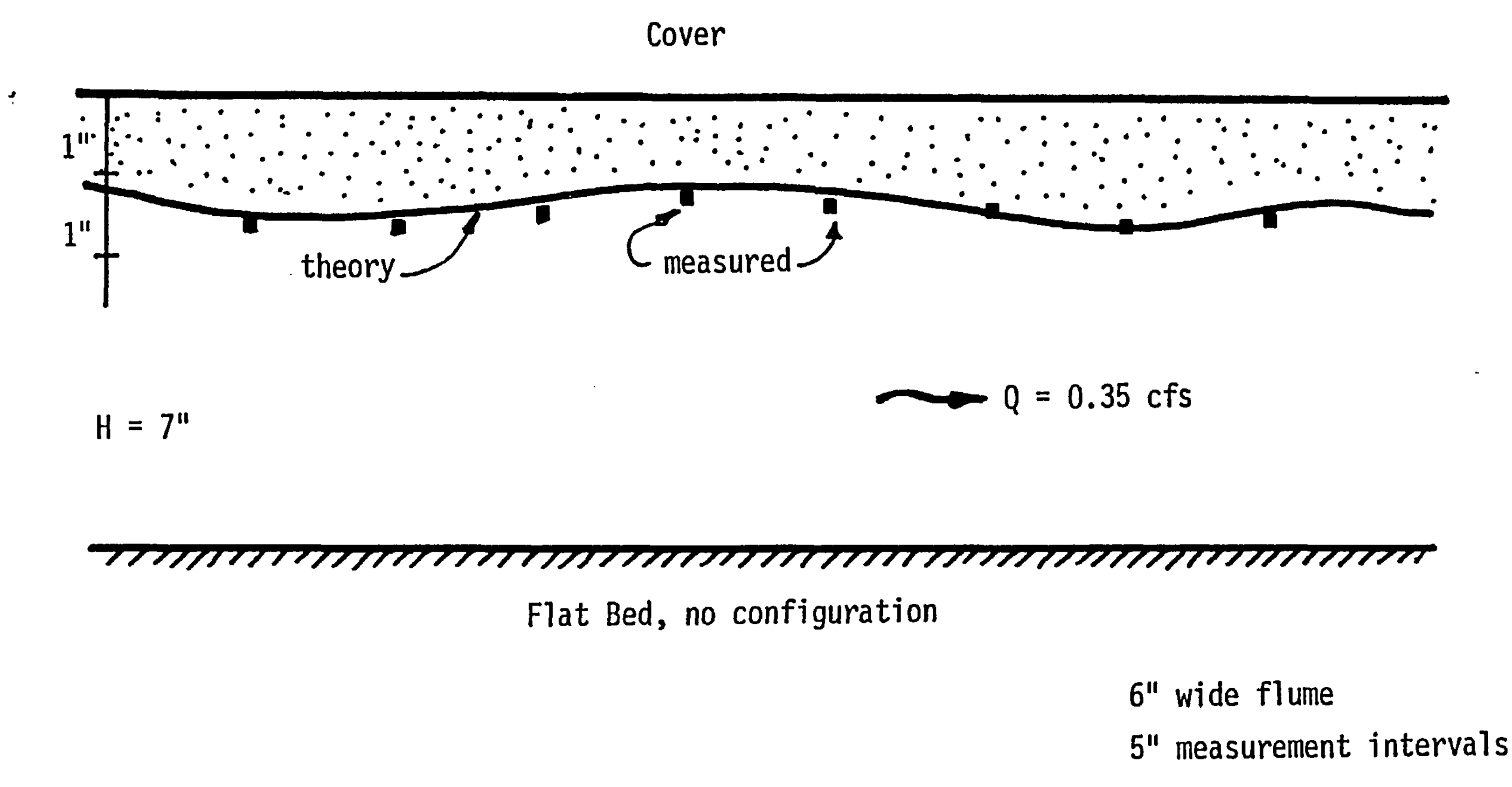

Figure 5.22: Underside Configuration, Flat Bed

	DATA			CALCULATIONS			
No	X	$\bar{b}$	$\frac{dn_b}{dx}$	Y	n_s	$\frac{dy}{dx}$	Remarks
0	x_0	n_{b0}	$\left.\frac{dn_b}{dx}\right\rvert_0$	Y_0	$n_{s0} \rightarrow$	$\left.\frac{dy}{dx}\right\rvert_0$	Given Line
1	x_1	n_{b1}	$g \left.\frac{dn_b}{dx}\right\rvert_1$	Y_1	$n_{s1} \rightarrow$	$\left.\frac{dy}{dx}\right\rvert_1$	
2	x_2	n_{b2}	$g \left.\frac{dn_b}{dx}\right\rvert_2$	$Y_2 \rightarrow$	$n_{s2} \rightarrow$	$\left.\frac{dy}{dx}\right\rvert_2$	
3	x_3	n_{b3}	$g \left.\frac{dn_b}{dx}\right\rvert_3$	Y_3	....		

Δx can be changed for each step.

Δx should be reduced at the maximum and minimum points of n_s (i.e. crests and troughs)

TABLE 5.1: Details of Direct Step Method Calculations

interest, or cannot be defined, an estimate of Y_0 can be assumed and the solution should be iterated to establish the final configuration.

In this solution the forward difference scheme was used. The model results might improve if the central or backward differences are adopted; this depends on the particular problem under investigation.

Special care should be given to the chosen step size dx due to the wavy nature of the underside configuration. A long step can mislead the solution by underestimating the rapid change in the slope. Generally the shorter the step the more accurate the solution will be.

The following examples demonstrate the application of this method to channel flow with different bedforms.

1. <u>Triangle Bed-Form</u>

In this article , the underside configuration of a loose cover in the presence of triangle bed-forms is studied. Table 5.2 illustrates the detailed calculations for a typical experiment. The last two columns were added to show the corresponding experimental results while Figure 5.23 shows the computed and measured configurations.

The measured values at station 0 were used as initial values for the solution. The computations were carried at one inch intervals while the measurements were taken every five inches. The datum was taken at the lowest point in the bed to avoid any negative η_b values. The bed slope $d\,\eta_b/dx$ at crests and troughs was assumed to be zero since the tangent is actually horizontal at these locations. As can be seen from the graphs, the experiments and the theory agree very well.

2. <u>Dune Bed-Form</u>

The underside configuration of the cover was studied in the

X	η_b	dy/dx	Y	dy/dx	η_s	Y_m	η_{sm}
0	1.55	0.22	6.10	0.180	1.40	5.97	1.39
1	1.77	0.22	5.92	0.179	1.31		1.31
2	2.00	0.00	5.74	-0.005	1.25		
3	1.50	-0.50	5.75	-0.510	1.75		
4	1.00	-0.50	6.25	-0.480	1.73		
5	0.50	-0.50	6.73	-0.470	1.76	6.85	1.31
6	0.00	0.00	7.20	-0.006	1.79		
7	0.22	0.22	7.21	0.180	1.57		
8	0.44	0.22	7.03	0.179	1.52		
9	0.66	0.22	6.85	0.178	1.48		
10	0.88	0.22	6.67	0.178	1.44	6.39	1.625
11	1.11	0.22	6.50	0.177	1.39		
12	1.33	0.22	6.32	0.176	1.34		
13	1.55	0.22	6.14	0.175	1.31		
14	1.77	0.22	5.96	0.175	1.26		
15	2.00	0.00	5.78	-0.006	1.21	5.54	1.48
16	1.50	-0.50	5.78	-0.500	1.71		
17	1.00	-0.50	6.28	-4.810	1.72		
18	0.50	-0.50	6.76	-0.466	1.74		
19	0.00	0.00	7.22	-0.006	1.78		
20	0.22	0.22	7.23	0.178	1.55	7.06	1.76
21	0.44	0.22	7.05	0.177	1.50		

all dimensions in inches.

TABLE 5.2: Calculations with Triangular Bed-form

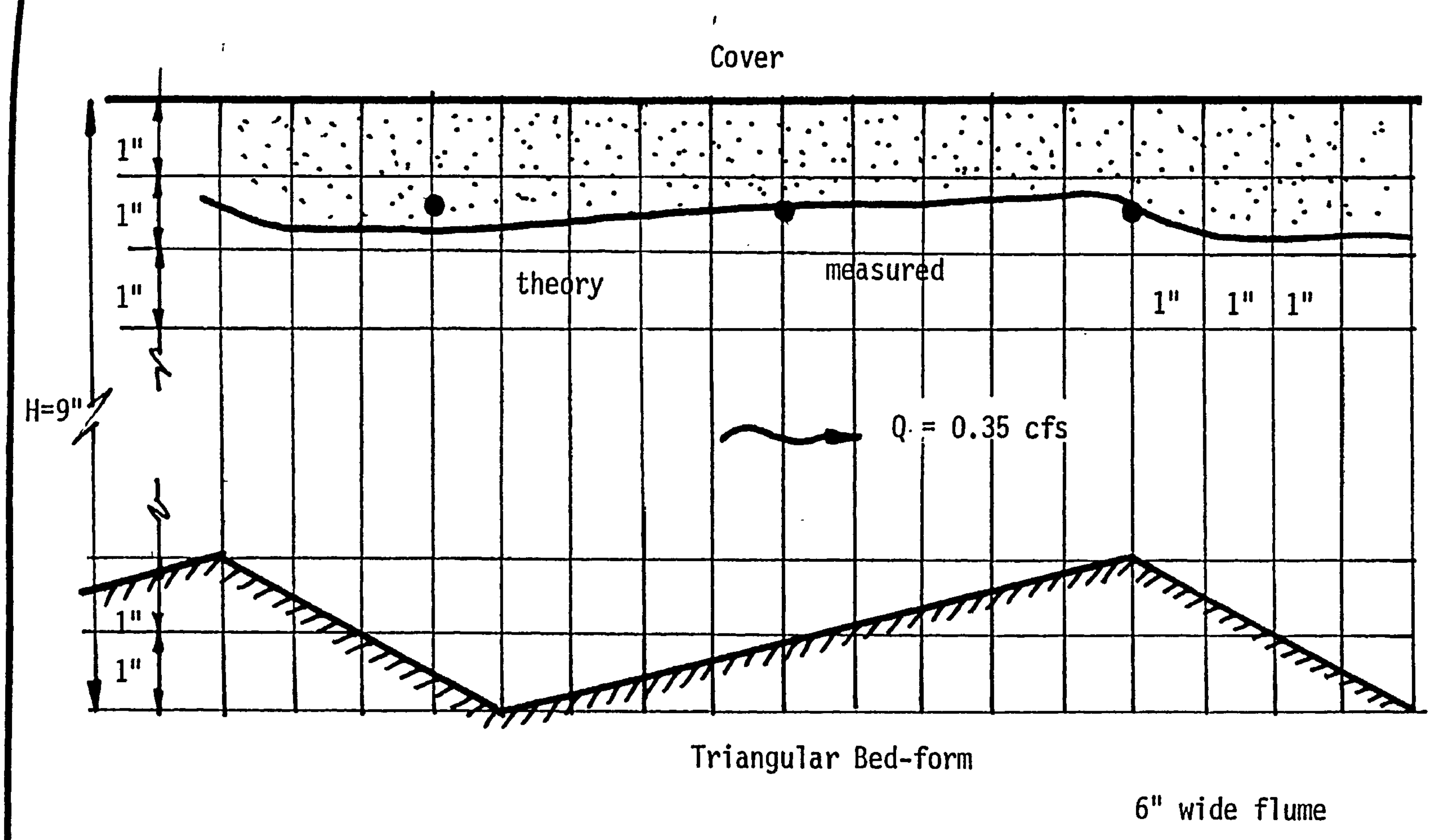

Figure 5.23: Underside Configuration, Triangular Bed-form

presence of immobile dune bed-forms as explained in Chapter IV. The same basic assumptions used in the triangular bed-forms solution were applied here.

The measurements were carried out at three in. intervals while the calculations were performed at one in.. Figures 5.24 and 5.25 reproduce pictures of the experimental results, while Figure 5.26 shows the experimental and computed results which were found to agree.

5.3.3 General Remarks on the Predicted Configuration

From the figures it is generally noticed that a uniform regular wave configuration existed. The increase of the cover thickness with the flow-rate can be explained by the stability requirements. The wave length also increased with the discharge.

It is also noticed that the waves were steeper in the downstream face than the upstream one. This may be attributed to the bed-form influence since both the triangular and dune bed-forms were shaped in that way.

An ice load, similar to the sediment bed-load, was noticed to increase with the flow. The cover particles moved only by intermittent leaps and/or by a creeping process. Neither saltation nor any kind of suspended movements were observed due to the high buoyancy force on the light particles.

Although both the flow and the bed-forms were assumed to be two dimensional, a change in phase angle between the central and the side sections of the configuration, Figure 5.24, was noticed. This change was attributed to the effect of the sides.

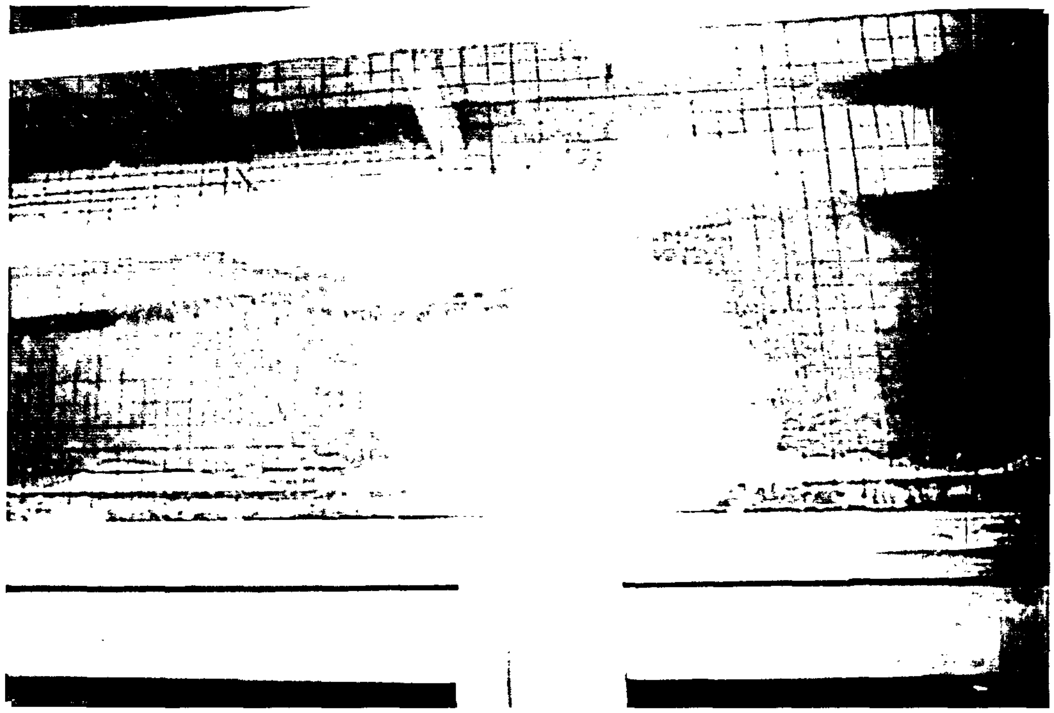

Figure 5.24: Underside Configuration for Dune Bed-form

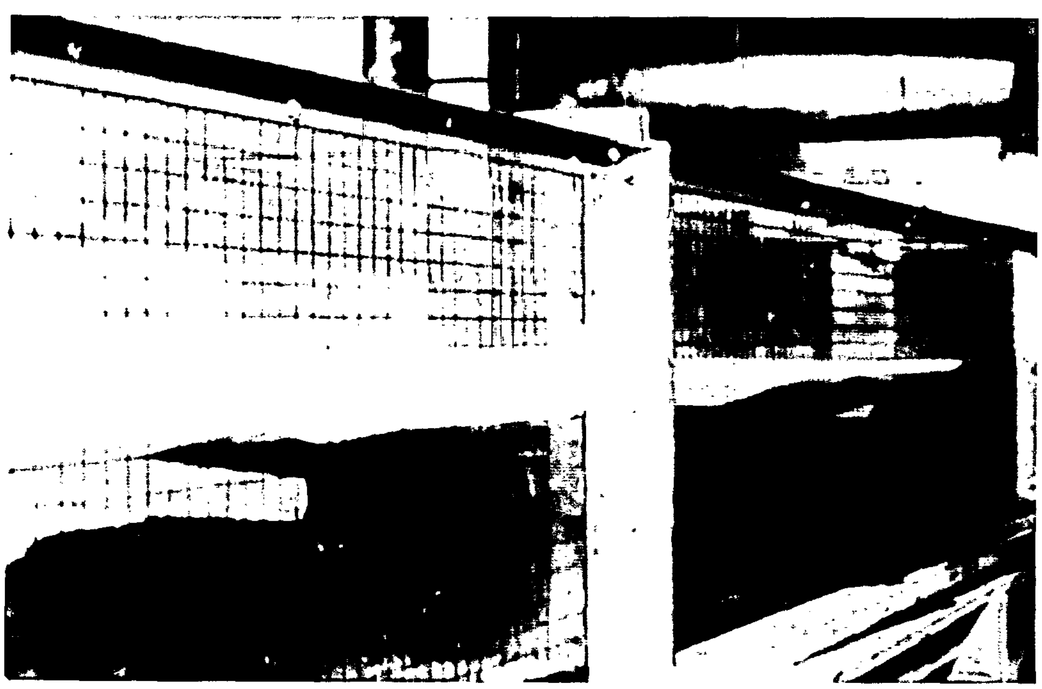

Figure 5.25: Underside Waves for Dune Bed-form

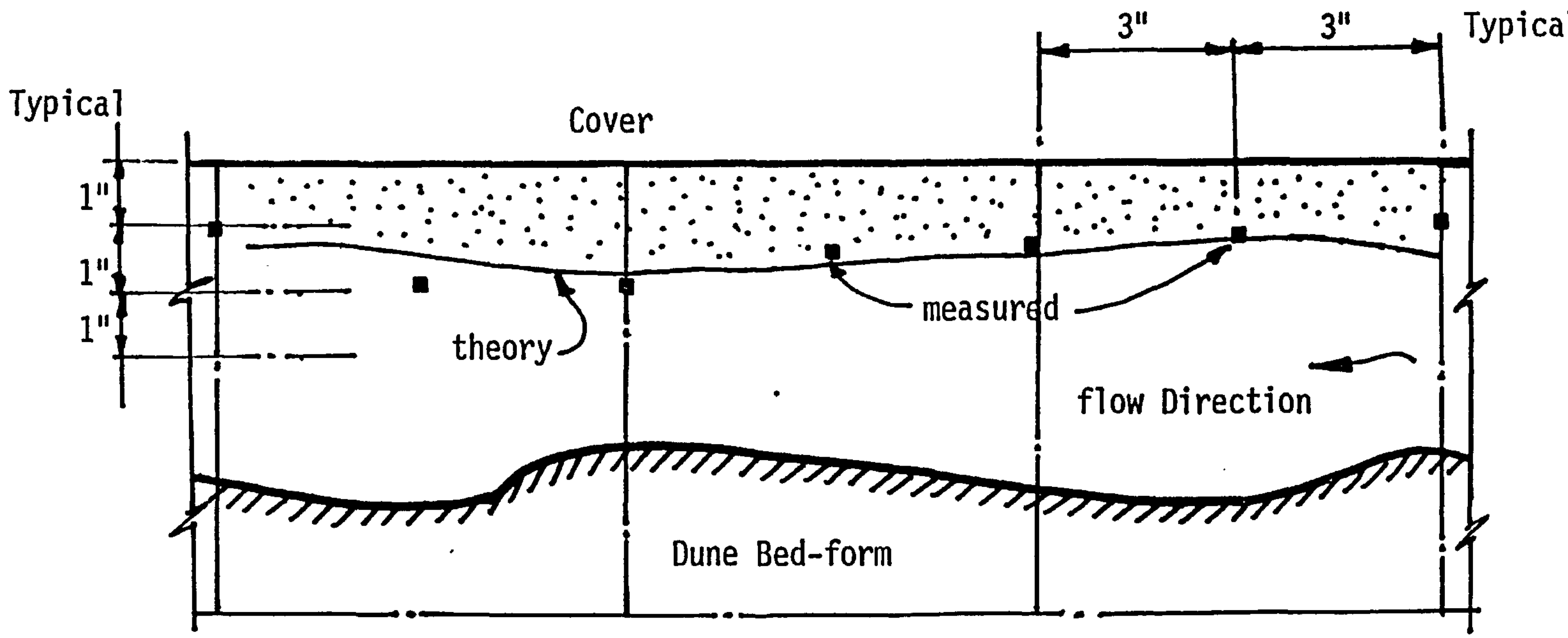

Q = 1.0 cfs
H = 15.8 inches

Figure 5.26: Underside Configuration; Dune Bed-form Example

The difference in phase between the cover configurations at different longitudinal sections gives rise to different cross-sectional shapes. This can be seen in Figure 5.27 cases 1 to 6. The cover may be thicker at the central part, case 5, or at the sides, case 4. It may consist of one wave as in case 4 or more than one wave, such as cases 1,2 and 3. The reason for these differences is the change in phase explained before.

5.3.4 Three-Dimensional Underside Configuration

In this article the experiments carried out in the 56" wide flume are analyzed. A typical set of measurements is presented in Figure 5.28. The velocity profile established in this flume consisted of a main stream in the central portion of the channel. Then the flow was reduced towards the sides. The inlet condition was arranged in such a way that it will amplify and maintain this transverse flow pattern. The typical measured velocity pattern for the test results of the model is shown in Figure 5.28.

In the longitudinal direction it can be seen that the cover edge assumes a very gentle slope. This slope varies with the flow rate; it is much gentler at higher velocities. The wave height decreases as the velocity increases; this can be seen by inspecting the central and side portion of the channel. At high flows, the cover in some runs was found to diminish at certain locations along the main stream forming a partial cover. This was usually accompanied by a thickening of the other parts of the cover.

An approximate solution was tried using the measured velocity profiles for vertical strips of the channel cross-section, but further

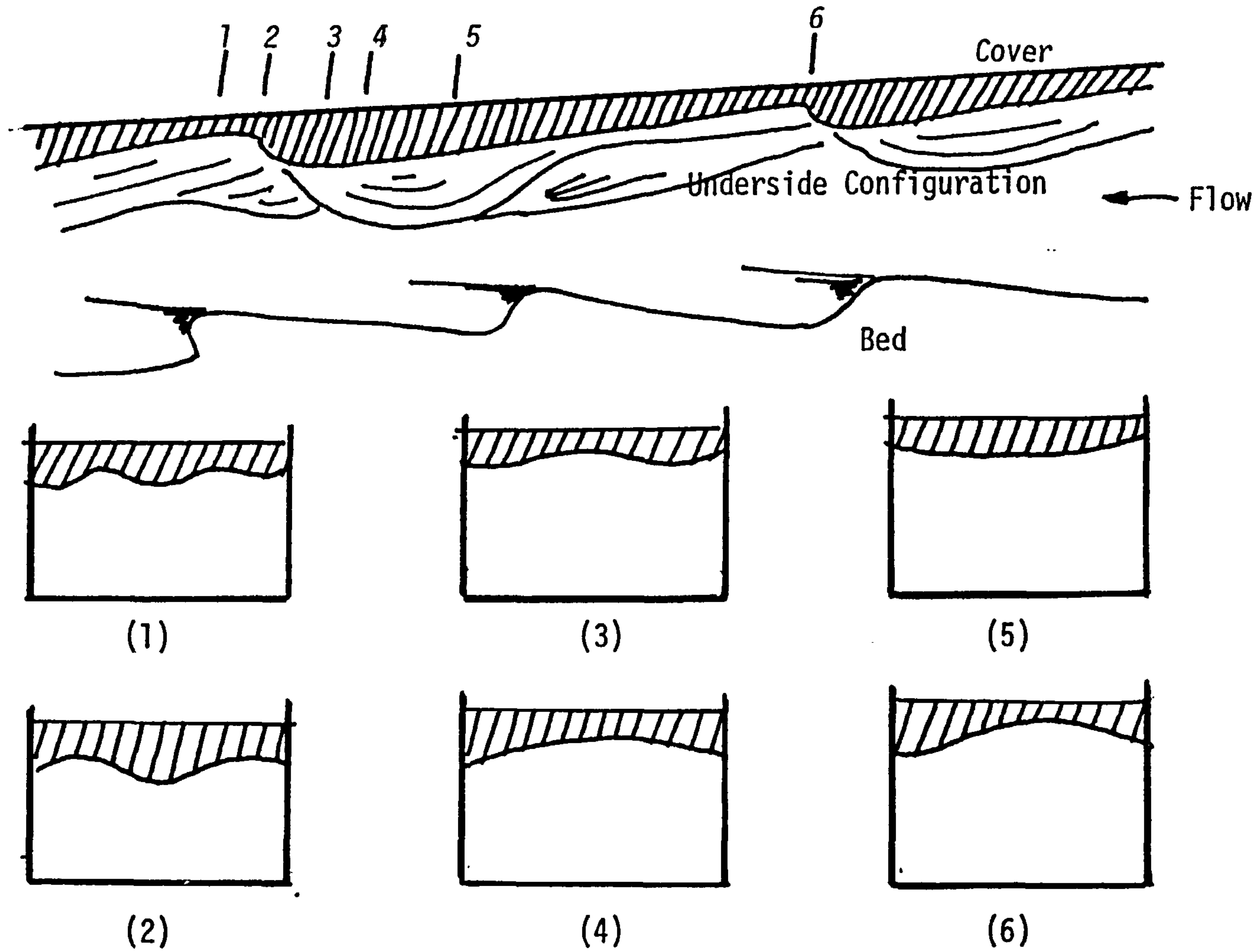

Figure 5.27: Underside Configuration - Dune Bed-Form

Run # 1 Q = 1.50 cfs

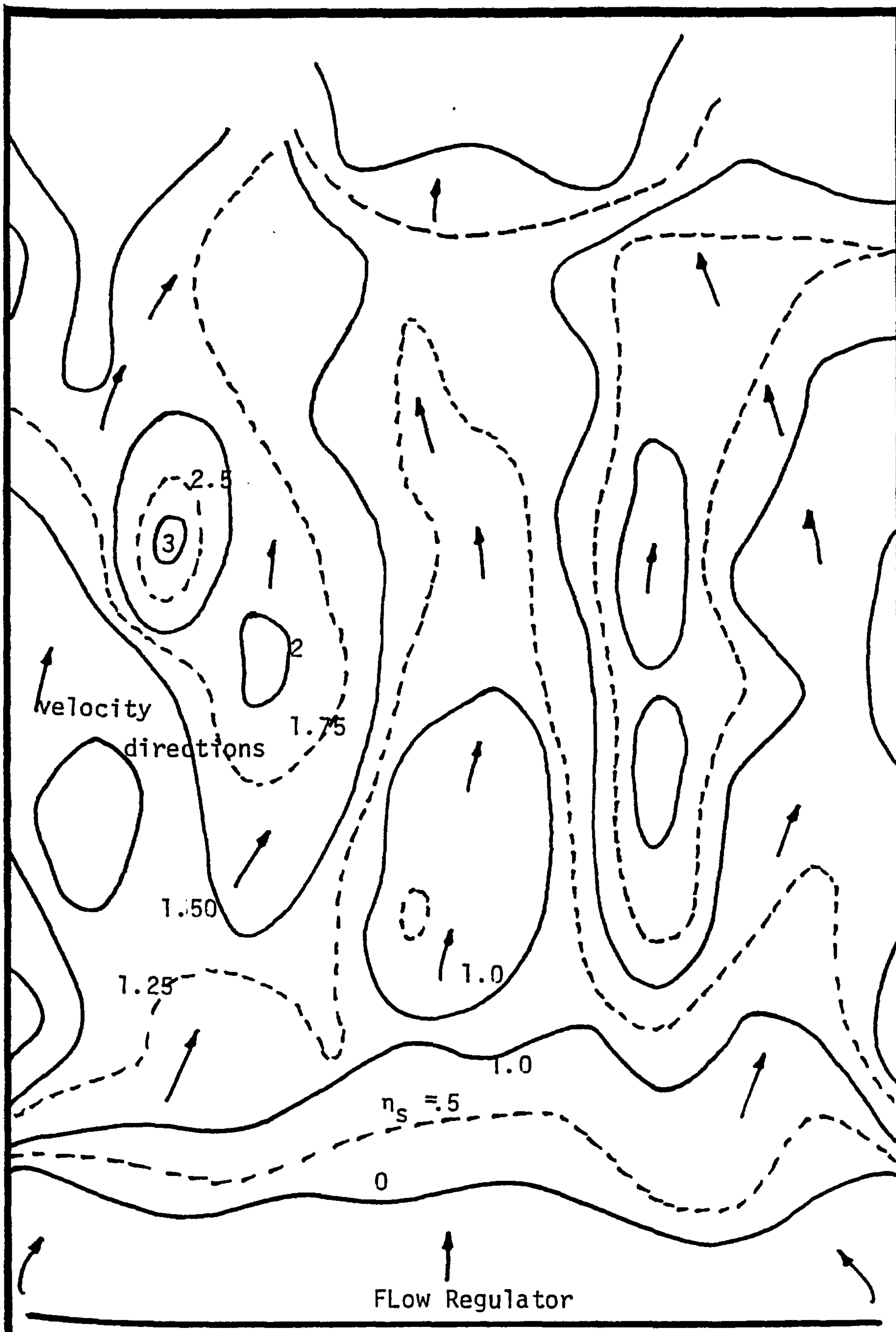

Figure 5.28: Three Dimensional Configuration

investigations are needed to enable a complete judgement on the success of this technique.

5.4 Equilibrium Thickness and Extension Mechanism

In this article the equilibrium thickness and extension mechanism of the cover are discussed based on the mathematical model presented in Chapter III.

5.4.1 Behavior of the model

The basic concept used in this model was the block's freedom to move in any direction as long as it stayed in contact with the cover and within the stability range. This freedom of motion was not analyzed in the literature, although it was reported. The stability criteria considered in this model are the equilibrium of forces and moments acting on the block. In the literature, however, the no-spill condition was the dominant assumption. This model shows this criterion to be true only in some cases. It further shows that a block can have a submerged edge without being unstable.

Inspecting the equilibrium conditions, it can be seen that a heavy block tends to become unstable in the positive rotational modes. In fact if S_g become greater than unity the block will automatically submerge. On the other hand a light block is usally stable but not in its original position. It tends to follow the upturn mode.

A longer block is more sensitive to the variation in the flow conditions than a short one. Also a thicker block becomes unstable much faster than a thinner one. The bed material and flow depth affect the forces on the block. A smoother bed will exert larger forces on the block underside than a rough bed will.

The block edge guides the flow around the block. A streamlined, gently sloped edge, 2:1 edge for example, will pass a higher flow-rate with less disturbance than a blunt edge,for example a rectangular one. This allows the block to withstand severe flow conditions without reaching instability.

5.4.2 Modes of Instability

The freedom of the block to move vertically and to rotate in any direction about the point of contact with cover gave rise to eight different modes of instability, Figure 3.13. The experimental investigation confirmed these modes as can be seen from Figure 5.29 and 5.30.

The experiments also showed that the thickening process can be broadly divided into two categories that define the stage of the blocks motion. When the arrested block encounters favourable hydraulic conditions it becomes unstable through one of the forementioned modes; this is the first thickening process. Once the block rests under or on top of the cover edge it can be moved by the flow to form a new cover leading edge or to free the existing one. This will be referred to as the second thickening process, Figure 5.31.

If the first thickening is an undercover type, the second thickening can assume a rolling, sliding or saltating motion, or any combination of these movements. On the other hand, if the first thickening is an overcover one, the cover leading edge will thicken; then, depending on the flow conditions, a sliding process could occur

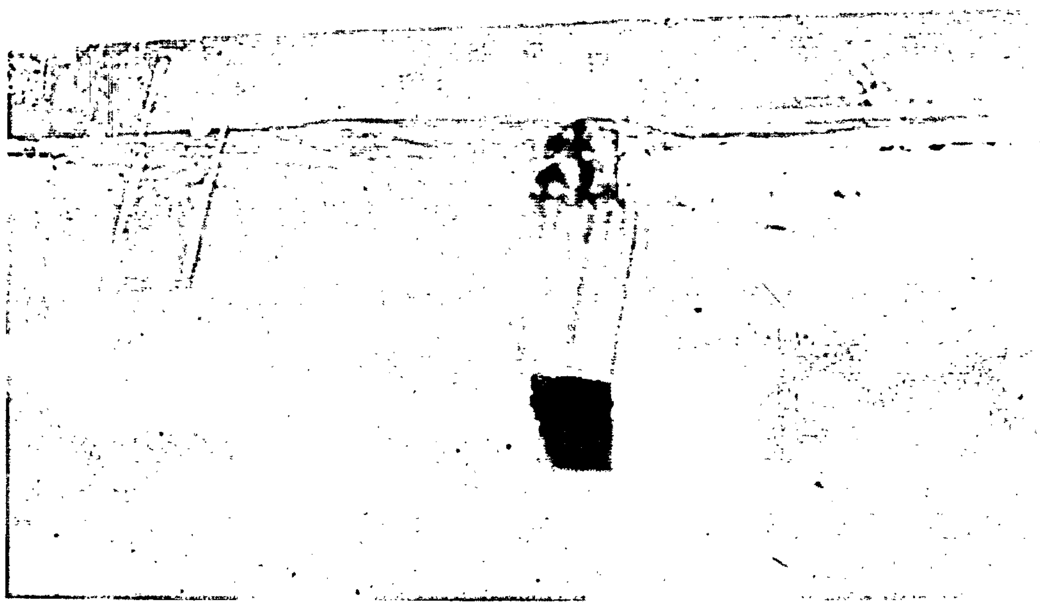

Figure 5.29: Underturning Instability

Figure 5.30: Upturning Instability

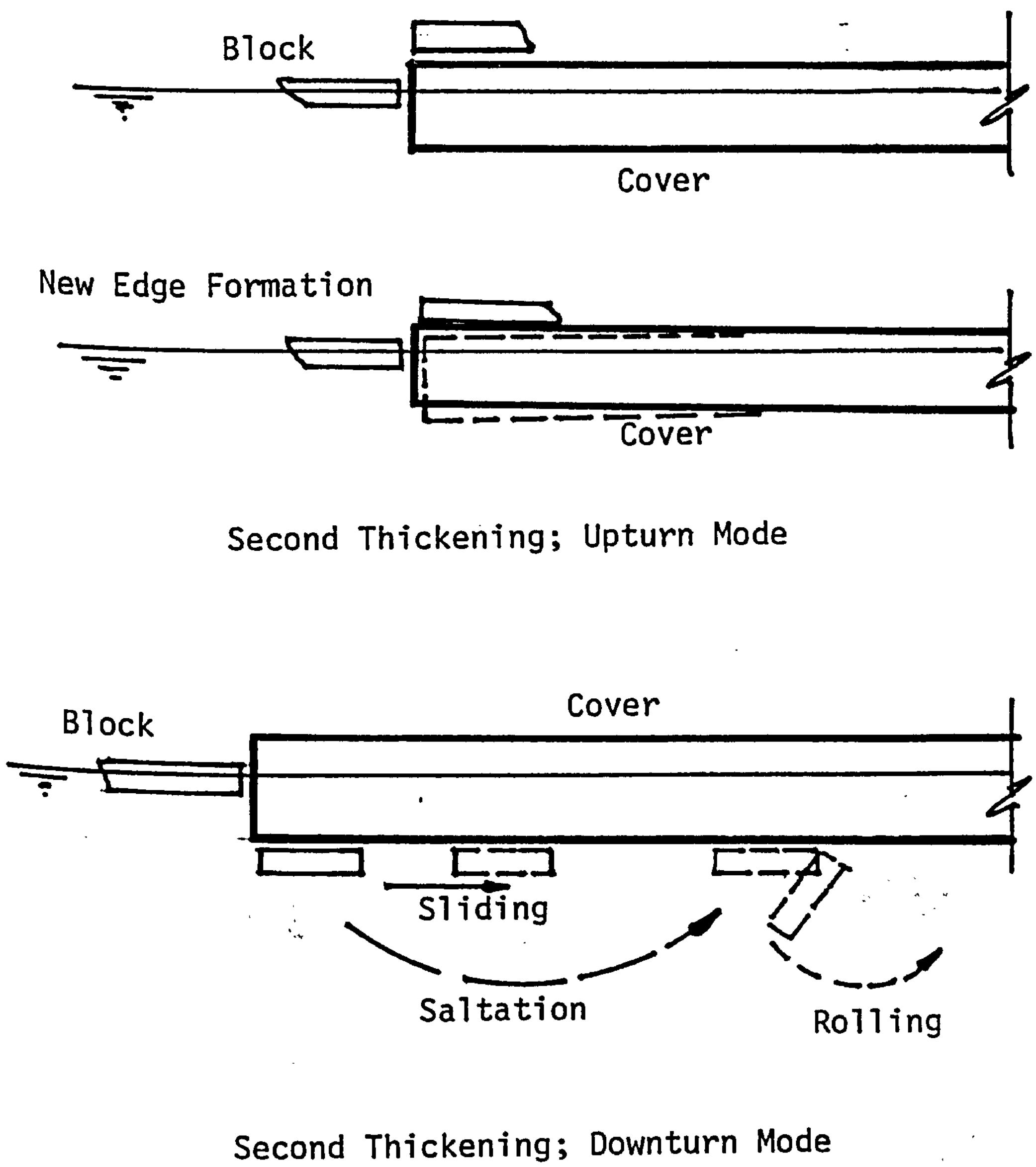

Figure 5.31: Second Thickening Process

or another first thickening mode could start to emerge.

Another interesting aspect of the instability process was observed experimentally with a series of short blocks placed back to back in front of the cover. A unified mode was noticed in which all the blocks acted as one unit.

The group of blocks were found to become unstable in almost all the rotational modes of a single block. Further more, when they reached the instability condition and rotated for their final position they either rotated as one piece, Figure 5.32 or blew up with each piece landing at a different position.

In general, it was observed that the steeper the edge geometry the greater was the block's tendency to underturn. For blocks with rectangular edges only underturning modes were observed. For blocks with other edges, this mode was observed only for long blocks;short blocks experienced upturn modes.

5.4.3 <u>Numerical Solution</u>

The equations that constitute the mathematical model assume a non-linear behaviour for the Δ and α values . This necessitates a numerical solution for the equations. To facilitate the solution the following assumptions were made:

1. The surface tension forces were neglected.
2. The flow is only affected in a limited distance X_o, from the cover where

$$X_o = L + 5\ L_e \text{ or } 5t \qquad 5.10$$

whichever is greater.

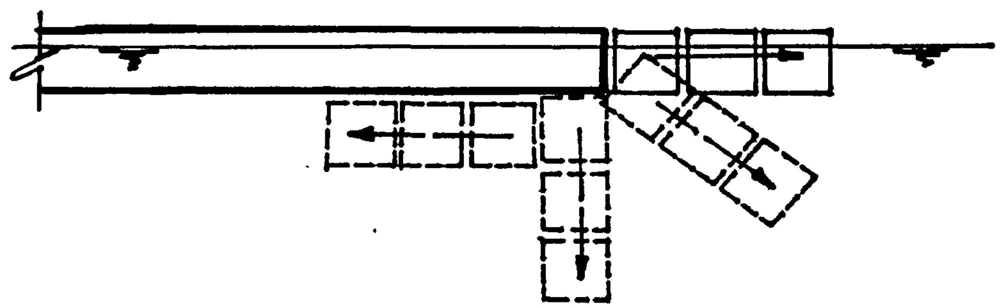

Unified Mode

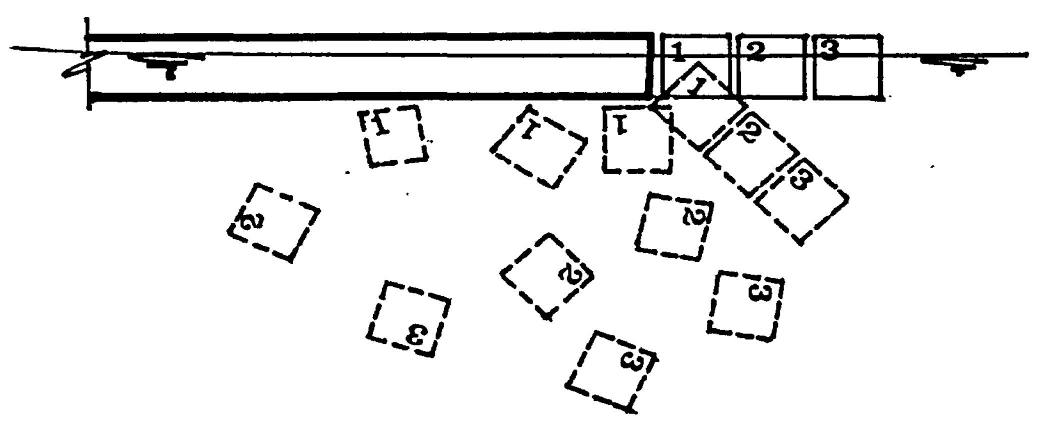

Blow-up Mode

Figure 5.32: Group Instability

3. The angle θ varies linearly with the distance Y from zero at the top to the tangent at the edge's exit point. It is given as

$$\theta(y) = (dy/dx)_2 \cdot y / Y_2 \qquad 5.11$$

4. The pressure coefficient C_p and the velocity coefficient (a) equal to unity.
5. No seepage through the bed nor any phase change between the cover and the fluid is allowed.
6. The angle ϕ is taken as the slope of the dividing line of the depths Y_2 and Y_3 and hence ϕ at any distance x will be.

$$\phi(x) = \frac{x - X_2}{X_3 - X_2} \cdot \mathrm{Tan}^{-1} \tfrac{1}{2} \frac{Y_2 - Y_3}{X_2 - X_3} \qquad 5.12$$

7. The bottom shear coefficient C_τ equals $(1 + \lambda) / \lambda$.

5.4.4 Comparison with Experimental Data

The theory was tested against the experimental data obtained and they were found to agree in general. Due to the non-linearity of the equations only comments of a generalized type could be made.

The horizontal forces on different edges were measured using very short block to minimize the undercover shear effect. The vertical forces were difficult to measure; hence, no comment can be presented about them.

The results, Figure 5.33, indicated that the edge forces increase with the increase in the Froude number. A gentle edge of 2:1 slope, offers less resistance than the more abrupt ones, such as rectangular edges. The difference is not constant; it rather increases

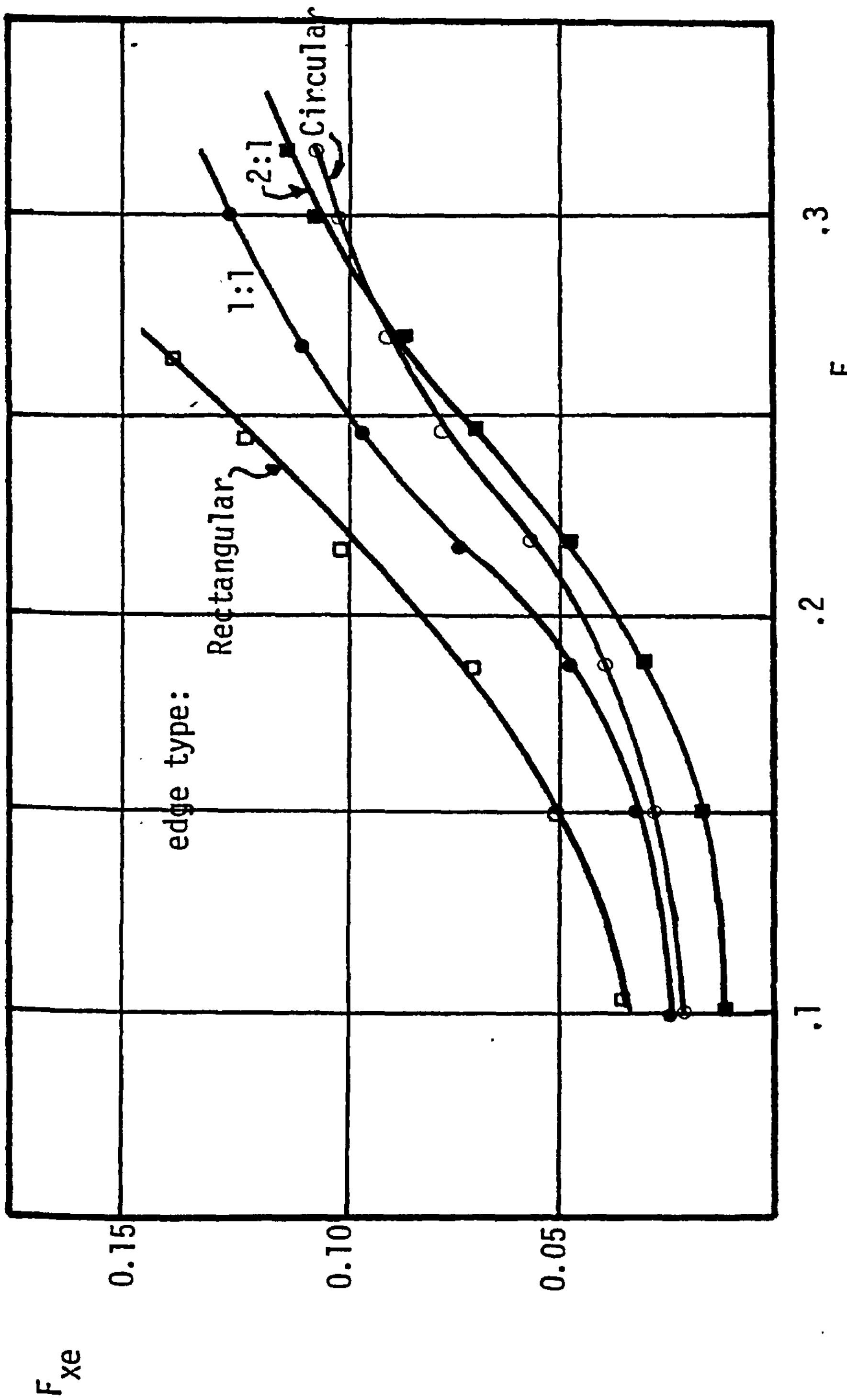

Figure 5.33: Edge Forces

with the force itself, which speeds the instability process. Circular edges experience less resistance at high flow-rate and Froude number, while the 2:1 edges have the lesser resistance at lower flows.

The force on the block underside was difficult to measure. Therefore the total force on the block was measured and the edge force was then subtracted. The underside forces follow almost the same pattern, Figure 5.34. The improved edge condition facilitates a smooth entry of the flow, allowing less shear to develop.

The shear on the block underside was very close for the three sloping edges. This can be explained by the fact that this shear consists of a skin frictional resistance and an induced resistance due to the edge effect. The skin resistance was almost the same; the same block was used with the different edges. Hence, the difference is mainly due to the induced resistance. The total shear and edge forces compromise the reaction of the block on the cover. This reaction was measured and the results are given in Figure 5.35 for the 2:1 edge. It can be seen that the reaction increases slowly at a low Froude number; then it changes sharply as the Froude number increases.

The vertical pressure on the block underside was measured and typical results for rectangular and circular edged blocks are reproduced in Figure 5.36. From the figure it can be seen that a zone of negative pressure develops under the cover up to a certain distance after which the cover assumes a uniform resistance. For shorter blocks, the behavior in general will remain the same, but the extension of the pressure drop area will be accompanied by secondary zones causing the non-uniform reach

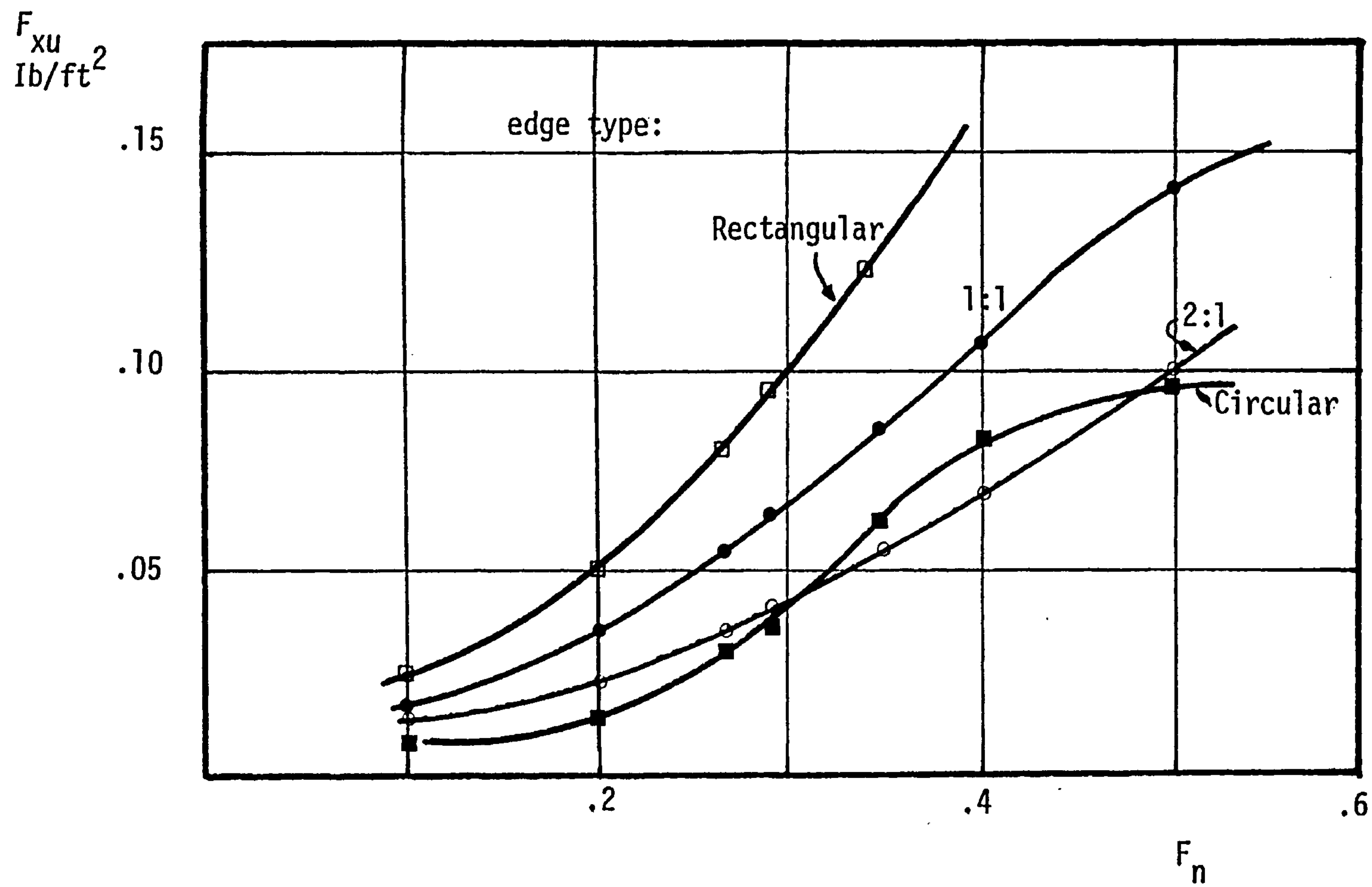

Figure 5.34: Shear on Block Underside

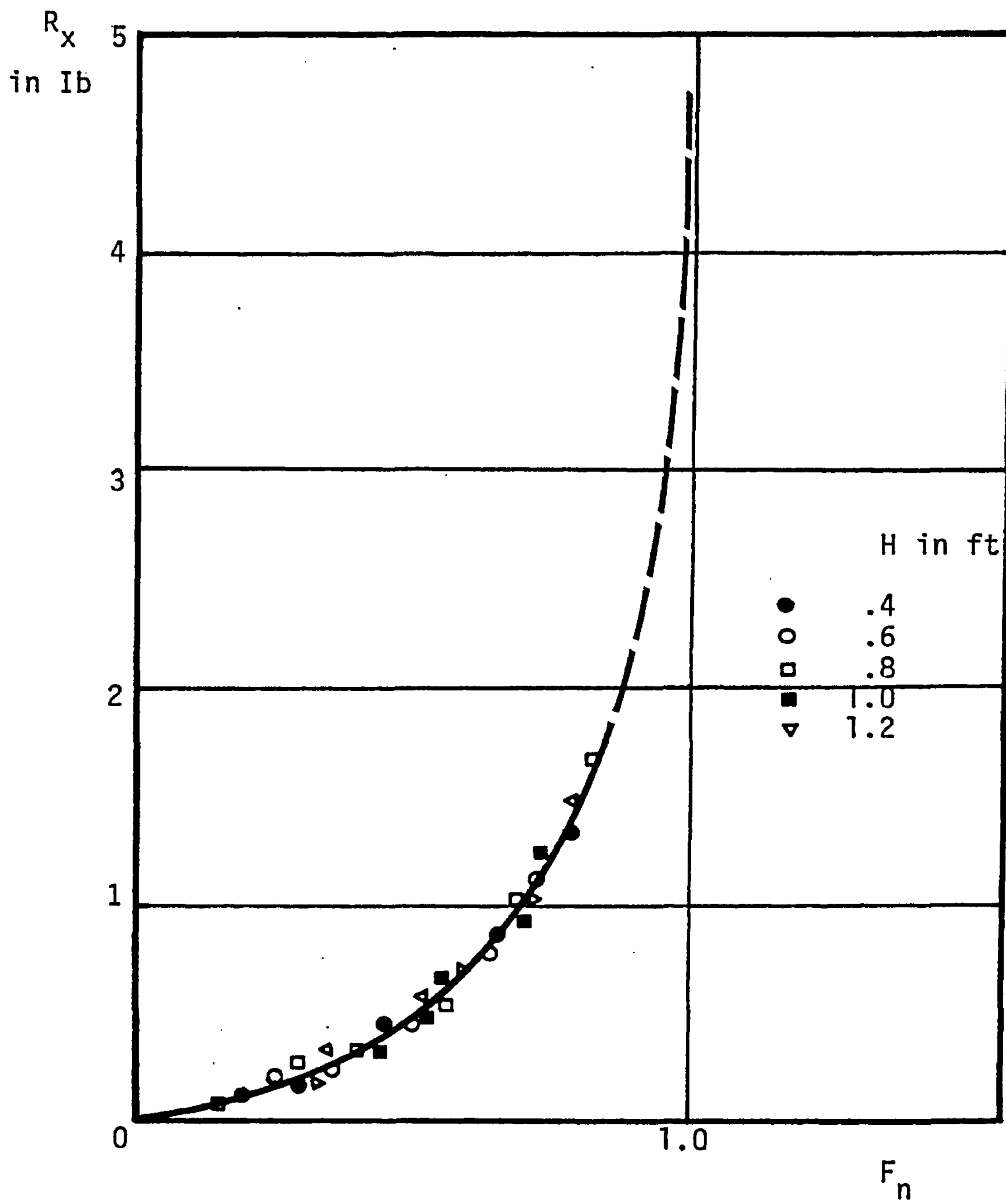

Figure 5.35: Horizontal Reaction of the Cover

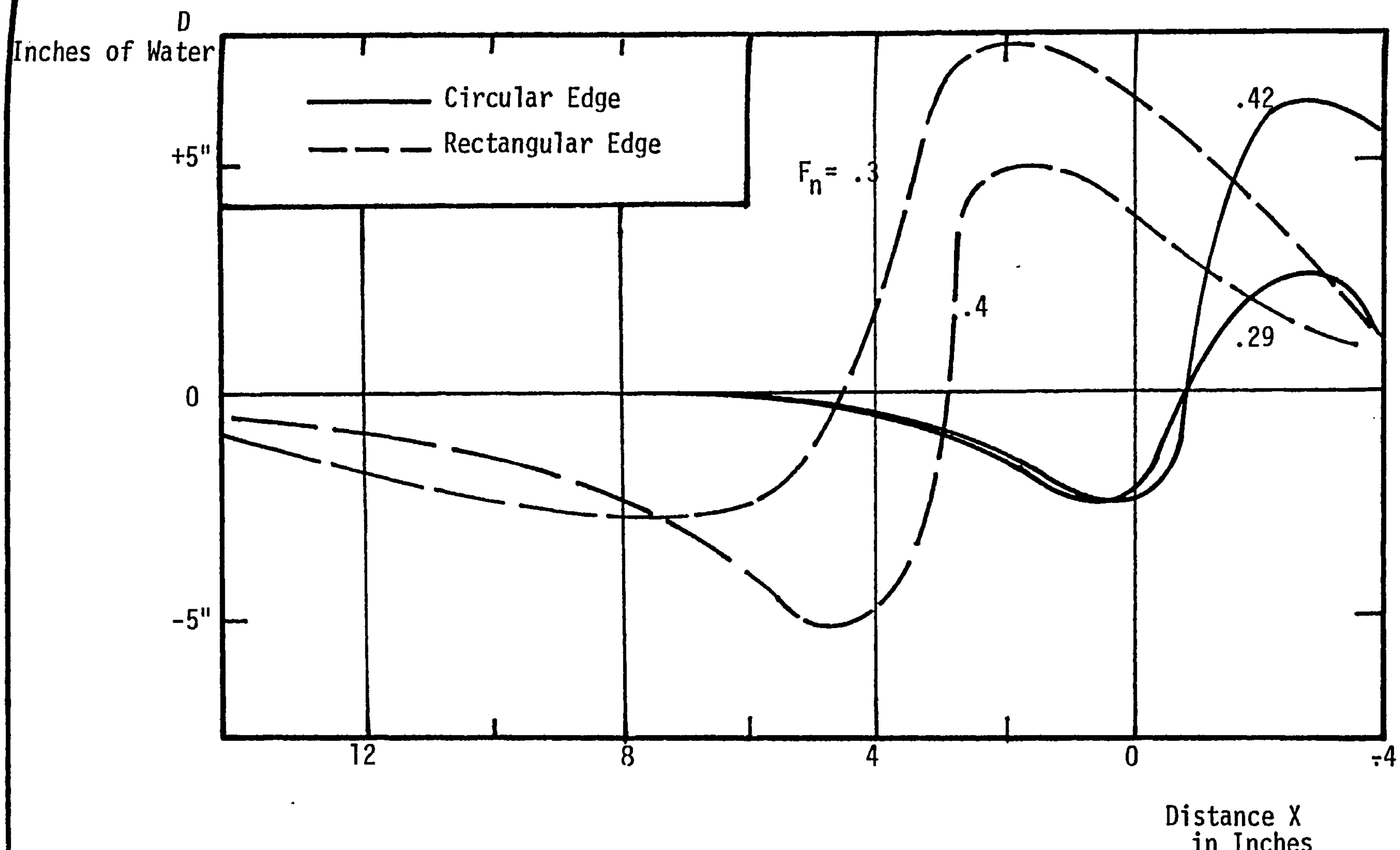

Figure 5.36: Undercover Pressure

to extend downstream.

The negative pressure increases with a blunt edge; it is greater for the block with a rectangular edge than for the one with a circular edge which emphasizes the importance of the edge shape on the process. Other edges were also found to experience similar underside pressure distribution. The increase in the pressure at the edge tip due to the heading up was also common. From Figures 5.37 and 5.38, it can be seen that the longer the block the lower its tendency to be stable, due to the increase in the moments around the rotation center. On the other hand, the longer the edge length the more stable the block will be, due to the improved flow entry to the cover underside.

Thicker blocks or shallower channels (large t/Y ratio) cause the instability conditions to be reached faster, Figure 5.39. Thin blocks reduce the non-uniform edge zones which result in less disturbance to the flow. The theory was used to obtain the values of the displacement Δ under different flow conditions. The results for long blocks are shown in Figure 5.40. At low Froude numbers small negative displacement was noticed, but as the F_n value increased the displacement became positive and increased with F_n until the flow becomes supercritical, when it decreases again. No similar distinct relations were obtained for the rotation α ; but generally α was found to be always positive except for short blocks (t/L less than 0.3) with gentle sloping edges (2:1 or 1:1 for example).

To test the validity of the model for the general instability problem a stage curve for blocks with different edges was obtained theoretically. A comparison of this curve with the experimental results

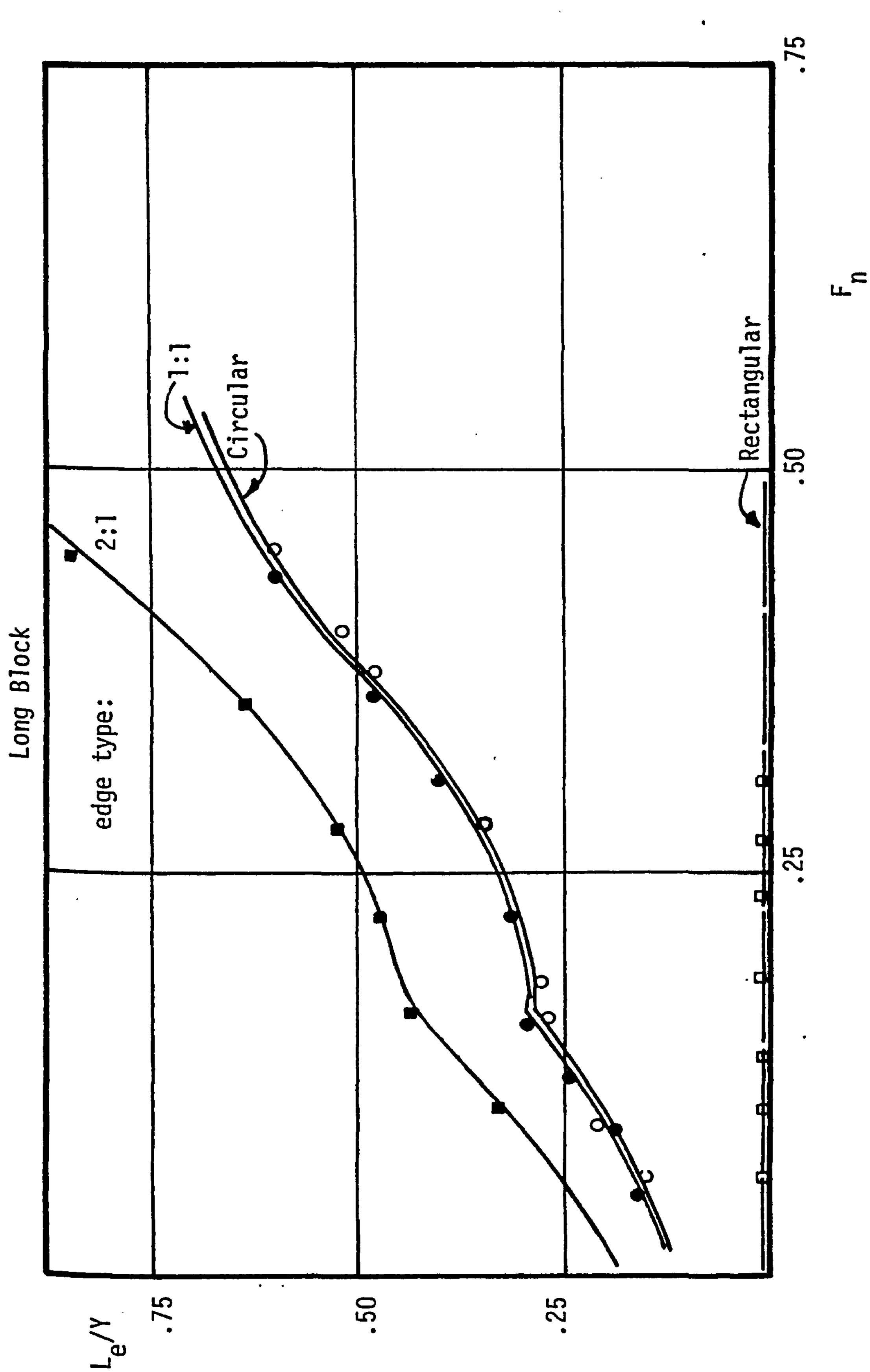

Figure 5.37: Length Effect on Stability

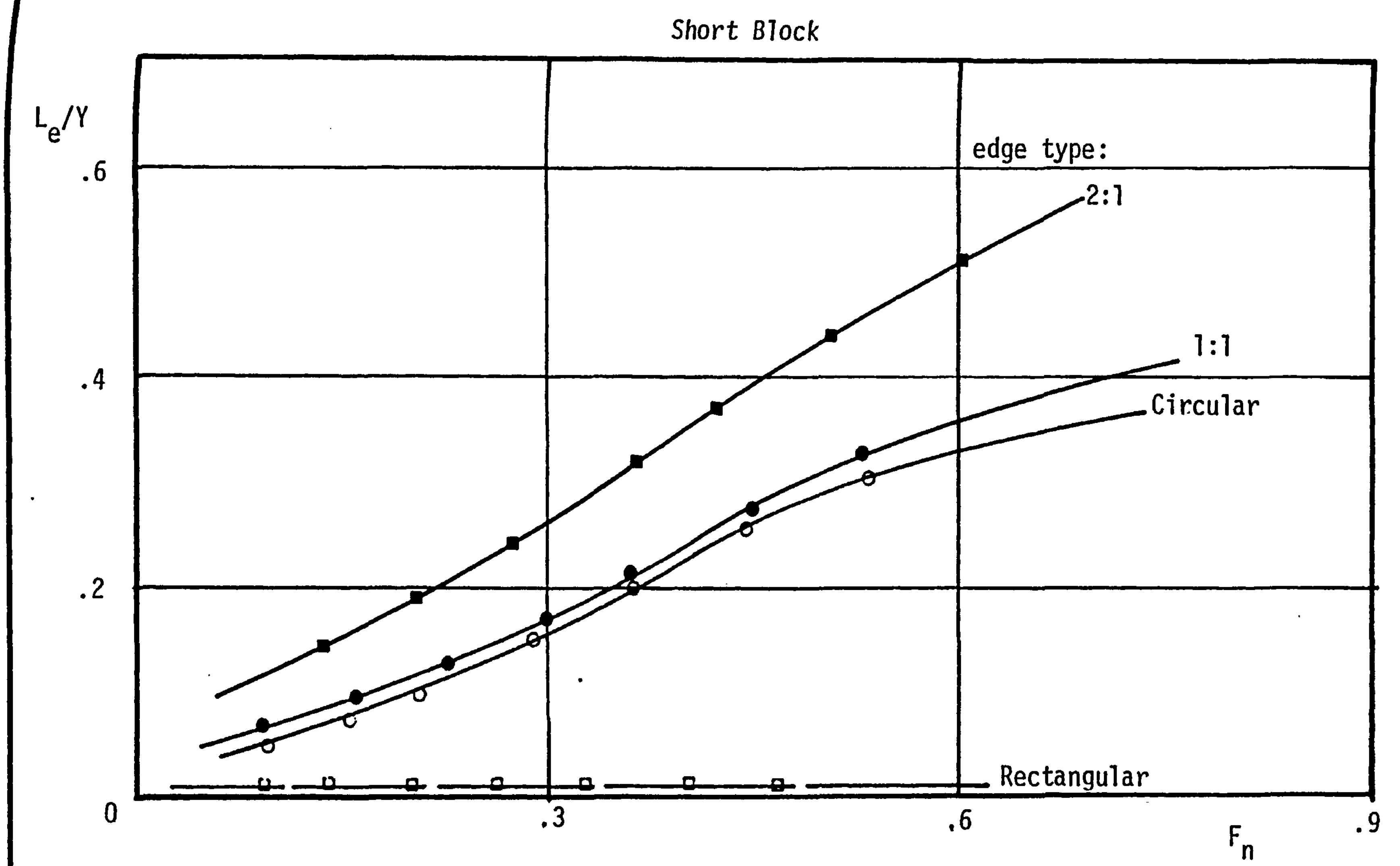

Figure 5,38; Length Effect on Stability

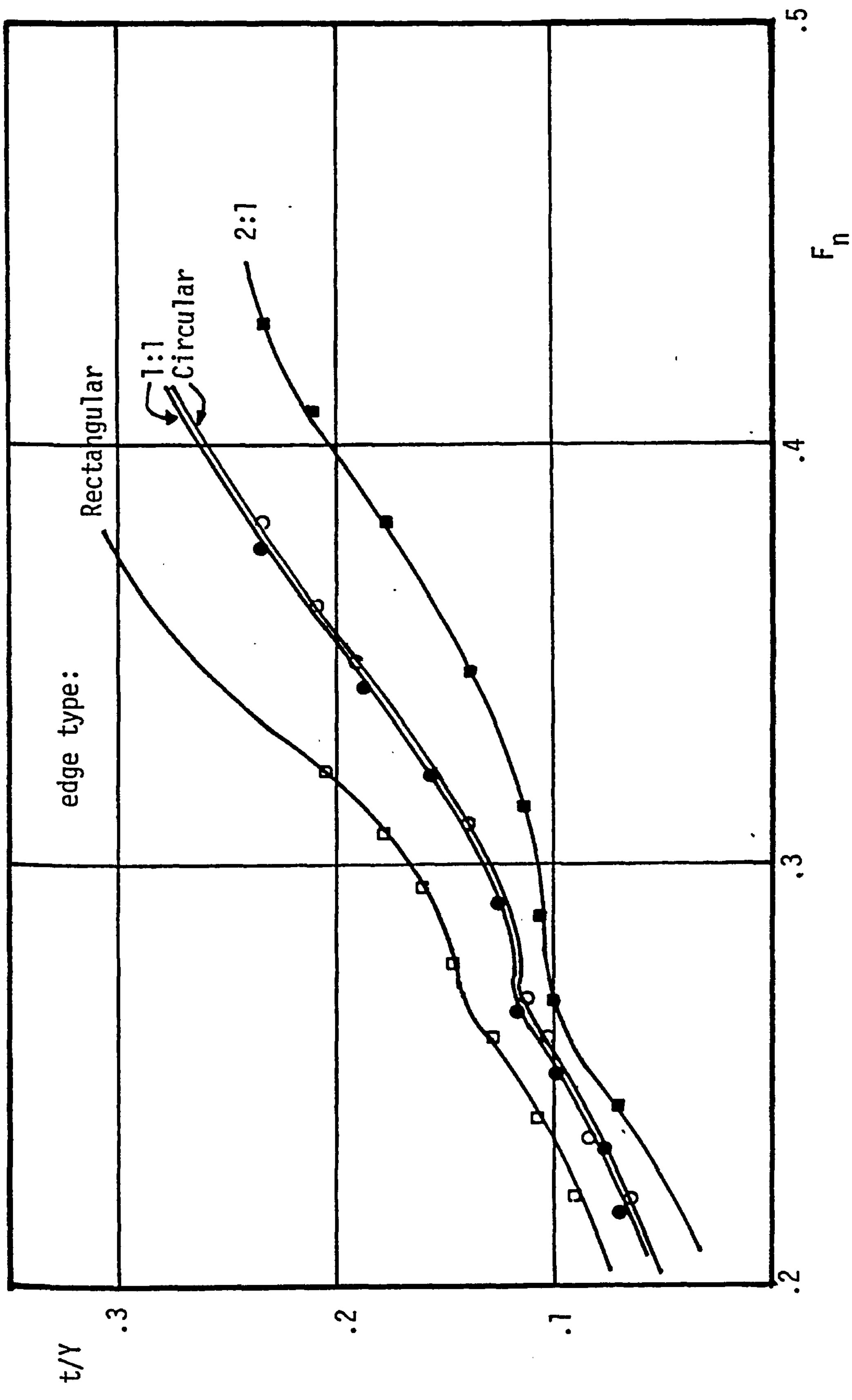

Figure 5.39: Thickness to Depth Ratio Effect

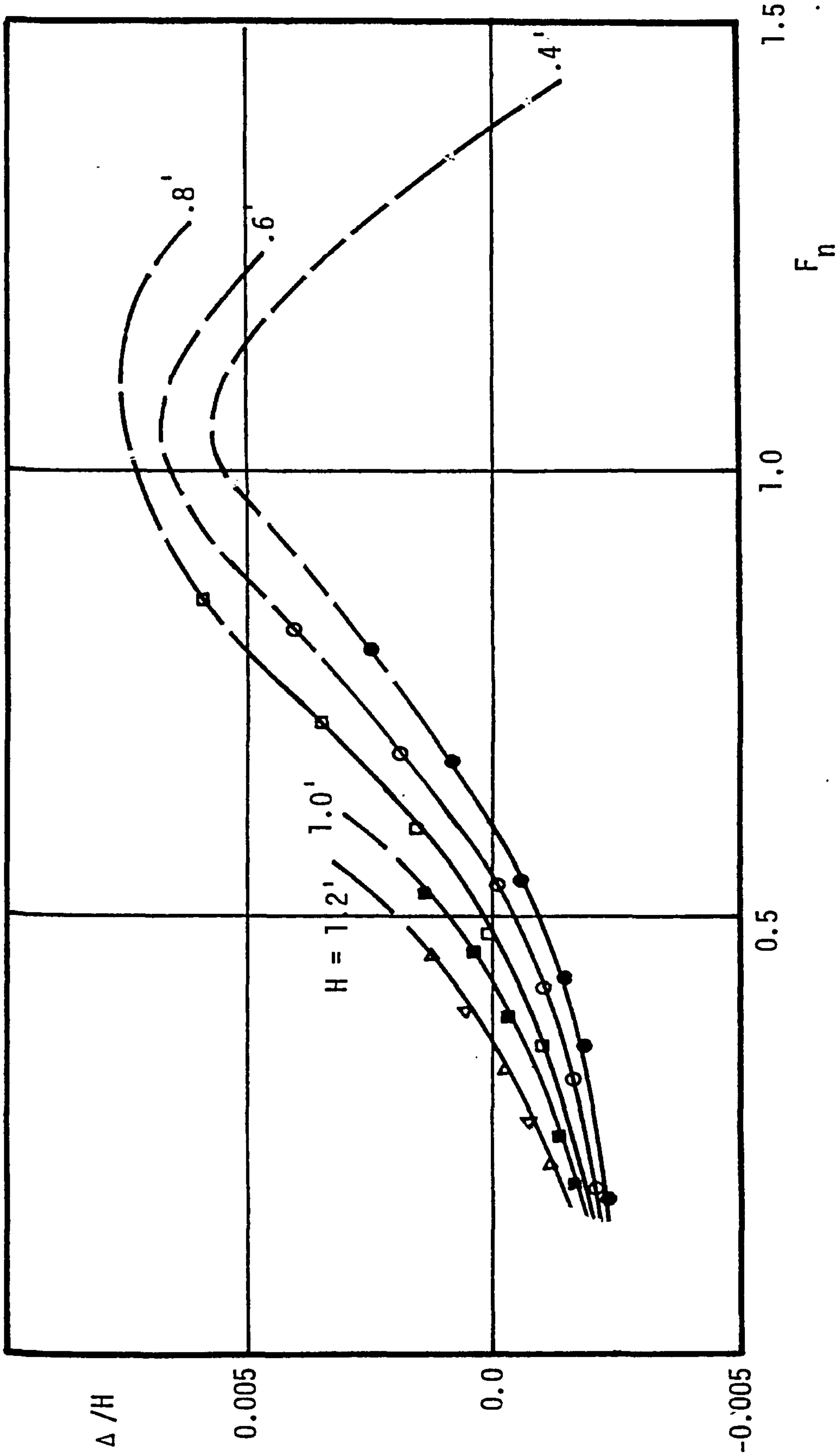

Figure 5.40: Variation of Δ.

is given in Figure 5.41 from which good agreement can be noticed.

As shown in the curve, the blocks can sustain higher flow-rates by allowing deeper flow to develop. This phenomena, heading up, should be investigated when designing any channel that will be exposed to cover formation. The theory and the experiments, under the tested conditions, were found to be in good agreement.

The proposed model can be modified to allow for any orientation for the block or any shape for the cover leading edge to be investigated. This modification should only involve the location of the rotation center and the stability range. None of the force and stability equations need to be adjusted.

5.5 Remarks on Discussion of Theoretical and Experimental Data

The theoretical model presented in Chapter III and discussed in this chapter constitutes a framework for the analysis and design of covered channels.

The mutual dependence of the velocity profile, friction factor and underside configuration suggests that they should be treated as one unit in any in-depth analysis of the problem. Their effects should be included if the extension mechanism of the cover is to be investigated.

The design process of a covered channel should begin with choosing the cross-section dimensions as for an open channel. A modification to the design should then follow, based on assumed resistance factors to the cover underside, gathered from experience or collected field data.

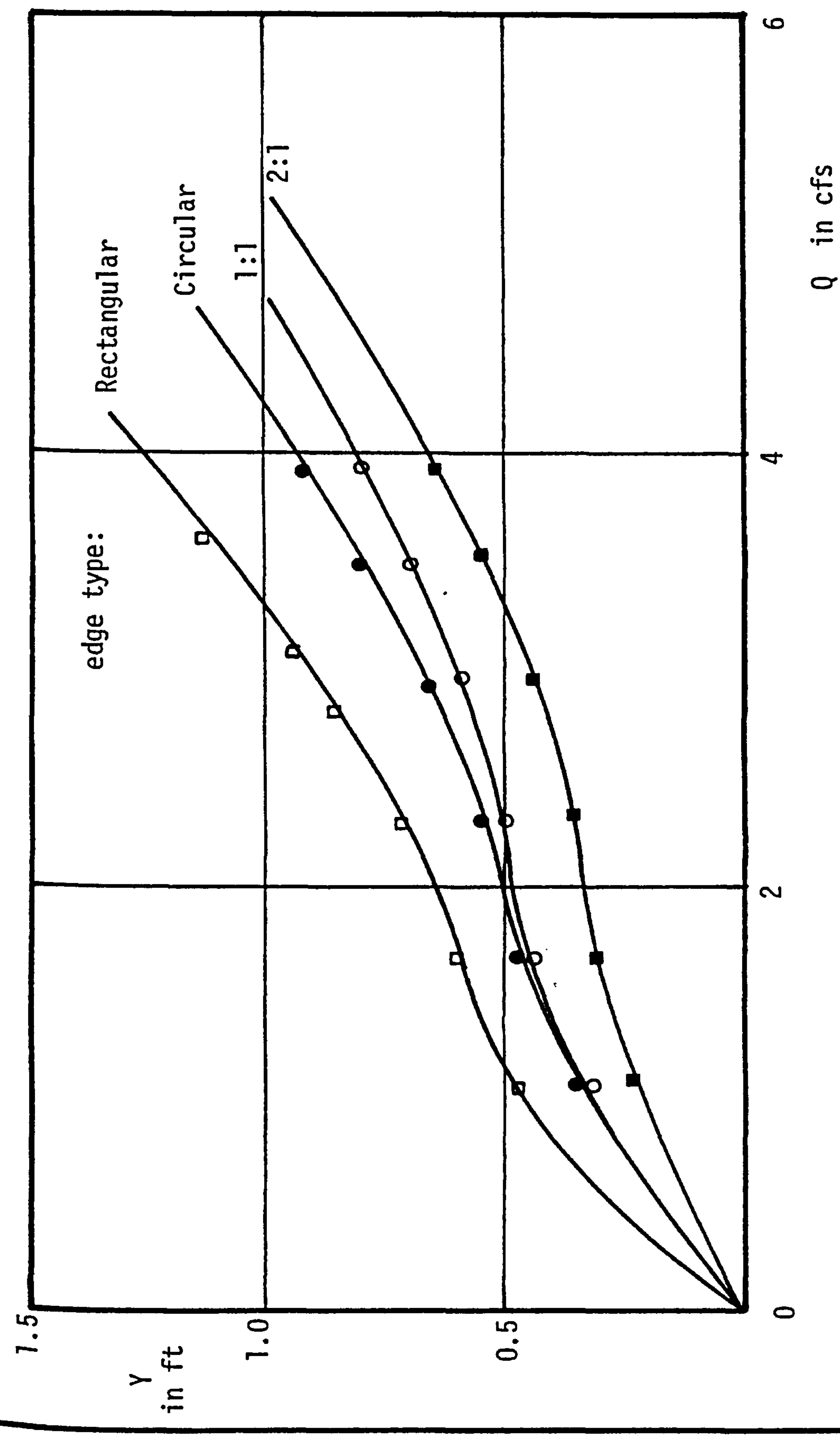

Figure 5.41: Rating Curves

A check for the carrying capacity will then reveal the optimum flow depth.

The underside configuration can be computed along with a check on the extension mechanism of the cover. A final verification of the assumed resistance factor should be carried out using the obtained underside configuration. If the predicted value is found to be different from the assumed one, a new value should be considered and the design should be modified accordingly.

Generally, the model was tested in each of its aspects and good agreement was obtained between the theory and experiments. The model needs to be tested against field measurements to prove its general validity. No field data were obtained in this research nor were any found in the literature that could serve this puropse. A comprehensive field data collection program should be implemented to fill this need.

CHAPTER VI

EMPIRICAL RELATIONS

VI. EMPIRICAL RELATIONS

In this chapter, semi-empirical relations are developed to predict the critical Froude number at which the block will become unstable without the necessity of knowing, in detail, the forces acting on the block.

6.1 Analysis of Block Stability

The analysis of the block stability was first made for the case of uniform submergence caused by a uniform pressure reduction at the base of the block. With this assumption the length of the block will not be a parameter in the equation. The no-spill conditon was used where the water surface just reached the top of the block. In this case the rise in the water level, due to the stagnation pressure at the upstream face, was equal to the approach velocity head. This rise was considered in addition to the submergence of the block in arriving at the final water level.

6.1.1 Uniform Submergence Analysis

For this case it was assumed that the block would experience a uniform submergence (Δ) as shown in Figure 6.1. The governing equations are the continuity, energy and the no-spill condition.

The continuity equation can be expressed as:

$$VH = V_u (H - S_g t - \Delta) \qquad 6.1$$

where, V = upstream velocity

H = upstream flow depth

V_u = flow velocity under the block

t = block thickness

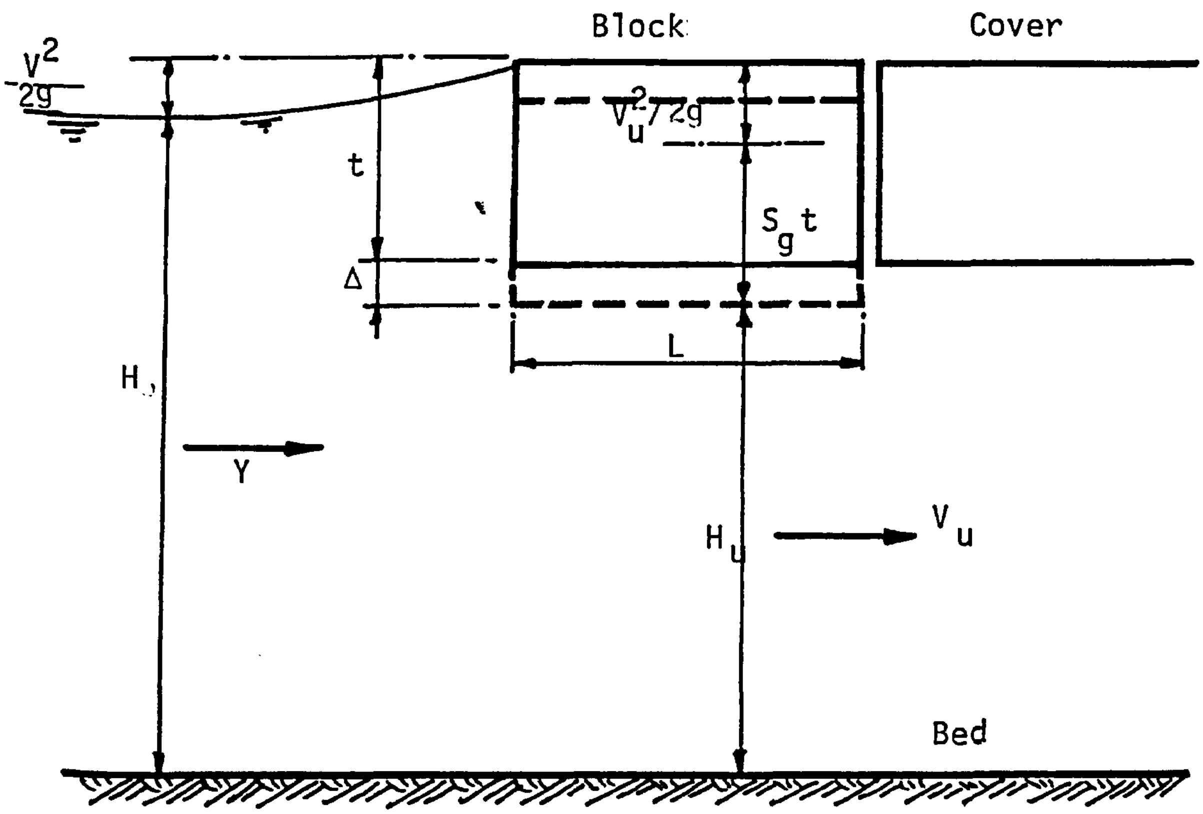

Figure 6.1: Definitions and Notations

S_g = specific gravity of the block material

The energy loss between the upstream section and the cover underside was considered to be proportional to the velocity head upstream, i.e.

$$H_L = K\,V^2/\,2g \tag{6.2}$$

where, K = energy loss coefficient

The application of the energy equation between these two sections yielded

$$H + (1-K)\,\frac{V^2}{2g} = (H-\Delta) + \frac{V_u{}^2}{2g} \tag{6.3}$$

The no-spill condition provided

$$\Delta = (1-S_g)\,t - \frac{V^2}{2g} \tag{6.4}$$

The solution of these equations, neglecting the energy loss, gave

$$V/\sqrt{2\,g\,H} = \sqrt{\frac{t}{H}\,(1-S_g)}\,\left(1-\frac{t}{H}+\frac{V^2}{2gH}\right) \tag{6.5}$$

Using the dimensionless grouping to give the upstream Froude number ($F_n = V/\sqrt{gH}$) as one variable transformed Equation 6.5 into a second degree equation in F_n. Solving this quadratic equation for F_n resulted in

$$F_n = \sqrt{\frac{2H}{t}}\,\left(Z - \sqrt{Z^2 - \frac{t}{H}\,(1-\frac{t}{H})}\,\right) \tag{6.6}$$

in which

$$Z = 1/2\,\sqrt{(1-S_g)} \tag{6.7}$$

6.1.2 Submergence with Rotation

If the submergence is accompanied by a rotation, it can then be argued that the length, L, of the block can influence the mechanism of the instability process. In such an instance, Equation 6.6 can be modidied to give

$$F_n = \sqrt{\frac{H}{t}} \left(Z - \sqrt{Z^2 - \frac{t}{H} \left(1 - \frac{t}{H}\right)} \right) M \qquad 6.8$$

where M is a function that would express the effect of the rotation of the block.

The dimensional analysis revealed that M should be a function of the relative dimensions of the block, Froude number and edge geometry i.e.

$$M = M\left(\frac{t}{L} ,\ F_n ,\ \text{edge geometry} \right) \qquad 6.9$$

The experimental data were used to yield the required expressions for M.

6.2 Results

6.2.1 Modes of Instability

Two modes of instability were considered in this chapter. The underturning mode of instability, in which the block underturns and comes to rest beneath the cover, and the upturning one, where the block terminates above the cover. No further subdivisions of these modes were considered.

In the following articles the results of the experimental investigation as well as the best fit expressions for the M function are discussed.

6.2.2 Blocks with Rectagular Edges

The value of M, as given by Equation 6.8 was plotted against the block thickness to length ratio, Figure 6.2, and a family of curves was obtained. In each of these constant Froude number curves two branches were distinguished. The steep portion of the curve represents long blocks while the flatter part of the curve describes the stability of short blocks. The least square method was used to develop the following expressions for the M function

for long blocks,

$$M = 0.0076\ F_n^{-0.56} / (t/L) + 2.15\ F_n + 2/3 \qquad 6.10$$

for short blocks,

$$M = 0.05\ F_n^{-0.56}\ (t/L) + 2.15\ F_n + 2/3 \qquad 6.11$$

The change-over point between long and short blocks is denoted by the point of intersection of these two curves.

6.2.3 Blocks with Circular Edge

The laboratory results of blocks with circular edge were plotted in Figure 6.3. All the experimental points fell sensibly into a single curve indicating that for blocks with a circular edge the block length has a negligible influence, within the experimental range. The M function was found to follow these relations:

$$M = 4.0\ F_n + 0.75 \qquad F_n < 0.3 \qquad 6.12$$

and

$$M = 4.0\ F_n^3 + 1.50 \qquad F_n > 0.3 \qquad 6.13$$

6.2.4 Blocks with 1:1 Edge

For this type of edge the M-F_n plot is shown in Figure 6.4. The

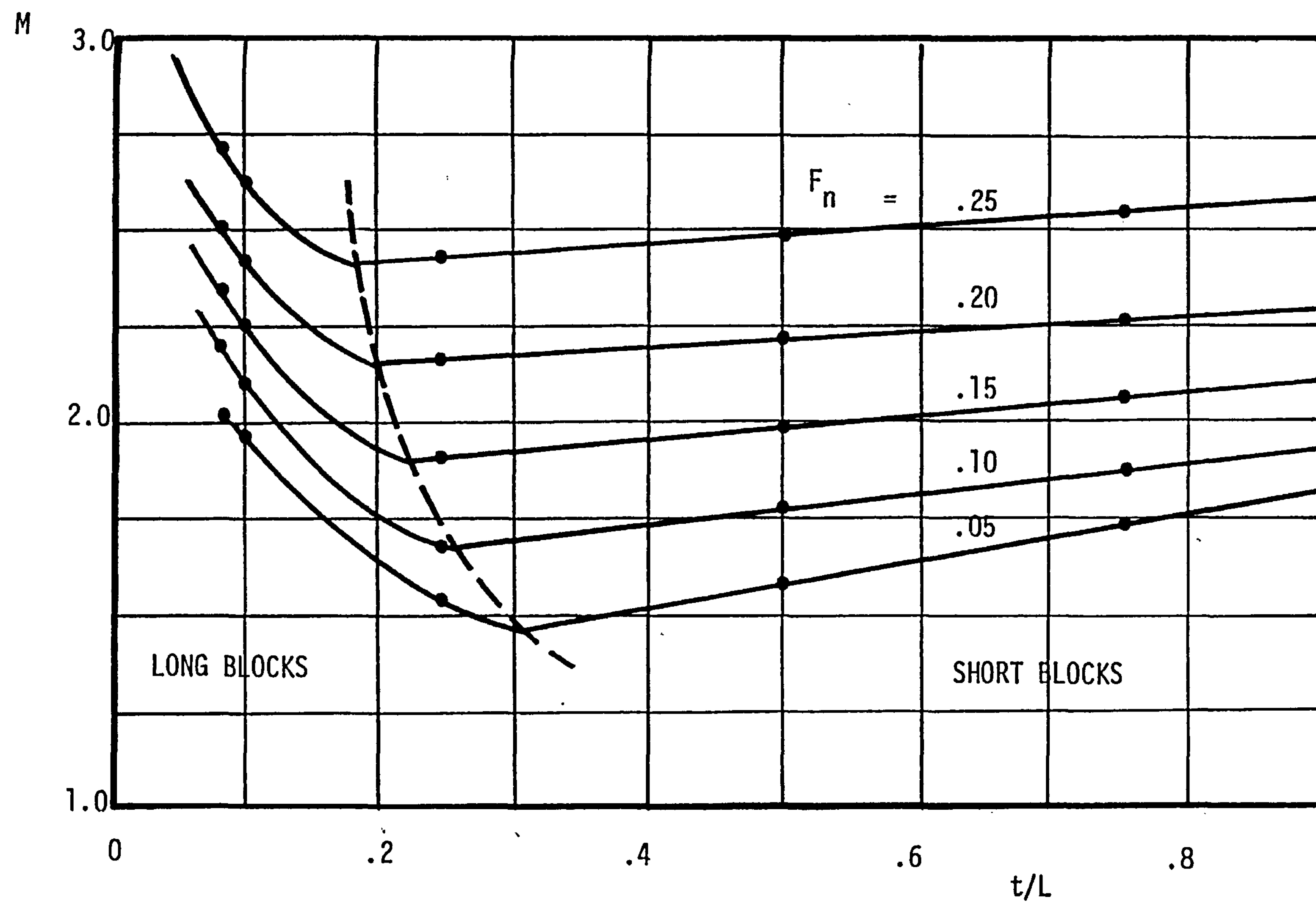

Figure 6.2: M-funtion for Rectangular Edge

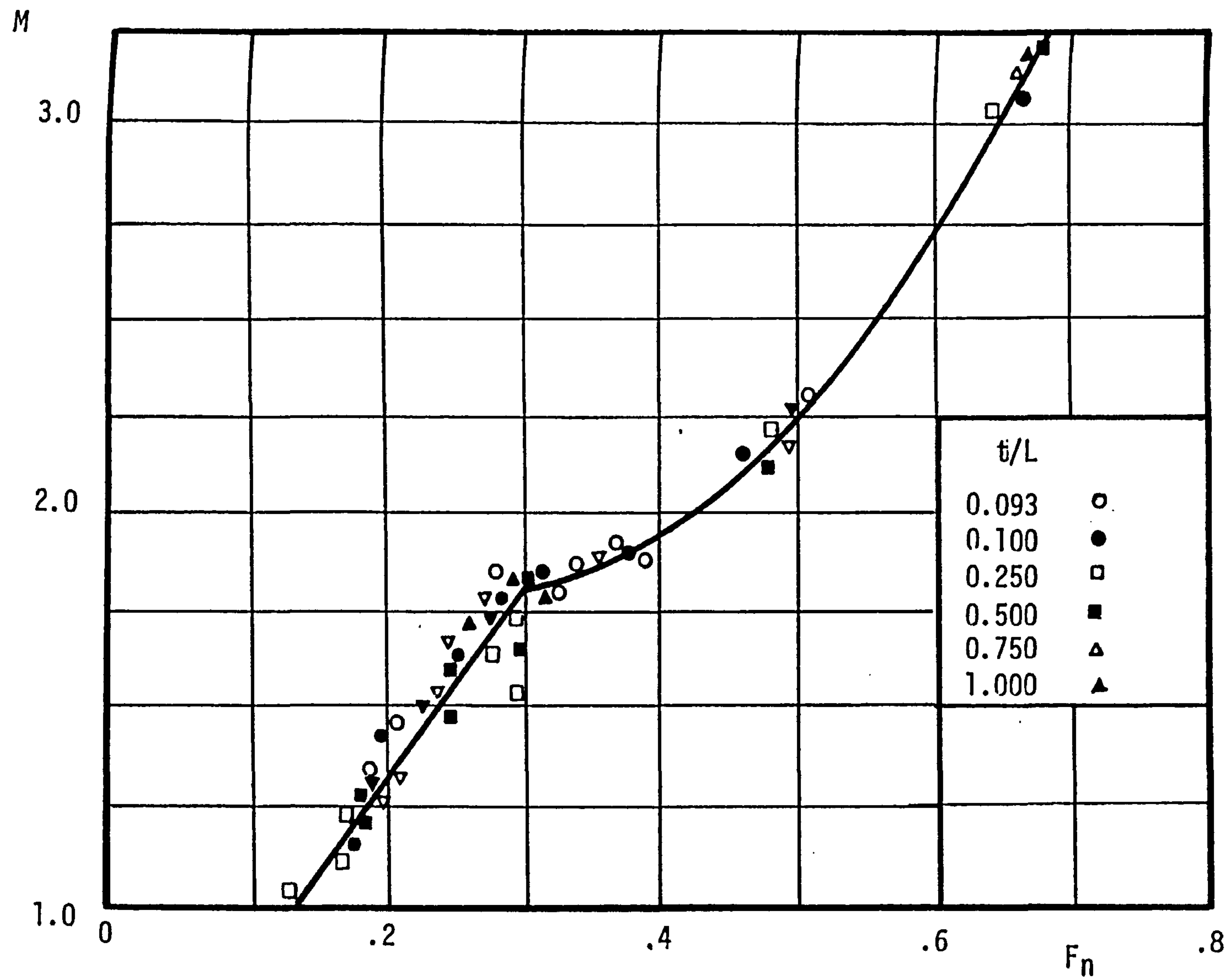

Figure 6.3: M-Function for Circular Edge

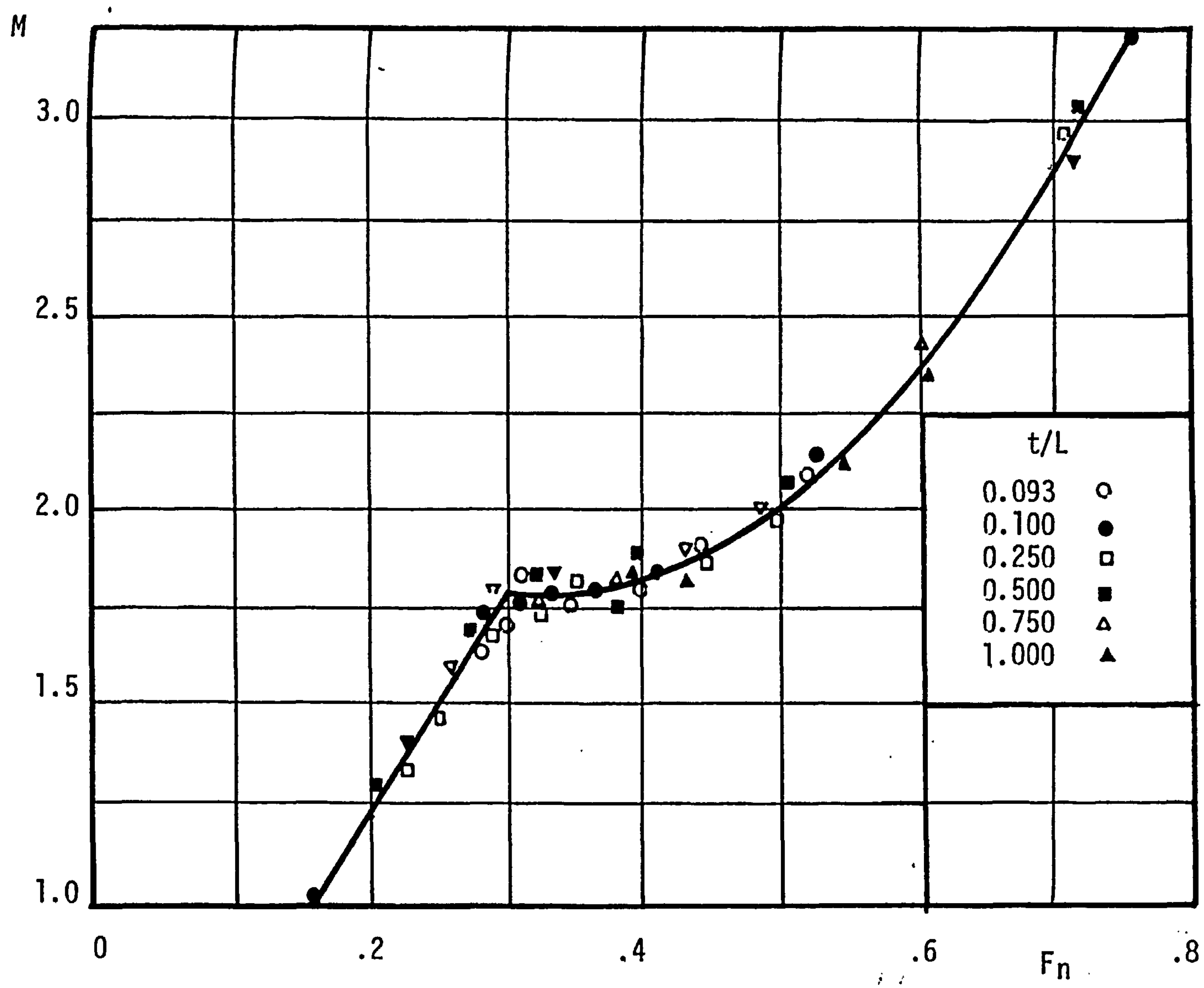

Figure 6.4: M-Function for 1:1 Edge

existence of the sloping edge reduces the entry disturbance and thus the pressure reduction is reduced limiting the length effect. The M function was found to be best expressed as

$$M = 5.5\ F_n + 1/8 \qquad F_n < 0.3 \qquad 6.14$$

and

$$M = 4.0\ F_n^{3.5} + 1.5 \qquad F_n > 0.3 \qquad 6.15$$

These expressions are similar to those obtained for the block with a circular edge. This can be attributed to the fact that both have the same extension of the leading edge and hence the reduction in the pressure will be almost the same in the two cases.

6.2.5 Blocks with 2:1 Edge

The results for this type are plotted in Figure 6.5. For Froude numbers less then 1/3, a single equation giving a straight line describes the behavior of the function M, namely,

$$M = 2.75\ F_n + 0.83 \qquad 6.16$$

This equation was also found to represent the behavior of the M function for long blocks (t/L < 0.1) at higher Froude numbers. For shorter blocks the following equation was found to give the best fit:

$$M = 5.66\ F_n^{4} + 1.85 \qquad 6.17$$

6.2.6 Upturning Instability Mode

In this mode the block becomes unstable at a higher Froude number than the underturning mode block, and the M value, corresponding to a certain Froude number, was also found to be higher.

The main factors in causing a block to follow the upturning mode were found to be the block dimensions and the leading edge geometry. With the leading edge sloping at 2:1 all the blocks with a thickness-to-length

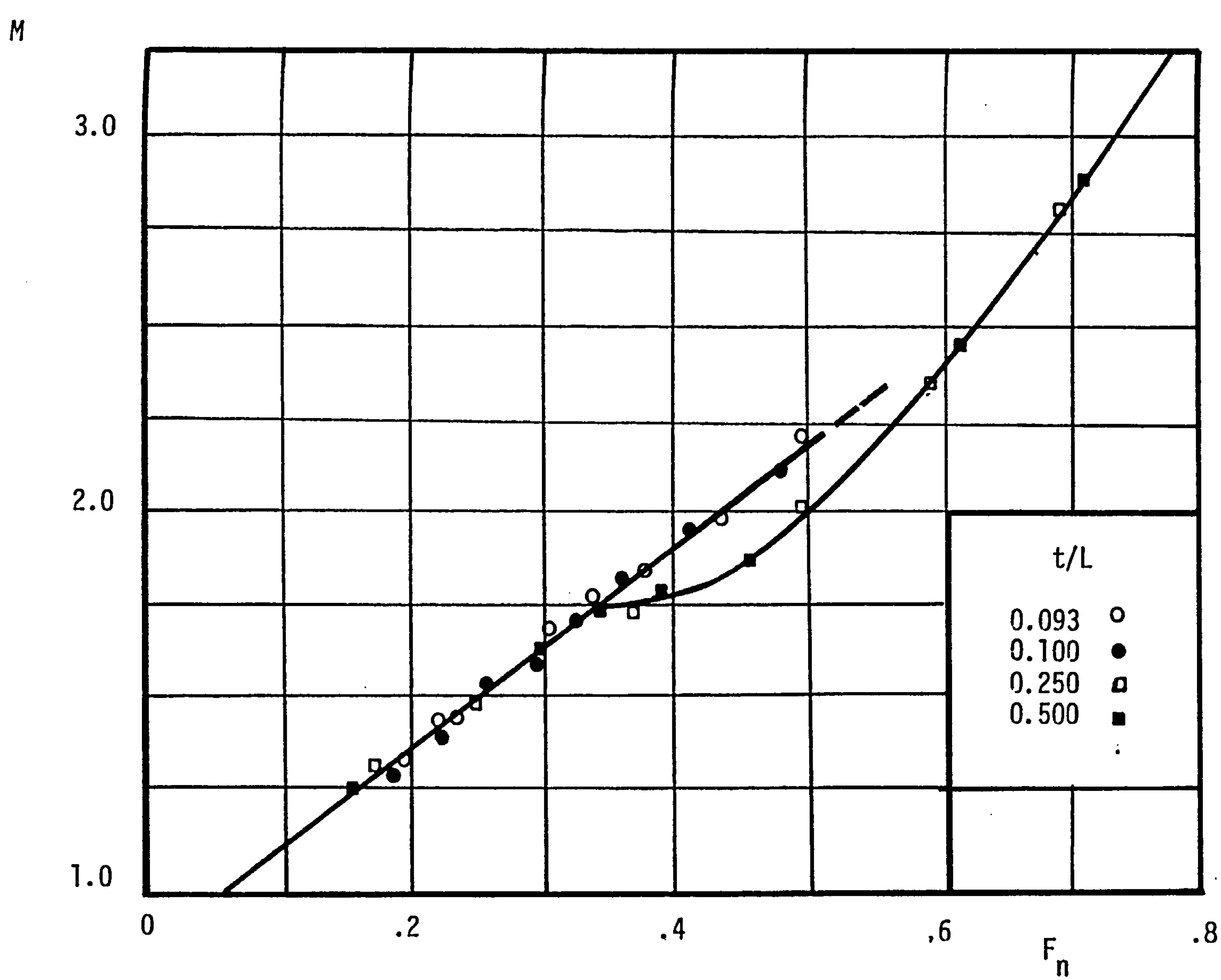

Figure 6.5: Results for 2:1 Edge

ratio greater than ½ were found to follow the upturning instability mode. This mode was also found to occur for circular as well as 1:1 sloping edges for blocks with (t/L) greater than 0.75.

The experimental results obtained for this mode are reproduced in Figure 6.6. Two branches of the curve are shown. These branches can be described by the following equations:

$$M = 2.75\, F_n + 1.15 \qquad \text{for } F_n < 0.45 \qquad 6.18$$

and

$$M = 3.3\, F_n^{4.5} + 2.75 \qquad \text{for } F_n > 0.45 \qquad 6.19$$

The line between the two modes of instability, namely the underturning and the upturning modes, is drawn using the guidelines for the edge shape and t/L ratio indicated earlier. For mixed blocks the lower critical Froude number should be considered for design purposes.

6.3 Behavior of the Equations

Equation 6.8 can be expressed in the form

$$F_n = \frac{Z\,M}{\sqrt{t/H}} \left(1 - \sqrt{1 - \frac{1}{Z^2}(t/H)\left(1 - \frac{t}{H}\right)} \right) \qquad 6.20$$

where M can generally be expressed as

$$M = a\, F_n^{\,b} + c \qquad 6.21$$

and the values of a, b and c are summarized in Table 6.1.

Since

$$\frac{1}{Z^2}\;\frac{t}{H}\left(1 - \frac{t}{H}\right) \ll 1$$

the equation can be expanded to

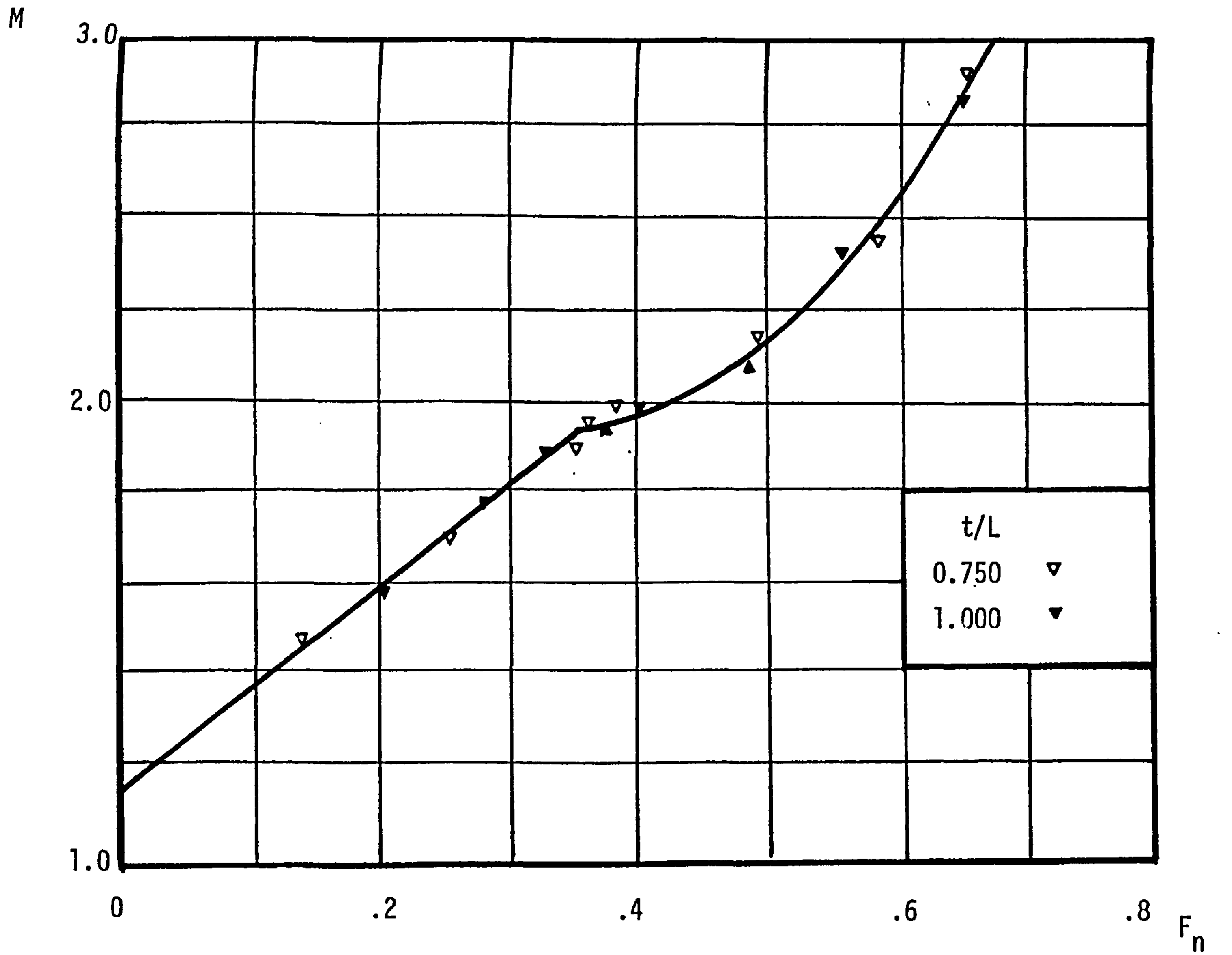

Figure 6.6: M-Function for Upturn Mode

Edge	L_e/t	a	b	e	Remarks
Rectangular	0	$.0076/(t/L)$	-0.56	$2.15F_n + 2/3$	Long Blocks
	0	$.05\ (t/L)$	-0.56	$2.15F_n + 2/3$	Short Blocks
1:1 Slope	1	5.5	1	0.125	$F_n < .3$
	1	4.0	3.5	1.50	$F_n > .3$
Circular	1	4.0	1	0.75	$F_n < .3$
	1	4.0	3	1.50	$F_n > .3$
2:1 Slope	2	2.75	1	0.83	$F_n < 1/3$
	2	5.66	4	1.	$F_n > 1/3$

TABLE 6.1: General Expression for Underturning Mode

$$F_n = (Z\ M/\ \ t/H)\ \left(\frac{1}{2\ Z^2}\ \frac{t}{H} (1 - \frac{t}{H}) + \ldots\ldots. \right) \qquad 6.22$$

If only the first term is considered, this equation will be reduced to Equation 2.19 with A = 0 and B is a function of M and K.

The literature equations, presented in Chapter II, were tested against the experimental data obtained in this research. The results are shown in Figures 6.7 through 6.10. It is clear from these figures that the literature equations are only applicable to blocks with a rectangular edge. For other edges the literature equations have a very limited applicability.

Figure 6.11 shows a typical set of curves that indicate the behavior of the equation suggested in this chapter as well as those in the literature. It can be seen from the figure that the proposed equation covers a wider range of flow conditions and relative block thicknesses.

It should be noted that the suggested expressions were developed utilizing the experimental data and were subject to the experimental errors given in Appendix D. These expressions should be used cautiously since they were established for a limited range of data. Further experimental and field measurements are needed to verify and extend the range of their applicability.

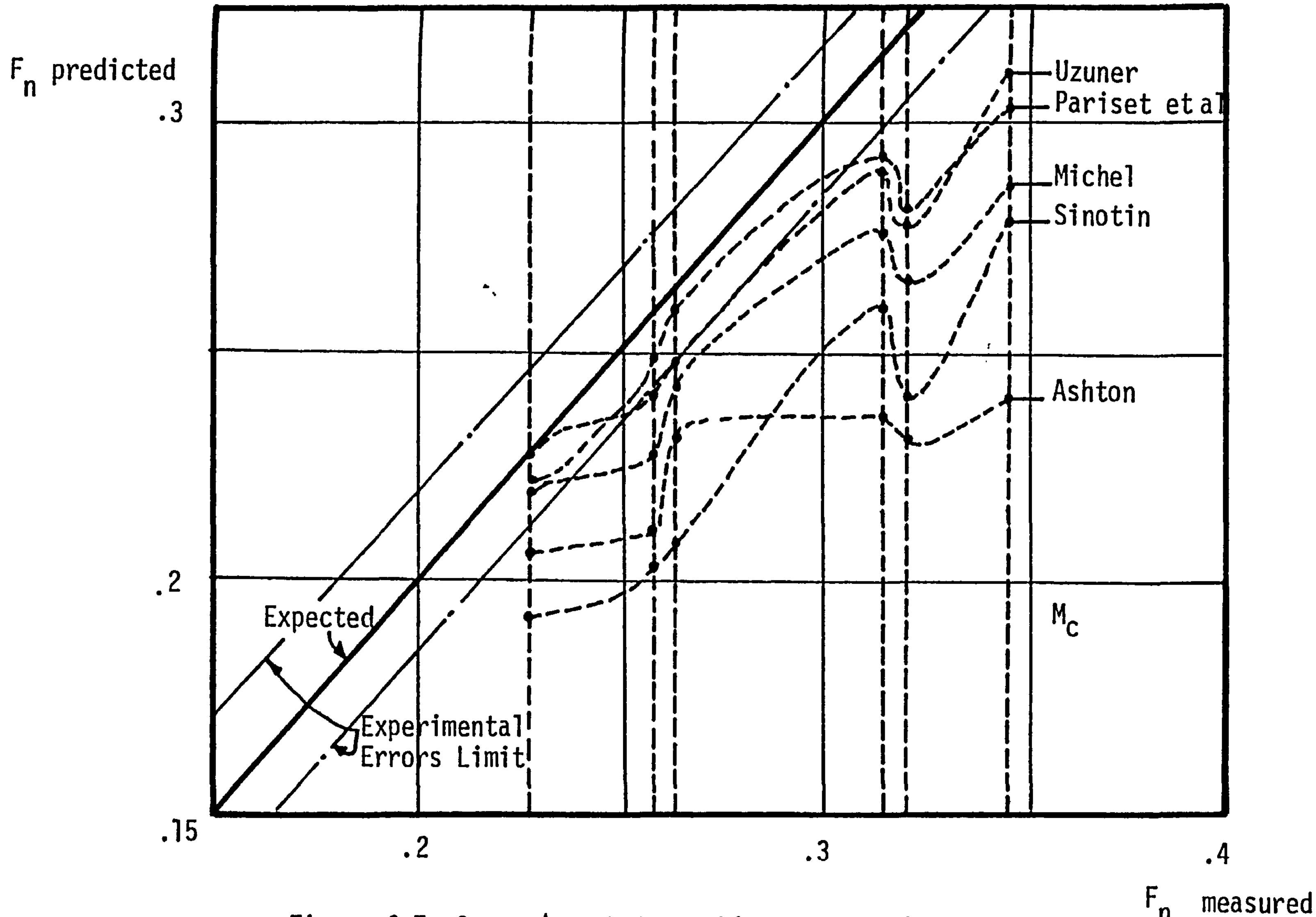

Figure 6.7: Comparison Between Literature and Experimental Results for Rectangular Edge

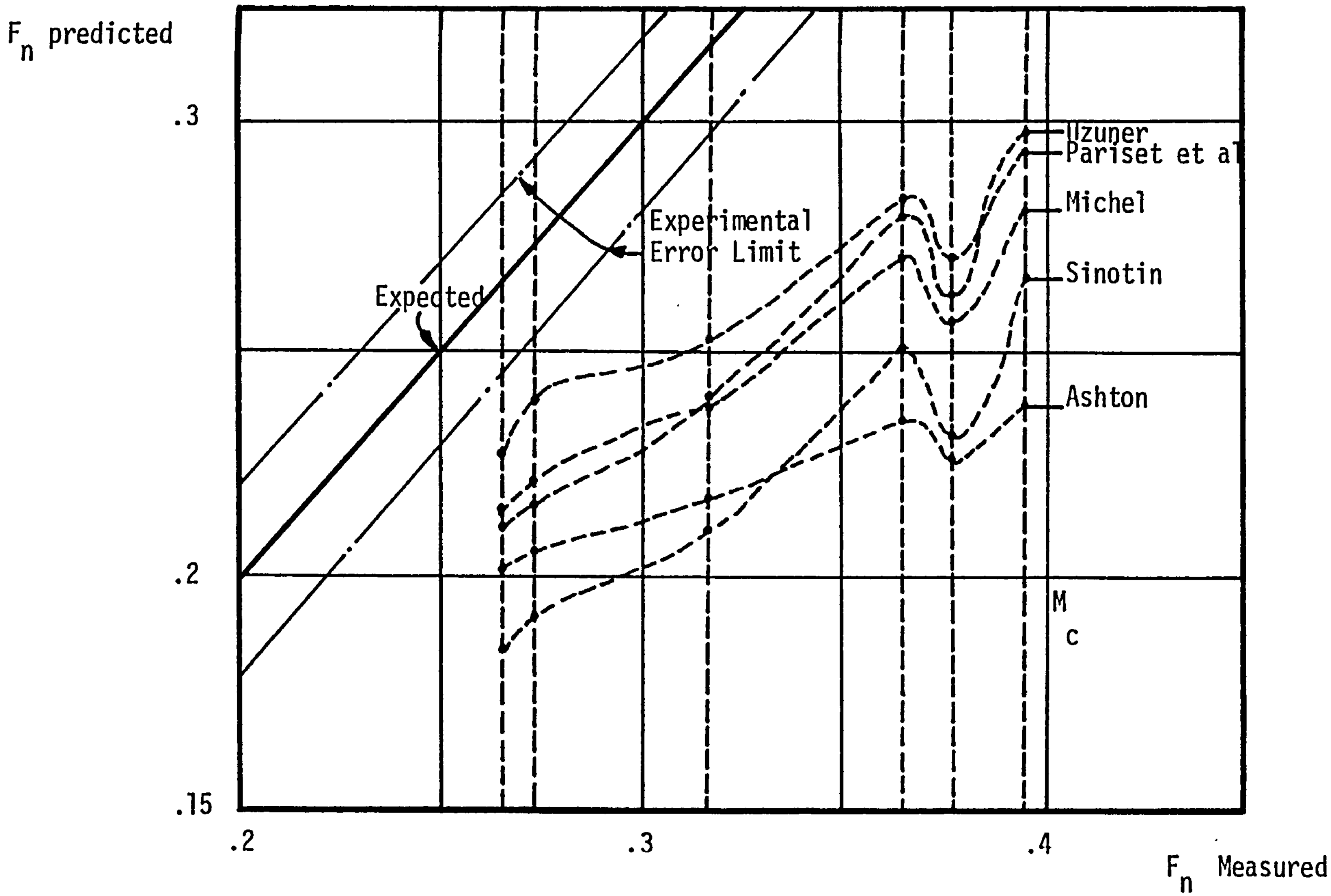

Figure 6.8: Comparison Between Literature and Experimental Results for Circular Edge

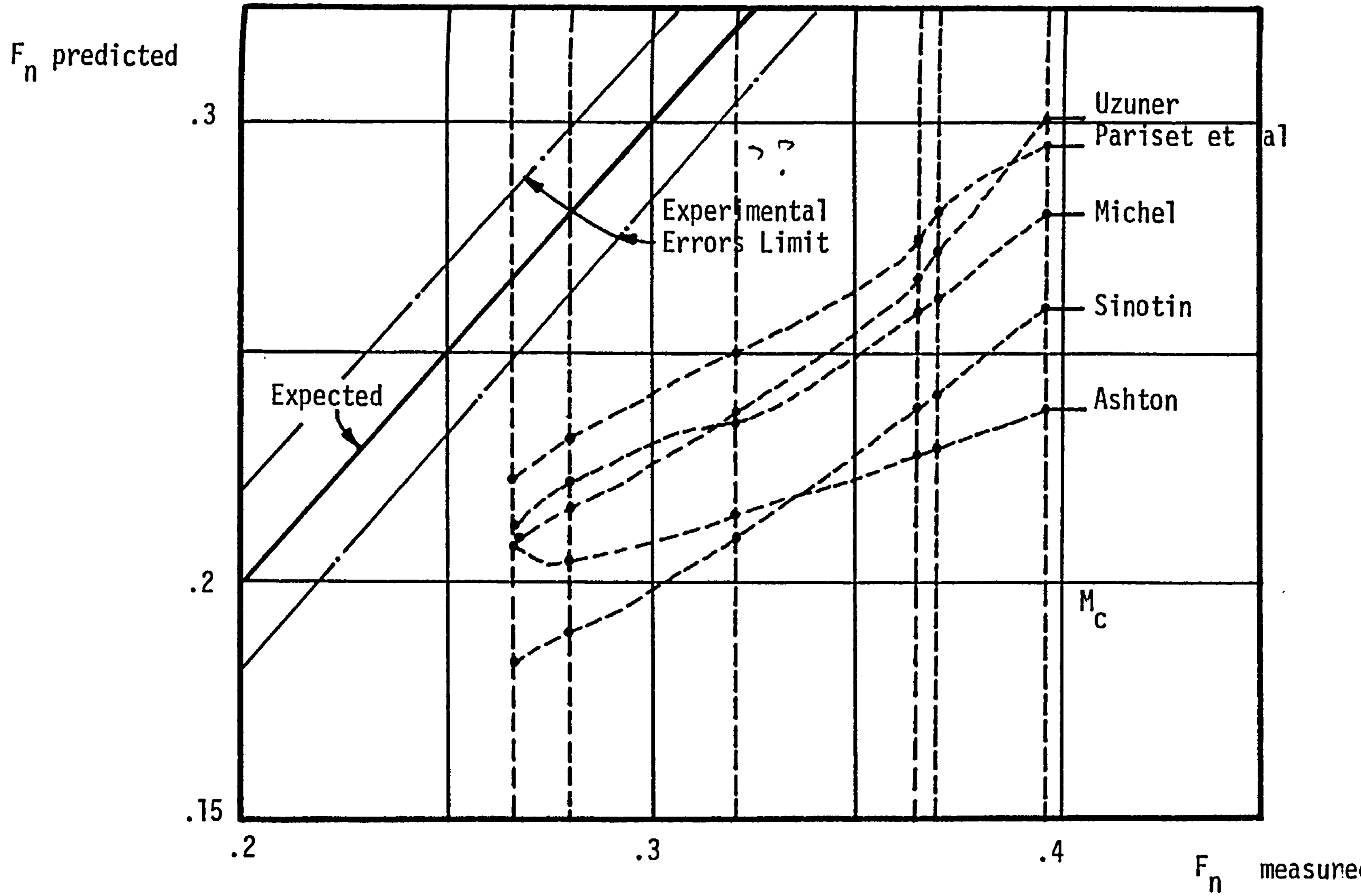

Figure 6.9: Comparison Between Literature and Experimental Results for 1:1 Edge

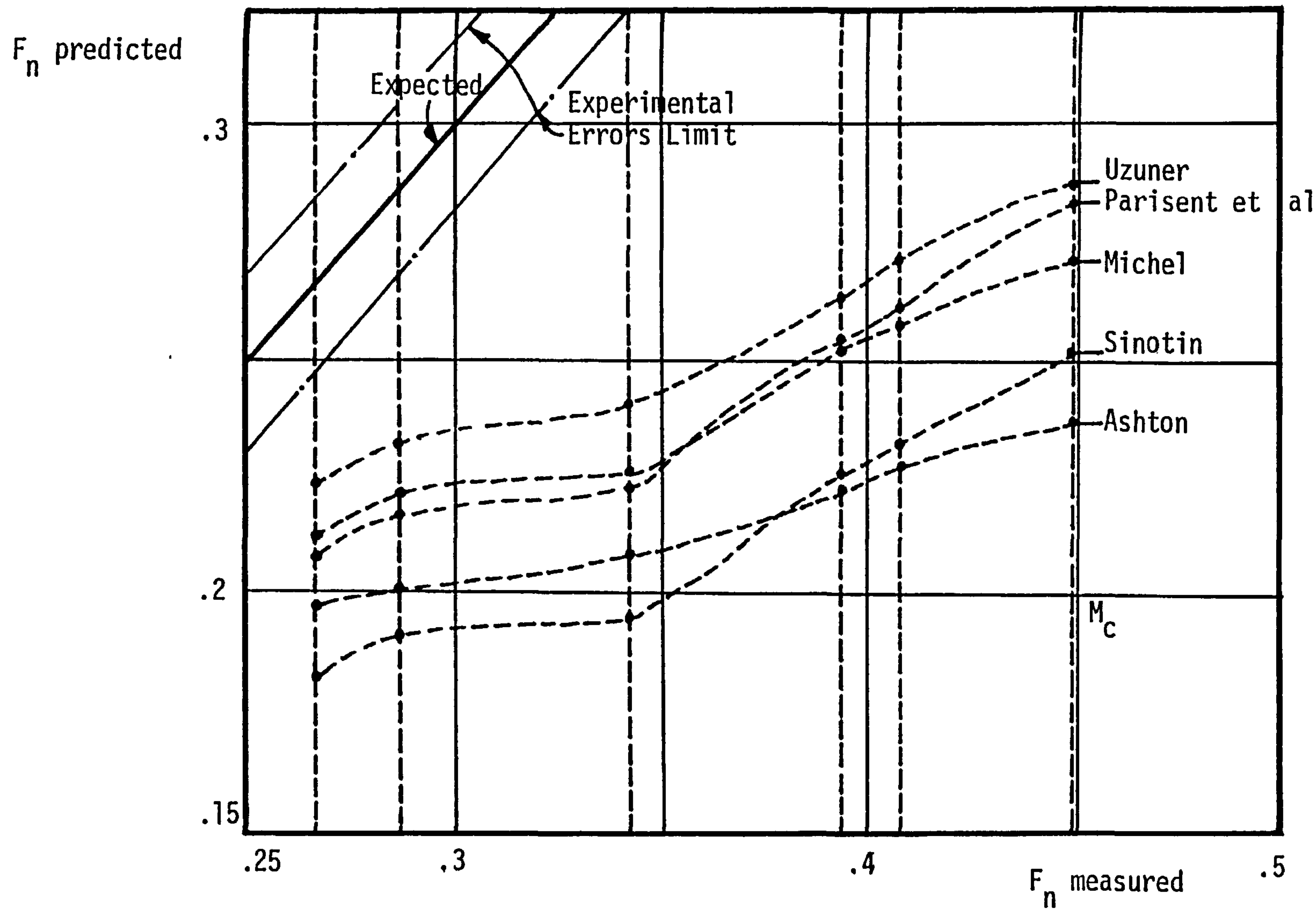

Figure 6.10: Comparison Between Literature and Experimental Results for 2:1 Edge

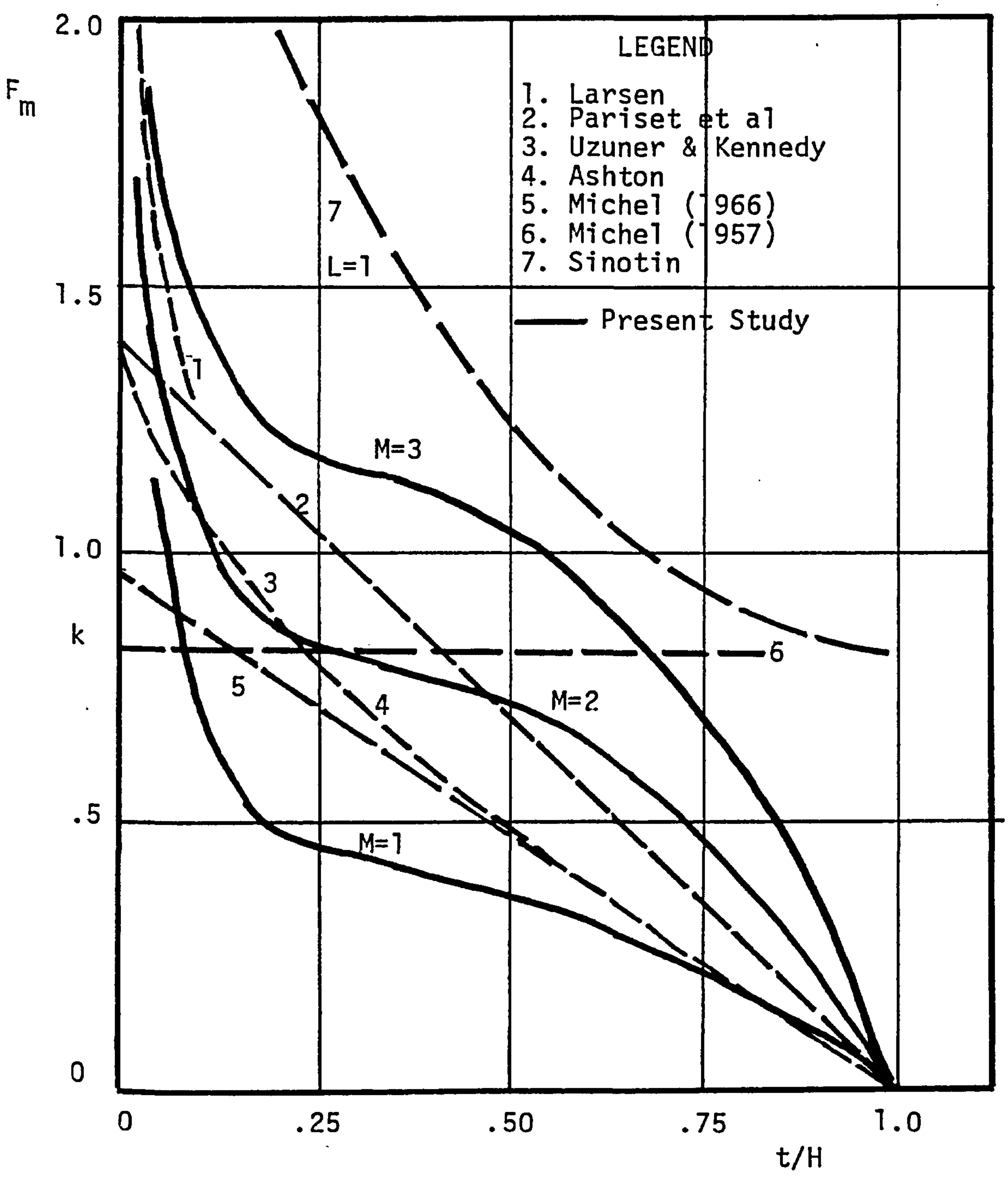

Figure 6.11: Stability Comparison for the Theory and Literature

CHAPTER VII

CONCLUSIONS AND RESEARCH SUGGESTIONS

VII CONCLUSIONS AND RESEARCH REMARKS

In this chapter a summary of the conclusions obtained from this research is presented followed by suggestions for further investigations.

7.1 Conclusions

The following conclusions can be drawn from the previous dicussions:

1. A technique was developed for predicting the velocity distribution in covered channels with different boundary roughnesses.
2. A method for estimating the composite roughness was developed using Manning's roughness as

$$n_1/n = (\alpha + (1-\alpha)\lambda)^{-5/3}\,(\alpha + (1-\alpha)\frac{n_1}{n_2}\lambda^{5/3})$$

where λ is the solution of

$$\frac{R^{1/6}}{n_1\sqrt{g}} = \frac{0.44}{\kappa}(\sqrt{\lambda}-1)\,(\alpha + (1-\alpha)\lambda)^{1/6} / (1 - \frac{n_1}{n_2}\lambda^{2/3})$$

Similar relations using Chezy's friction factor were also developed.

3. An empirical expression for the friction factor of the cover underside expressing the skin and form resistances was obtained in the form

$$C_{2m} = 6.25 + 5.75 \text{ Log } \frac{R}{k} - 44\left(\frac{\Delta}{L} \cdot \frac{\Delta}{Y}\right)^{1/4}$$

where $C_{2m} = C_2/\sqrt{g}$

and C_2 = the cover underside Chezy's coefficient.

The first two terms represent the skin friction and were adopted from the literature (9), (31), (44) while the form resistance function, expressed by the last term, was developed using the experimental data obtained in this research and is valid only within their limits. Further tests are needed before the equation could be extended beyond the experimental limits.

4. A study of the forces acting on a block arrested at the cover leading edge was presented. Only the case of rotation about the contact point was investigated. A method was developed to predict the extension mechanism and to test the stability conditons.
5. An empirical relation for the block instability problem was also developed to facilitate a less complicated solution to the problem.
6. A mathematical model for predicting the underside configuration of loose floating boundaries was presented.
7. The experimental investigation proved the applicability of the proposed models within the experimental range. Further data are needed to extend the rage of applicability of the developed technique.

7.2 Remarks on Further Investigations

The study presented in this thesis gives rise to some topics that warrant further research. Some of these topics are summarized as follows:

1. Further studies of the applicability of the proposed velocity distribution technique to prismatic channels are needed.

2. Experimental investigation of the shear distribution in open and covered channels is necessary to verify the theoretical solution.
3. A method for the definition of a friction factor that is a property of the boundary alone and a flow equation that satisfies such a condition can be a subject of further research.
4. The study of the instability problem for different geometrical shapes of either the cover leading edge or the block tail is necessary to complement the proposed model. Also the case of the block rotation about its center of buoyancy rather than its contact point needs to be investigated.
5. The lack of any field data on the floating boundary problems restricted the results to those of the laboratory models. A comprehensive field program is needed to compensate for such missing data.

APPENDICES

APPENDIX A

METHODS OF COMPUTING THE SEPARATION LINE POSITION AND COMPOSITE ROUGHNESS

APPENDIX A

In this appendix the necessary equations for the determination of the composite roughness in covered channels are developed. A numerical example is also given to verify and illustrate the application of the equations.

A.1 Velocity Profile Relations

The velocity profile presented in Chapter III with the notatiions adopted in Figure 3.1 was given in the form

$$V_i - U_i(\varepsilon_i) = V_{*i}\, F_1(\varepsilon_i) \qquad ,i = 1,2 \qquad 3.16$$

and

$$V_{max} - U_i(\varepsilon_i) = V_{*i}\, F_2(\varepsilon_i) \qquad ,i = 1,2 \qquad 3.17$$

where

$$\varepsilon_i = y_i \,/\, Y_i \qquad ,i = 1,2$$

and

$$V_{*i} = \sqrt{g\, R_i\, S} \qquad ,i = 1,2$$

From these equations the difference between the average velocities of the bed and cover subsections V_1 and V_2 respectively is given as

$$V_1 - V_2 = \frac{-2}{3\kappa}\,(V_{*1} - V_{*2}) \qquad A.1$$

where κ is the Von-Karman constant and equals 0.4. This relation can be combined with the continuity equation to obtain the mean velocity in the channel V, as

$$V = \frac{1}{2}(V_1 + V_2) - \frac{1}{3\kappa}(V_{*1} - V_{*2})\left(\frac{A_1 - A_2}{A}\right) \qquad \text{A.2}$$

where A_1 and A_2 are the cross-sectional areas of the bed and cover subsections and A is the total cross-sectional area.

A.2 Geometric Definitions

The following definitions are adopted to describe the channel geometry:

1. The relative wetted perimeter ratio α is the ratio between the bed subsection wetted perimeter, P_1, and the total covered channel wetted perimeter, P, or

$$\alpha = P_1 / P \qquad \text{A.3}$$

2. The hydraulic radii ratio λ is defined as the ratio between the cover and bed subsections hydraulic radii, or

$$\lambda = R_2 / R_1 \qquad \text{A.4}$$

where R is defined as

$$R_1 = A_i / P_i \qquad i = 1,2 \qquad \text{A.5}$$

3. The ratio between the areas of the two subsections and the total area can be expressed as

$$(A_1 - A_2)/ A = (\alpha - (1-\alpha)\lambda) / (\alpha + (1-\alpha)\lambda) \qquad \text{A.6}$$

A.3 Expressions For Composite Roughness

In this article the expressions for the determination of the hydraulic radii ratio λ and the composite roughness of the channel will be presented in terms of Chezy's C and Manning's n roughness coefficients.

A.3.1 Application to Chezy's Equation

The Chezy's equation can be written for each subsection as

$$V_i = C_i \sqrt{R_i\, S} \qquad ,i = 1,2 \qquad \text{A.7}$$

which can be combined with Equation A.1 to yield the value of λ as

$$\lambda = \left((C_1 + J) \;/\; (C_2 + J) \right)^2 \qquad \text{A.8}$$

where $J = 2\sqrt{g} \;/\; 3\,\kappa$ A.9

Combining these relations with Equation A.2, the composite roughness can be expressed as

$$\frac{C}{C_1} = (\alpha + (1 - \alpha)\lambda)^{-3/2} \left(\alpha + (1-\alpha)\frac{C_2}{C_1}\lambda^{3/2}\right) \qquad \text{A.10}$$

A.3.2 Application to Manning's Equation

The flow equations according to Manning, written in foot-second units for each subsection, are

$$V_i = \frac{1.486}{n_i} R_i^{2/3} S^{1/2} \qquad ,i = 1,2 \qquad \text{A.11}$$

The introduction of this equation into Equation A.1 will end in the expression

$$\frac{R^{1/6}}{n_1\sqrt{g}} = \frac{0.44}{\kappa} \frac{(\sqrt{\lambda} - 1)}{(1 - n_1 \lambda^{3/2}/n_2)} (\alpha + (1 - \alpha)\lambda)^{1/6} \qquad \text{A.12}$$

For any value of R and known values of n_1 and n_2, this equation can be solved to estimate the λ value. Combining the previous equations with Equation A.2 will result in estimating the composite roughness n from

$$\frac{n_1}{n} = (\alpha + (1 - \alpha)\ \lambda\ )^{-5/3}\ (\alpha\ + (\ 1- \alpha\ )\ \frac{n_1}{n_2}\ \lambda^{5/3}\ ) \qquad \text{A.13}$$

EXAMPLE

Given (39): wide channel

$Y = 2.12$ ft

$n_1 = 0.0240$

$n_2 = 0.0122$

Required: λ, n, C, check velocity profile relations.

Solution: Using Manning's n:

For wide channel $\alpha = 0.5$, $R = Y/2 = 1.06$

$R^{1/6}/\ n_1\sqrt{g} = 7.416$, $n_1/n_2 = 1.967$, $\kappa = 0.4$

From Equation A.12

$$7.416 = 1.11\ (\sqrt{\lambda} - 1)(0.5 + 0.5\lambda\ )^{1/6}/(1 - 1.967\lambda^{2/3})$$

solving for λ : $\lambda = 0.3916$

From Equation A.13: $n = 0.0186$

which agrees with the values reported by Uzuner,

Levi 0.0198, Carey 0.0191, Hancu 0.0207, Larsen 0.0186

Using Chezy's relation

$\lambda = Y_2/Y_1 = 0.3916$, $Y_1 + Y_2 = Y = 2.12$, hence

$Y_1 = 1.523$, $Y_2 = 0.597$

Subistituting in Chezy's equation: $C_1 = 66.41$, $C_2 = 111.75$

From Equation A.8: $\lambda = ((66.41 + 9.5)/(111.75 + 9.5))^2 = 0.3916$

From Equation A.10: $C = 80.47$

which agrees well with Uzuner's data.

<u>Check for velocity relations</u>:

Using arbitrary slope S,

$V_1 - V_2 = 66.41\sqrt{1.523\ S} - 111.75\sqrt{0.597\ S} = -4.38\sqrt{S}$

$(-2/3\kappa)(V_{*1} - V_{*2}) = (-2/3\text{x}0.4)(\sqrt{32.18\text{x}1.523\text{x}S} - \sqrt{32.18\text{x}0.597\text{x}S})$

$= -4.36\sqrt{S}$

which confirms Equation A.5.

$V = 80.47\sqrt{1.06\ S} = 82.85\sqrt{S}$

$V_1 + V_2 = 168.29\sqrt{S}$

$(A_1 - A_2)/A = (0.5 - 0.5\text{x}0.3916)/(0.5 + 0.5\text{x}0.3916) = 0.7186$

$(V_{*1} - V_{*2})/3\kappa = 2.18\sqrt{S}$

From Equation A.6,

$V = \frac{1}{2}\text{x}168.29\sqrt{S} - 2.18\sqrt{S}\ \text{x}\ 0.7186 = 82.6\sqrt{S}$

which agrees with the previously obtained value; this confirms Equation A.6.

APPENDIX B

FORCES AND MOMENTS ACTING ON BLOCKS ARRESTED AT THE LEADING EDGE OF THE COVER

In this appendix the different forces acting on the block and their moments about the centre of rotation are developed. The notation and definitions are explained in Figure B.1.

B.1 Weight of Block Core

The weight of the block core W is

$$W = \gamma S_g \, t \, L \qquad \text{B.1}$$

acting on the positive y direction. The moment caused by this force in the general position is

$$M_W = W \left(\tfrac{1}{2} L \cos\alpha - \left(\tfrac{1}{2} t - S_{g1} t + \Delta - Y_r \right) \sin\alpha \right) \qquad \text{B.2}$$

B.2 Weight of Block Edge

The weight of block edge is W_e, where

$$W_e = \gamma \, S_g \, V_e \qquad \text{B.3}$$

where V_e = Volume of Edge

Shown in Figure B.1 are the points of action of this force. The moment due to this force is

$$M_{we} = W_e \left((L + e_x) \cos\alpha - (e_y - S_{g1} t + \Delta - Y_r) \sin\alpha \right) \qquad \text{B.4}$$

Different types of block edges can be found in nature. The two cases suggested in this research are the linear and circular edges, Figure B.2, Equations B.3 and B.4 for these types are reduced to :

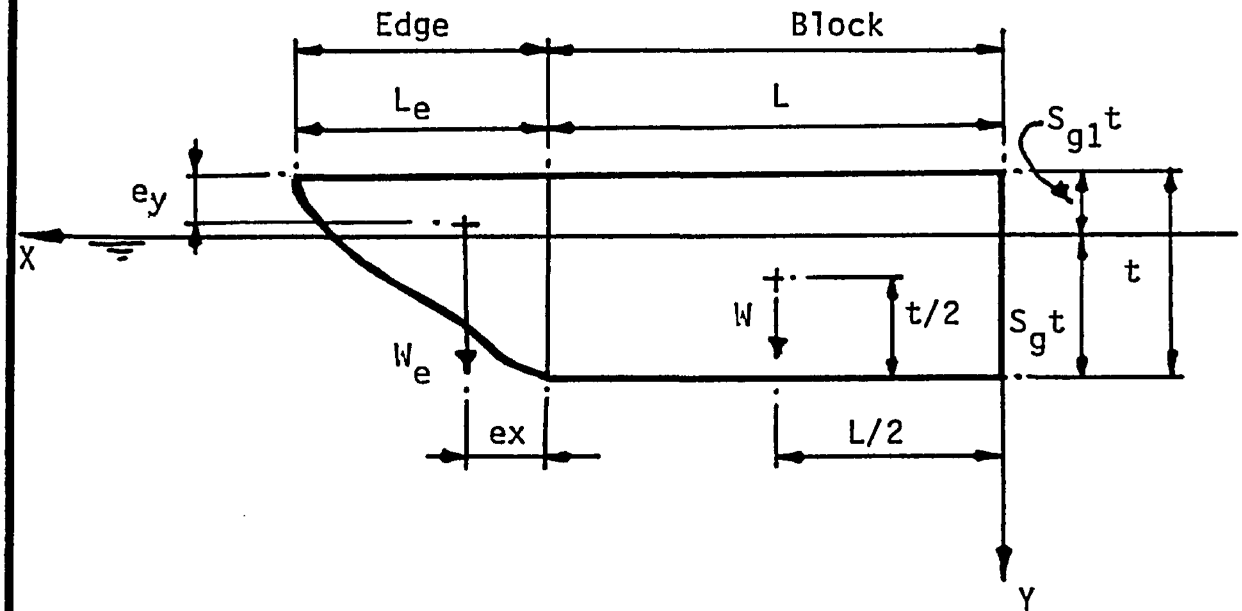

Figure B.1: Definitions

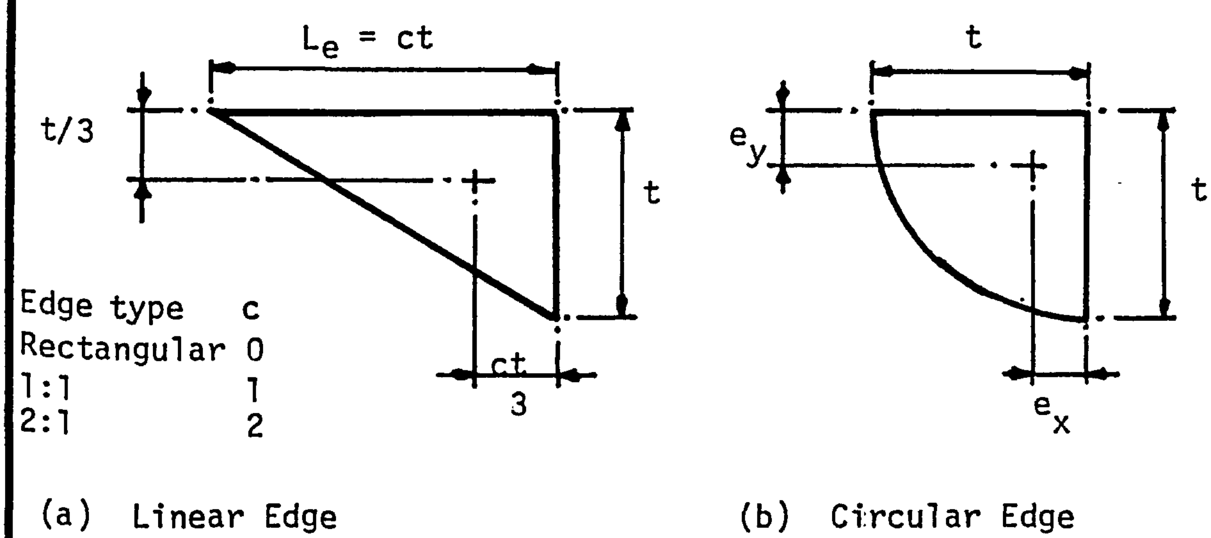

Figure B.2 Types of Block Edges

a) Linear Edges:

$$W_e = \tfrac{1}{2}\,\gamma\, S_g\, c\, t^2 \qquad \text{B.5}$$

b) Circular Edge:

$$W_e = \tfrac{1}{4}\,\gamma\, S_g\, t^2 \qquad \text{B.6}$$

B.3 Additional Weight of Water due to Submergence

This weight will only appear if the block is stable in such a position that its top leading corner has plunged under the flow surface, Figure B.3. This force. W_a, is

$$W_a = \tfrac{1}{2}\,\gamma\, Y_1^{\,2} \,/\, \mathrm{Tan}\,\alpha \qquad \text{B.7}$$

where Y_1 is the vertical ordinate of the top leading corner after displacement Δ and rotation α . Its moment, M_{wa}, is

$$M_{wa} = W_a\,\left(L + L_e - \tfrac{1}{3}\, Y_1 \,/\, \mathrm{Tan}\,\alpha \right) \qquad \text{B.8}$$

In the case of a sink-upturn mode a similar condition can happen then

$$W_a = \tfrac{1}{2}\,\gamma\, Y_4^{\,2} \,/\, \mathrm{Tan}\,\alpha \qquad \text{B.9}$$

and

$$M_{wa} = W_a\,\left(\tfrac{1}{3}\, Y_4 \,/\, \mathrm{Tan}\,\alpha \right) \qquad \text{B.10}$$

where Y_4 is the vertical ordinate of the back top corner of the block.

B.4 Surface Tension Force

This is the force that develops between the two adjacent faces

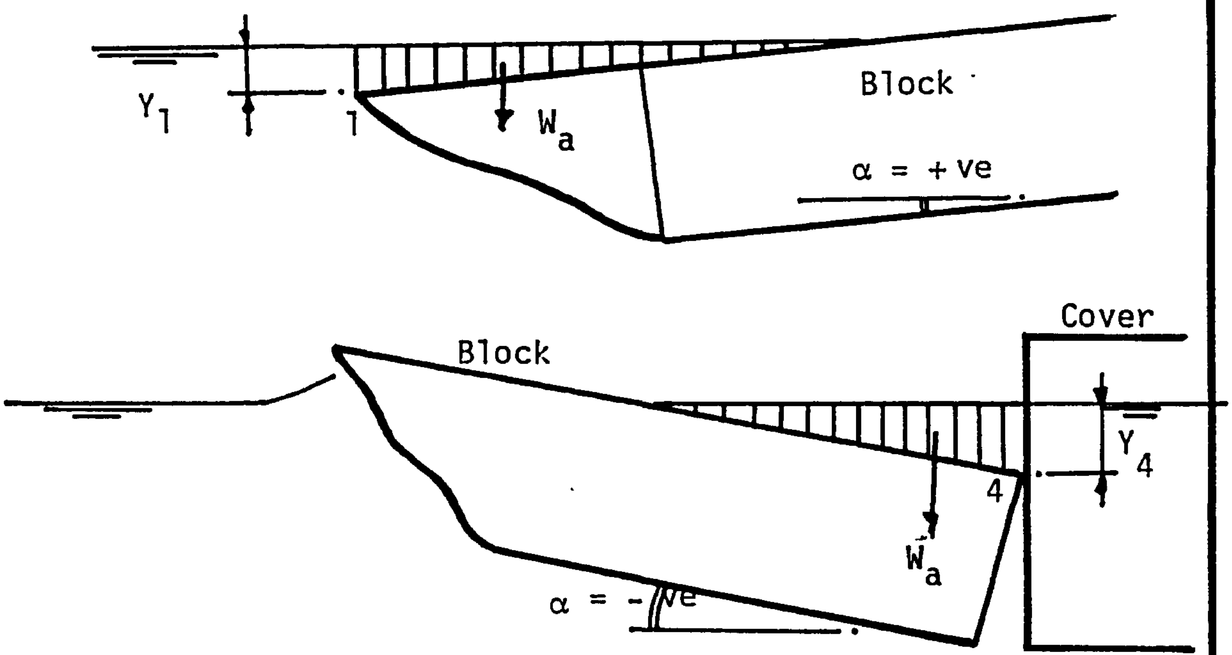

Figure B.3: Additional Weight due to Submergence

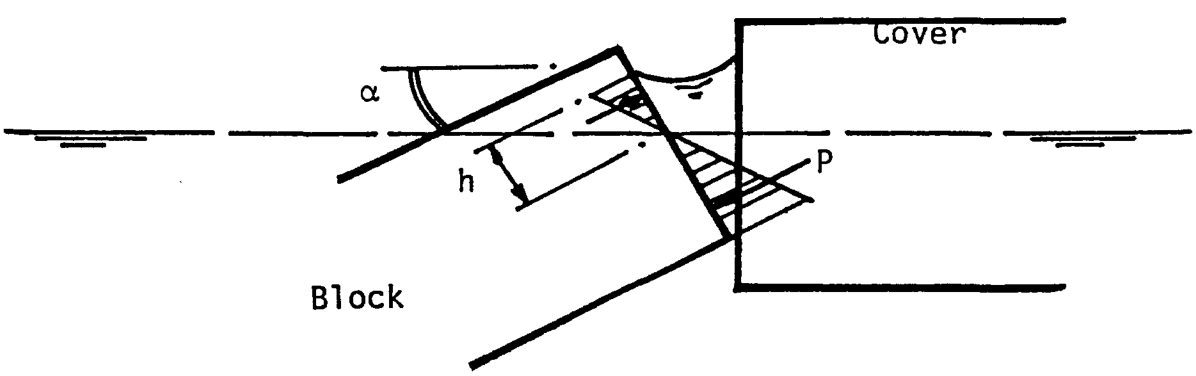

Figure B.4: Surface Tension Forces

of the blcok and cover. This force is very small and only acts when the block and cover are very close. It can be safely neglected without any disturbace to the results. This force is shown in Figure B.4.

B.5 Edge Forces

The edge force was estimated by applying the momentum principle to the differential volume shown in Figure B.5. The edge surface, in the displaced position, Figure B.5, was described generally as $y_e = y_e(x)$.

B.5.1 In the x direction

The application of the momentum equation to the differential element, considering the pressure to be hydrostatic, gives the horizontal component of the edge force as

$$dF_{xe} = \gamma\, y_e\, dy + \rho\, V_s^2\, d\left(y_e + y_e^2 \operatorname{Tan} \theta \,/\, (X_o - x)\right) \qquad \text{B.11}$$

where V_s is the surface velocity and equals

$$V_s = C_s\, V$$

and C_s is the surface velocity coefficient that can be obtained through the developed velocity profile in Chapter III.

The distance from the cover face to the farthest point , up-stream of the block, that feels the block's existence is denoted by X_o. This distance was considered as

$$X_o = L + 5L_e \text{ or } 5t \qquad \text{B.12}$$

whichever is greater.

Integrating this equation will yield the edge force F_{xe} as

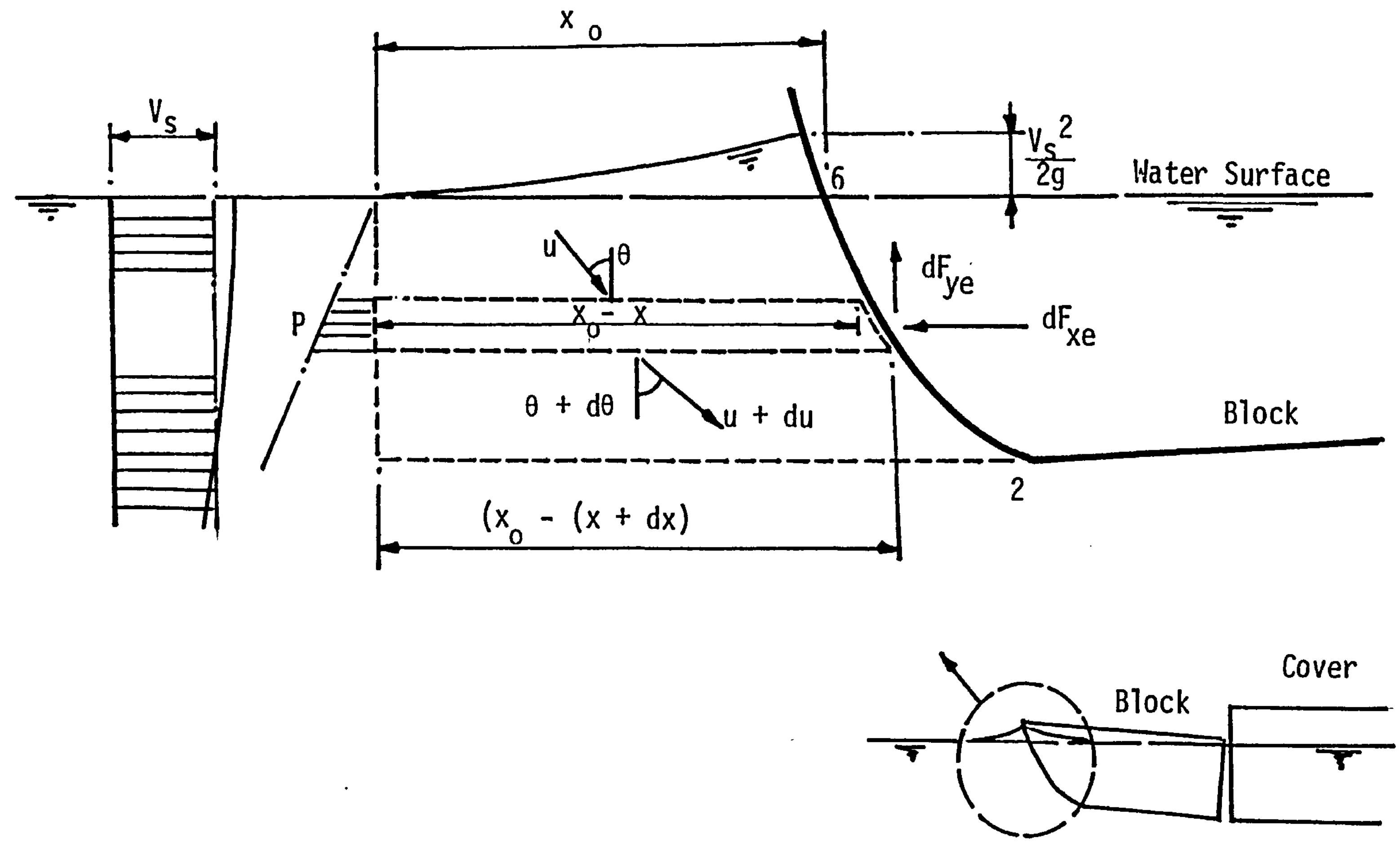

Figure B.5: Estimation of the Forces on the Block Edge

$$F_{xe} = \left[\rho V_s^2 y_e - \frac{1}{2} \gamma y_e^2 - \frac{y_e^2 \rho V_s^2 \operatorname{Tan} \theta}{X_o - x} \right]_{p1}^{p6} \quad B.13$$

The local moment about the point of rotation due to this force is

$$M_{xe} = \int_{edge} (y_e - Y_r)\, dF_{xe} \quad B.14$$

B.5.2 In the Y direction

Following the same approach as the horizontal force, the local vertical force is

$$dF_{ye} = -\gamma y_e - \rho V_s^2 y_e^2 / (X_o - x) \quad B.15$$

The total force accordingly will be

$$F_{ye} = \int_{edge} dF_{ye} \quad B.16$$

and the total moment due to this force will be

$$M_{ye} = \int_{edge} x\, dF_{ye} \quad B.17$$

It should be noticed that if the leading top corner drops below the static water level in any sinking mode, the integration limits should be modified.

B.6 Forces on the Block Underside

The forces acting on the block underside and their moments are obtained using the momentum equation, Figure B.6. The application of the momentum principle to the differential element will yield the variation of both the X and Y components of the underside forces with the X direction as

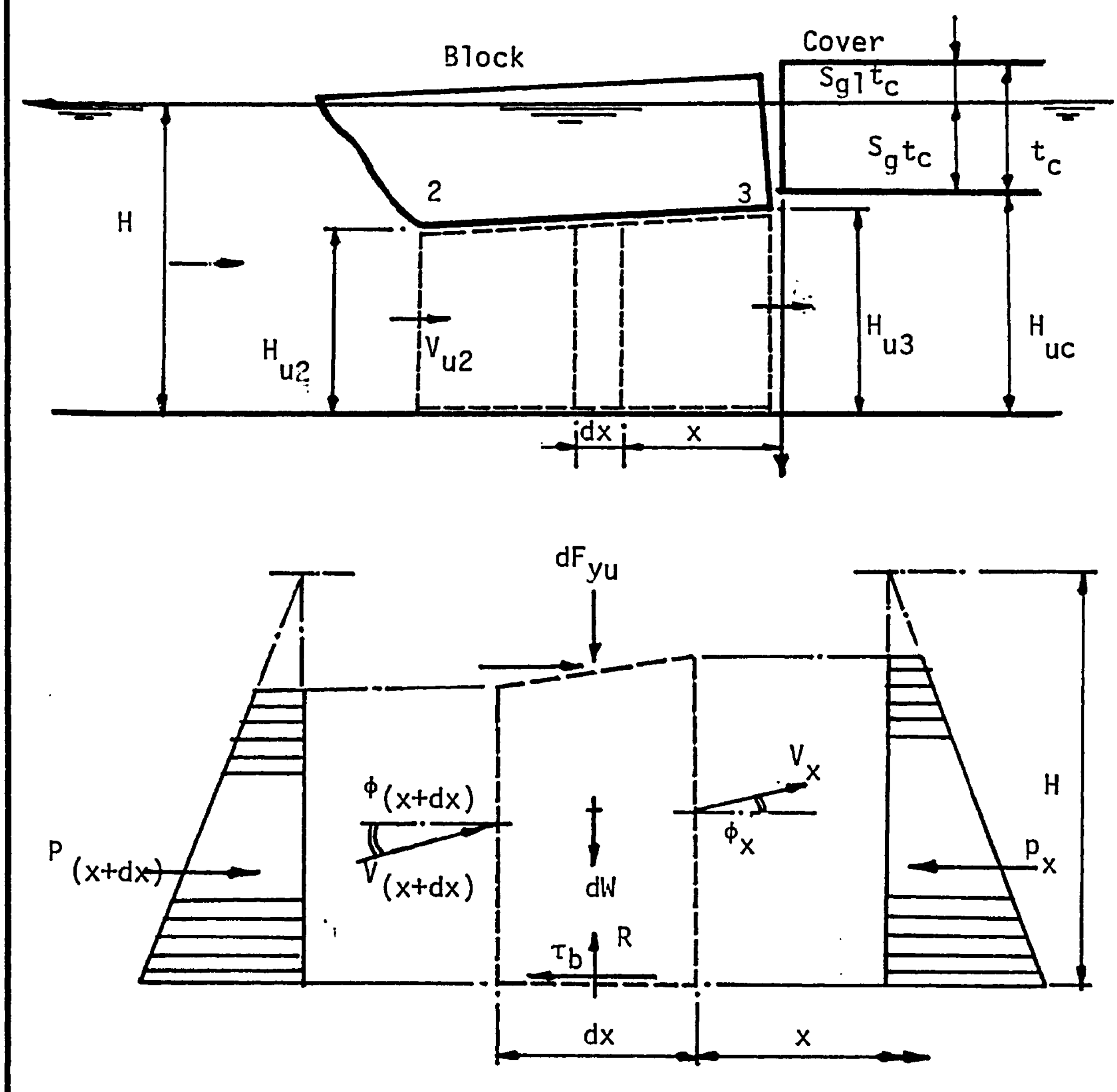

Figure B.6: Forces on Block Underside

$$\frac{dF_{yu}}{dx} = \frac{dR_b}{dx} - \frac{dW}{dx} + \rho\ q \frac{d}{dx} (a\ V_u \operatorname{Sin} \phi\ ) \qquad \text{B.18}$$

and

$$\frac{dF_{xu}}{dx} = \frac{d\tau'_b}{dx} + \frac{dP_x}{dx} - \rho\ q \frac{d}{dx} (a\ V_u \operatorname{Cos} \phi\ ) \qquad \text{B.19}$$

where the different terms will be determined subsequently.

The moments caused by these forces can then be calculated as

$$M_{yu} = \int_{\text{block underside}} x_u \frac{dF_{yu}}{dx}\ dx \qquad \text{B.20}$$

and

$$M_{xu} = \int_{\text{block underside}} (y_u - Y_r) \frac{dF_{xu}}{dx}\ dx \qquad \text{B.21}$$

In the previous expressions the total pressure was assumed to be proportional to the static one. Hence, the pressure was expressed as

$$P_x = C_p\ \gamma\ H_u(H - \tfrac{1}{2} H_u) \qquad \text{B.22}$$

The water weight, W, was taken as the weight of the water column above the bed at the section. The variation of this weight along the X axis is

$$dW / dx = \gamma\ H_u \qquad \text{B.23}$$

The bed reaction, on the other hand, equals the total weight of the fluid and the cover above the bed, i.e.

$$dR_b / dx = \ \ H \qquad \text{B.24}$$

The bed shear, τ_b, is the shear that developes at the bottom in the bed subsection. This shear is estimated at

$$d\tau_b'/dx = \gamma H_u S / (1 + \lambda) \qquad B.25$$

where C_τ is a factor that accounts for the nonuniform conditions at the leading edge and the redistribution of the energy under the cover. and λ is the hydraulic radii ratio as expressed in Appendix A.

The continuity relation shows the variation of the flow in the X direction to be

$$dq / dx = d(V_u H_u \mathrm{Cos}\ \phi)/ dx \qquad B.27$$

which can be used to express the variation in the velocity components as per the momentum equation. These variations will be

$$\frac{d}{dx}\ (a\ V_u \mathrm{Cos}\ \phi) = \frac{a\ q}{H_u}\ \left(\frac{1}{a}\frac{da}{dx} + \frac{1}{H_u}\mathrm{Tan}\ \alpha + \frac{1}{q}\frac{dq}{dx} \right) \qquad B.28$$

and

$$\frac{d}{dx}\ (a\ V_u \mathrm{Sin}\ \phi) = \frac{a\ q}{H_u}\ \mathrm{Tan}\ \phi \left(\frac{\mathrm{Tan}\ \alpha}{H_u} + \frac{1}{a}\frac{da}{dx} + \frac{1}{q}\frac{dq}{dx} + \frac{2}{\mathrm{Sin}\ 2\phi}\frac{d\phi}{dx} \right) \qquad B.29$$

The expressions developed in the forementioned equations, namely Equations B.18 to B.29 can be used to obtain the forces on the block underside, F_{xu} and F_{yu}, as well as their moments M_{xu} and M_{yu}.

B.7 The Cover Reaction

In order for the block to be stable the sum of all the forces acting on it in as well as their corresponding moments should vanish. Hence the cover reactions at the point of contact can estimated as

$$R_x = F_{xe} + F_{xu} \qquad \text{B.30}$$

and

$$R_y = F_{ye} + F_{yu} - W - W_e - W_a \qquad \text{B.31}$$

and the values of the different forces were estimated earlier.

The tangential reaction R_t can be expressed as

$$R_t = R_y \text{ Cos } \alpha - R_x \text{ Sin } \alpha \qquad \text{B.32}$$

while the sum of all the moments is

$$\Sigma M = M_w + M_{we} + M_{wa} - M_{ye} - M_{xe} - M_{yu} + M_{xu} \qquad \text{B.33}$$

and the different moments were developed earlier. For the block to be stable this sum of moments should vanish, i.e.

$$\Sigma M = 0 \qquad \text{B.34}$$

APPENDIX C

LIST OF NUMERICAL PROGRAMS

Block Instability Problem

```
      COMMON/AREA1/L,LE,T,TC,C,SG,NU,NE,GM,S,XR,YR,X6,Y6
      COMMON/AREA2/XO(5),X(5),YO(5),Y(5),XS(20),YS(20),XU(20),YU(20)
      COMMON/AREA3/W,MW,WE,MWE,WW,MWA,FEX,MEX,FEY,MEY,FUX,MUX,FUY,MUY,RX
     *,RY,RT,MT
      COMMON/AREA4/VO,HO
      DIMENSION XX(2),WA(8)
      DIMENSION AL(6)
      DOUBLE PRECISION XX,WA,EPS,ALF,DLT,F
      EXTERNAL F
      REAL MT,MW,MWE,MWA,MEY,MEX,MUY,MUX,L,LE,NC
      G=32.18
      GM=62.4
      SG=0.65
      NE=11
      NU=11
      T=1.5/12.
      TC=T
      NC=0.01
       SGI=1.-SG
      READ(5,17) (AL(I),I=1,6)
 17   FORMAT(6F5.2)
      DO 999 KC=1,3
      C=KC-1.
      DO 999 KL=1,6
      L=AL(KL)
      L=L/12.
      DO 999 KH=1,5
      HC=0.2+0.2*KH
      WRITE(6,2)
 2    FORMAT('XXXXXXXXXXXXXXXXXXXXXXXXXXXXXXXXXXXXXXXXXXXXXXXXXXXX')
      WRITE(6,71) C,L,HC
 71   FORMAT(' FOR: C=',F5.2,'  L=',F8.4,'  HC=',F8.4)
      DO 999 KQ=1,10
      Q=0.25*KQ
      LE=C*T
      VO=Q/HC
      HU=HC-SG*TC
      VU=Q/HU
      FNO=VO/SQRT(G*HC)
      FNU=VU/SQRT(G*HU)
      S=VU*VU*NC/(1.49*(HU**(3./2.)))
      XO(1)=L+LE
      YO(1)=-SGI*T
      XO(2)=L
      YO(2)=SG*T
      XO(3)=0.0
      YO(3)=SG*T
      XO(4)=0.0
      YO(4)=-SGI*T
      XO(5)=L
      YO(5)=-SGI*T
      XX(1)=T*1.0D-1
      XX(2)=0.1*3.14/180.
      EPS=1.0D-3
      NSIG=4
      N=2
      IMAX=100
      CALL ZSYSTM (F,EPS,NSIG,N,XX,IMAX,WA,PAR,IER)
      ALF=XX(2)
      DLT=XX(1)
      DLH=DLT/HC
      DLTT=DLT/T
      CALL STABL(DLT,ALF,1,AUX)
      WRITE(6,72) Q,FNO,DLT,ALF,DLH,FEX,FEY,FUX,FUY,RX,RY
 72   FORMAT(1X,11F9.4)
 999  CONTINUE
      WRITE(6,2)
      STOP
      END

      DOUBLE PRECISION FUNCTION   F(XX,K,PAR)
      DIMENSION XX(2)
      DOUBLE PRECISION XX
      GO TO (5,10),K
 5    CALL STABL(XX(1),XX(2),1,AA)
      F=AA
      RETURN
 10   CALL STABL(XX(1),XX(2),2,AA)
      F=AA
```

```
      RETURN
      END

      SUBROUTINE STABL (DLT,ALF,MK,AA)
      COMMON/AREA1/L,LE,T,TC,C,SG,NU,NE,GM,S,XR,YR,X6,Y6
      COMMON/AREA2/XO(5),X(5),YO(5),Y(5),XE(20),YE(20),XU(20),YU(20)
      COMMON/AREA3/W,MW,WE,MWE,WW,MWA,FEX,MEX,FEY,MEY,FUX,MUX,FUY,MUY,RX
     *,RY,RT,MT
      COMMON/AREA4/VC,HC
      DIMENSION TTH(20),Z(20),DFYUDX(20),DMYUDX(20),DFXUDX(20),DMXUDX(20
     *)
      DIMENSION TH(20)
      DOUBLE PRECISION XX,WA,EPS,ALF,DLT
      REAL MT,MW,MWE,MWA,MEY,MEX,MUY,MUX,L,LE,NC
      G=32.18
      PI=3.14
      SGI=1.-SG
      IF(ALF.EQ.0.0) ALF=0.0001
CCCCCCPOINT OF ROTATION
      AALF=DABS(ALF)
      SGE =SG-0.5+0.5*ALF/AALF
      IF( SGE * DLT ) 2,1,1
    1 YR=SGE*TC
      GO TO 3
    2 YR=SGE*T+DLT
    3 XR=0.0
CCCCCCDETERMINATION OF ROTATED POINTS
      CALF=1.0
      SALF=ALF
      TALF=ALF
      DO 11 I=1,5
      X(I)=XO(I)*CALF-(YO(I)+DLT-YR)*SALF
      Y(I)=XO(I)*SALF+(YO(I)+DLT-YR)*CALF+YR
   11 CONTINUE
      DO 12 I=1,NU
      XUO=L*(I-1)/(NU-1)
      YUO=SG*T
      XU(I)=XUO*CALF-(YUO+DLT-YR)*SALF
      YU(I)=XUO*SALF+(YUO+DLT-YR)*CALF+YR
   12 CONTINUE
CCCCCCEDGE INTERSECTION AND POINTS (LINEAR EDGES ONLY)
      Y6=0.0
      A1=(Y(2)-Y(1))/(X(2)-X(1))
      B1=Y(1)-A1*X(1)
      X6=X(1)-Y(1)/A1
      IF(X6.LE.X(1)) GO TO 13
      X6=X(1)
      Y6=Y(1)
   13 DY=(Y(2)-Y6)/(NE-1)
      DO 17 I=1,NE
      YE(I)=Y6+(I-1)*DY
      XE(I)=(YE(I)-B1)/A1
   17 CONTINUE
CCCCCCDETERMINATION OF FORCES AND THEIR MOMENTS
CCCCCCWEIGHT W
      W=SG*GM*T*L
      MW=W*(0.5*L*CALF-((0.5-SGI)*T+DLT-YR)*SALF)
CCCCCCEDGE WEIGHT WE
      WE=0.5*C*GM*SG*T*T
      MWE=WE*((L+C*T/3.)*CALF-(T/3.-SGI*T+DLT-YR)*SALF)
CCCCCCADDITIONAL WEIGHT DUE TO SUBMERGENCE
      WW=0.0
      MWA=0.0
CCCCCCCCCCC  EDGE FORCES AND MOMENTS
      RO=GM/G
      VS=VC*1.1
      XCO=5.*T+L+LE
      TTH2=A1*(1.-Y6/Y(2))
      TTH2=ABS(TTH2)
      TH2=TTH2
      FEX=RO*VS*VS*Y(2)*Y(2)*TTH2/(XCO-X(2))+0.5*GM*Y(2)*Y(2)+1.[illegible]*RO*Y(2
     *)*VS*VS
      FEY=-FEX
      AZ=0.0
      DO 31 I=1,NE
      TH(I)=TH2*YE(I)/Y(2)
      TTH(I)=TH(I)
   31 Z(I)=(YE(I)*YE(I)*TTH(I)/ (XCO-XE(I)))
      WS=SQRT((X6-X(2))*(X6-X(2))+(Y6-Y(2))*(Y6-Y(2)))/(NE-1)
      CALL SIMSON (Z,WS,1,NE,AZ)
```

```
      MFX=RO*VS*VS*((YR-Y(2))*(1.5*Y(2)+Y(2)*Y(2)*TTH2/(XCO-X(2)))
     1+AZ)+GM*Y(2)*Y(2)*(0.5*YR-Y(2)/3.+.75*VS*VS/G)
      FEY=0.5*GM*(Y(2)-Y6)*(X6-X(2))-RO*VS*VS*Y(2)*Y(2)/(XOO-X(2))
      AI=Y(2)/(X(2)-X6)
      BI=-X6*AI
      AZ=0.0
      DO 33 I=1,NE
   33 Z(I)=(AI*AI*XE(I)*XE(I)+2.*AI*BI*XE(I)+BI*BI)/(XOO-XE(I))
      WS=L/(NE-1)
      CALL SIMSON(Z,WS,1,NE,AEY)
      MFY=GM*Y(2)*(X6*X6/6.+X6*X(2)/6.-X(2)*X(2)/3.)-RO*VS*VS
     1*((X(2)*Y(2)*Y(2)/(XOO-X(2)))-AEY)
      IF(Y(2).LE.0.0) FEX=0.0
      IF(Y(2).LE.0.0) MFX=0.0
      IF(Y(2).LE.0.0) FEY=0.0
      IF(Y(2).LE.0.0) MFY=0.0
CCCCCCFORCES AND MOMENTS ON BLOCK UNDERSIDE
      CT=1.0
      Q=VO*HO
      FI=2.0*ALF
      TFI=2.0*TALF
      DO 41 I=1,NU
      H=HO-YU(I)
      DFYUDX(I)=-GM*YU(I)-RO*Q*Q*TFI*TALF/(H*H)
      DFYUDX(I)=-DFYUDX(I)
      DMYUDX(I)=DFYUDX(I)*XU(I)
      DFXUDX(I)=CT*GM*H*S-GM*TALF*YU(I)-RO*Q*Q*TALF/(H*H)
      DMXUDX(I)=(YR-YU(I))*DFXUDX(I)
   41 CONTINUE
      WS=L/(NU-1)
      CALL SIMSON(DFYUDX,WS,1,NU,FUY)
      CALL SIMSON(DMYUDX,WS,1,NU,MUY)
      CALL SIMSON(DFXUDX,WS,1,NU,FUX)
      CALL SIMSON(DMXUDX,WS,1,NU,MUX)
CCCCCCCCCCCCCC TOTAL FORCES
      RX=FEX+FUX
      RY=FEY+FUY-W-WF-WW
      RT=RY*CALF-RX*SALF
      MT=MW+MWF+MWA-MFY-MFX-MUY+MUX
      AA=RY
      IF(YR.EQ.(SG*TC).OR.YR.EQ.(SGI*TC)) AA=RT
      IF(MK.EQ.2) AA=MT
      RETURN
      END

      SUBROUTINE SIMSON(X,WS,IS,IL,A)
      DIMENSION X(20)
      IIS=IS+1
      IL1=IL-1
      A=0.0
      DO 9 IK=IIS,IL1,2
    9 A=A+4.*X(IK)+2.*X(IK+1)
      A=(A+X(IS)-X(IL))*WS/3.
      RETURN
      END
```

Subroutine ZSYSTM is an IBM library subroutine.

FOR: C= 2.00 L= 0.2500 HO= 1.0000

0.2500	0.0441	-0.0237	0.1263	-0.0237	-0.2680	0.7042	-0.1409	1.1454	-0.4089	-0.0517
0.5000	0.0831	-0.0243	0.1281	-0.0243	-0.3258	0.7005	-0.1311	1.1421	-0.4579	-0.0586
0.7500	0.1322	-0.0257	0.1319	0.0257	-0.4236	0.6957	-0.1164	1.1344	-0.5400	-0.0712
1.0000	0.1763	4.3651	-5.3329	4.3651	-309.8062	-85.3821	314.4067	62.7495	4.6006	-24.5338
1.2500	0.2204	-0.0353	0.1661	-0.0353	-0.7290	0.6731	-0.1119	1.0884	-0.8409	-0.1397
1.5000	0.2644	0.0069	0.0131	0.0059	-1.0100	0.4893	0.2527	1.4020	-0.7572	-0.0099
1.7500	0.3085	-0.0148	0.0897	-0.0148	-1.2301	0.5629	0.1325	1.2398	-1.0976	-0.0985
2.0000	0.3526	-0.0174	0.0967	-0.0174	-1.5132	0.5456	0.1863	1.2273	-1.3270	-0.1284
2.2500	0.3966	-0.0188	0.0994	0.0188	-1.8329	0.5199	0.2583	1.2248	-1.5747	-0.1566
2.5000	0.4407	0.0366	-0.2106	0.0366	-1.6256	0.0946	1.8742	1.7543	0.2486	-0.0523

XXXXXXXXXXXXXXXXXXXXXXXXXXXXXXXXXXXXXXXXXXXXXXXXX

FOR: C= 2.00 L= 0.2500 HO= 1.2000

0.2500	0.0335	-0.0235	0.1259	-0.0196	-0.2620	0.7039	-0.1422	1.1465	-0.4043	-0.0509
0.5000	0.0671	-0.0242	0.1277	-0.0201	-0.3028	0.7024	-0.1377	1.1426	-0.4405	-0.0562
0.7500	0.1006	-0.0251	0.1301	-0.0209	-0.3703	0.6987	-0.1301	1.1374	-0.5005	-0.0651
1.0000	0.1341	-0.0271	0.1361	-0.0226	-0.4629	0.6974	-0.1231	1.1240	-0.5860	-0.0798
1.2500	0.1676	-0.0322	0.1518	-0.0269	-0.5751	0.7071	-0.1257	1.0878	-0.7009	-0.1064
1.5000	0.2012	1.3347	-0.4144	1.1123	-65.0957	-19.2000	27.4161	36.7166	-37.6797	15.6153
1.7500	0.2347	-0.0033	0.0507	-0.0028	-0.9549	0.5378	0.1144	1.3208	-0.8405	-0.0426
2.0000	0.2682	-0.0119	0.0801	0.0099	-1.1476	0.5584	0.0938	1.2584	-1.0538	-0.0845
2.2500	0.3017	-0.0150	0.0895	-0.0125	-1.3709	0.5498	0.1193	1.2394	-1.2517	-0.1120
2.5000	0.3353	-0.0167	0.0938	-0.0139	-1.5205	0.5324	0.1599	1.2319	-1.4606	-0.1370

XXXXXXXXXXXXXXXXXXXXXXXXXXXXXXXXXXXXXXXXXXXXXXXXX

FOR: C= 2.00 L= 0.5000 HO= 0.4000

0.2500	0.1742	-0.0093	0.0413	-0.0232	-0.3990	0.5865	0.0966	2.5698	-0.3024	-0.0125
0.5000	0.3484	-0.0032	0.0266	-0.0080	-0.7791	0.5224	0.7675	2.6461	-0.0116	-0.0003
0.7500	0.5226	0.0059	0.0035	0.0149	-1.3839	0.4232	1.9806	2.7476	0.5967	0.0021
1.0000	0.6968	0.0221	-0.0618	0.0551	-1.8069	0.1938	4.3611	2.8170	2.5542	-0.1579
1.2500	0.8710	0.0190	-0.0768	0.0476	-2.3065	0.0984	7.0494	2.7061	4.7428	-0.3643
1.5000	1.0452	0.0124	-0.0772	0.0309	-2.8863	0.0427	10.1637	2.5645	7.2772	-0.5616
1.7500	1.2194	0.0055	-0.0725	0.0138	-3.5505	0.0026	13.7444	2.4274	10.1839	-0.7388
2.0000	1.3936	-0.0008	-0.0668	-0.0021	-4.2915	-0.0310	17.8352	2.2947	13.5437	-0.9050
2.2500	1.5678	-0.0120	-0.0650	-0.0301	-4.1975	-0.0427	22.8817	1.9973	18.6841	-1.2141
2.5000	1.7420	-0.0262	-0.0628	-0.0655	-3.3082	-0.0288	28.8192	1.5964	25.5110	-1.6012

XXXXXXXXXXXXXXXXXXXXXXXXXXXXXXXXXXXXXXXXXXXXXXXXX

Velocity Profile Problem

```
$JCB      WATFIV   XXXXXXXXXX  REDA
          COMMON/AREA1/NI,NJ,Q
          COMMON/AREA2/DUX(25,25),DUY(25,25),TX(25,25),TY(25,25)
          COMMON/AREA3/X(25,25),Y(25,25),XL(25,25),YL(25,25),U(25,25)
          COMMON/AREA4/EXX(25,25),EYY(25,25)
          DIMENSION UOV(25,25),F(25),FF(25)
          EA=1.
          G=32.18
          GM=62.4
          EEPS=0.05
          ETH=1.0
          READ,NI,NJ
          READ,NIJK
          DO 999 IJK=1,NIJK
          READ,BB,BT,H,HI,Q,S
          READ,RC1,RC2,RC3,RC4
          DO 999 K1=1,2
          IF(K1.EQ.2) RC2=0.0
          PRINT 2
    2     FORMAT(' XXXXXXXXXXXXXXXXXXXXXXXXXXXXXXXXXXXXXXXXXXXXXXXXXXXXXXXXX')
          PRINT,NI,NJ
          PRINT,RC1,RC2,RC3,RC4
          PRINT,BB,BT,H,HI,Q,S
          A=BT*H-HI*(BT-BB)/2.
          P=BT+BB+2.*(H-HI)+2.*SQRT(HI*HI-(BT-BB)*(BT-BB)/4.)
          IF(RC2.EQ.0.0) P=P-BT
          R=A/P
          V=Q/A
          PRINT,A,P,R,V
          PRINT,EA
          PRINT 2
          DO 90 J=1,NJ
          DO 90 I=1,NI
          Y(I,J)=(J-1)*H/(NJ-1)
          X(I,J)=(I-1)*BT/(NI-1)
          WE=0.0
          IF(HI.NE.0.0) WE=(BT-BB)*(HI-Y(I,J))/HI
          IF(Y(I,J).LE.HI) X(I,J)=(I-1)*(BT-WE)/(NI-1)+.5*WE
   90     CONTINUE
          CALL PRINT(X)
          CALL PRINT(Y)
          DO 91 J=1,NJ
          DO 91 I=1,NI
          W=X(NI,J)-X(1,J)
          D=Y(I,NJ)-Y(I,1).
          RCX1=RC3
          RCX2=RC4
          RCY2=RC2
          RCY1=RC1
          IF(X(I,J).LT.X(1,1)) RCY1=RC3
          IF(X(I,J).GT.X(NI,1)) RCY1=RC4
          XE=X(I,J)-X(1,J)
          CALL EPSFNC(XE,W,RCX1,RCX2,0.5,EX,EFNX,CRX,RFX,RRX,UOVX)
          EXX(I,J)=EX
          XL(I,J)=EX*RRX
          YE=Y(I,J)-Y(I,1)
          CALL EPSFNC(YE,D,RCY1,RCY2,0.5,EY,EFNY,CRY,RFY,RRY,UOVY)
          EYY(I,J)=EY
          YL(I,J)=EY*RRY
          UOV(I,J)=UOVX*UOVY
   91     CONTINUE
          CALL PRINT(EXX)
          CALL PRINT(EYY)
          CALL PRINT(UOV)
          DO 77 I=1,NI
          DO 77 J=1,NJ
          U(I,J)=(UOV(I,J)**EA)*V
   77     CONTINUE
          CALL PRINT(U)
          AT=0.0
          DO 92 J=1,NJ
          EW=X(NI,J)-X(1,J)
          DO 93 I=1,NI
   93     F(I)=U(I,J)
          CALL SIMSON(F,EW,1,NI,AI)
          FF(J)=AI
   92     CONTINUE
          HE=H
          CALL SIMSON(FF,HE,1,NJ,AA)
          E=Q/AA
```

```
      DE=(E-ETH)/ETH
      PRINT,Q,AA,E,DE
      DO 94  J=1,NJ
      DO 94  I=1,NI
      U(I,J)=U(I,J)*E
94    CONTINUE
      CALL PRINT(U)
      CALL SHEAR(TSH)
      S=TSH/(GM*A)
      CN=1.49*(R**(2./3.))*A*SQRT(S)/C
      PRINT,TSH,A,S,CN
      CALL PRINT(DUX)
      CALL PRINT (DUY)
      PRINT 2
      PRINT 2
      PRINT 2
999   CONTINUE
      STOP
      END

      SUBROUTINE PRINT(F)
       COMMON/AREA1/NI,NJ,Q
      DIMENSION F(25,25)
      PRINT 1,((F(I,J),I=1,NI),J=1,NJ)
1     FORMAT(1X,11F10.5)
      PRINT 82
82    FORMAT (/,'********************************',/)
      RETURN
      END

      SUBROUTINE SIMSON(F,WS,IS,IL,A)
      DIMENSION F(25)
      WS=WS/(IL-1)
      I1S=IS+1
      IL1=IL-1
      A=0.0
      DO 9 IK=I1S,IL1,2
9     A=A+4.*F(IK)+2.*F(IK+1)
      A=(A+F(IS)-F(IL))*WS/3.
      RETURN
      END

      SUBROUTINE EPSFNC(XE,R,RF1,RF2,ALF,EP,EPF,CR,RF,RR,UDV)
      EPS=0.01
      G=32.18
      VK=0.4
      IF(RF2.NE.0.0) GO TO 1
      ALM=0.0
      CR=RF1
      GO TO 10
1     IF(RF1.NE.RF2 ) GO TO 2
      ALM=1.
      CR=RF1
      GO TO 10
2     RF21=RF2/RF1
      RF12=RF1/RF2
      XR=0.9*(R**(1./6.))/(RF1*SQRT(G))
      T=0.95*RF21*SQRT(RF21)
      KN=50
      DO 32 K=1,KN
      C=((1.+T)**(1./6.))*(SQRT(T)-1.)*(1./(1.-RF12*(T**(2./3.))))
      F=C-0.445*VK*(R**(1./6.))/RF1
      DF=C*((1./(6.*(T+1.)))+(1./(2.*(T-SQRT(T))))+(2.*RF12/
     1(3.*(T**(1./3.)-RF12*T))))
      TI=T-F/DF
      IF(ABS((TI-T)/TI).LE.EPS) GO TO 34
32    T =TI
      PRINT 33, KN
33    FORMAT('  AFTER',I4,'  ITTERATICNS.. NO SOLUTION WAS FOUND',/,/)
34    ALM=TI
      Z=(ALF+(1.-ALF)*RF12*(ALM**1.6667))/((ALF+(1.-ALF)*ALM)**1.66667)
      CR=RF1/Z
10    X2=R*ALM/(1.+ALM)
      X1=R/(1.+ALM)
      IF(XE.GT.X1) GO TO 20
      EP=XE/X1
      RR=X1
      RF=RF1
      GO TO 30
20    EP=(R-XE)/X2
```

```
      RR=X2
      RF=RF2
   30 CRF=1.49*(RR**(1./6.))/(RF*SQRT(G))
      IF(EP.EQ.0.0) GO TO 40
      EP1=SQRT(1.-EP)
      EPF=2.*(ALOG(SQRT(EP)/(1.-EP1))-EP1-.3333)/VK
      UOV=1.-EPF/CRF
      GO TO 50
   40   EPF=CRF
      UOV=0.0
   50 CONTINUE
      RETURN
      END

      SUBROUTINE SHEAR(TSH)
      COMMON/AREA1/NI,NJ,Q
      COMMON/AREA2/DUX(25,25),DUY(25,25),TX(25,25),TY(25,25)
      COMMON/AREA3/X(25,25),Y(25,25),XL(25,25),YL(25,25),U(25,25)
      COMMON/AREA4/EXX(25,25),EYY(25,25)
      DIMENSION F(25)
      REAL MU
      G=32.18
      RO=62.4/G
      MU=RO*0.000014
      VK=0.4
      NI1=NI-1
      NJ1=NJ-1
      NI2=NI-2
      NJ2=NJ-2
      DO 90 J=1,NJ
      DX=(X(NI,J)-X(1,J))/(NI-1)
      DO 91 I=3,NI2
      DUX(I,J)=(U(I+1,J)-U(I-1,J))/(2.*DX)
      TX(I,J)=DUX(I,J)*(MU+RO*VK*VK*XL(I,J)*XL(I,J)*ABS(DUX(I,J)))
   91 CONTINUE
      TX(1,J)=TX(3,J)/(1.-EXX(3,J))
      TX(2,J)=TX(1,J)*(1.-EXX(2,J))
      TX(NI,J)=TX(NI-3,J)/(1.-EXX(NI-3,J))
      TX(NI1,J)=TX(NI,J)*(1.-EXX(NI1,J))
      CALL DU (TX(1,J),XL(1,J),DUX(1,J))
      CALL DU (TX(2,J),XL(2,J),DUX(2,J))
      CALL DU (TX(NI,J),XL(NI,J),DUX(NI,J))
      CALL DU(TX(NI1,J),XL(NI1,J),DUX(NI1,J))
   90 CONTINUE
      DO 92 I=1,NI
      DO 93 J=3,NJ2
      DY=SQRT((Y(I,J+1)-Y(I,J))*(Y(I,J+1)-Y(I,J))+(X(I,J+1)
     *-X(I,J))*(X(I,J+1)-X(I,J)))
      DUY(I,J)=(U(I,J+1)-U(I,J-1))/(2.*DY)
      TY(I,J)=DUY(I,J)*(MU+RO*VK*VK*YL(I,J)*YL(I,J)*ABS(DUY(I,J)))
   93 CONTINUE
      TY(I,1)=TY(I,3)/(1.-EYY(I,3))
      TY(I,2)=TY(I,1)*(1.-EYY(I,2))
      TY(I,NJ)=TY(I,NJ-3)/(1.-EYY(I,NJ-3))
      TY(I,NJ1)=TY(I,NJ)*(1.-EYY(I,NJ1))
      CALL DU (TY(I,1),YL(I,1),DUY(I,1))
      CALL DU (TY(I,2),YL(I,2),DUY(I,2))
      CALL DU (TY(I,NJ),YL(I,NJ),DUY(I,NJ))
      CALL DU (TY(I,NJ1),YL(I,NJ1),DUY(I,NJ1))
   92 CONTINUE
      CALL PRINT(TX)
      CALL PRINT(TY)
      TSH=0.0
      DO 94 I=1,NI,NI1
      DO 95 J=1,NJ
   95 F(J)=ABS(TX(I,J))
      WS=0.0
      DO 951 J=1,NJ
      JKK=J+1
      IF(J.EQ.NJ) JKK=J-1
      WA=SQRT((Y(I,JKK)-Y(I,J))*(Y(I,JKK)-Y(I,J))+(X(I,JKK)
     *-X(I,J))*(X(I,JKK)-X(I,J)))
  951 WS=WS+WA
      CALL SIMSON(F,WS,1,NJ,AA)
      TSH=TSH+AA
   94 CONTINUE
      DO 96 J=1,NJ,NJ1
      DO 97 I=1,NI
   97 F(I)=ABS(TY(I,J))
      WS=X(NI,J)-X(1,J)
```

```
      CALL SIMSUM(F,WS,I,NI,AA)
      TSH=TSH+AA
   56 CONTINUE
      RETURN
      END

      SUBROUTINE DU(T,Y,DV)
      VK=0.4
      RO=62.4/32.18
      AMU=RO*0.000014
      IF(Y.EQ.0.0) GO TO 10
      K=1
      IF(T.LT.0.0) K=-1
      T=T*K
      EP=RO*VK*VK*Y*Y
      DV=0.5*(SQRT(AMU*AMU+4.*T*EP)-AMU)/EP
      DV=DV*K
      RETURN
   10 DV=T/AMU
      RETURN
      END

     $ENTRY
*XXXXXXXXXXXXXXXXXXXXXXXXXXXXXXXXXXXXXXXXXXXXXX
        11              21
 0.1000000E-01   0.1000000E-01   0.1000000E-01   0.1000000E-01
 0.1000000E 01   0.1000000E 01   0.1000000E 01   0.0000000E 00   0.1000000E 01   0.1000000E-01
 0.1000000E 01   0.4000000E 01   0.2500000E 00   0.1000000E 01
 0.1000000E 01
*XXXXXXXXXXXXXXXXXXXXXXXXXXXXXXXXXXXXXXXXXXXXXX
 0.00000  0.10000  0.20000  0.30000  0.40000  0.50000  0.60000  0.70000  0.80000  0.90000  1.00000
 0.00000  0.10000  0.20000  0.30000  0.40000  0.50000  0.60000  0.70000  0.80000  0.90000  1.00000
 0.00000  0.10000  0.20000  0.30000  0.40000  0.50000  0.60000  0.70000  0.80000  0.90000  1.00000
 0.00000  0.10000  0.20000  0.30000  0.40000  0.50000  0.60000  0.70000  0.80000  0.90000  1.00000
 0.00000  0.10000  0.20000  0.30000  0.40000  0.50000  0.60000  0.70000  0.80000  0.90000  1.00000
 0.00000  0.10000  0.20000  0.30000  0.40000  0.50000  0.60000  0.70000  0.80000  0.90000  1.00000
 0.00000  0.10000  0.20000  0.30000  0.40000  0.50000  0.60000  0.70000  0.80000  0.90000  1.00000
 0.00000  0.10000  0.20000  0.30000  0.40000  0.50000  0.60000  0.70000  0.80000  0.90000  1.00000
 0.00000  0.10000  0.20000  0.30000  0.40000  0.50000  0.60000  0.70000  0.80000  0.90000  1.00000
 0.00000  0.10000  0.20000  0.30000  0.40000  0.50000  0.60000  0.70000  0.80000  0.90000  1.00000
 0.00000  0.10000  0.20000  0.30000  0.40000  0.50000  0.60000  0.70000  0.80000  0.90000  1.00000
 0.00000  0.10000  0.20000  0.30000  0.40000  0.50000  0.60000  0.70000  0.80000  0.90000  1.00000
 0.00000  0.10000  0.20000  0.30000  0.40000  0.50000  0.60000  0.70000  0.80000  0.90000  1.00000
 0.00000  0.10000  0.20000  0.30000  0.40000  0.50000  0.60000  0.70000  0.80000  0.90000  1.00000
 0.00000  0.10000  0.20000  0.30000  0.40000  0.50000  0.60000  0.70000  0.80000  0.90000  1.00000
 0.00000  0.10000  0.20000  0.30000  0.40000  0.50000  0.60000  0.70000  0.80000  0.90000  1.00000
 0.00000  0.10000  0.20000  0.30000  0.40000  0.50000  0.60000  0.70000  0.80000  0.90000  1.00000
 0.00000  0.10000  0.20000  0.30000  0.40000  0.50000  0.60000  0.70000  0.80000  0.90000  1.00000
 0.00000  0.10000  0.20000  0.30000  0.40000  0.50000  0.60000  0.70000  0.80000  0.90000  1.00000
 0.00000  0.10000  0.20000  0.30000  0.40000  0.50000  0.60000  0.70000  0.80000  0.90000  1.00000
 0.00000  0.10000  0.20000  0.30000  0.40000  0.50000  0.60000  0.70000  0.80000  0.90000  1.00000

*****************************

 0.00000  0.00000  0.00000  0.00000  0.00000  0.00000  0.00000  0.00000  0.00000  0.00000  0.00000
 0.05000  0.05000  0.05000  0.05000  0.05000  0.05000  0.05000  0.05000  0.05000  0.05000  0.05000
 0.10000  0.10000  0.10000  0.10000  0.10000  0.10000  0.10000  0.10000  0.10000  0.10000  0.10000
 0.15000  0.15000  0.15000  0.15000  0.15000  0.15000  0.15000  0.15000  0.15000  0.15000  0.15000
 0.20000  0.20000  0.20000  0.20000  0.20000  0.20000  0.20000  0.20000  0.20000  0.20000  0.20000
 0.25000  0.25000  0.25000  0.25000  0.25000  0.25000  0.25000  0.25000  0.25000  0.25000  0.25000
 0.30000  0.30000  0.30000  0.30000  0.30000  0.30000  0.30000  0.30000  0.30000  0.30000  0.30000
 0.35000  0.35000  0.35000  0.35000  0.35000  0.35000  0.35000  0.35000  0.35000  0.35000  0.35000
 0.40000  0.40000  0.40000  0.40000  0.40000  0.40000  0.40000  0.40000  0.40000  0.40000  0.40000
 0.45000  0.45000  0.45000  0.45000  0.45000  0.45000  0.45000  0.45000  0.45000  0.45000  0.45000
 0.50000  0.50000  0.50000  0.50000  0.50000  0.50000  0.50000  0.50000  0.50000  0.50000  0.50000
 0.55000  0.55000  0.55000  0.55000  0.55000  0.55000  0.55000  0.55000  0.55000  0.55000  0.55000
 0.60000  0.60000  0.60000  0.60000  0.60000  0.60000  0.60000  0.60000  0.60000  0.60000  0.60000
 0.65000  0.65000  0.65000  0.65000  0.65000  0.65000  0.65000  0.65000  0.65000  0.65000  0.65000
 0.70000  0.70000  0.70000  0.70000  0.70000  0.70000  0.70000  0.70000  0.70000  0.70000  0.70000
 0.75000  0.75000  0.75000  0.75000  0.75000  0.75000  0.75000  0.75000  0.75000  0.75000  0.75000
 0.80000  0.80000  0.80000  0.80000  0.80000  0.80000  0.80000  0.80000  0.80000  0.80000  0.80000
 0.85000  0.85000  0.85000  0.85000  0.85000  0.85000  0.85000  0.85000  0.85000  0.85000  0.85000
 0.90000  0.90000  0.90000  0.90000  0.90000  0.90000  0.90000  0.90000  0.90000  0.90000  0.90000
 0.95000  0.95000  0.95000  0.95000  0.95000  0.95000  0.95000  0.95000  0.95000  0.95000  0.95000
 1.00000  1.00000  1.00000  1.00000  1.00000  1.00000  1.00000  1.00000  1.00000  1.00000  1.00000

*****************************

 0.00000  0.20000  0.40000  0.60000  0.80000  1.00000  0.80000  0.60000  0.40000  0.20000  0.00000
 0.00000  0.20000  0.40000  0.60000  0.80000  1.00000  0.80000  0.60000  0.40000  0.20000  0.00000
```

0.00000	1.02100	1.08865	1.12163	1.13972	1.14750	1.13972	1.12163	1.08865	1.02100	0.00000
0.00000	1.01951	1.08622	1.11912	1.13717	1.14494	1.13717	1.11912	1.08622	1.01951	0.00000
0.00000	1.01497	1.08127	1.11402	1.13199	1.13972	1.13199	1.11402	1.08127	1.01497	0.00000
0.00000	1.00806	1.07402	1.10655	1.12440	1.13208	1.12440	1.10655	1.07402	1.00806	0.00000
0.00000	0.99876	1.06411	1.09634	1.11432	1.12163	1.11402	1.09634	1.06411	0.99876	0.00000
0.00000	0.98628	1.05091	1.08264	1.10011	1.10762	1.10011	1.08264	1.05091	0.98628	0.00000
0.00000	0.96939	1.03292	1.06411	1.08127	1.08865	1.08127	1.06411	1.03292	0.96939	0.00000
0.00000	0.94572	1.00760	1.03812	1.05486	1.06207	1.05486	1.03812	1.00760	0.94572	0.00000
0.00000	0.90986	0.96939	0.99876	1.01497	1.02100	1.01497	0.99876	0.96939	0.90986	0.00000
0.00000	0.84453	0.89978	0.92704	0.94199	0.94843	0.94199	0.92704	0.89978	0.84453	0.00000
0.00000	0.00000	0.00000	0.00000	0.00000	0.00000	0.00000	0.00000	0.00000	0.00000	0.00000

****

0.1000000E 01   0.9340369E 00   0.1070621E 01   0.7062149E-01

0.00000	0.00000	0.00000	0.00000	0.00000	0.00000	0.00000	0.00000	0.00000	0.00000	0.00000
0.00000	0.90417	0.96333	0.99251	1.00852	1.01540	1.00852	0.99251	0.96333	0.90417	0.00000
0.00000	0.97412	1.03785	1.06929	1.08654	1.09396	1.08654	1.06929	1.03785	0.97412	0.00000
0.00000	1.01251	1.07875	1.11143	1.12936	1.13707	1.12936	1.11143	1.07875	1.01251	0.00000
0.00000	1.03785	1.10576	1.13925	1.15763	1.16553	1.15763	1.13925	1.10576	1.03785	0.00000
0.00000	1.05593	1.12502	1.15910	1.17780	1.18584	1.17780	1.15910	1.12502	1.05593	0.00000
0.00000	1.06929	1.13925	1.17377	1.19270	1.20084	1.19270	1.17377	1.13925	1.06929	0.00000
0.00000	1.07925	1.14987	1.18470	1.20381	1.21202	1.20381	1.18470	1.14987	1.07925	0.00000
0.00000	1.08654	1.15763	1.19270	1.21194	1.22021	1.21194	1.19270	1.15763	1.08654	0.00000
0.00000	1.09151	1.16292	1.19815	1.21748	1.22579	1.21748	1.19815	1.16292	1.09151	0.00000
0.00000	1.09396	1.16553	1.20084	1.22021	1.22854	1.22021	1.20084	1.16553	1.09396	0.00000
0.00000	1.09151	1.16292	1.19815	1.21748	1.22579	1.21748	1.19815	1.16292	1.09151	0.00000
0.00000	1.08654	1.15763	1.19270	1.21194	1.22021	1.21194	1.19270	1.15763	1.08654	0.00000
0.00000	1.07925	1.14987	1.18470	1.20381	1.21202	1.20381	1.18470	1.14987	1.07925	0.00000
0.00000	1.06929	1.13925	1.17377	1.19270	1.20084	1.19270	1.17377	1.13925	1.06929	0.00000
0.00000	1.05593	1.12502	1.15910	1.17780	1.18584	1.17780	1.15910	1.12502	1.05593	0.00000
0.00000	1.03785	1.10576	1.13925	1.15763	1.16553	1.15763	1.13925	1.10576	1.03785	0.00000
0.00000	1.01251	1.07875	1.11143	1.12936	1.13707	1.12936	1.11143	1.07875	1.01251	0.00000
0.00000	0.97412	1.03785	1.06929	1.08654	1.09396	1.08654	1.06929	1.03785	0.97412	0.00000
0.00000	0.90417	0.96333	0.99251	1.00852	1.01540	1.00852	0.99251	0.96333	0.90417	0.00000
0.00000	0.00000	0.00000	0.00000	0.00000	0.00000	0.00000	0.00000	0.00000	0.00000	0.00000

****

0.00000	0.00000	0.00000	0.00000	0.00000	0.00000	0.00000	0.00000	0.00000	0.00000	0.00000
0.00406	0.00324	0.00243	0.00143	0.00065	0.00000	-0.00065	-0.00143	-0.00243	0.00286	-0.00358
0.00471	0.00376	0.00282	0.00166	0.00076	0.00000	-0.00076	-0.00166	-0.00282	0.00332	-0.00415
0.00508	0.00407	0.00305	0.00179	0.00082	0.00000	-0.00082	-0.00179	-0.00305	0.00359	-0.00449
0.00534	0.00427	0.00320	0.00189	0.00086	0.00000	-0.00086	-0.00189	-0.00320	0.00377	-0.00471
0.00553	0.00442	0.00332	0.00195	0.00089	0.00000	-0.00089	-0.00195	-0.00332	0.00390	-0.00488
0.00567	0.00453	0.00340	0.00200	0.00091	0.00000	-0.00091	-0.00200	-0.00340	0.00400	-0.00500
0.00577	0.00462	0.00346	0.00204	0.00093	0.00000	-0.00093	-0.00204	-0.00346	0.00408	-0.00510
0.00585	0.00468	0.00351	0.00207	0.00094	0.00000	-0.00094	-0.00207	-0.00351	0.00413	-0.00517
0.00591	0.00472	0.00354	0.00209	0.00095	0.00000	-0.00095	-0.00209	-0.00354	0.00417	-0.00521
0.00593	0.00475	0.00356	0.00209	0.00096	0.00000	-0.00096	-0.00209	-0.00356	0.00419	-0.00524
0.00591	0.00472	0.00354	0.00209	0.00095	0.00000	-0.00095	-0.00209	-0.00354	0.00417	-0.00521
0.00585	0.00468	0.00351	0.00207	0.00094	0.00000	-0.00094	-0.00207	-0.00351	0.00413	-0.00517
0.00577	0.00462	0.00346	0.00204	0.00093	0.00000	-0.00093	-0.00204	-0.00346	0.00408	-0.00510
0.00567	0.00453	0.00340	0.00200	0.00091	0.00000	-0.00091	-0.00200	-0.00340	0.00400	-0.00500
0.00553	0.00442	0.00332	0.00195	0.00089	0.00000	-0.00089	-0.00195	-0.00332	0.00390	-0.00488
0.00534	0.00427	0.00320	0.00189	0.00086	0.00000	-0.00086	-0.00189	-0.00320	0.00377	-0.00471
0.00508	0.00407	0.00305	0.00179	0.00082	0.00000	-0.00082	-0.00179	-0.00305	0.00359	-0.00449
0.00471	0.00376	0.00282	0.00166	0.00076	0.00000	-0.00076	-0.00166	-0.00282	0.00332	-0.00415
0.00406	0.00324	0.00243	0.00143	0.00065	0.00000	-0.00065	-0.00143	-0.00243	0.00286	-0.00350
0.00000	0.00000	0.00000	0.00000	0.00000	0.00000	0.00000	0.00000	0.00000	0.00000	0.00000

****

0.00000	0.00459	0.00521	0.00553	0.00570	0.00578	0.00570	0.00553	0.00521	0.00459	0.00000
0.00000	0.00413	0.00469	0.00497	0.00513	0.00520	0.00513	0.00497	0.00469	0.00413	0.00000
0.00000	0.00367	0.00416	0.00442	0.00456	0.00463	0.00456	0.00442	0.00416	0.00367	0.00000
0.00000	0.00285	0.00324	0.00344	0.00355	0.00360	0.00355	0.00344	0.00324	0.00285	0.00000
0.00000	0.00235	0.00267	0.00283	0.00292	0.00296	0.00292	0.00283	0.00267	0.00235	0.00000
0.00000	0.00193	0.00218	0.00232	0.00239	0.00243	0.00239	0.00232	0.00218	0.00193	0.00000
0.00000	0.00152	0.00173	0.00184	0.00190	0.00192	0.00190	0.00184	0.00173	0.00152	0.00000
0.00000	0.00114	0.00129	0.00137	0.00141	0.00143	0.00141	0.00137	0.00129	0.00114	0.00000
0.00000	0.00075	0.00085	0.00090	0.00093	0.00094	0.00093	0.00090	0.00085	0.00075	0.00000
0.00000	0.00035	0.00039	0.00042	0.00043	0.00044	0.00043	0.00042	0.00039	0.00035	0.00000
0.00000	0.00000	0.00000	0.00000	0.00000	0.00000	0.00000	0.00000	0.00000	0.00000	0.00000
0.00000	-0.00035	-0.00039	-0.00042	-0.00043	-0.00044	-0.00043	-0.00042	-0.00039	-0.00035	0.00000
0.00000	-0.00075	-0.00085	-0.00090	-0.00093	-0.00094	-0.00093	-0.00090	-0.00085	-0.00075	0.00000
0.00000	-0.00114	-0.00129	-0.00137	-0.00141	-0.00143	-0.00141	-0.00137	-0.00129	-0.00114	0.00000
0.00000	-0.00152	-0.00173	-0.00184	-0.00190	-0.00192	-0.00190	-0.00184	-0.00173	-0.00152	0.00000
0.00000	-0.00193	-0.00218	-0.00232	-0.00239	-0.00243	-0.00239	-0.00232	-0.00218	-0.00193	0.00000
0.00000	-0.00235	-0.00267	-0.00283	-0.00292	-0.00296	-0.00292	-0.00283	-0.00267	-0.00235	0.00000

0.00000	0.20000	0.40000	0.60000	0.80000	1.00000	0.80000	0.60000	0.40000	0.20000	0.00000
0.00000	0.20000	0.40000	0.60000	0.80000	1.00000	0.80000	0.60000	0.40000	0.20000	0.00000
0.00000	0.20000	0.40000	0.60000	0.80000	1.00000	0.80000	0.60000	0.40000	0.20000	0.00000
0.00000	0.20000	0.40000	0.60000	0.80000	1.00000	0.80000	0.60000	0.40000	0.20000	0.00000
0.00000	0.20000	0.40000	0.60000	0.80000	1.00000	0.80000	0.60000	0.40000	0.20000	0.00000
0.00000	0.20000	0.40000	0.60000	0.80000	1.00000	0.80000	0.60000	0.40000	0.20000	0.00000
0.00000	0.20000	0.40000	0.60000	0.80000	1.00000	0.80000	0.60000	0.40000	0.20000	0.00000
0.00000	0.20000	0.40000	0.60000	0.80000	1.00000	0.80000	0.60000	0.40000	0.20000	0.00000
0.00000	0.20000	0.40000	0.60000	0.80000	1.00000	0.80000	0.60000	0.40000	0.20000	0.00000
0.00000	0.20000	0.40000	0.60000	0.80000	1.00000	0.80000	0.60000	0.40000	0.20000	0.00000
0.00000	0.20000	0.40000	0.60000	0.80000	1.00000	0.80000	0.60000	0.40000	0.20000	0.00000
0.00000	0.20000	0.40000	0.60000	0.80000	1.00000	0.80000	0.60000	0.40000	0.20000	0.00000
0.00000	0.20000	0.40000	0.60000	0.80000	1.00000	0.80000	0.60000	0.40000	0.20000	0.00000
0.00000	0.20000	0.40000	0.60000	0.80000	1.00000	0.80000	0.60000	0.40000	0.20000	0.00000
0.00000	0.20000	0.40000	0.60000	0.80000	1.00000	0.80000	0.60000	0.40000	0.20000	0.00000
0.00000	0.20000	0.40000	0.60000	0.80000	1.00000	0.80000	0.60000	0.40000	0.20000	0.00000
0.00000	0.20000	0.40000	0.60000	0.80000	1.00000	0.80000	0.60000	0.40000	0.20000	0.00000
0.00000	0.20000	0.40000	0.60000	0.80000	1.00000	0.80000	0.60000	0.40000	0.20000	0.00000
0.00000	0.20000	0.40000	0.60000	0.80000	1.00000	0.80000	0.60000	0.40000	0.20000	0.00000

+++++++++++++++++++++++++++

0.00000	0.00000	0.00000	0.00000	0.00000	0.00000	0.00000	0.00000	0.00000	0.00000	0.00000
0.10000	0.10000	0.10000	0.10000	0.10000	0.10000	0.10000	0.10000	0.10000	0.10000	0.10000
0.20000	0.20000	0.20000	0.20000	0.20000	0.20000	0.20000	0.20000	0.20000	0.20000	0.20000
0.30000	0.30000	0.30000	0.30000	0.30000	0.30000	0.30000	0.30000	0.30000	0.30000	0.30000
0.40000	0.40000	0.40000	0.40000	0.40000	0.40000	0.40000	0.40000	0.40000	0.40000	0.40000
0.50000	0.50000	0.50000	0.50000	0.50000	0.50000	0.50000	0.50000	0.50000	0.50000	0.50000
0.60000	0.60000	0.60000	0.60000	0.60000	0.60000	0.60000	0.60000	0.60000	0.60000	0.60000
0.70000	0.70000	0.70000	0.70000	0.70000	0.70000	0.70000	0.70000	0.70000	0.70000	0.70000
0.80000	0.80000	0.80000	0.80000	0.80000	0.80000	0.80000	0.80000	0.80000	0.80000	0.80000
0.90000	0.90000	0.90000	0.90000	0.90000	0.90000	0.90000	0.90000	0.90000	0.90000	0.90000
1.00000	1.00000	1.00000	1.00000	1.00000	1.00000	1.00000	1.00000	1.00000	1.00000	1.00000
0.90000	0.90000	0.90000	0.90000	0.90000	0.90000	0.90000	0.90000	0.90000	0.90000	0.90000
0.80000	0.80000	0.80000	0.80000	0.80000	0.80000	0.80000	0.80000	0.80000	0.80000	0.80000
0.70000	0.70000	0.70000	0.70000	0.70000	0.70000	0.70000	0.70000	0.70000	0.70000	0.70000
0.60000	0.60000	0.60000	0.60000	0.60000	0.60000	0.60000	0.60000	0.60000	0.60000	0.60000
0.50000	0.50000	0.50000	0.50000	0.50000	0.50000	0.50000	0.50000	0.50000	0.50000	0.50000
0.40000	0.40000	0.40000	0.40000	0.40000	0.40000	0.40000	0.40000	0.40000	0.40000	0.40000
0.30000	0.30000	0.30000	0.30000	0.30000	0.30000	0.30000	0.30000	0.30000	0.30000	0.30000
0.20000	0.20000	0.20000	0.20000	0.20000	0.20000	0.20000	0.20000	0.20000	0.20000	0.20000
0.10000	0.10000	0.10000	0.10000	0.10000	0.10000	0.10000	0.10000	0.10000	0.10000	0.10000
0.00000	0.00000	0.00000	0.00000	0.00000	0.00000	0.00000	0.00000	0.00000	0.00000	0.00000

+++++++++++++++++++++++++++

0.00000	0.00000	0.00000	0.00000	0.00000	0.00000	0.00000	0.00000	0.00000	0.00000	0.00000
0.00000	0.84453	0.89978	0.92704	0.94199	0.94943	0.94199	0.92704	0.89978	0.84453	0.00000
0.00000	0.90986	0.96939	0.99876	1.01487	1.02180	1.01487	0.99876	0.96939	0.90986	0.00000
0.00000	0.94572	1.00760	1.03812	1.05486	1.06207	1.05486	1.03812	1.00760	0.94572	0.00000
0.00000	0.96939	1.03282	1.06411	1.08127	1.08865	1.08127	1.06411	1.03282	0.96939	0.00000
0.00000	0.98628	1.05081	1.08264	1.10011	1.10762	1.10011	1.08264	1.05081	0.98628	0.00000
0.00000	0.99876	1.06411	1.09634	1.11402	1.12163	1.11402	1.09634	1.06411	0.99876	0.00000
0.00000	1.00806	1.07402	1.10655	1.12440	1.13208	1.12440	1.10655	1.07402	1.00806	0.00000
0.00000	1.01487	1.08127	1.11402	1.13199	1.13972	1.13199	1.11402	1.08127	1.01487	0.00000
0.00000	1.01951	1.08622	1.11912	1.13717	1.14494	1.13717	1.11912	1.08622	1.01951	0.00000
0.00000	1.02180	1.08865	1.12163	1.13972	1.14750	1.13972	1.12163	1.08865	1.02180	0.00000
0.00000	1.01951	1.08622	1.11912	1.13717	1.14494	1.13717	1.11912	1.08622	1.01951	0.00000
0.00000	1.01487	1.08127	1.11402	1.13199	1.13972	1.13199	1.11402	1.08127	1.01487	0.00000
0.00000	1.00806	1.07402	1.10655	1.12440	1.13208	1.12440	1.10655	1.07402	1.00806	0.00000
0.00000	0.99876	1.06411	1.09634	1.11402	1.12163	1.11402	1.09634	1.06411	0.99876	0.00000
0.00000	0.98628	1.05081	1.08264	1.10011	1.10762	1.10011	1.08264	1.05081	0.98628	0.00000
0.00000	0.96939	1.03282	1.06411	1.08127	1.08865	1.08127	1.06411	1.03282	0.96939	0.00000
0.00000	0.94572	1.00760	1.03812	1.05486	1.06207	1.05486	1.03812	1.00760	0.94572	0.00000
0.00000	0.90986	0.96939	0.99876	1.01487	1.02180	1.01487	0.99876	0.96939	0.90986	0.00000
0.00000	0.84453	0.89978	0.92704	0.94199	0.94843	0.94199	0.92704	0.89578	0.84453	0.00000
0.00000	0.00000	0.00000	0.00000	0.00000	0.00000	0.00000	0.00000	0.00000	0.00000	0.00000

+++++++++++++++++++++++++++

0.00000	0.00000	0.00000	0.00000	0.00000	0.00000	0.00000	0.00000	0.00000	0.00000	0.00000
0.00000	0.84453	0.89978	0.92704	0.94199	0.94843	0.94199	0.92704	0.89978	0.84453	0.00000
0.00000	0.90986	0.96939	0.99876	1.01487	1.02180	1.01487	0.99876	0.96939	0.90986	0.00000
0.00000	0.94572	1.00760	1.03812	1.05486	1.06207	1.05486	1.03812	1.00760	0.94572	0.00000
0.00000	0.96939	1.03282	1.06411	1.08127	1.08865	1.08127	1.06411	1.03282	0.96939	0.00000
0.00000	0.98628	1.05081	1.08264	1.10011	1.10762	1.10011	1.08264	1.05081	0.98628	0.00000
0.00000	0.99876	1.06411	1.09634	1.11402	1.12163	1.11402	1.09634	1.06411	0.99876	0.00000
0.00000	1.00806	1.07402	1.10655	1.12440	1.13208	1.12440	1.10655	1.07402	1.00806	0.00000
0.00000	1.01487	1.08127	1.11402	1.13199	1.13972	1.13199	1.11402	1.08127	1.01487	0.00000
0.00000	1.01951	1.08622	1.11912	1.13717	1.14494	1.13717	1.11912	1.08622	1.01951	0.00000

APPENDIX D

EXPERIMENTAL ERRORS

THEIR SOURCES AND EVALUATION

D.1 Sources of Errors

The sources of experimental errors in performing the laboratory tests in this study can be summarized as follows:

1. Errors in measuring the flow depth:

   a) Variation of the floor ±0.100 inch (0.254 cm).

   b) Reference level reading ±0.050 inch (0.127 cm).

   c) Electric point gauge reading ±0.010 inch (0.025 cm).

   d) Water surface fluctuation errors:

      Upstream ±0.120 inch (0.305 cm).

      Downstream ±0.080 inch (0.203 cm)

   e) Longitudinal distances ±0.100 inch (0.254 cm).

2. Errors in the velocity measurements:

I. Using the Pitot-tube:

   a) A common instrument precision of ±1% was assumed.

   b) Manometer reading of ±0.050 inch (0.127 cm) which caused a possible error in the observed velocity of about ±1.2% at low velocities and ±1.0% at high velocities.

   c) Vertical distance measured by the attached point gauge of ± 0.060 inch (0.153 cm).

II. Miniature Current Meter:

   a) A common instrument precision of ±1.00%.

   b) Averaging of dial readings error of ±5.00%.

   c) Vertical distance measured by the attached point gauge of ±0.060 inch (0.153 cm).

3. The shear measurements were subject to an error of ±5.00% in measuring the balance angle due to the common errors of reading and the error due to the fluctuations in the shear value caused by the unsteadiness in the flow was ±10.00 %.

D.2 Composite Error

The general equation of the theory of errors states that if

$$Q = Q\ (X_1, X_2, \ldots) \qquad \text{D.1}$$

is a defined relation that relates the dependent variable Q to its independent variables X_1, X_2, ... etc, then the total error in Q is:

$$(\delta Q)^2 = (\partial Q/\partial X_1)^2\ (\delta X_1)^2 + (\partial Q/\partial X_2)^2\ (\delta X_2)^2 + \cdots \qquad \text{D.2}$$

where δX_1, δX_2 ,... are the specific errors in X_1, X_2 ,... that are made during their measurements. This equation can be applied to each experiment to estimate its expected experimental error.

D.3 Estimation of Errors

In this section the experimental errors are presented:

1. Velocity Profiles

   The total error was estimated at ±2.5%.

2. Underside Configuration

   This error was estimated at less than ±2.00% on the average.

3. The Roughness Coefficients

   The error in computing Manning's n was estimated as follows:

$$n = \frac{1.49}{V} R^{2/3} S^{1/2} \qquad \text{D.3}$$

$$\frac{E_n}{n} = \left(\left(\frac{E_v}{V} \right)^2 + \frac{4}{9} \left(\frac{E_r}{R} \right)^2 + \frac{1}{4} \left(\frac{E_s}{S} \right)^2 \right)^{1/2} \qquad \text{D.4}$$

where,

E_v / V = relative error in V estimated as ±2.0%

E_r / R = relative error in R estimated as $2R\,(E_y/Y)^2$

E_s / S = relative error in S estimated as $(E_y/L)\sqrt{2 + S^2}$ but as S is very small compared to the 2 it will be considered as $(E_y/L)\sqrt{2}$ and E_y is the error in the water depth measurements assumed to be constant in both upstream and downstream ends.

The value of the relative error in the composite roughness is different from one run to another. The error in measuring Chezy's C was computed in the same manner. An average error in estimating the friction factor was estimated as ±18.00%.

4. Instability of Blocks

a) The error in shear measurements was estimated at ±5.00%.

b) The error in the pressure measurement was 0.010 inch (0.025 cm).

c) The error in the instability flow was estimated at ±10 GPM (0.630 L/s).

APPENDIX E

EXPERIMENTAL RESULTS

APPENDIX E

This appendix summarizes the data obtained in the course of the experimental investigation. The results obtained are presented as follows:

E.1 Velocity Profiles

The two and three dimensional velocity profiles, measured experimentally, are given in Chaper V.

E.2 Friction Factor

The measurements for the estimation of the cover underside friction factor are presented in Table E.1, Table E.2

E.3 Underside Configuration

The data collected for the underside configuration of loose covers are presented as follows:

Table E.3 Data measured in the 6" wide flume with triangular bed form.

Table E.4 Three-dimensional configuration corresponding to the flat bed in the 56" wide flume.

The data for dune bed-form were taken after Haggag (27).

E.4 Cover Extension Mechanism

Typical measurements of the pressure distribution of the cover underside are presented in Table E.5, while Table E.6 is a summary of the critical flow (Maximum Stability Flow) for blocks of diffreent geometry and dimensions.

In this Appendix all the intermediate collected data and necessary calculations were omitted to avoid lengthy presentation of the experimental data.

No.	Q_{cfs}	Y_{ft}	R_{ft}	$C_{ft^{1/2}/s}$	L_{inch}	Δ_{inch}	$\frac{L}{\Delta} \cdot \frac{Y}{\Delta}$	$C_{2\,ft^{1/2}/s}$
1	0.92	0.950	0.240	58.00	17.00	0.75	354	30.00
2	1.36	1.040	0.306	53.00	17.00	0.75	379	29.10
3	0.78	1.112	0.319	40.80	17.00	0.75	407	22.65
4	2.22	1.182	0.330	42.40	17.00	0.75	432	23.34
5	1.08	0.996	0.299	67.60	17.00	1.50	91	42.20
6	1.48	1.053	0.309	64.70	17.00	1.50	96	39.91
7	1.96	1.155	0.326	52.90	17.00	1.50	106	30.34
8	2.43	1.214	0.336	53.65	17.00	1.50	110	30.51
9	0.97	0.955	0.292	41.25	17.00	2.25	39	23.69
10	1.43	1.073	0.313	36.94	17.00	2.25	43	20.45
11	1.97	1.142	0.324	42.16	17.00	2.25	46	23.36
12	2.41	1.211	0.333	43.87	17.00	2.25	49	24.11
13	1.04	0.964	0.293	99.44	11.33	0.75	233	83.13
14	1.48	1.038	0.307	74.62	11.33	0.75	252	48.90
15	1.97	1.150	0.325	59.90	11.33	0.75	280	35.41
16	2.51	1.224	0.337	64.37	11.33	0.75	248	38.33
17	1.04	0.970	0.295	45.65	11.33	1.50	59	26.50
18	1.50	1.054	0.309	53.27	11.33	1.50	64	31.22
19	1.94	1.137	0.323	47.39	11.33	1.50	69	26.74
20	2.40	1.190	0.332	50.73	11.33	1.50	72	28.67
21	0.97	0.951	0.291	39.55	11.33	2.25	26	22.62
22	1.48	1.063	0.311	35.65	11.33	2.25	29	19.71
23	1.94	1.133	0.323	39.64	11.33	2.25	31	21.84
24	2.49	1.206	0.334	43.60	11.33	2.25	33	24.00
25	1.03	0.972	0.295	50.70	5.66	0.75	118	30.00
26	1.52	1.064	0.311	66.00	5.66	0.75	128	41.00
27	2.04	1.144	0.325	69.00	5.66	0.75	140	42.80
28	2.57	1.221	0.337	61.50	5.66	0.75	149	36.10
29	1.00	0.957	0.292	48.00	5.66	1.50	29	28.16
30	1.50	1.058	0.310	51.00	5.66	1.50	32	29.60
31	1.92	1.129	0.322	60.00	5.66	1.50	34	35.60
32	2.34	1.206	0.334	60.00	5.66	1.50	37	35.10
33	1.01	0.966	0.294	50.00	5.66	2.25	13	29.50
34	1.48	1.057	0.310	54.00	5.66	2.25	14	31.92
35	1.92	1.135	0.323	56.00	5.66	2.25	15	32.64
36	2.46	1.216	0.336	56.00	5.66	2.25	16	32.19

TABLE E-1; Friction Factors Data

NO.	R ft	C_2' $ft^{\frac{1}{2}}/s$	C_2	$-\delta C_2$	$\frac{L}{\Delta}\frac{Y}{\Delta}$	$\delta C_2/(\frac{L}{\Delta}\frac{Y}{\Delta})$ x-1
1	0.29	125.8			354	
2	0.31	116.6	109.1	12.5	379	0.031
3	0.32	117.1	22.6	94.5	407	0.250
4	0.33	117.6	23.3	94.3	432	0.218
5	0.30	116.2	42.2	74.0	91	0.813
6	0.31	116.7	39.9	76.8	96	0.800
7	0.33	117.4	30.3	87.1	106	0.822
8	0.34	117.9	30.5	87.4	110	0.794
9	0.29	115.9	23.7	92.2	39	2.380
10	0.31	116.9	20.5	96.4	43	2.230
11	0.32	117.4	23.4	94.0	46	2.040
12	0.33	117.7	24.1	93.6	49	1.910
13	0.29	115.6	83.1	32.5	233	0.141
14	0.31	116.6	48.9	67.7	252	0.268
15	0.33	117.4	35.4	82.0	280	0.293
16	0.34	117.9	38.3	95.6	298	0.321
17	0.30	116.0	26.5	89.5	59	1.517
18	0.31	116.7	31.2	85.5	64	1.335
19	0.32	117.3	26.7	90.6	69	1.312
20	0.33	117.7	28.6	89.1	72	1.240
21	0.29	115.8	22.6	93.2	26	3.630
22	0.31	116.8	19.7	97.1	29	3.400
23	0.32	117.3	21.8	95.5	31	3.120
24	0.33	117.7	24.0	93.7	33	2.890
25	0.30	116.1	30.0	86.1	118	0.730
26	0.31	116.8	41.0	75.8	128	0.590
27	0.33	117.4	42.8	75.6	140	0.540
28	0.34	117.9	36.1	81.8	149	0.550
29	0.29	115.9	28.2	87.7	29	3.020
30	0.31	116.7	29.6	87.1	32	2.720
31	0.32	117.3	35.6	81.7	34	2.390
32	0.33	117.7	35.1	82.6	37	2.250
33	0.29	116.0	29.5	84.5	13	6.500
34	0.31	116.7	31.7	85.0	14	5.980
35	0.32	117.3	32.6	84.7	15	5.570
36	0.34	117.9	32.2	85.7	16	5.220

Table E.2: Underside Friction Factor Data

note: all units in ft.-sec.

$Q_{measured}$ (cfs)	Distance from the Head Tank (In.)												
	30	35	40	45	50	55	60	65	70	75	80	85	90
0.0362	5.2	4.5	6.0	5.0	4.3	6.0	4.6	5.0	4.9	4.4	5.8	4.7	4.5
0.0506	5.8	4.6	5.9	5.3	5.8	6.4	5.1	5.3	6.0	4.7	6.3	5.4	4.6
0.0593	6.2	4.9	6.2	5.7	4.8	6.5	5.3	5.5	6.2	4.7	6.3	5.4	4.7
0.0723	6.5	5.5	6.0	5.5	5.3	6.7	5.2	5.6	5.9	4.0	5.1	5.6	5.3
0.0795	6.6	5.6	6.4	6.0	5.2	5.9	5.7	5.7	6.2	5.0	6.2	5.7	5.1
0.0919	7.2	5.6	6.3	6.0	5.2	7.3	5.7	6.6	5.4	6.8	5.8	5.4	4.4
0.1031	7.2	6.0	6.8	6.6	5.4	7.3	6.0	6.1	6.9	5.6	5.8	6.1	5.5

TABLE E-3a: Depth of Water for Various Flows (Inches) for 6" Flume with Triangular Bed-form

$Q_{measured}$ (cfs)	Distance from the Head Tank (In.)												
	30	35	40	45	50	55	60	65	70	75	80	85	90
0.0362	1.8	1.4	1.4	1.9	1.3	1.5	1.7	1.2	2.1	1.5	1.4	2.0	1.3
0.0506	1.7	1.8	1.4	1.9	1.7	1.4	1.7	1.2	1.6	1.7	1.2	1.6	1.6
0.0593	1.6	1.8	1.4	1.7	1.5	1.5	1.5	1.3	1.4	1.8	1.4	1.8	1.4
0.0723	1.5	1.5	1.6	2.0	1.3	1.7	1.7	1.3	2.0	1.7	1.5	1.8	1.3
0.0795	1.2	1.4	1.4	1.7	1.6	1.6	1.4	1.5	1.9	1.7	1.7	1.9	1.5
0.0919	1.3	1.7	1.7	1.9	1.7	1.5	1.7	1.6	1.6	1.6	1.7	2.0	1.5
0.1031	1.5	1.3	1.3	1.6	1.5	1.5	1.6	1.3	1.4	1.6	1.6	1.8	1.5

TABLE E-3b: Loose Cover Thickness for Various Flows (Inches) for 6" Flume with Triangular Bed-form

Test	Distance Away from the Head Tank in inches																			
	5	10	15	20	25	30	35	40	45	50	55	60	65	70	75	80	85	90	95	100
1	1.5	1.6	1.5	1.7	2.0	2.2	2.3	2.2	1.8	1.6	1.9	1.9	2.0	2.2	2.4	2.4	2.4	2.3	2.3	1.2
2	1.3	1.5	1.0	0.9	0.8	1.2	1.9	2.3	2.8	2.3	1.7	1.9	2.1	2.3	2.3	1.9	1.9	2.0	2.3	2.2
3	1.5	1.4	1.0	1.0	1.0	1.3	2.4	2.5	2.6	2.4	1.8	1.9	2.2	2.2	2.1	1.8	1.7	1.9	2.1	2.2
4	1.0	1.0	1.2	1.4	1.4	1.8	2.1	2.5	2.6	2.5	2.5	2.1	1.4	1.4	1.5	2.0	2.1	2.5	2.7	3.0
5	1.3	1.7	1.9	2.0	2.4	2.1	2.0	1.8	1.8	2.3	2.3	2.3	2.2	2.0	1.9	1.9	2.0	2.4	2.8	3.0
6	1.5	1.6	1.9	2.2	2.5	2.5	2.4	2.1	1.9	1.6	1.7	1.6	1.7	1.8	2.0	2.2	2.5	2.8	3.0	3.0
7	1.2	1.5	1.3	1.2	1.4	1.5	1.6	1.9	2.0	2.0	2.0	2.1	2.4	2.4	1.2	1.3	1.7	2.0	2.5	3.0
8	1.2	1.7	1.6	1.7	2.0	1.8	1.9	1.9	1.9	2.2	2.2	2.2	2.1	2.0	1.8	1.8	1.9	2.3	2.7	2.9

TABLE E-3c: The Ice-Cover Thickness for Various Experiments (Inches) for 6" Flume with Plane Bed

No.	L. Inch	Cover Thickness at Different X Values											
		0	6	12	18	24	30	36	42	48	54	60	66 inches
1	27.0	0.00	0.00	0.00	0.00	0.00	0.00	0.25	0.25	0.25	0.25	0.00	0.00
2	39.0	0.00	0.00	0.00	0.25	0.25	0.25	0.25	0.25	0.25	0.25	0.00	0.00
3	50.5	0.00	0.00	0.00	0.82	1.47	1.60	1.20	1.04	1.48	0.74	0.00	0.00
4	62.5	0.00	0.00	0.00	0.47	1.38	2.07	1.93	1.11	1.44	2.04	1.22	1.25
5	71.5	0.00	1.59	2.00	2.00	1.47	1.04	0.99	1.37	1.87	2.24	2.01	2.60
6	86.0	3.25	2.21	2.03	1.49	1.23	1.07	1.02	1.29	1.33	1.48	1.12	1.25
7	98.0	1.75	1.77	1.58	1.30	1.25	1.17	1.00	1.45	1.65	1.78	1.59	1.50
8	110.0	1.25	1.45	1.49	1.50	1.56	1.20	1.30	1.30	1.59	2.00	1.52	1.28
9	122.0	1.60	1.71	1.57	1.02	1.19	1.27	1.39	1.58	1.82	1.41	----	1.60
10	134.0	HIGH ONE UP TO THE WEIR EFFECT											

Q = 1.63 cfs

TABLE E-4: Three Dimensional Underside Configuration

No.	L. Inch	Cover Thickness at Different X Values											
		0	6	12	18	24	30	36	42	48	54	60	66 inches
1	20.5	0.00	0.00	0.00	0.00	0.00	0.00	0.00	0.00	0.00	0.25	0.25	0.25
2	32.5	0.00	0.00	0.00	0.00	0.00	0.00	0.00	0.00	1.02	1.22	0.78	0.00
3	44.5	0.00	0.00	0.10	0.60	0.74	1.28	2.12	2.10	1.74	1.42	0.00	0.00
4	57.0	0.00	0.00	0.49	1.90	1.63	1.80	0.98	1.10	1.46	2.07	1.12	0.60
5	68.0	1.50	1.86	1.86	1.76	1.65	0.92	0.08	1.05	1.58	2.00	1.83	2.50
6	80.0	2.00	1.96	2.12	2.08	1.45	1.19	1.00	1.16	1.52	1.51	1.58	1.40
7	92.0	1.20	1.43	1.63	1.47	1.33	1.08	1.18	1.27	1.47	1.45	1.15	1.20
8	104.0	1.36	1.44	1.54	1.55	1.39	1.28	1.10	1.27	1.28	1.56	1.31	1.00
9	116.0	1.25	1.43	1.52	1.43	1.26	1.13	1.01	1.27	1.37	1.66	1.43	1.25
10	128.0	1.40	1.48	1.43	1.29	1.24	1.05	1.10	1.14	1.26	1.50	1.33	1.20

Q = 1.77 cfs

TABLE E-4 Cont'd

		Cover Thickness at Different X Values											
No.	L. Inch	0	6	12	18	24	30	36	42	48	54	60	66 inches
1	20.5	0.00	0.72	1.17	0.00	0.00	0.00	0.00	0.00	1.16	0.92	0.91	2.50
2	32.5	3.00	0.87	1.16	1.55	1.49	0.45	0.95	1.85	2.10	1.27	0.91	0.50
3	44.5	1.10	0.84	0.97	1.68	1.22	0.52	0.42	0.86	1.33	0.90	0.68	0.60
4	56.5	1.00	1.10	1.25	1.11	1.94	0.95	0.68	0.90	1.85	1.54	1.14	1.00
5	68.5	1.50	1.45	1.54	1.53	1.80	0.88	0.65	0.80	1.63	1.42	1.08	1.50
6	80.0	1.70	1.63	1.68	1.71	1.89	1.22	0.80	0.95	1.69	1.81	1.18	1.20
7	92.0	1.20	1.28	1.60	1.69	1.44	1.19	1.11	1.16	1.36	1.32	1.64	1.25
8	104.0	1.25	1.42	1.48	1.25	1.34	1.29	1.15	1.16	1.27	1.24	1.09	1.20
9	116.0	1.15	1.28	1.29	1.22	1.21	1.06	1.14	1.07	1.34	1.79	1.74	1.40
10	128.0	1.2	1.24	1.24	1.27	1.54	1.36	1.44	1.08	1.18	0.97	1.35	1.20

Q = 1.02 cfs

TABLE E-4 Continued

No.	L.Inch	Cover Thickness at Different X Values											
		0	6	12	18	24	30	36	42	48	54	60	66 inches
1	20.5	0.00	0.00	0.00	0.00	0.00	0.00	0.00	0.00	0.00	0.25	0.25	0.00
2	32.5	0.00	0.00	0.00	0.00	0.00	0.00	0.00	0.00	1.36	1.55	0.46	0.00
3	45.5	0.00	0.00	0.63	0.70	0.44	0.60	1.59	2.12	1.98	1.36	1.13	0.00
4	56.5	1.50	1.66	1.76	1.71	1.66	1.29	1.26	1.12	1.07	1.57	2.20	2.00
5	68.5	1.80	1.51	2.38	2.12	1.71	1.18	1.02	1.26	0.96	1.28	1.28	1.30
6	80.0	1.80	1.82	2.02	1.88	1.43	1.08	1.17	1.15	1.14	1.31	1.04	1.10
7	92.0	1.20	1.62	1.81	1.75	1.28	1.52	1.27	1.39	1.02	1.33	1.32	1.00
8	104.0	1.15	1.52	1.23	1.14	1.19	1.18	1.25	1.34	1.13	1.23	1.17	1.00
9	116.0	1.00	1.13	1.03	1.28	1.31	1.26	1.52	1.43	1.42	1.53	1.16	0.75
10	128.0	1.30	1.46	1.45	1.24	1.10	1.10	1.14	1.19	1.04	0.91	1.08	1.00

Q = 1.70 cfs

TABLE E-4 Cont'd

No.	L. Inch	Cover Thickness at Different X Values											
		0	6	12	18	24	30	36	42	48	54	60	66 inches
1	20.5	0.00	0.10	0.10	0.00	0.00	0.00	0.00	0.00	0.00	0.10	0.90	0.00
2	32.5	0.00	0.10	0.10	0.00	0.00	0.00	0.00	0.00	1.26	2.20	0.48	0100
3	44.5	3.60	2.16	1.55	2.14	1.52	0.87	1.26	1.65	1.85	1.46	2.10	1.40
4	56.0	1.50	2.05	1.92	1.93	1.65	0.65	0.72	1.27	1.94	1.12	0.89	0.90
5	68.5	1.50	1.65	1.47	2.16	2.06	1.03	0.76	1.36	2.07	1.40	1.03	1.00
6	80.0	1.60	1.60	1.56	2.39	1.96	1.17	0.79	1.42	2.00	1.64	1.12	1.25
7	92.0	1.25	1.35	1.53	2.02	2.02	1.55	1.26	1.52	1.98	1.84	1.38	1.35
8	104.0	1.00	1.37	1.20	1.30	1.28	1.17	1.20	1.36	1.38	1.35	1.24	1.30
9	110.0	1.15	1.16	1.03	1.23	1.30	1.18	1.44	1.35	1.18	1.50	1.31	1.20
10	128.0	1.50	1.35	1.47	1.29	1.35	1.15	1.30	1.15	1.14	1.16	1.05	1.20

Q = 1.25 cfs

TABLE E-4 Cont'd

No.	t inches	Le inches	Q cfs	Y ft	Pressure on Cover Underside (inches of Water)								
					F	0	2	4	6	8	10	12	14
1	2.25	0	3.04	1.06	0.84	0.48	1.16	1.22	1.44	1.46	1.45	1.44	1.34
2	2.25	0	2.31	1.07	0.96	0.17	1.10	1.17	1.28	1.28	1.31	1.32	1.32
3	2.25	0	3.22	1.11	0.65	0.44	1.37	1.26	1.41	1.50	1.54	1.52	1.52
4	2.25	0	1.59	0.62	0.51	0.27	1.06	1.22	1.34	1.44	1.45	1.45	1.43
5	2.25	0	3.95	1.53	0.63	0.23	1.34	1.42	1.47	1.52	1.49	1.51	1.50
6	2.25	0	2.68	0.99	0.59	0.46	1.03	1.10	1.28	1.31	1.41	1.39	1.39
7	2.25	0	2.13	0.83	0.52	0.62	1.08	1.12	1.28	1.35	1.44	1.43	1.41
8	2.25	12.25	3.65	1.14	0.56	0.37	1.27	1.42	1.45	1.33	1.30	1.30	1.35
9	2.25	12.25	3.56	1.06	0.73	0.23	1.32	1.46	1.53	1.39	1.38	1.36	1.33
10	2.25	12.25	2.47	0.91	0.48	0.29	1.12	1.29	1.26	1.23	1.30	1.29	1.30
11	2.25	12.25	2.20	0.71	0.60	0.41	1.19	1.26	1.26	1.26	1.26	1.28	1.30
12	2.25	12.25	2.65	0.92	0.42	0.29	1.23	1.27	1.33	1.25	1.29	1.32	1.28
13	2.25	12.25	4.36	1.45	0.33	0.17	1.26	1.33	1.36	1.39	1.39	1.39	1.38
14	2.25	12.25	3.97	1.29	0.58	0.22	1.39	1.43	1.42	1.42	1.43	1.38	1.60
15	2.25	2.25	3.77	1.21	0.60	0.29	1.56	1.44	1.47	1.49	1.48	1.48	1.48
16	2.25	2.25	3.68	1.50	0.42	0.80	1.46	1.56	1.56	1.52	1.51	1.55	1.53
17	2.25	2.25	4.22	1.45	0.63	0.55	1.35	1.43	1.48	1.49	1.55	1.58	1.50
18	2.25	2.25	4.31	1.35	0.61	0.32	1.13	1.55	1.59	1.57	1.58	1.59	1.51
19	2.25	2.25	1.84	0.65	0.53	0.63	1.07	1.42	1.48	1.47	1.46	1.43	1.40
20	2.25	2.25	3.47	1.13	0.69	0.50	1.21	1.39	1.46	1.50	1.50	1.52	1.49
21	2.25	2.25	2.65	0.90	0.48	0.31	1.16	1.38	1.41	1.39	1.38	1.39	1.37
22	2.25	4.50	1.59	0.47	0.65	0.48	1.42	1.48	1.42	1.44	1.49	1.49	1.45
23	2.25	4.50	3.27	0.91	0.75	0.24	1.49	1.60	1.61	1.61	1.60	1.61	1.66
24	2.25	4.50	3.84	1.13	0.21	0.00	1.61	1.46	1.57	1.56	1.64	1.60	1.55

TABLE E-5: Pressure Distribution Under Cover

No	t inches	Le inches	Q cfs	Y ft	Pressure on Cover Underside (inches of Water) F	0	2	4	6	8	10	12	14
25	2.25	4.50	4.06	1.40	0.20	0.01	1.44	1.41	1.46	1.45	1.51	1.52	1.54
26	2.25	4.50	3.44	1.05	0.56	0.17	1.23	1.33	1.40	1.37	1.38	1.36	1.36
27	2.25	4.50	2.20	0.71	0.22	0.21	1.27	1.36	1.36	1.36	1.35	1.34	1.34
28	2.25	4.50	2.65	0.92	0.38	0.25	1.37	1.36	1.35	1.40	1.37	1.37	1.32

TABLE E-5: Continued

TABLE E-6: Maximum Block Stability Conditions

Run No.	Edge	J	Q cfs	Y ft	L inches	L_e inches
1	Rectangular	0.093	820	10.00	16	0
2	Rectangular	0.093	960	10.75	16	0
3	Rectangular	0.093	1270	15.00	16	0
4	Rectangular	0.093	1240	16.13	16	0
5	Rectangular	0.093	0550	7.50	16	0
6	Rectangular	0.093	0650	8.75	16	0
7	Rectangular	0.093	1090	13.60	16	0
8	Rectangular	0.093	1160	15.75	16	0
9	Rectangular	0.093	0440	6.00	16	0
10	Rectangular	0.093	0860	11.25	16	0
11	Rectangular	0.093	0625	8.25	16	0
1	Rectangular	0.250	0510	7.75	6	0
2	Rectangular	0.250	0350	5.87	6	0
3	Rectangular	0.250	0460	7.65	6	0
4	Rectangular	0.250	0575	9.25	6	0
5	Rectangular	0.250	0860	11.65	6	0
6	Rectangular	0.250	0875	12.90	6	0
7	Rectangular	0.250	0460	5.91	6	0
8	Rectangular	0.250	0500	7.61	6	0
9	Rectangular	0.250	0740	10.55	6	0
10	Rectangular	0.250	0880	12.86	6	0
11	Rectangular	0.250	1060	14.50	6	0
12	Rectangular	0.250	1060	16.19	6	0
13	Rectangular	0.250	0890	13.33	6	0
14	Rectangular	0.250	0410	6.52	6	0

Run No.	Edge	J	Q	Y	L	L_e
1	Rectangular	0.10	0380	5.54	15	0
2	Rectangular	0.10	0560	7.92	15	0
3	Rectangular	0.10	0830	10.92	15	0
4	Rectangular	0.10	1020	12.95	15	0
5	Rectangular	0.10	1150	14.93	15	0
6	Rectangular	0.10	1190	16.50	15	0
7	Rectangular	0.10	1080	13.90	15	0
8	Rectangular	0.10	0500	6.94	15	0
1	Rectangular	0.50	0440	5.83	3	0
2	Rectangular	0.50	0540	7.80	3	0
3	Rectangular	0.50	0710	10.42	3	0
4	Rectangular	0.50	0950	13.12	3	0
5	Rectangular	0.50	0980	14.16	3	0
6	Rectangular	0.50	1150	16.35	3	0
7	Rectangular	0.50	1030	13.82	3	0
8	Rectangular	0.50	0480	6.90	3	0
1	Rectangular	0.75	0360	5.38	2	0
2	Rectangular	0.75	0570	7.90	2	0
3	Rectangular	0.75	0770	10.69	2	0
4	Rectangular	0.75	1030	9.50	2	0
5	Rectangular	0.75	1030	14.35	2	0
6	Rectangular	0.75	1240	16.86	2	0
7	Rectangular	0.75	1170	14.25	2	0
8	Rectangular	0.75	0470	6.80	2	0

TABLE E-6 Cont'd

Run No.	Edge	J	Q	Y	L	L_e
1	Rectangular	0.99	400	6.10	1.5	0
2	Rectangular	0.99	580	7.92	1.5	0
3	Rectangular	0.99	850	10.90	1.5	0
4	Rectangular	0.99	1020	13.40	1.5	0
5	Rectangular	0.99	1220	15.02	1.5	0
6	Rectangular	0.99	1200	16.69	1.5	0
7	Rectangular	0.99	1020	13.85	1.5	0
8	Rectangular	0.99	560	7.27	1.5	0
1	1:1	1.093	1070	10.75	16	1.5
2	1:1	1.093	1380	13.75	16	1.5
3	1:1	1.093	1560	16.25	16	1.5
4	1:1	1.093	1660	16.50	16	1.5
5	1:1	1.093	760	8.25	16	1.5
6	1:1	1.093	940	9.87	16	1.5
7	1:1	1.093	1475	15.00	16	1.5
8	1:1	1.093	1550	16.75	16	1.5
9	1:1	1.093	610	6.62	16	1.5
10	1:1	1.093	875	9.50	16	1.5
1	1:1	1.100	1500	16.18	15	1.5
2	1:1	1.100	1210	13.62	15	1.5
3	1:1	1.100	790	9.58	15	1.5
4	1:1	1.100	440	5.58	15	1.5
5	1:1	1.100	910	16.73	15	1.5
6	1:1	1.100	1320	15.00	15	1.5

TABLE E-6 Cont'd

Run No.	Edge	J	Q	Y	L	L_e
7	1:1	1,100	1000	11.55	15	1.5
8	1:1	1,100	320	3.20	15	1.5
1	1:1	1,250	1220	16.14	6	1.5
2	1:1	1,250	1050	13.17	6	1.5
3	1:1	1,250	720	9.33	6	1.5
4	1:1	1,250	360	5.15	6	1.5
5	1:1	1,250	780	9.96	6	1.5
6	1:1	1,250	1210	14.72	6	1.5
7	1:1	1,250	850	10.82	6	1.5
8	1:1	1.250	220	2.98	6	1.5
1	1:1	1,500	1500	16.18	3	1.5
2	1:1	1.500	1190	13.33	3	1.5
3	1:1	1.500	740	9.43	3	1.5
4	1:1	1.500	460	5.62	3	1.5
5	1:1	1.500	980	10.72	3	1.5
6	1:1	1.500	1210	14.72	3	1.5
7	1:1	1.500	900	11.12	3	1.5
8	1:1	1.500	230	2.90	3	1.5
1	1:1	1,750	1330	16.10	2	1.5
2	1:1	1,750	1040	13.10	2	1.5
3	1:1	1,750	730	9.40	2	1.5
4	1:1	1,750	520	5.88	2	1.5
5	1:1	1,750	990	10.78	2	1.5

TABLE E-6 Cont'd

Run No.	Edge	J	Q	Y	L	L_e
6	1:1	1.750	1250	14.82	2	1.5
7	1:1	1.750	890	10.90	2	1.5
8	1:1	1.750	250	2.73	2	1.5
1	1:1	1.990	1440	16.50	1.5	1.5
2	1:1	1.990	1250	13.92	1.5	1.5
3	1:1	1.990	910	10.09	1.5	1.5
4	1:1	1.990	420	5.54	1.5	1.5
5	1:1	1.990	1050	10.98	1.5	1.5
6	1:1	1.990	1350	15.32	1.5	1.5
7	1:1	1.990	950	11.12	1.5	1.5
8	1:1	1.990	300	3.40	1.5	1.5
1	2:1	2.093	1340	11.75	16	3
2	2:1	2.093	1750	15.25	16	3
3	2:1	2.093	1600	16.25	16	3
4	2:1	2.093	1740	17.90	16	3
5	2:1	2.093	1060	9.30	16	3
6	2:1	2.093	1250	11.00	16	3
7	2:1	2.093	1550	15.40	16	3
8	2:1	2.093	1660	17.00	16	3
9	2:1	2.093	940	7.80	16	3
10	2:1	2.093	1190	10.40	16	3

TABLE E-6 Cont'd

Run No.	Edge	J	Q	Y	L	L_e
1	2:1	2.100	1770	17.00	15	3
2	2:1	2.100	1320	14.30	15	3
3	2:1	2.100	1230	14.10	15	3
4	2:1	2.100	550	6.10	15	3
5	2:1	2.100	1100	11.12	15	3
6	2:1	2.100	1520	15.80	15	3
7	2:1	2.100	1280	12.20	15	3
8	2:1	2.100	440	4.02	15	3
1	2:1	2.250	1470	16.58	6	3
2	2:1	2.250	1220	13.88	6	3
3	2:1	2.250	1010	10.63	6	3
4	2:1	2.250	520	5.88	6	3
5	2:1	2.250	1040	10.96	6	3
6	2:1	2.250	1300	15.03	6	3
7	2:1	2.250	1250	12.22	6	3
8	2:1	2.250	340	3.62	6	3
1	2:1	2.500	1600	16.88	3	3
2	2:1	2.500	2500	17.30	3	
3	2:1	2.500	1870	13.95	3	3
4	2:1	2.500	1140	8.20	3	3
5	2:1	2.500	1100	11.02	3	3
6	2:1	2.500	2380	17.00	3	3
7	2:1	2.500	2200	14.90	3	3
8	2:1	2.500	560	5.00	3	3

TABLE E-6 Cont'd

Run No.	Edge	J	Q	Y	L	L_e
1	2:1	2.750	2350	16.00	2	3
2	2:1	2.750	1940	13.23	2	3
3	2:1	2.750	1190	8.20	2	3
4	2:1	2.750	1950	13.70	2	3
5	2:1	2.750	2282	18.55	2	3
6	2:1	2.750	1970	14.96	2	3
7	2:1	2.750	900	5.70	2	3
1	2:1	2.990	2330	16.95	1.5	3
2	2:1	2.990	1810	12.95	1.5	3
3	2:1	2.990	1240	8.40	1.5	3
4	2:1	2.990	1940	13.55	1.5	3
5	2:1	2.990	2240	17.40	1.5	3
6	2:1	2.990	2100	14.60	1.5	3
7	2:1	2.990	750	5.05	1.5	3
1	Circular	10.93	1170	11.25	16	1.5
2	Circular	10.93	1330	13.50	16	1.5
3	Circular	10.93	1510	16.05	16	1.5
4	Circular	10.93	1650	17.40	16	1.5
5	Circular	10.93	780	8.40	16	1.5
6	Circular	10.93	890	9.60	16	1.5
7	Circular	10.93	1430	15.00	16	1.5
8	Circular	10.93	1525	16.75	16	1.5
9	Circular	10.93	600	6.60	16	1.5
10	Circular	10.93	870	9.30	16	1.5

TABLE E-6 Cont'd

Run No.	Edge	J	Q	Y	L	L_e
1	Circular	11.00	570	6.02	15	1.5
2	Circular	11.00	950	10.02	15	1.5
3	Circular	11.00	1400	13.90	15	1.5
4	Circular	11.00	1600	16.05	15	1.5
5	Circular	11.00	1660	17.49	15	1.5
6	Circular	11.00	1540	15.81	15	1.5
7	Circular	11.00	1240	12.66	15	1.5
8	Circular	11.00	380	13.70	15	1.5
1	Circular	12.50	550	5.98	6	1.5
2	Circular	12.50	800	9.36	6	1.5
3	Circular	12.50	1250	13.43	6	1.5
4	Circular	12.50	1290	15.20	6	1.5
5	Circular	12.50	1380	16.83	6	1.5
6	Circular	12.50	1300	15.02	6	1.5
7	Circular	12.50	1100	12.12	6	1.5
8	Circular	12.50	300	3.40	6	1.5
1	Circular	15.00	500	5.78	3	1.5
2	Circular	15.00	860	9.60	3	1.5
3	Circular	15.00	1200	13.22	3	1.5
4	Circular	15.00	1330	15.48	3	1.5
5	Circular	15.00	1570	17.35	3	1.5
6	Circular	15.00	1320	15.11	3	1.5
7	Circular	15.00	1100	12.12	3	1.5
8	Circular	15.00	450	4.00	3	1.5

Table E-6 Cont'd

Run No.	Edge	J	Q	Y	L	L_e
1	Circular	17.50	550	6.02	2	1.5
2	Circular	17.50	980	10.10	2	1.5
3	Circular	17.50	1240	13.36	2	1.5
4	Circular	17.50	1400	15.45	2	1.5
5	Circular	17.50	1660	17.00	2	1.5
6	Circular	17.50	1450	15.50	2	1.5
7	Circular	17.50	1200	12.60	2	1.5
8	Circular	17.50	370	3.70	2	1.5
1	Circular	19.99	600	6.23	1.5	1.5
2	Circular	19.99	910	9.82	1.5	1.5
3	Circular	19.99	1340	13.70	1.5	1.5
4	Circular	19.99	1490	15.70	1.5	1.5
5	Circular	19.99	1650	17.62	1.5	1.5
6	Circular	19.99	1450	15.50	1.5	1.5
7	Circular	19.99	1250	12.83	1.5	1.5
8	Circular	19.99	340	3.50	1.5	1.5

TABLE E-6 Cont'd

Note:

J is a shape geometric factor when $INT(J) = L_e/t$

$FRACTIONAL\ (J) = t/L$

Except for Circular Edge where, $J = J \times 10$

APPENDIX F

NQMENCLATURE

In this appendix, the nomenclature and subscripts used in this thesis are presented. Each term is also defined as it first appears.

F.1 Nomenclature

A - Channel cross-section area

A_1, A_2 - Cross-sectional area of channel and cover subsections respectively

a, a' - Constants

B - Channel top width, constant in general instability equation

b - Channel bed width, width of roughness elements

b' - Constant

C - Chezy's coefficient

C_1, C_2 - Chezy's coefficient for bed and cover subsections

C_{12} - Roughness ratio = C_1/C_2

C^* - Non-dimensional modified Chezy's coefficient

C^*_1, C^*_2 - Modified Chezy's coefficient for bed and cover subsections respectively

C_L, C_D - Lift and Drag coefficients respectively

C_p - Dynamic pressure coefficient

C_τ - Shear distribution coefficient

c - Edge shape factor

D - Total flow depth

d - Local flow depth

E - Total energy, absolute error

E_R - Error in measuring hydraulic radius

E_S - Error in measuring friction slope

E_v	-	Error in measuring velocity
E_y	-	Error in measuring flow depth
e	-	Base for natural logarithms, eccentricity for edge weight
F	-	Force
F_n	-	Froude number = $V/\sqrt{gD}$
F_1, F_2	-	Velocity distribution functions
f	-	Darcy's coefficient of roughness
g	-	Acceleration due to gravity
H	-	Total height between two datums, total energy head
H_L	-	Total head lost
h	-	Local height of elements
i	-	Universal subscript
K	-	Specific gravity constant for instability of blocks
k	-	Roughness height of boundary
k_1, k_2	-	Roughness height for bed and cover underside boundaries respectively
L	-	Length of channel reach, block length, wave length
L_e	-	Length of block edge
l	-	Mixing length, local length
M	-	Moment caused by a force, rotational instability function
m	-	Atmospheric pressure in original Manning's formula
n	-	Manning's roughness coeffecient
n_1, n_2	-	Bed and cover Manning's roughness coeffecients respectively
n_{12}	-	The roughness factor = n_1/n_2
p	-	Channel wetted perimeter, pressure
P_v	-	Vapour pressure
P_1, P_2	-	Wetted perimeter for bed and cover subsections respectively

P_{st}	-	Static pressure
p	-	Porosity, general point location
Q	-	Total flow rate
q	-	Flow rate per unit width
q_i, q_s	-	Ice and sediment load respectively
R	-	Hydraulic radius = A/P ; reaction
R_n	-	Reynolds' number = $\rho VD/\mu$
R_1, R_2	-	Hydraulic radii of bed and cover subsections respectively
r	-	General exponent, rotation point subscript
S	-	Slope
S_o	-	Channel bed slope
S_f	-	Friction slope
S_g	-	Specific gravity
T	-	Total shear force
t	-	Block thickness
t_c	-	Cover thickness
U	-	Local average velocity in a strip
$\overline{U}$	-	Averaged velocity in turbulent flow
u	-	Local velocity in a strip
u'	-	Fluctuation in u due to turbulence
V	-	Average flow in the channel
V_{max}	-	Maximum velocity in the channel
V_1, V_2	-	Average velocities in bed and channel subsections respectively
V_*	-	Shear velocity = $\sqrt{\tau/\rho}$
$\mathcal{V}$	-	Volume
v	-	Local velocity at a point in the cross-section
v_s	-	Surface velocity

v' - Turbulent fluctuation in v

W - Weight, channel waveyness

X - Axis X

x - Distance along axis X

x_o - Distance between the cover edge and first point of effect U/S.

Y - Axis Y, total depth of flow

Y_1, Y_2 - Flow depth to separation line for bed and cover subsections respectively

y - Local flow depth, distance along Y axis

y_1, y_2 - Local depths in bed and cover subsections respectively

Z - Loss weight factor for instability in blocks

α - Angle of block rotation, wetted perimeter ratio = P_1/P

β - Coefficient

γ - Unit weight of water

δ - Thickness of boundary layer

Δ - Vertical displacement of blocks; height of roughness elements; and underside waves height

ε - Relative depth = y/Y

ε_1, ε_2 - Relative depths in bed and cover subsections respectively

κ - Von Karman's constant

ξ - Local vertical coordinates for block

η - Local horizontal coordinates for block

η_b, η_s - Thickness of bed and cover layers respectively

θ - Angle of flow direction at the block edge

λ - Hydraulic radii ratio = R_2/R_1

μ - Dynamic viscosity

ρ - Density

σ - Surface tension

τ - Shear stress

ϕ - Flow angle under the cover

ψ - General function

F.2 Subscripts

1 - Bed subsection

2 - Cover subsection

ABS - absolute value

b - Bed

c - Cover

C_r - Critical condition

d/dx - Derivative w.r.t.x

E - Error function

EXPC - Exponent Exp (x) = e^x

e - Edge

f - Friction

i - General subscript

J - General subscript

Log - Logarithm to base 10

ln - Logarithm to base e

O - Order to magnitude of

o - Initial or boundary value

u - Underside of the cover or under cover generally

x - In the X direction, horizontal acting horizontally

Y - In the Y direction, acting vertically, vertical strip

APPENDIX G

REFERENCES

REFERENCES

1. Ashton, G., and Kennedy, J.F., 1972, Ripples on Underside of River Ice Covers, Journal of the Hydraulics Division, ASCE, HY 9, Pgs. 1603-1624.
2. Bolsegna, S.J., June 1968, River Ice Jams, State of the Art Report, U.S. Army, CRREL.
3. Burgi, P.H., August 1978, Winter Ice Jam Observation on the Gunnison River, IAHR, Symposium on Ice Problems, Lulea, Sweden.
4. Carey, K.L., 1967, Analytical Approach to Computation of Discharge of an Ice Covered Stream, U.S. Geological Survey Professional Paper S75-C, Geol. Survey Research, Pgs. C200-C207.
5. Carey, K.L., 1967, The Underside of River Ice, St. Croix River Wisconsin, U.S. Geol. Survey Professional Paper S75-c, Geological Survey Research, Pgs. C195-C199.
6. Carey, K.L., 1966, Observed Configurations and Computed Roughness of the Underside of River Ice, St. Croix River, Wisconsin, U.S. Geological Survey Professional Paper 550 B, Geological Survey Research, Pgs. B197-B198.
7. Cartier, L., Feb. 1979, Field Investigation of Some Ice Cover Problems in an Experimental Canal, Eastern Snow Conference, Vol. 6, Pgs. 45-54.
8. Chang, F.M., Simons D., and Richardson, E.V., 1966, Total Bed Material Discharge in Alluvial Channels, IAHR, Hydraulics Conference.

9. Chow, V.T., 1959, Open Channel Hydraulics, McGraw-Hill, N.Y.

10. Devik, O., 1964, Present Experience on Ice Problems Connected with the Utilization of Water Power in Norway, IAHR, Volume 2, No. 1, Pgs. 25-40.

11. Drage, B., and Carlson, R., 1977, Hydraulic Geometry Relations for Northern Braided Rivers, CSCE, 3rd Hydrotechnical Conference.

12. Haggag, M.R., July 1976, Hydraulics of Ice Covered Channels, An M.A.Sc thesis presented to the Faculty of Graduate Studies, The University of Windsor, Windsor, Ontario, Canada.

13. Ismail, F, et al, 1978, Resistance to Channel Flow Under a Very Rough Top Boundary -Analogues to Broken Ice Cover, IAHR, Symposium on Ice Problems, Lulea, Sweden, August 1978, Pgs. 443-448.

14. Kanavin, E.V., August 1975, Water Velocity in Open and Frozen Rivers Control of Ice Production, IAHRA, Journal of Hydraulic Research.

15. Kennedy, J,and Neville, A.M., 1978, Bsic Statistical Methods for Engineers and Scientists, International Scranton, Pennsylvania.

16. Kivisild, H.R., 1956, Hanging Ice Dams, 8th Congress, ZAHR, Vol. 2, Paper 23-F1/30, Montreal, Canada.

17. Larsen, P.A., 1966, Head Losses Caused by an Ice Cover on Open Channels, Boston society of Civil Engineers. Pgs. 45-67.

18. Larsen, P.A., Jan. 1973, Hydraulic Roughness of Ice Covers, ASCE, Journal of the Hydraulics Division, HY 1, Pgs. 111-119.

19. Larsen, P.A., Aug. 1975, Notes on the Stability of Floating Ice Blocks, IAHR, 3rd International Symposium on Ice Problems.

20. Mathieu, B., Michel, B., 1967, Formation of Soft Ice Jams, 3AHR, 12th Congress, Vol. 4., Part 2, Colorado.

21. Mercer, A.G., and Cooper, A.H., 1977, River Bed Scour Related to the Growth of a Major Ice Jam, 3rd National Hydraulics Conference Pgs. 291-308.

22. Michel, B., Nov. 1966 Ice Covers in Rivers, Proceedings from the Conference on Ice Pressure Against Structures, Appendix IV (C),Laval University, Quebec, NRC Technical Memorandum, No. 92.

23. Michel, B., April 1971, Winter Regieme of Rivers and Lakes, Research Report, U. S. Army, CRREL.

24. Michel, B., and Abd-Elnoor, R., 1974, Break-up of a Solid River Ice Cover, 3rd Hydrotechnical Conference, CSCE.

25. NRC Working Group on Hydraulics of Ice Covered Channels, May 1979, Resistance to flow in Ice Covered Rivers, Canadian Hydrology Symposium 1979, Vancouver, B.C.

26. Osterkamp, T.E., Sept. 1978, Frazil Ice Formation, a Review, ASCE, Journal of the Hydraulics Division, HY 9, Pgs. 1239-1255.

27. Pariset, E., and Hausser, R., 1959, Some Theoretical and Laboratory Research on Ice Cover Problems, Eastern Snow Conference, Vol.6, Pgs. 71-93.

28. Pariset, E, and Hausser, R, 1961, Formation and Evolution of Ice Covers on Rivers, Transaction of the Engineering Institute of Canada, Vol. 5., No. 1, Pgs. 1-9.

29. Petryk, S., June 1978, Simulation of Ice Conditions in Channels, CSCE, Computer Application Conference, Toronto, Ontario.

40. Uzuner, M.S., July 1977, Stability Analysis of Floating and Sumberged Ice Floes, ASCE, Journal of the Hydraulics Division, HY7, Pgs. 713-722.

41. Uzuner, M., and Kennedy, J.F., December 1972, Stability of Floating Ice Blocks, ASCE, Journal of the Hydraulics Division, Vol.98,HY12, Pgs. 2117-2133.

42. Uzuner, M., and Kennedy, J., September 1974, Theoretical Model of River Ice Jams, ASCE, Journal of the Hydraulics Division, HY9, Pgs. 1365-1383.

43. Wong, Y.F., 1979, Hydraulics of Covered Channels, An M.A.Sc thesis presented to the Faculty of Graduate Staudies, the University of Windsor, Windsor, Ontario, Canada.

44. Yalin, M.S , 1970, Mechanics of Sediment Transport, Pergamon Press, New York.

45. Yu, K.H., Graff, W.H., and Levine, G., The Effect of Ice on the Roughness Coefficients of the St. Croix River, Proceedings of the 11th Conference, Great Lakes Research, Association of Great Lakes Research, 1968, Pgs. 668-680.

46. Zhidkikh, V.M. Sinotin, V.L., and Guenken, Z ,1974, Kinematics of Flow Under Ice Cover, IAHR, International Symposium on River and Ice, Budapest, Hungary.

47. Zsilak, E., August 1978, Approach to Stream Resistance in Case of Jammed Ice Motion, IAHR, Symposium on Ice Problems, Lulea, Sweden, Pgs. 403-414.

30. Richardson, E., and Simons, D., Resistance to Flow in Sand Channels, IAHR, Hydraulics Journal, Pgs, A18.1-A18.10.

31. Senturk, H. A, 1978, Resistance to Flow in Sand Bed Channels, ASCE, Journal of the Hydraulics Division, HY2, Pgs 421-438.

32. Synotin, V.I., 1965, Velocity Structure of Flow Under Ice Cover, IAHR, Ice Symposium, Montreal.

33. Task Force on Friction Factors, March 1963, Friction Factors in Open Channels, ASCE, Journal of the Hydraulics Division, HY2, Pgs. 97-143.

34. Tatinclaux, J.C., Sept. 1977, Equilibrium Thickness of Ice Jams, ASCE, Journal of the Hydraulics Division, HY9, Pgs. 949-974.

35. Tatinclaux, J., and Lee, C.,1978, A Laboratory Investigation of the Mechanics and Hydraulics of River Ice Jams, IAHR Report 186, Iowa Institute of Hydraulic Research, University of Iowa, Iowa City, Iowa.

36. Tatinclaux, J. C. and Chung, S.T., Characteristics of River Ice Jams, IAHR Symposium on Ice Problems, Lulea, Sweden, August 1978,Pgs. 461-475.

37. Tesaker, E., 1970, Measurements of Ice Cover Roughness and the Effect of Ice Cover on Water Levels in Three Norwegian Rivers, IAHR Symposium on Ice, Reykjavik, Iceland.

38. Tsang, G., 1970, Change of Velocity Distribution in a Cross-Section of Freezing River and the Effect of Frazil Ice Loading on Velocity Distribution, IAHR Ice Symosium, Reykjavik, Iceland, Pgs. 3.2-1-3.2-11.

39. Uzuner, M.S., 1975, The Composite Roughness of Ice Covered Streams, IAHR,Journal of Hydraulics, Vol. 3, No. 1, Pgs. 79-102.

VITA AUCTORIS

1951 Born on the 15th of May in Cairo, Egypt

1967 Matriculated from Ibrahimia Secondary School, Cairo, Egypt

1972 Graduated with a B.Sc. in Civil Engineering (Distinction with Honour Degree) from the Faculty of Engineering, Cairo University, Giza, Egypt

1972 Appointed as instructor of Hydraulic and Coastal Engineering at the Hydraulics and Irrigation Department, Faculty of Engineering, Cairo University, Giza, Egypt

1976 Graduated with a M.A.Sc in Civil Engineering, University of Windsor, Windsor, Ontario, Canada

1976 Enrolled in the Civil Engineering Ph.D. programme at the University of Windsor, Ontario, Canada.